

FLOW AND FILLING CHARACTERISTICS IN
PLANE STRAIN AND
AXISYMMETRICAL DEFORMATION IN FORGING

FLOW AND FILLING CHARACTERISTICS IN
PLANE STRAIN AND
AXISYMMETRICAL DEFORMATION IN FORGING

A thesis presented for the degree of

DOCTOR OF PHILOSOPHY

of the

UNIVERSITY OF ASTON IN BIRMINGHAM, ENGLAND.

BY

Tai Chiu LEE

THESIS
621.73011 LEE

190399 27 APR 1975

August, 1975.

SUMMARY

The flow and filling characteristics of a forging process are important because they are related to the study of the forgeability of metal which is the cornerstone of forging technology.

The usual conception of forgeability is the extent ^{which} to _^the metal being deformed without failure. The old criterion of failure is the appearance of cracks, whereas this criterion is now found to be inadequate by the fact that cracks can appear anywhere in the forging. Furthermore, a non-homogeneously deformed or incompletely filled forging can also be called a failure. Since it is for strength that the forging is to serve, any damage to the strength through deformation of the forging can be considered as failure. It is on the study of the deterioration of strength through deformation that this project is based.

The deformation from point to point in the forging is not only non-uniform but very large as compared with the small deformations commonly analysed in the analysis of small strain. So a new mathematical tool, namely, the analysis of large deformation, has been developed in Part A of this thesis. This method is a combination of the work by Professor Hsü and the mathematical method of Truesdell and other mathematical physicists.

The objective of this project is to use this mathematical tool to analyse the deformation in upsetting processes, and consequently explore the implications to the loss of strength of the forging through deformation. With the use of this analytical tool, a scalar value called the deformation intensity value Γ , is developed to represent the extent of the deformation

of an element. Subsequently, contour maps with varying deformation intensity values of the forging are produced to represent the distribution of the various levels of damage due to deformation. Such contour maps are essential tools for forging designers in deciding the shape of the forging.

Deformation is so non-uniformly distributed in a forging that a homogeneity value has been developed to indicate how much the most damaged part deviates from the least damaged part in the forging.

It has been revealed that the initial filling of the die cavity which is also one of the criteria included in the study of forgeability, is dominated by the folding of metal from the side face of the forging.

The analysis presented in this thesis cannot claim to be the solution to all the problems in the study of forgeability, but a proper route has been found to further this study.

C O N T E N T S

	<u>Page</u>
SUMMARY	(i)
Notation	(xii)
Chapter 1	Introduction 1
Chapter 2	Literature Review 13
2.1	Introduction 13
2.2	Predictive Theories 13
2.2.1	The Analytical Method using the approximate Theory 14
2.2.2	Finite Element Method 16
2.2.3	Slip Line Field Method 18
2.2.4	Extremum or Bounding Theorem 19
2.3.1	Experimental Methods in the Analysis of Deformation Processes 21
2.3.2	The Behaviour of Metal on the Surface of the Specimen under Compression 22
2.3.3	Visioplasticity 24
2.3.4	The Welded Tube Method 25
2.4	General Remarks 26
Part A	Theoretical Derivation of Large Deformation Analysis
Chapter 3	Deformation, Strain and Rate of Deformation-- the Analysis of 27
3.1	Introduction 27
3.1.1	Definition of Conventional Engineering Strain and Natural Strain in One Dimension 27

	<u>Page</u>
3.2	General Consideration of Deformation Analysis 28
3.2.1	Deformation in terms of the Affine Transformation of a Point and Line Element 28
3.2.2	Matrix Algebra in Deformation Analysis and its Displacement Gradient and Deformation Gradient Matrices 30
3.2.3	Various Measures of Finite Deformation and their Relationships 31
3.2.4	Decomposition of the Deformation Gradient Matrix 34
3.3	Deformation in Two Dimensions 35
3.3.1	The Analysis 35
3.3.2	Some Typical Examples of Deformation Modes Repre- sented by Matrices 36
3.3.3	Principal Values and Directions of a Stretch (Strain) Matrix \mathbf{U} 37
3.3.4	Practical Analysis of a Deformation 39
3.4	Velocity Field and Rate of Deformation 40
3.4.1	Motion of a Particle -- Velocity 40
3.4.2	The Decomposition of the Velocity Field into the Rate of Deformation Matrix and Spin Matrix 41
3.4.3	The Principal Axis of Stretching 42
3.4.4	Some Examples of Velocity Gradient Field in Two Dimensions 42
3.4.5	General Analysis of a Velocity Field 44
3.5	Axisymmetrical Deformation Analysis 45
3.5.1	Uniform Dilation in Two Dimensions 45

	<u>Page</u>
3.5.2	Axisymmetrical Deformation 46
3.5.3	Velocity Field of a Uniform Dilatation in Two Dimensions 48
3.5.4	Velocity Field for an Axisymmetrical Deformation 49
Chapter 4	The Behaviour and the Distribution of Finite Deformation of Metal under Load 51
4.1	General Consideration 51
4.2	Graphical Representation of Deformation 51
4.2.1	The Triangular Co-ordinate System 52
4.2.2	Coaxial and Non-Coaxial Path 53
4.2.3	Coaxial Strain Path 55
4.2.4	Non-Coaxial Strain Path 55
4.2.5	Strain Path in Plane Strain Condition 56
4.2.6	Finite Deformation -- its Meaning and its Measure 57
4.3	Distribution of Deformation of a Workpiece in Simple Plane Strain Upsetting Process 57
4.3.1	Finite Strain Distribution of a Deformed Work- Piece 58
4.3.2	Finite Strain Distribution Histogram 58
4.3.3	Non-Dimensional Strain Distribution Histogram 58
4.3.4	Homogeneous Deformation 59
4.4	Examples of Deformation Models in Plane Strain Upsetting 59
4.4.1	Ideal Reduction Model 59
4.4.2	A Theoretical Zonal Model 61
4.4.3	Comparis <u>i</u> on of the Two Models 62

		<u>Page</u>
Chapter 5	The Incremental Theory in Deformation Analysis	63
5.1	Basic Principles	63
5.1.1	The Incremental Strain	63
5.1.2	Frame of Reference	64
5.1.3	Change of Frame and Frame Indifference	64
5.1.4	Equivalent Motion and Equivalent Deformation Path	65
5.2	Total Deformation Analysis	66
5.2.1	The Extent of Deformation and the Curvature of the Strain Path	66
5.2.2	Pure Deformation	68
5.2.3	Total Deformation of a Process	69
5.2.4	Total Deformation with Superimposed Rigid Body Rotation	69
5.3	The Determination of the Total Deformation Intensity Γ of a Non-Coaxial Strain Path	70
5.3.1	An Equivalent Deformation Path	71
5.3.2	The Derivation of the Incremental Strain or Rate of Deformation Matrix \mathbf{D} in terms of a Fixed Configuration	71
5.3.3	The Calculation of Total Deformation Intensity of this Equivalent Path	75
Chapter 6	Work, Path Characteristic and Redundant Work of a Perfectly Plastic Body	76
6.1	Introduction	76
6.1.1	Work Done by an Element in a Perfectly Plastic Deformable Medium	76
6.1.2	Apparent Work Done by the Element	78

	<u>Page</u>	
6.2	Ideal Work Path and the Path Characteristics of an Element in a Deformable Body	78
6.2.1	Ideal Deformation Path of a Particle in a De- formable Body	78
6.2.2	Curved Coaxial Path	79
6.2.3	Path Characteristic for Non-Coaxial Plane Strain Deformation	80
6.3	Distribution of Work Done by a Deformed Body	82
6.3.1	Distribution Pattern represented by means of a Contour Map	82
6.3.2	Distribution Pattern in term of a Histogram	82
6.4	Total Work Done and Redundant Work for a Simple Reduction Process	82
6.4.1	Total Work Done	82
6.4.2	Redundant Work	83
6.4.3	Apparent Redundant Work	84
Chapter 7	The Filling and Spreading Characteristics in a Closed Die Forging Process	86
7.1	The Spreading of the Metal	86
7.1.1	General Considerations	86
7.1.2	An Ideal Spreading Process	86
7.1.3	Actual Spreading of Metal at the Interface	87
7.1.4	The Spreading Coefficient	87
7.1.5	The Bulge Profile	88
7.2	Filling Characteristic	89
7.2.1	General Consideration	89
7.2.2	The Filling Coefficient	90

		<u>Page</u>
Chapter 8	Experimental Equipment and Technique	91
8.1	The Experimental Methods and Data	91
8.2	Experimental Technique in the Investigation of Flow Characteristic of Metal under Simple Upsetting	91
8.2.1	Specimen Data	91
8.2.2	Preparation of the Checker Board (Master Grid)	92
8.2.3	The Printing Technique	93
8.2.4	Experimental Procedure	95
8.2.5	Analysis of Data	97
8.3	Experimental Method for the Investigation of the Filling Characteristic	98
8.3.1	The Specimen and its Preparation	98
8.3.2	Equipment	99
8.3.3.	The Forging Procedure	99
8.3.4	The Measuring Procedure	100
8.3.5	Computation of Data	100
Part B	Discussion of Results	
Chapter 9	The Distribution of Deformation under Contin- uous Loading	101
9.1	Introduction	101
9.2.1	The Development of the Pattern of Distribution of Deformation under Continuous Loading	102
9.2.2	The Principal Directions of the Finite Strains	103
9.2.3	The Development of the Zonal Patterns	104
9.3	The Distinction of Deformation Zones in terms of the Behaviour of the Zonal Elements	106
9.3.1	Introduction	106

		<u>Page</u>
9.3.2	The Path Characteristics	107
9.3.3	The Behaviour of Strain Paths in Different Deformation Zones	107
9.3.4	Curvature of the Strain Path	108
9.3.5	Rigid Body Rotation of the Zonal Element	111
9.4	The Effect of Lubrication on the Deformation Distribution Pattern	112
9.4.1	The Zonal Pattern and the Orientation of the Plateau	112
9.4.2	The Effect of Lubrication on the Behaviour of the Zonal Elements	113
9.5	Concluding Remarks	114
Chapter 10	The Homogeneity of Deformation	116
10.1	General Introduction	116
10.2.1	The Criteria of Homogeneity in Deformation Process	117
10.2.2	The Meaning of Homogeneity	117
10.2.3	The Characteristic Equation of Homogeneity	118
10.2.4	Some Aspects of the Homogeneity of Deformation	119
10.2.5	The Homogeneity of Deformation in Upsetting Processes	120
10.3	Concluding Remarks	121
Chapter 11	Redundant Work and Redundant Deformation of a Perfectly Plastic Medium	123
11.1	Introduction	123
11.2	The Total Work Done in Upsetting Process	124
11.2.1	Deformation Distribution Curves	124

		<u>Page</u>
11.2.2	The Work Done on a Perfectly Plastic Body	125
11.2.3	The Effect of Strain Hardening on the Total Work Done	127
11.3	Redundant Deformation and Redundant Work in a Perfectly Plastic Body	128
11.3.1	The Redundant Deformation and Redundant Work	128
11.3.2	The Efficiency of Deformation Dispersion	130
11.4	Concluding Remarks	131
Chapter 12	The Spreading and Filling Characteristics of the Forming Process	134
12.1	General Consideration	134
12.2.1	The Spreading Phenomenon and the Bulge Profile of the Specimen under Continuous Loading	135
12.2.2	The Relationship between the Two Spreading Mechanisms	136
12.2.3	The Effect of Rigid Body Rotation on Folding	137
12.3	The Filling of the Die Cavity	137
12.3.1	The Height to Diameter Ratio (H/D) of the Specimen	138
12.3.2	The Effect of Extra Volume of Metal	139
12.3.3	The Loading Factor in the Filling Process	139
12.4	Concluding Remarks	141
Chapter 13	Conclusions	142

		<u>Page</u>
Chapter 14	Future Work	154
14.1	The Improvement in Experimental Technique	154
14.2	The Detection of Structural Failure	155
14.2.1	The Density Evaluation Method	155
14.2.2	Fatigue Test	160
14.3	The Flash Behaviour and its Effects	160
Appendix I		162
Acknowledgements		164
Bibliography		165

NOTATIONS

The notation used throughout this thesis closely follows the format used in Truesdell's "Classical Field Theory" (85).

Italic letters or Greek letters -- A, a, \dots etc.; Scalar or indices of the vectors.

Bold-face letters or Greek letters -- $\mathbf{A}, \mathbf{F}, \mathbf{v}, \dots$ etc., are vectors, matrices or tensors.

A number in a bracket for example, (5) the number of reference in the Bibliography.

B	Hencky's logarithmic strain matrix.
C	right Cauchy-Green deformation matrix.
D	rate of deformation matrix.
E	Lagrangy strain matrix.
F	deformation gradient matrix.
H	displacement gradient.
I	unit matrix.
L	velocity gradient.
R	rotational matrix.
T	traction force.
U	right stretch.
V	left stretch matrix.
W	spin matrix.

X	initial undeformed column matrix.
dX	elements of arc before transformation.
a	acceleration vector.
c	left Cauchy-Green deformation matrix.
e	Eulerian strain matrix.
u	displacement vector.
v	velocity vector.
x	final or terminal position matrix.
dx	element of arc after deformation.
Φ	rotational matrix for the principal angle of the deformation matrix.
Θ	rotational matrix for the principal angle for the stretch matrix.
$\dot{\epsilon}$	strain rate matrix.
$\dot{\epsilon}_0$	principal strain rate matrix.
ϵ	strain matrix.
ϵ_0	principal strain matrix.
$d\epsilon$	incremental strain matrix.
σ	stress matrix.
$d\sigma$	incremental stress matrix.
A	dimensionless work per unit volume.
A_R	redundant work.
B	apparent work.
\dot{E}	rate of work.
K	shear stress
L	load required.

S	spread coefficient.
SD	sideway displacement coefficient.
W	work per unit volume.
$X, (X, X_2, X_3)$	co-ordinates of a point.
a	total area.
b	width of the specimen.
d, d_i	horizontal displacement; ideal horizontal displacement.
f	function.
g	function.
h, h_0, h'	heights of the specimen.
l	length.
m	uniform dilatation.
p	hydrostatic pressure.
r	radius of the specimen.
t	time.
δt	element of time.
u	displacement.
u_{x_1}	displacement in the x_1 direction.
x, x_1, x_2, x_3	co-ordinates of a point.
Γ	deformation intensity.
\wedge	filling coefficient.
Υ	% of reduction ⁱⁿ height.
$\bar{\Upsilon}_e$	average reduction strain.
Φ	principal angle of the rate of deformation matrix.
Ω	rate of spin.

β	non-coaxiality angle.
$\epsilon_1, \epsilon_2, \epsilon_3$	principal strains.
$\bar{\epsilon}$	effective strain.
$\dot{\epsilon}_0$	principal strain rate.
$d\epsilon_1, d\epsilon_2, d\epsilon_3$	principal incremental strain.
$d\bar{\epsilon}$	effective incremental strain.
ξ	homogeneity value.
η	characteristic index of strain.
θ	principal angle of stretch matrix.
λ	stretch.
λ_0	principal stretch.
μ	coefficient of friction.
ν	folding coefficient.
ξ	deformation dispersion efficiency.
ρ	the radius of curvature of the strain path.
$\sigma_1, \sigma_2, \sigma_3$	principal stresses.
$\bar{\sigma}$	effective stress.
σ_0	yield stress.
ω	angle of the rigid body rotation.

ALAN S. WATSON

CHAPTER ONE

Introduction

Forging is a basic production process and it has dominated the manufacturing industry for centuries past. Its history can be traced back to the primitive age when men used stones or heavy objects to beat pieces of metal into usable objects, such as knives and tools. Long after its existence, people seldom tried to explain the mechanism behind the forming processes till sometime in the 17th century, when Galileo established the foundation of the mechanics of solids in his book "Two New Sciences". But, not much progress was made until the end of the 19th century. Material scientists and mathematicians such as Tresca, Coulomb, Saint Venant and Lévy began their study of the plastic behaviour of metals. After these pioneers' work, the research done in this field began to gather momentum. Especially since the second world war, many great advances have been made and theories concerning the mechanism of the various deformation processes have been established.

Although various theories have been proposed in the analysis of ^{the} forging process in which simple upsetting is a basic one, many aspects of its mechanism are still a mystery because of the complexity involved. One fundamental area of research which has been done for several years past is the forgeability of metal. ~~the~~ ~~the~~ ~~process~~

The idea of forgeability is often demonstrated in text books on production engineering or manufacturing technology by photographs of progressively compressed cylindrical slugs of the same material, some with and some without cracks at the periphery of the severely **compressed** specimens. The idea of forgeability illustrated in such pictures is a very rudimentary

one, namely, that metal can crack if sufficiently compressed, as in forging processes. Such^a demonstration is, however, also misleading. In the first place, cracks can as easily appear inside the workpiece as on its surface, indeed, in some cases they start inside the metal before the surface begins to crack. In the second place, cracks big enough to be visible to the naked eye can hardly serve as the criterion for the end or exhaustion of forgeability, rather, they indicate that the work is falling apart. Forgings fail long before they fall apart; they fail when their static, dynamic or fatigue strength has seriously deteriorated. Whether the static, or the impact, or the fatigue strength should be used as the criterion depends on the use which the forged product is to serve.

The research reported in this thesis is based on a wider and at the same time more precise conception of forgeability. Forgeability is conceived in terms of the retainment of strength in general, rather than in terms of the appalling visible cracks alone, hence it is a wider conception. Such an idea of forgeability is not based on a refined criterion of crack detection, say, from those comfortably visible in photographs, to those visible with a lens, to those detectable under more and more powerful microscopes, till one begins to question what qualifies as a crack. If, however, ductility is based on the idea of strength, then such an idea is both more realistic and more easily measurable, because it is for strength that components are forged rather than fabricated or cast, and the methods of measuring various types of strength are well established and standardized. A forging must be thought of as having failed if its dynamic or fatigue strength, for example, is below the admissible, no

matter what size of cracks are detectable in it, with what microscope. Equally, a forging is counted as a successful one if it is sufficiently strong, no matter what size of cracks are detectable in it with some microscope or other.

This conception of forgeability opens up a whole field of research, of which it is the aim of this thesis to provide a starting point. In delineating the scope of this thesis, therefore, it is necessary to survey the broad outlines of this new field of research and to choose an area as the starting point.

There are obviously two aspects in this new area of research, the loss of strength (or structural damage) due to forging and a definition of the degree of forging. Information on forgeability is then seen as a quantitative relationship between the degree of forging and the internal damage or weakening of the workpiece. This being a field in which little research results are available, a choice has to be made in the manner of tackling the problem. Either some degree of forging is taken as a working criterion in some specimens and some tests for strength are conducted on them; or a narrow area is to be covered at a greater depth. It is recognized that even if only ad hoc forging processes and tests for strength were used, the results would be more sound than looking for cracks. However, it is also recognized that research on manufacturing processes in general and forging in particular suffers precisely ^{from} a lack of depth and thoroughness. It was therefore decided to make a start in this general area by concentrating on the degree of forging. That the definition of the ~~degree of forging~~ degree of forging is in itself a topic of sufficient complexity and

difficulty to warrant a major effort in research will become evident in the course of this thesis.

The degree of forging is usually thought of as the reduction in height of a cylindrical slug compressed along its axis. The simplicity of this definition covers a concealed illusion. The illusion that this is a good measure of the degree of at least upsetting lies in the fact that the reduction in height is thought of both as a compressive strain and as the degree to which the specimen is compressed. Now, the reduction in height can represent both a strain and the general deformation of a slug only if the deformation is homogeneous. In most actual cases of upsetting, the deformation is far from being homogeneous. If then the reduction in height is thought of as strain, it represents the strain of no particular element in the specimen. All that can be said of it then, is that it is an "average strain", the averaging being so rough and ready as to be practically meaningless. If, on the other hand, the reduction in height is meant to represent the general deformation of the specimen, then it becomes of dubious validity when the specimen is not a cylindrical slug with flat and parallel ends and the die faces are not flat and parallel.

To find a better basis for the degree of forging it is necessary to take the major, and apparently negative step of abandoning the reduction in height, as a representation of strain. (It is only useful as a practical parameter to represent the progress of the upsetting process, like time or cross-head travel.) From this rejection of the reduction in height, emerges a method of measuring the degree of forging in which both the

unsatisfactory "average strain" and the limitation to cylindrical slugs with parallel ends, are avoided. This method consists of the analysis of large deformations in depth.

The analysis of large deformation is, curiously, a relatively unfamiliar and uncommon topic among the research workers in applied plasticity. This relative neglect is curious because it is almost tautological to say that metal forming always involves large deformations and the basic investigation of any metal forming process must include the analysis of large deformation. Although this thesis does not cover all the ground in the topic of forgeability, the method and the approach adopted here can legitimately be claimed to be germane to all metal forming processes. Of course, the avoidance of the analysis of large deformations is understandable. The mechanics of solids begin in the analysis of small deformations, as in the Theory Of Elasticity. The ease of superposition, the simplicity of the Mohr circle and the apparent generality of the definitions of small strains conspire to encourage a mental inertia visible in many attempts to force large deformation, especially theoretical ones, willy-nilly into the moulds of small strains. Thus, strain analysts sometimes still talk of simple shear where the deformation is not simple shear at all, and of direct strain, when only a longitudinal displacement gradient exists. In this manner, the analysis adequate only for small strains is overworked and stretched into the area of large strains where it is either inadequate and erroneous, or severely limited and impotent.

The reduction in height is a useless measure because the deformation in a compressed specimen is practically never homogeneous. The analysis of large

deformation begins, therefore, with the recognition that the deformation in forgings is always a point function, in other words, it varies from point to point. It is more helpful to talk of ^a deformation field, or the distribution of deformation, than to talk simply of deformation. Once deformation is analyzed on the basis of the deformation at (or in the vicinities of) a point, then it is at once unnecessary to think in terms of a cylindrical slug compressed along its axis, or to imply homogeneous deformation in such a specimen. Any forging produced in any die is now open to this analysis, because in it there must be various points, and at each point there is a particular deformation. Such an approach is far more incisive than the imprecise reduction in height.

Apart from being more precise and more widely applicable, the analysis of large deformations can rightly be claimed to be the proper way to study forgeability. The whole idea of forgeability hinges on the damage to strength through deformation. Since deformation is never homogeneous in a forging, whatever other factors enter into the damage to strength — such as hydrostatic stress and surface friction — the damage to strength is also never uniformly distributed in a forging. The only adequate way to investigate the damage to strength through deformation must begin, therefore, with ^{an} analysis of the deformation from point to point. So now in the study of forgeability we investigate the deformation from point to point in a forging to see how much the damage to the strength at any point in the product approaches an unacceptable value.

As has been previously explained, the analysis of large deformation is not an exercise indulged in for its elegance or profundity, but is an

inevitable route to a better understanding of forgeability.

An engineer, to whom mathematics is always only a means to an end, is entitled to the less aesthetic but more practical approach of seeking the simplest mathematics adequate for his purpose. As will be seen in Part A of this thesis, to establish a relatively simple mathematical technique requires some labour and it may require some justification. The justification is explained in the following.

Unlike jet propulsion and nuclear explosives, forging is not a technique arising out of theoretical studies. It has existed since primitive times. The Industrial Revolution stimulated the theoretical studies of thermodynamics because the source of mechanical power in heat became a major concern, but the Industrial Revolution had little immediate effect on the mechanics of solids, because the strength of materials was not at first an acute issue, people simply built thicker foundations or used heavier chains. Processes of metal forming proliferated and were developed, but the developments ^{were} dangerously based on unhealthy exclusive faith in empirical methods and an unfounded scepticism against theoretical research. This type of conservatism of the engineers in the metal forming industries is well known. Nevertheless, small achievements of empirical experience and guess-work can continue to maintain a distrust of theoretical studies, till the pressure of commercial competition forces industry to seek all possible means of staying commercially on top, even among the possibilities of theoretical studies. This has been the climate of studies of applied plasticity since world war I, and more so after world war II. In such a climate, one important task of a research engineer

is to provide a bridge between the theoretical physicists and the engineers who design and operate the metal forming processes. The mathematical physicists are hardly interested in the actual problems of metal forming because they are too bedeviled by a multitude of real but irritating effects, or because the basic equations are too simple and lack structural beauty; whereas the die makers and press operators are shy of the simplest differential equations and try to excuse their ignorance by a self generated scorn for any theory whatsoever. Left to these two groups of people, little progress can be expected in the basic studies of metal forming. The engineer has the advantage over the technician in that he, the engineer, is not daunted by the complexity of the mathematics, and he has the advantage over the mathematical physicist in that he is not daunted by the simplicity of the mathematics either. To him the mathematics is a tool only, the simpler the better, so long as it is adequate. He is neither committed to the beauty of mathematical displays, nor has he an interest in shunning equations. In fact, he is uniquely qualified to make use of the necessary mathematical technique, however plain it may seem to the mathematician, to further the understanding and serve the improvement of metal forming, even though he may have to brave the rejection of the technicians and mechanics. He needs only occasionally to excuse himself to the mathematical physicists for simplifying the mathematics from its full generality and beauty, and to excuse himself to the press operators for introducing more mathematics than is required for sums.

In order to study these forging processes methods of deformation analysis have to be developed. In particular, methods for strain analysis with the use of matrix algebra originally developed by Hsü (29,30,31,32) coupled with the mathematical approach of Truesdell, Malvern, Toupin, Eringen, Noll, and Hill (85,86,16,64,57,25) are chosen and extended further to be used in our analysis. The development of this mathematical tool is described in chapters three and four in this thesis in which the changes in the co-ordinates of a distorted square grid (used to represent a minute homogeneous deformation field) are used to calculate the state of strain.

In chapter six, a deformation intensity Λ^{Γ} is introduced. The use of this deformation intensity Λ (a scalar quantity) is to indicate the degree or extent of deformation that the element has experienced. The deformation intensity is different from the effective strain. Even in a co-axial strain path in which the principal straining directions do not rotate with respect to the material throughout the history of deformation of an element, the effective strain is a poor measure for the extent of deformation owing to the varying strain ratio resulting in a curved strain path. In a forging process such as simple upsetting, most elements within the metal body during deformation behave non-coaxially due to the non-homogeneity of deformation, that is, their principal straining directions rotate with respect to the material. These rotations throughout their history require extra work to be done even if the deformation does not involve changing the shapes of the elements. From our

strain analysis, for non-coaxial paths, the extent of deformation can be represented by a scalar quantity which is the summation of all its incremental principal strains referred to a fixed configuration, from the initial state of strain, through the strain history to the final state. The scalar value is the deformation intensity factor Γ .

In most literature on the deformation analysis of the upsetting process, researchers (25,38,45,52,2,44) have either concerned themselves with theories to predict the load and stresses required for the process or were just satisfied with the investigation of the flow of metal on the surface of the specimen only (47,48,81,50,41). So, the objective of this project is to look into how the metal flows and how the deformation is distributed in the cross-section of the specimen with the aid of the strain analysis method developed in this thesis.

Most of Part A of this thesis is devoted to the development of the mathematical tool to analyse the large deformation. Part B is the adoption of this analytical method in analysing the upsetting processes in a thorough and precise way. In Chapter two of this thesis, the various past methods in the analysis of deformation in upsetting processes are reviewed in two groups (i) the predictive theories and (ii) the experimental methods. Chapter three, which begins with a brief description of the various strain measures, describes the development of the analysis of large deformation by matrix algebra by Professor Hsü. Different modes of deformation and velocity field are presented to provide a guide to

the actual deformation analysis. This analysis has also ^{been} extended to cover deformation in both plane strain and axisymmetrical conditions. The representation of the state of strain in a triangular co-ordinate system developed by Professor Hsü is described in Chapter four. The distinction between different types of strain paths such as coaxial and non-coaxial paths is also included. The resulting strain distribution of a deformed specimen analysed by means of a histogram is also presented in the later section of the chapter. Chapter five goes back to the analysis of large deformation in which the essential feature is the derivation of a scalar value — deformation intensity factor Γ to represent the extent of deformation that an element has experienced. The work done in various upsetting processes and their differences are explained and developed in Chapter six. The curvature of the strain path, which, under certain conditions, determines the work is also included. Chapter seven involves the study of the bulk reactions of the deformed specimen such as the spreading of the metal and the filling of the forging. The experimental technique and equipment used are described in Chapter eight.

Part B of this thesis is mainly the discussion of results. In it, Chapters nine and ten contain the discussion of the deformation distribution patterns, the significance of the zonal paths and the resulting homogeneity of deformation. Chapters eleven and twelve are concerned with the work consumed in the various upsetting processes and the significance in the filling and spreading of the metal when compressed between the dies. The conclusions are in Chapter thirteen and ^{are} followed by **a** descriptions

and suggestions for the various unresolved and remodelled theoretical as well as experimental methods in Chapter fourteen.

These various studies are intended to clarify some obscure areas in the study of forgeability in upsetting processes and it is hoped that they will contribute to solving some of the complex problems faced by the industry.

CHAPTER TWO

Literature Review

2.1 Introduction

Metal deformation processes are well established even in the primitive period of human history. Yet, the analysis of deformation was not started until after 1900 and during the period since 1900, the material scientist began to realise the importance of these studies. The application of the various theories of plasticity to the analysis of the phenomenon of forging gives rise to the prediction of strain, stress, load and energy consumption in forging. The simple upsetting process which is the beginning of most forging processes, is most frequently used as a test or model for either the experimental determination of the various measurable quantities in the process or the establishment of the theoretical models for prediction. This review is just a brief study of the vast quantity of literature in this field which is related to our project and it is divided into two main parts : -

- (i) the predictive theories and
- (ii) the experimental methods.

2.2 Predictive theories

As far as literature goes, the publications on the predictive theories started at around 1900. From then onwards, the aims of these predictions can be grouped into : -

- (i) to predict the distribution of the state of strain in the deformed specimen,
- (ii) to predict the distribution of the stresses,
- (iii) to find the average load or the energy required by the process,
- and (iv) the geometrical changes in the specimen.

In order to achieve these objectives, several basic assumptions have been made such as : -

- (i) the isotropy and incompressibility of the material,
- (ii) simple forming shapes are considered such as in plane strain or axisymmetrical conditions, Bauschinger effect is neglected,
- and (iii) a certain stress-strain relationship such as Lévy Mises flow rule.

The following is a brief review of the predictive theories used in analysing forging, both in simple upsetting and in closed die forming of simple shape.

2.2.1 The analytical method using the approximate theory

The essence of this method is that the whole forging ^{specimen} is viewed at different stages as composed of several components. Forces and stresses are calculated for each component and then added together to give the total forging load. For each component, an approximate theory is used such as the slab method.

This elementary approach in the approximate solution was proposed by Siebel (77) as early as 1930. On top of the assumptions made in the previous section, he added that the

- (i) concentric cylindrical surfaces in the material remain concentric cylindrical i.e., barrelling of the free surface is neglected and
- (ii) frictional force is governed by the Coulomb's friction law.

This approach was further improved by others such as Kobayashi (43,82), Lippmann (55) and Altan (2). Under the plane strain condition as given in fig.(2.1), by considering the equilibrium of the forces acting on the element and equating them, we have the following : -

$$\frac{\sigma_y}{\sigma_0} = \frac{2}{\sqrt{3}} \exp\left(\frac{2\mu}{h} \left(\frac{b}{2} - x\right)\right) \quad 2.1$$

where σ_y stress in the y-direction ;

σ_0 = yield stress;

μ the frictional coefficient;

b width of the slab.

Therefore, at any stage of deformation, the forging load is : -

$$\text{Load} = L = 2 w \int_0^{b/2} (-\sigma_y) dx$$

and
$$L = \sigma_0 \left(\frac{2h}{\sqrt{3}\mu}\right) \left(e^{\frac{\mu b}{h}} - 1\right) \text{ per unit length.}$$

where w is the length of the specimen.

Similarly, in axially symmetrical cases, the total forging load is

$$L = \frac{1}{2} \pi \sigma_0 \left(\frac{h}{\mu}\right)^2 \left(e^{\frac{2\mu}{h} r_d} - \frac{2\mu}{h} r_d - 1\right)$$

where r_d is the radius of the specimen.

Naturally, if the frictional condition changes to sticking condition, the load equation will be quite different.

These researchers (2,43,55,82,7) made use of these refined approximate solutions in analysing forging of axially symmetrical shapes. Such a forging specimen is assumed to have several components and each individual component is analysed by the approximate solution most suitable to it. In particular, Altan and his colleagues (2) applied this method to analyse the closed die forging problems and with the help of a digital computer, have calculated the forging load required and it is found to be in reasonably good agreement, Fig.(2.2) with the experimental results.

2.2.2 Finite element method

Most analytical methods on deformation have neglected the effects of both the elastic properties and the strain hardening of the material. For this type of elastic-plastic problem, an exact analytical solution can hardly be found, and it is usually solved by a numerical method such as ^{the} finite element method.

This method was developed as early as 1958 by Clough (11) in analysing elastic structures. At a later date, Yamada (89) used it and assumed that the material behaves as an elastic-plastic material and is linearly strain hardened. Calculation was carried out by a step-by-step incremental method through elastic, partially plastic, and fully plastic ranges.

The finite element approach is basically governed by three sets of relationships. These are : -

(i) the stress equilibrium condition

$$\sigma + T = 0$$

(ii) stress strain relationship

$$\sigma = M \epsilon$$

(iii) strain displacement relationship

$$\epsilon = H u$$

where T is the traction forces

σ is the stress matrix

ϵ is the strain matrix

M is the strain stress relation matrix

H is the displacement gradient matrix

and these relationships together can be formulated according to the variational principle.

Nagamatsu, Murota and Jimma (62) followed Yamada's lead and applied the above approach to solve both the cylindrical and plane strain compression problems. Half of the body is divided into 288 elements and by analysing them step by step, plastic zones development, loading curve, and stress strain distribution can all be computed.

Lee (52,53) made use of the same incremental method and a large digital computer, and computed a contour map of the deformed specimen as in fig. (2.3).

2.2.3 Slip line field method

This method is one of the most commonly used theories in deformation analysis of metal under plane strain conditions. The theory originated in Hencky's and Geiringer's papers, (23,20) and was improved by Hill (25).

Basically, the theory is restricted by the following assumptions : -

- (i) the metal is perfectly plastic and isotropic
- and (ii) the deformation is under plane strain conditions.

Accordingly, if the material is compressed in the plane strain condition, the deformation will consist of pure shear only. Also the hydrostatic pressure P and the shear stress K which is a constant are included.

Therefore, the characteristic of the differential equation of the stress equation and of the velocity equation should coincide. There are two orthogonal characteristic directions at any point in the plastic field, and they coincide with the directions of the maximum and minimum shear stress and strain rate $\dot{\epsilon}$ and are called the α and β lines. The equation governing the variation of P along the line is, according to Hencky (23).

$$P + 2 K \phi = \text{constant along the } \alpha \text{ lines}$$

$$P - 2 K \phi = \text{constant along the } \beta \text{ lines}$$

where K is the shear stress,

P is the hydrostatic pressure,

ϕ is the anticlockwise system of orientation of the slip line with respect to a fixed space frame.

The set of equations governing the velocity field proposed by Geiringer (20) is

$$du - v d\phi = 0 \text{ along } \alpha \text{ line}$$

$$dv + u d\phi = 0 \text{ along } \beta \text{ line}$$

i.e. the rate of stretching along any slip line is nil.

where u is the velocity in the α direction.

v is the velocity in the β direction.

With the known boundary condition and the assumed yield criterion, the construction of slip line field can be achieved. In any slip line field solution, a complete solution is one which must satisfy both

- (1) the kinematically admissible velocity field and,
- (2) the statically admissible stress field.

But in most cases, only the partial solution is obtainable and they are called bounding theories.

Johnson (37,38), Thomsen, Shabaik (82,72), Green (21) and Alexander (1) have all developed their own slip line field solution for the simple upsetting process under various conditions (fig.2.4). One author (15) has even developed a complete computer program to calculate the solution by this method but his prediction of average load and stress distribution is not quite accurate.

2.2.4 Extremum or Bounding theorem

A bounding solution proposed by Hill (25) is a partial solution of the slip line field and is an overestimate or an underestimate of the load actually required to cause plastic flow. The aim of these methods is to replace the laborious way of constructing the slip line field net, by some assumed boundary lines thus permitting a quicker way to compute the average forging load.

A. Lower bound method

In a lower bound solution in Kobayashi (44), ^{and Avitzur} Johnson (37,38,4), it is stated that lower bound is an under-estimate of the load required to cause metal flow and can be calculated from an admissible stress field σ^* which satisfies the equilibrium equation, stress boundary conditions and the yield criteria. The surface traction force T over the surface S with the velocity v and the product Tv will give the rate of work on the surface, with the assumed stress field inside the body. The rate of work for the actual equilibrium stress field σ is

$$\dot{E} = \int_S \text{tr} (Tv) dS = \int_V \text{tr} (\sigma d\dot{\epsilon}) dV$$

where $\text{tr}(\)$ is a trace of

and the rate of work for any other statically admissible stress field σ^*

$$\int_S \text{tr} (T^* v) dS = \int_V \text{tr} (\sigma^* d\dot{\epsilon}) dV$$

The lower bound theorem states that

$$\int_S \text{tr} ((T - T^*) v) dS = \int_V \text{tr} ((\sigma - \sigma^*) d\dot{\epsilon}) dV \geq 0$$

In other words, when a body is yielding and is undergoing small incremental displacement, the increment of work done by the actual force on S is greater than or equal to, that done by the force of any other statically admissible stress field.

B. Upper bound method

Again Johnson, Kudo and others (37,38,45,46,4,5,) have taken this concept of assuming a kinematically admissible velocity field to calculate the average forming load. The essence of the over-estimation of load which

is called the upper bound solution, is that, if a velocity field can be found as \mathbf{v} , the rate of work due to the over-estimated load, exceeds the rate of internal energy dissipation. Therefore, the rate of energy dissipated will be : -

$$\dot{E} = L_v \leq \int_V \text{tr} (\boldsymbol{\sigma} \dot{\boldsymbol{\epsilon}}) dV + \int_S \text{tr} (K \mathbf{v}) dS$$

The first term on the right hand side expresses ^{the} power required for internal deformation over the volume of the body V and the second term includes the shear power over the surface of velocity discontinuity or boundary surfaces. The actual power consumed by the external body is never greater than the computed \dot{E} and that is why it is called the upper bound theorem for the assumed kinematical velocity field.

Johnson and Kudo, Kobayashi and Thomsen and Avitzur (38,44,45,4) have all applied this method to calculate the average load required for deforming a plane strain specimen and an axisymmetrical one (fig. 2.5).

2.3.1 Experimental methods in the analysis of deformation processes

Experimental methods applied to the analysis of deformation processes began way back in the early days of this century. Marks and flow lines were observed in the specimen so that the deformation pattern or flow lines can be qualitatively described (8,61,51). Later on, grid marks or photo-grid patterns were put on the surface of the metal and distortion was measured as a means of quantifying the deformation. These approaches are significantly different from the predictive theories in

that they are not trying to predict but to quantify the degree of deformation evaluated by different experimental techniques on various basis of strain measures. These methods are just **used** to find out the distribution of stresses based on an assumed stress strain relationship and to solve the problems of failure in deformation.

2.3.2 The behaviour of metal on the surface of the specimen under compression

These researchers (47,54,41,81) tend to neglect the non-uniform distribution inside the body of the specimen and concentrate on the flow of metal on the circumferential surfaces. Strain measurements are carried out on these surfaces to find the state of strain and stress under the assumptions they made.

Kudo and his colleagues (47,48) were the first to apply this technique to analyse the forgeability of metal. Indentation marks were made on the circumferential surface of the cylindrical specimen along the equator and used to compute the circumferential and tangential strain values. The variation of these two strains during the process were plotted till microscopic cracks appeared as in (fig. 2.6). By adopting the Lévy-Mises flow rule, stresses were calculated. This method was repeated with different lubricants and shapes of dies and followed by an analysis of various fracture criteria applicable in the forging process.

Thomason (81) also followed Kudo's approach but he included the consideration of anisotropy in the calculation of stress. In the experimental

method, he used a very ductile metal, aluminium, as an analogue model material to steel so that the complete history of deformation could be traced so as to eliminate inaccuracy in measuring the fracturing strain of a steel specimen. The inclusion of anisotropy in the calculation of stress shows significant differences from Kudo's results.

Kobayashi, Lee and Kuhn (41,42,50,54) closely extended this idea by refining the technique and included a few more interface conditions and metals in consideration. Furthermore, fracture criteria proposed by Cockcroft and Latham (12,13) were used in a failure equation for the definition of the forgeability of metal.

Hsü and Young (35) developed an ingenious idea by using a properly adjusted quantity of lubricant to eliminate the frictional effect on the bulk material so that an almost ideal uniaxial compression was achieved. In fact, this method has rectified one main defect in this kind of semi-experimental analytical method because the deformation is homogeneous throughout the whole bulk of the metal.

All these workers have tried to analyse the deformation patterns and their final collapsing criteria. But, most of them either neglected ^{the} internal distribution of deformation or, by perfecting the experiments into nearly those of homogeneous deformation, succeeded in theorising only the ideal deformation rather than the actual one.

2.3.3 Visioplasticity

As the name of this method implies, it is a semi-analytical method in which the velocity field is computed from actual data for the deformed specimen. This is essentially an experimental means to find out the flow of the metal not just on the surface but in the cross-section of the specimen under certain restrictions such as ^{the} plane strain condition. Originally, this method was applied to analysing the metal flow in the steady state condition as extrusion and rolling (59,73). Shabaik and his colleagues (73,72,74) perfected the system so that in the non-steady state such as forging, the particle paths in the cross-section are measured by means of a scanning machine and are used in a computer program they developed to compute the velocity. From the definition of strain rate, the components of the strain rate matrix will be : -

$$\dot{\epsilon}_x = \frac{\partial u}{\partial x} \quad \dot{\epsilon}_y = \frac{\partial v}{\partial y} \quad \dot{\gamma}_{xy} = \frac{\partial u}{\partial y} + \frac{\partial v}{\partial x}$$

and the effective strain rate is equal to : -

$$\dot{\bar{\epsilon}} = \frac{2}{3} \left(3\dot{\epsilon}_x^2 + \frac{3}{4}\dot{\gamma}_{xy}^2 \right)^{\frac{1}{2}}$$

Consequently, the total effective strain $\bar{\epsilon}$ can be derived from integrating the $\dot{\bar{\epsilon}}$ along the flow lines with respect to time

$$\bar{\epsilon} = \int_0^t \dot{\bar{\epsilon}} dt$$

By assuming that the material behaves in a perfectly plastic manner and follows the Lévy-Mises flow rule, the state of stress at various instances can be derived and its distribution is given in (fig.2.7) after computation. This is an effective way to analyse the detailed mechanism during deformation

since it is based on an actual flow field of the metal, and the final stress results are found to be in close agreement with other experimental results. One defect in that research is that the state of strain at various stages and its history are omitted. Although the effective strain gives an index of deformation yet, it does not show the history of that deformation.

2.3.4 The welded tube method.

In order to visualise the distribution of deformation within the body of the specimen, Bühler and Bobbert (9) and others (63) had proposed a direct method in which the cylindrical specimen was prepared by brazing 10m.m. thick steel discs together. The deformed specimen was cut and etched so that the sharp brazed lines can be measured. Local compression ratio can thus be calculated to show the degree of deformation. Some non-homogeneous contour maps are shown in (fig.2.8). Furthermore, they analysed the pattern of deformation and came up with a distribution curve of local deformation (fig.2.9). One conclusion from their work is that the lubricants have no significant effect on the deformation patterns.

This kind of measure of distribution of deformation is rather crude because the plate is too thick to represent a minute area and the deformation measure does not indicate how the element is being deformed. The brazing would also affect the real performance of the solid metal.

2.4 Concluding Remarks

The above brief summary covers only a part^{of} a vast amount of work done in the field of deformation by upsetting. It can be seen that most of the recent work done in this field revolves around the predictive theories; mostly, by refining the theory in terms of more realistic velocity fields etc., so as to calculate the average load required. Computer programs have also been developed to help to calculate the work load of the various approaches. Comparative curves in (fig.2.10) have predicted^{the} non-dimensional load of the various theories. Table 2.1 is an abstract of the various authors' predictions and assumptions. An experimental or semi-analytical method such as viscoplasticity is another way to eliminate this kind of inaccurate assumption as the flow fields are those measured by experimental techniques. But this kind of semi-analytical method is still defective in that some essential aspects are not included, such as the state of deformation, the principal directions, the degree of rigid body rotation of the particle, its final alignment directions and their total deformation. These authors' achievements and methods are summarised in table 2.2. Fig.(2.11) shows the variation of the principal strains at the equatorial free surface of a cylindrical specimen with unlubricated die by the various researchers. These different theories and experimental results are presented on a triangular co-ordinate system for comparison. The triangular co-ordinate system developed by Professor Hsü (30) is used to record the variation of the three principal strains of a deformation on the same graph. On it, a number called the characteristic index for strain, η , varying from 0 to 12, is used because it is analogous to the number on the clock face and all the odd numbers represent pure shear. This system has been shown to be very useful in clarifying the difference between the lubricated and those unlubricated paths.

Table 2.1

Predictive Theories Authors	Objections	Assumptions	Results
<u>A. Slip line field</u>			
Hill	(i) To find a complete solution	(i) plane strain condition	results are usually compared to the other methods only
Johnson	(ii) To determine the average load.	(ii) ideal or sticking friction	
Alexander	1	(iii) perfect plastic material	
Green	21 (1951)	(iv) isotropic and incompressible material	
		(v) co-axial strain paths	
		(vi) small strain measure	
Shabaik	(i) To determine the geometrical changes in the bulge profile. (ii) To find the load required.	Assumptions the same as above	The correlation between the calculated measured results are quite good.
<u>B. Bounding theorem</u>			
Kudo and Johnson	(i) To find the average dimensionless load required.	(i) plane strain condition and symmetrical problems	Correlation with other methods and experimental results are good.
Kobayashi and Thomsen	44 (1965)	(ii) perfect plastic, isotropic and incompressible material (iii) co-axial paths	

Table 2.1 (continued)

Predictive Theories C. Finite Element.	Authors	Objections	Assumptions	Results
C.H. Lee and Kobayashi Nagamattsu, Murota and Jimma	52, 53 (1970, 1971)	(i) find the development of plastic zones (ii) the load required (iii) the ϵ distribution (iv) the σ distribution	(i) Elastic-plastic material (ii) Plane strain and axisymmetrical (iii) isotropic and incompressible material (iv) von-Mises yield criterion (v) sticking frictional condition	Computer must be used in these calculations, results are comparable with other predictive theories.
<u>D. Analytical Methods.</u>				
Altan	2 (1968)	(i) To determine the load required.	(i) either plane strain or axisymmetrical conditions	Computer programs have been developed for the analysis of complex forgings. Results calculated are comparable to the actual experiments.
Biswas	7 (1972)	(ii) The variation in geometrical shape of the bulge profile	(ii) perfectly plastic, isotropic and incompressible material (iii) assumed a certain linear stress distribution (iv) follow a stress strain relationship	
Kobayashi	43 (1958)			

Authors	Objective	Assumptions	Strain Measurement	Notes and Comments
Kudo and Aoi 47,48 (1967,1968)	<ol style="list-style-type: none"> 1. To find the strain distribution. 2. To find the stress distribution. 3. The fracture criterion. 	<ol style="list-style-type: none"> 1. Isotropic and incompressible material. 2. According to Lévy-Mises flow rule. 3. Cockcroft fracture criterion. 	<p>Marks on the surface along the equator.</p> <ol style="list-style-type: none"> 1. Cracks by eye examine. 2. Coaxial strain path only. 	
Thomason 81 (1968)	<ol style="list-style-type: none"> 1. strain distribution. 2. stress distribution. 3. The effect of anisotropy. 	<ol style="list-style-type: none"> 1. Anisotropic material. 2. Follows Lévy-Mises flow rule. 	<p>Two grid marks are made along the equator.</p> <ol style="list-style-type: none"> 1. Anisotropy does affect the stress level. 2. Coaxial strain path. 	
Lee and Kuhn 50,54 (1973)	<ol style="list-style-type: none"> 1. To find the strain distribution. 2. To find the stress distribution. 3. Fracture of the specimen. 	<ol style="list-style-type: none"> 1. Isotropic and incompressible material. 2. Follows Lévy-Mises flow rule. 3. Use Cockcroft fracture criterion. 	<p>Two sets of grid lines along the equator of 0.12 in. apart.</p> <ol style="list-style-type: none"> 1. Cracks observed by eyes. 2. Coaxial strain path. 	

Table 2.2 (continued)

Authors	Objective	Assumptions	Strain Measurement	Notes and Comments
Hsü and Young 35 (1967)	<ol style="list-style-type: none"> To find the strain distribution. To simulate uniaxial compression condition. To find the stress strain curve. 	<ol style="list-style-type: none"> Isotropic and incompressible material. St. Venant flow rule. 	Grid lines mark on the surface in a helix shape.	<ol style="list-style-type: none"> Bollard shape specimens was found. Coaxial strain path.
Kobayashi 41,42 (1970)	<ol style="list-style-type: none"> To find the strain distribution. To find the stress distribution. To apply the fracture criterion. 	<ol style="list-style-type: none"> Isotropic and incompressible material. Follows Lévy-Mises flow rule. Cockcroft fracture criterion. 	Use grid marks on the equatorial face.	<ol style="list-style-type: none"> Coaxial strain path.
A.H. Shabaik 72,73,74 (1970,1972)	<ol style="list-style-type: none"> To find the strain distribution. To find the stress distribution. Computer calculation of effective strain. 	<ol style="list-style-type: none"> Follow Lévy-Mises flow rule. Isotropic and incompressible material. 	Use 0.040 inch grid mark.	

Table 2.2 (continued)

Authors	Objective	Assumptions	Strain Measurement	Notes and Comments
M. Al-Chalabi and others 10 (1974)	<ol style="list-style-type: none"> To find the strain distribution. To find the stress distribution. Theoretical and experimental comparison. To find the frictional effect. 	<ol style="list-style-type: none"> Isotropic, incompressible and perfect plastic material. Small deformation analysis. Coaxial strain path. 	Measured with strain gauges.	Good correlation between experimental theoretical results.
Bühler 9 (1966)	<ol style="list-style-type: none"> To find the strain distribution. The distribution contour map. 	<ol style="list-style-type: none"> Use reduction in thickness of the sandwiched disc as strain measure. 	By measuring the variation in the thickness of the sandwiched discs	Contour maps with distribution of local thickness strain. Deformation is non-symmetrical.

PART A

Theoretical Derivation

of Large

Deformation Analysis

CHAPTER THREE

Deformation, Strain and Rate

of

Deformation -- the Analysis of

3.1 Introduction

Deformation is a continuous process and the progress of it can be evaluated with respect to time or other variables. The trace of the progress of deformation from one stage to the other of an element in a deformed specimen is called the strain history or strain path. If the step taken is finite, then the state of strain is called finite strain whereas if the step taken is vanishingly small, then this state is called incremental strain. The deformation of an element in a specimen is the culmination of all the incremental deformations or incremental strains along the path or history and the total deformation of the deformed specimen is the sum of all the individual deformations of the specimen. The strain rate is the ratio between the incremental strain and the increment itself.

3.1.1 Definition of conventional engineering strain and natural strain in one dimension.

The conventional engineering strain e is defined as the ratio of the extended (or compressed) length of the element and its original length. As in (fig. 3.1), the engineering strain is equal to

$$e = \frac{L - L_0}{L_0} \quad 3.1$$

For large strains, this conventional strain cannot cope with the real deformation. Therefore, in large deformations, the natural strain ϵ is used which is :-

$$\epsilon = \int_{L_0}^L \frac{dl}{L} = \ln \frac{L}{L_0} \quad 3.2$$

3.2 General consideration of deformation analysis

3.2.1 Deformation in terms of the affine transformation of a point and line element.

Consider a particle P in a three dimensional space displaced from the initial undeformed position P (X₁, X₂, X₃) to a terminal position P'(x₁, x₂, x₃) as in (fig.3.2). The deformation is represented by the ordinate transformation of this system i.e.,

$$x_1 = f_{X_1}(X_1, X_2, X_3) \quad x_2 = f_{X_2}(X_1, X_2, X_3) \quad x_3 = f_{X_3}(X_1, X_2, X_3)$$

If the motion is continuous and differentiable, the displacement vector **u** will also be a function of the undeformed (X₁, X₂, X₃) co-ordinates, or vice versa.

Hence, we can find out that the position of the deformed particle P'(x₁, x₂, x₃) which has undergone displacement **u** is

$$\begin{aligned} x_1 &= X_1 + u_{X_1}(X_1, X_2, X_3) \\ x_2 &= X_2 + u_{X_2}(X_1, X_2, X_3) \\ x_3 &= X_3 + u_{X_3}(X_1, X_2, X_3) \end{aligned} \tag{3.3a}$$

or equal to

$$\begin{aligned} x_1 &= x_1(X_1, X_2, X_3) \\ x_2 &= x_2(X_1, X_2, X_3) \\ x_3 &= x_3(X_1, X_2, X_3) \end{aligned} \tag{3.3b}$$

This is the general transformation of points.

When the particle P is displaced, a very close point Q (X₁+δX₁, X₂ +δX₂, X₃ +δX₃) is also displaced to its terminal position Q'(x₁ +δx₁, x₂ +δx₂, x₃ +δx₃) and is related to its initial position by **u**+d**u** as in (fig.3.2).

$$\begin{aligned} dx_1 &= dX_1 + du_{x_1} (dX_1, dX_2, dX_3) \\ dx_2 &= dX_2 + du_{x_2} (dX_1, dX_2, dX_3) \\ dx_3 &= dX_3 + du_{x_3} (dX_1, dX_2, dX_3) \end{aligned} \quad 3.4a$$

or equation 3.4a equal to

$$\begin{aligned} dx_1 &= dx_1 (dX_1, dX_2, dX_3) \\ dx_2 &= dx_2 (dX_1, dX_2, dX_3) \\ dx_3 &= dx_3 (dX_1, dX_2, dX_3) \end{aligned} \quad 3.4b$$

When this small amount $d\mathbf{u}$ is projected onto this initial position (X_1, X_2, X_3) in terms of the first order of dX_1, dX_2, dX_3 by neglecting the higher orders, the relation will be equal to the total differentials of its components.

$$\begin{aligned} du_{x_1} &= \frac{\partial u_{x_1}}{\partial X_1} dX_1 + \frac{\partial u_{x_1}}{\partial X_2} dX_2 + \frac{\partial u_{x_1}}{\partial X_3} dX_3 \\ du_{x_2} &= \frac{\partial u_{x_2}}{\partial X_1} dX_1 + \frac{\partial u_{x_2}}{\partial X_2} dX_2 + \frac{\partial u_{x_2}}{\partial X_3} dX_3 \\ du_{x_3} &= \frac{\partial u_{x_3}}{\partial X_1} dX_1 + \frac{\partial u_{x_3}}{\partial X_2} dX_2 + \frac{\partial u_{x_3}}{\partial X_3} dX_3 \end{aligned} \quad 3.5$$

By combining equation 3.5 and equation 3.4a, we have the transformation equation.

$$\begin{aligned} dx_1 &= dX_1 + \frac{\partial u_{x_1}}{\partial X_1} dX_1 + \frac{\partial u_{x_1}}{\partial X_2} dX_2 + \frac{\partial u_{x_1}}{\partial X_3} dX_3 \\ dx_2 &= \frac{\partial u_{x_2}}{\partial X_1} dX_1 + dX_2 + \frac{\partial u_{x_2}}{\partial X_2} dX_2 + \frac{\partial u_{x_2}}{\partial X_3} dX_3 \\ dx_3 &= \frac{\partial u_{x_3}}{\partial X_1} dX_1 + \frac{\partial u_{x_3}}{\partial X_2} dX_2 + dX_3 + \frac{\partial u_{x_3}}{\partial X_3} dX_3 \end{aligned} \quad 3.6$$

Equation 3.6 expresses the transformation of a line element (dx_1, dx_2, dx_3) in terms of the original element (dX_1, dX_2, dX_3) .

3.2.2 Matrix algebra in deformation analysis and its displacement gradient and deformation gradient matrices

The application of matrix algebra in strain analysis has been well developed by Professor Hsü and others (29,30,32,57,17,18,60,34) and its advantages can be illustrated by using a linear equation to represent the equations in the last sections and equation (3.3a) becomes

$$\mathbf{x} = \mathbf{X} + \boldsymbol{\mu}(\mathbf{X}) \quad 3.7$$

and also equation (3.3b) becomes

$$\mathbf{x} = \mathbf{x}(\mathbf{X}) \quad 3.8a$$

or
$$\mathbf{x} = \frac{\partial \mathbf{x}}{\partial \mathbf{X}} \mathbf{X} \quad 3.8b$$

and from equation (3.4a)

$$d\mathbf{x} = d\mathbf{X} + d\boldsymbol{\mu}(d\mathbf{X}) \quad 3.9$$

$$d\mathbf{x} = d\mathbf{x}(d\mathbf{X}) \quad 3.10$$

where \mathbf{x} is a column matrix

\mathbf{X} is a column matrix defining the point P (X_1, X_2, X_3)

$\boldsymbol{\mu}$ displacement column matrix

When applied to the linear transformation equation such as equation (3.5), it becomes

$$d\boldsymbol{\mu} = \mathbf{H} d\mathbf{X} \quad 3.11$$

The matrix \mathbf{H} is called the displacement gradient matrix. Again, when matrix algebra is applied to equation (3.4b), it becomes

$$d\mathbf{x} = \mathbf{F} d\mathbf{X} \quad 3.12$$

The matrix \mathbf{F} is called the deformation gradient matrix which is equal to a unit matrix plus the displacement gradient matrix.

$$\mathbf{F} = \mathbf{I} + \mathbf{H} \quad 3.13a$$

and in component form is

$$\begin{vmatrix} \frac{\partial x_1}{\partial X_1} & \frac{\partial x_1}{\partial X_2} & \frac{\partial x_1}{\partial X_3} \\ \frac{\partial x_2}{\partial X_1} & \frac{\partial x_2}{\partial X_2} & \frac{\partial x_2}{\partial X_3} \\ \frac{\partial x_3}{\partial X_1} & \frac{\partial x_3}{\partial X_2} & \frac{\partial x_3}{\partial X_3} \end{vmatrix} = \begin{vmatrix} 1 + \frac{\partial u_1}{\partial X_1} & \frac{\partial u_1}{\partial X_2} & \frac{\partial u_1}{\partial X_3} \\ \frac{\partial u_2}{\partial X_1} & 1 + \frac{\partial u_2}{\partial X_2} & \frac{\partial u_2}{\partial X_3} \\ \frac{\partial u_3}{\partial X_1} & \frac{\partial u_3}{\partial X_2} & 1 + \frac{\partial u_3}{\partial X_3} \end{vmatrix} \quad 3.13b$$

3.2.3 Various measures of finite deformation and their relationships

The change in length and in relative direction occasioned by deformation is called, roughly, strain.

As a result of the line element transformation during a deformation described in the previous section, the square of the length of the newly deformed element $|d\mathbf{x}|^2$ or ds^2 may define the magnitude of the deformed element in the body.

$$ds^2 = d\mathbf{x} \cdot d\mathbf{x} \quad 3.14a$$

The magnitude of the same element before deformation dS , will be :-

$$dS^2 = d\mathbf{X} \cdot d\mathbf{X} \quad 3.14b$$

A. Lagrangian and Eulerian Strain matrices

The change in the square of lengths can be found by substituting equation 3.12 into equations 3.14a and b., and they become

$$ds^2 - dS^2 = 2 d\mathbf{X} \mathbf{E} d\mathbf{X} \quad 3.15a$$

Here the matrix \mathbf{E} is called the Lagrangian strain matrix and similarly, the reciprocal representation will be

$$ds^2 - dS^2 = 2 d\mathbf{x} \mathbf{e} d\mathbf{x} \quad 3.15b$$

The matrix \mathbf{e} is called the Eulerian strain matrix. By combining equations 3.14a and b and 3.12, it can be seen that the strain matrices can be expressed in terms of the deformation gradient matrix.

$$2 \mathbf{E} = \mathbf{F}^T \mathbf{F} - \mathbf{I} \quad 3.16a$$

$$2 \mathbf{e} = \mathbf{I} - (\mathbf{F}^{-1})^T \mathbf{F}^{-1} \quad 3.16b$$

B. Cauchy and Green deformation matrices

There are, in the theory of plasticity, also two other measures of strain due to the creation of Cauchy and Green. They found that any changes in length and direction can be derived from just the squared element of length.

$$ds^2 = d\mathbf{X} \mathbf{C} d\mathbf{X} \quad 3.17a$$

The matrix \mathbf{C} is the Green's deformation matrix.

$$dS^2 = d\mathbf{x} \mathbf{c}^{-1} d\mathbf{x} \quad 3.17b$$

\mathbf{c} is the Cauchy's deformation matrix.

In terms of the deformation gradient matrix, the Green and Cauchy matrices become

$$\mathbf{C} = \mathbf{F}^T \mathbf{F} \quad 3.18a$$

$$\mathbf{c}^{-1} = \mathbf{F}^{-1T} \mathbf{F}^{-1} \quad 3.18b$$

C. Hencky's logarithmic strain matrix

There is another means to measure the deformation which was proposed by

Hencky called the logarithmic strain (84). He saw the advantages of taking the natural logarithm of the elongation factor in linear measures. So, he suggested to take the logarithm of the deformed squared length of the line element.

$$\ln (ds)^2 = d \mathbf{X} \mathbf{B} d \mathbf{X}$$

$$2 \ln (ds) = d \mathbf{X} \mathbf{B} d \mathbf{X}$$

and
$$\mathbf{B} = \frac{1}{2} \ln (\mathbf{F}^T \mathbf{F}) \quad 3.19$$

where \mathbf{B} is the Hencky's logarithmic strain matrix.

This measure of deformation is not popular because it is inconvenient to be used in the mathematical analysis of deformation.

D. Other measures.

There are a few more measures of deformation such as Murnaghan's who suggested the stretch matrix \mathbf{U} as the measure of deformation.

$$\mathbf{U} = \mathbf{C}^{\frac{1}{2}} \quad 3.20a$$

and
$$\mathbf{V} = \mathbf{c}^{\frac{1}{2}} \quad 3.20b$$

The advantage of using this measure is that its principal values are the principal stretches of the deformation but, the weakness is that it is rather difficult to expand in term of the displacement gradient matrix.

E. The relationship of various strain measures

By substituting equation 3.16 into equation 3.18, we have

$$2 \mathbf{E} = \mathbf{C} - \mathbf{I}$$

and similarly

$$2 \mathbf{e} = \mathbf{I} - \mathbf{e}^{-1} \quad 3.21$$

If equation 3.16 is substituted into Hencky's strain equation

$$2 \mathbf{B} = \ln \mathbf{C} = \ln (\mathbf{I} + 2 \mathbf{E}) \quad 3.22$$

Deformation measures by Cauchy, Green, Lagrangy etc., strain matrices are either expressed in the initial position or the final position of their principal axes which is inconvenient to use in the practical analysis. Therefore, a measure described in the next section will be always applied in all the analysis in this thesis.

3.2.4 Decomposition of the deformation gradient matrix

For large finite deformations, the pure strain and rotation components have a multiplicative relationship instead of the additive properties for small strain.

It is stated in the polar decomposition theorem (85,86,64) that any invertible linear transformation as \mathbf{F} has two unique multiplicatives.

$$\mathbf{F} = \mathbf{R}\mathbf{U} = \mathbf{V}\mathbf{R} \quad 3.23$$

in which \mathbf{R} is orthogonal and \mathbf{U} and \mathbf{V} are symmetric and positive definite matrices.

Therefore, when this theorem is applied to the linear transformation in a deformation, the deformation gradient matrix \mathbf{F} can then be decomposed accordingly. \mathbf{R} will be the rigid body rotation matrix and \mathbf{U} is the right stretch matrix or \mathbf{V} is the left stretch matrix of the deformation and they have the following properties : -

$$\mathbf{U}^2 = \mathbf{C} = \mathbf{F}\mathbf{F}^T \quad 3.24a$$

$$\mathbf{V}^2 = \mathbf{c} = \mathbf{F}\mathbf{F}^T = \mathbf{R}\mathbf{C}\mathbf{R}^T \quad 3.24b$$

As stated in section 3.2.3, these matrices \mathbf{U} or \mathbf{V} can be used as a measure of deformation but, the only weakness is that their components are irregular functions of the deformation gradient.

3.3 Deformation in two dimensions

In most of the manufacturing processes, such as rolling, drawing, forming and forging etc., the deformations are so large that superposition of strain, which is a routine in elastic analysis, cannot be applied. Therefore, this section is confined to the study of the large finite deformation in the simplified two dimensional cases such as axisymmetrical extrusion and plane strain forging.

The analysis of large deformation in two dimensions by matrix algebra was developed by Professor Hsü (29,30,32). The following sections are a condensed summary of his works.

3.3.1 The analysis

In large deformation, a square configuration in the undeformed state is deformed into a parallelogram as shown in (fig,3.3). In mathematical terms, this homogeneous deformation can be represented by the affine transformation of the configuration. The transformation equation is

$$\mathbf{x} = \mathbf{F}\mathbf{X} \quad 3.8b$$

and in terms of components

$$\begin{vmatrix} x_1 \\ x_2 \end{vmatrix} = \begin{vmatrix} f_{11} & f_{12} \\ f_{21} & f_{22} \end{vmatrix} \begin{vmatrix} X_1 \\ X_2 \end{vmatrix} \quad 3.8c$$

According to the axiom of continuity and permanence assumed in the matter (85,86), the deformation and its inverse are single valued and continuously differentiable. Furthermore, no region of the finite volume is deformed into zero or infinite volume. For this reason, it is necessary that the determinant of the the deformation gradient does not vanish.

$$\det \mathbf{F} > 0 \quad 3.25$$

In a two-dimensional plane strain deformation, the matrix \mathbf{F} is a 2 by 2 matrix and if the area of the configuration is assumed to be constant, the determinant of \mathbf{F} must always be equal to unity.

$$\det \mathbf{F} = 1 \quad 3.26$$

3.3.2 Some typical examples of deformation modes represented by matrices

A. Aligned pure shear

In this aligned pure shear, the principal axis of the deformation process coincides with the principal axis of the original undeformed configuration as in (fig.3.4). This affine transformation can be represented in the transformation equation

$$\mathbf{x} = \mathbf{F} \mathbf{X} \quad 3.8b$$

and in this case, the deformation gradient matrix \mathbf{F} will be in terms of components

$$\mathbf{F} = \begin{vmatrix} \lambda_0 & 0 \\ 0 & \frac{1}{\lambda_0} \end{vmatrix}$$

where λ_0 is the principal stretch of the deformation.

The natural strain in pure shear will be the logarithm of the principal stretches and therefore

$$\mathbf{F} = \begin{vmatrix} \lambda_0 & 0 \\ 0 & \frac{1}{\lambda_0} \end{vmatrix} = \begin{vmatrix} e^{\epsilon_0} & 0 \\ 0 & e^{-\epsilon_0} \end{vmatrix} \quad 3.27$$

where ϵ_0 is the principal pure shear strain in an aligned pure shear process and it is equal to

$$\epsilon_0 = \log_e \lambda_0$$

B. Pure rigid body rotation

Pure rigid body rotation is a special type of transformation without any deformation involved. In the physical sense, the configuration before the transformation will not be changed by this operation as in fig.3.5. The transformation equation representing this operation is again

$$\mathbf{x} = \mathbf{F}\mathbf{X} \quad 3.8b$$

and in this case, the components of the transformation matrix are

$$\mathbf{F} = \begin{vmatrix} \cos \omega & -\sin \omega \\ \sin \omega & \cos \omega \end{vmatrix} \quad 3.28$$

where ω is the angle through which the body is rigidly rotated during the operation and positive when it is rotating anti-clockwise.

3.3.3 Principal values and directions of a stretch (strain) matrix \mathbf{U}

It was stated in Cauchy's fundamental theorem (16,85) that at any point

\mathbf{X} , there exist a direction in which the stretch is not less than any other direction, ^{and} a second direction, perpendicular to it, in which the stretch is not greater than in any other direction. These stretches are called the principal stretches and their directions are the principal directions. The principal stretches are the most important quantities connected with the strain.

In mathematical terms, any real, symmetric and non-singular matrix will have real and distinct roots called eigenvalues and their corresponding directions are represented by what are called eigenvectors. Whereas in mechanics, the eigenvalues of a stretch (strain) matrix are the principal stretches λ_o (or strains ϵ_o) and the eigenvectors are along the principal directions (the angle θ). This transformation can be carried out by the matrix algebra called diagonalization, i.e., to transform a real and symmetric matrix into a diagonal matrix in which the diagonal components are the principal components. From the matrix algebra as shown in appendix I, the stretch matrix can be split into: -

$$U = \Theta \epsilon_o \Theta^{-1} \quad 3.29$$

where Θ is the rotational matrix with the principal vector at angle θ of the stretch matrix U .

In terms of components, equation 3.29 becomes

$$\begin{vmatrix} U_{11} & U_{12} \\ U_{21} & U_{22} \end{vmatrix} = \begin{vmatrix} \cos \theta & -\sin \theta \\ \sin \theta & \cos \theta \end{vmatrix} \begin{vmatrix} e^{\epsilon_o} & 0 \\ 0 & e^{-\epsilon_o} \end{vmatrix} \begin{vmatrix} \cos \theta & \sin \theta \\ -\sin \theta & \cos \theta \end{vmatrix} \quad 3.30$$

and by multiplying the right hand side of equation 3.30, it becomes

$$\begin{vmatrix} U_{11} & U_{12} \\ U_{21} & U_{22} \end{vmatrix} = \begin{vmatrix} \cosh \epsilon_o + \sinh \epsilon_o \cos 2\theta & \sinh \epsilon_o \sin 2\theta \\ \sinh \epsilon_o \sin 2\theta & \cosh \epsilon_o - \sinh \epsilon_o \cos 2\theta \end{vmatrix} \quad 3.31$$

In equation 3.30, we can see the middle matrix in the right hand side of the equation is the same matrix which in section 3.3.2 describes an aligned pure shear deformation. Therefore, we can clearly see that the matrix U represents a nonaligned pure shear deformation with the principal strain as ϵ_o and at a principal direction θ to the x-axis in fig.3.6.

Section 3.2.4 will show that the deformation gradient matrix \mathbf{F} can be decomposed into a rotation matrix and a stretch matrix. When this decomposition is combined with the diagonalization of the stretch matrix, we can find that any deformation will consist of

$$\mathbf{F} = \mathbf{R} \boldsymbol{\Theta} \boldsymbol{\epsilon}_0 \boldsymbol{\Theta}^{-1} \quad 3.32a$$

and in terms of components

$$\begin{vmatrix} f_{11} & f_{12} \\ f_{21} & f_{22} \end{vmatrix} = \begin{vmatrix} \cos \omega & -\sin \omega \\ \sin \omega & \cos \omega \end{vmatrix} \begin{vmatrix} \cos \theta & -\sin \theta \\ \sin \theta & \cos \theta \end{vmatrix} \begin{vmatrix} e^{\epsilon_0} & 0 \\ 0 & e^{-\epsilon_0} \end{vmatrix} \begin{vmatrix} \cos \theta & \sin \theta \\ -\sin \theta & \cos \theta \end{vmatrix} \quad 3.32b$$

or

$$= \begin{vmatrix} \cos \omega & -\sin \omega \\ \sin \omega & \cos \omega \end{vmatrix} \begin{vmatrix} \cosh \epsilon_0 + \sinh \epsilon_0 \cos 2\theta & \sinh \epsilon_0 \sin 2\theta \\ \sinh \epsilon_0 \sin 2\theta & \cosh \epsilon_0 - \sinh \epsilon_0 \cos 2\theta \end{vmatrix}$$

3.3.4 Practical analysis of a deformation.

At the end of the last section, we can see that any deformation gradient matrix which describes the deformation can be decomposed into a series of matrices on the right hand side. In the physical sense, the deformation of a configuration consists of : -

- (i) A rotation of the undeformed configuration in the principal direction at angle θ .
- (ii) The deformation is followed by a pure shear of the principal strain ϵ_0 .
- (iii) A reverse rotation of the deformed configuration through an angle θ i.e., the first angle.
- (iv) The deformation lastly followed by a rigid body rotation of the deformed configuration to its final position through a further angle ω .

The above sequences are shown in (fig.3.7) and the decomposition in equation (3.32b) is

$$\begin{vmatrix} f_{11} & f_{12} \\ f_{21} & f_{22} \end{vmatrix} = \begin{vmatrix} \cos \omega & -\sin \omega \\ \sin \omega & \cos \omega \end{vmatrix} \begin{vmatrix} \cosh \epsilon_0 + \sinh \epsilon_0 \cos 2\theta & \sinh \epsilon_0 \sin 2\theta \\ \sinh \epsilon_0 \sin 2\theta & \cosh \epsilon_0 - \sinh \epsilon_0 \cos 2\theta \end{vmatrix} \quad 3.32b$$

By comparing the components of the left hand side with the product in the right hand side, we can derive the three parameters ω , θ and ϵ_0 in terms of \mathbf{F} .

These are : -

$$\tan \omega = \frac{f_{12} - f_{21}}{f_{11} + f_{22}} \quad 3.33a$$

$$\tan 2\theta = \frac{2(f_{11}f_{12} + f_{21}f_{22})}{f_{11}^2 + f_{21}^2 - f_{12}^2 - f_{22}^2} \quad 3.33b$$

and
$$\cosh \epsilon_0 = \frac{\sqrt{(f_{11}^2 + f_{12}f_{21} + 1)^2 + (f_{21} - f_{12})^2 f_{11}^2}}{2 f_{11}} \quad 3.33c$$

If the co-ordinates of the deformed configuration are known, then the three parameters which define a deformation can be calculated by substituting the co-ordinates into the above equations.

3.4 Velocity field and rate of deformation

Basic principles.

3.4.1 Motion of a particle — velocity

The motion of a particle is defined relative to the same co-ordinate system by : -

$$\mathbf{x} = \mathbf{x}(\mathbf{X}, t) \quad 3.34$$

which means that $\mathbf{x} = \mathbf{x}(\mathbf{X}, t)$ is the position occupied at typical

time t by the particle whose original position is \mathbf{X} at time t_0 . Therefore, the motion in equation (3.34), chronicles the place \mathbf{x} occupied by the particle \mathbf{X} in the course of time.

If the motion is continuous, the axiom of continuity states that it possesses continuous partial derivatives. The velocity which is the rate of change of position of a given particle will be : -

$$\dot{\mathbf{x}} = \dot{\mathbf{x}}(\mathbf{X}, t)$$

This means that this velocity is a function of time for a given particle \mathbf{X} . But, we use velocity in terms of time at the current position \mathbf{x} . Therefore, the velocity

$$\mathbf{v} = \frac{\partial \mathbf{x}}{\partial t} = \frac{\partial}{\partial t} \mathbf{x}(\mathbf{x}, t) \quad 3.35a$$

and in a matrix transformation equation, the derivative of the function is called the velocity gradient \mathbf{L} and the above equation is equal to

$$\mathbf{v} = \frac{\partial}{\partial t} \mathbf{x} = \mathbf{L} \mathbf{x} \quad 3.35b$$

For a line element $d\mathbf{X}$ moving to $d\mathbf{x}$, the relative velocity of $d\mathbf{x}$ will be (provided it is homogeneous).

$$d\mathbf{v} = \frac{\partial \mathbf{v}}{\partial \mathbf{x}} d\mathbf{x} = \mathbf{L} d\mathbf{x} \quad 3.35c$$

3.4.2 The decomposition of the velocity field into the rate of deformation matrix and spin matrix

According to Euler and Stokes (85,86), any instantaneous state of motion may be resolved at each point into the sum of a symmetric matrix called the stretching or rate of deformation matrix \mathbf{D} and an anti-symmetric,

orthogonal matrix called the spin matrix \mathbf{W} .

$$\mathbf{L} = \mathbf{D} + \mathbf{W} \quad 3.36$$

where \mathbf{D} is an irrotational field in which $\text{curl } \mathbf{D} = 0$ and

\mathbf{W} is the solenoidal field in which $\text{div } \mathbf{W} = 0$

Furthermore, the rate of deformation matrix is equal to

$$\mathbf{D} = \frac{1}{2} (\mathbf{L} + \mathbf{L}^T) = \frac{1}{2} \text{div } \mathbf{L} \quad 3.37a$$

and the spin matrix equal to

$$\mathbf{W} = \frac{1}{2} (\mathbf{L} - \mathbf{L}^T) = \frac{1}{2} \text{curl } \mathbf{L} \quad 3.37b$$

Both \mathbf{D} and \mathbf{W} are pure rate matrices.

3.4.3 The principal axis of stretching

Since the rate of deformation matrix \mathbf{D} is a symmetrical one, its real principal axis is called the principal axis of stretching and along it, no shearing exists. Its real values are the principal stretching or the principal rate of deformation.

As suggested in section 3.3.3, the matrix operation can be applied to find the principal values and directions by diagonalization of the symmetric matrix \mathbf{D} .

$$\mathbf{D} = \Phi \dot{\epsilon}_0 \Phi^T \quad 3.38$$

where the $\dot{\epsilon}_0$ is the principal stretching matrix

Φ is the principal eigenvector of the matrix \mathbf{D}

3.4.4 Some examples of velocity gradient field in two dimensions

The analysis of velocity field by matrix algebra has also been developed by Professor Hsü (31,32) as part of the analysis of large deformation. Below is only a brief summary of some of his works.

A. Aligned velocity field.

In an aligned pure shear of an incompressible media as in (fig.3.8), the principal stretching axis is fixed throughout the process so that the velocity of the particle will be described as in the following equation.

$$\frac{\partial \mathbf{x}}{\partial t} = \mathbf{v} = \dot{\epsilon}_0 \mathbf{x}$$

or in terms of components

$$\begin{vmatrix} \frac{\partial x_1}{\partial t} \\ \frac{\partial x_2}{\partial t} \end{vmatrix} = \begin{vmatrix} \dot{\epsilon}_0 & 0 \\ 0 & -\dot{\epsilon}_0 \end{vmatrix} \begin{vmatrix} x_1 \\ x_2 \end{vmatrix} \quad 3.39$$

Here $\dot{\epsilon}_0$ is called the principal rate of stretch or rate of deformation.

B. Rotational field

At an instantaneous motion, the deforming body is assumed to have suddenly solidified and at the same time rotating rigid bodily at its local angular velocity Ω . The motion is called the rotational field and is represented by the following equation

$$\begin{vmatrix} \frac{\partial x_1}{\partial t} \\ \frac{\partial x_2}{\partial t} \end{vmatrix} = \begin{vmatrix} 0 & -\Omega \\ \Omega & 0 \end{vmatrix} \begin{vmatrix} x_1 \\ x_2 \end{vmatrix} \quad 3.40$$

where the first matrix in the right hand side is the rotational field and Ω is the rate of spin.

C. Velocity field for pure shear with rotated axis

Fig.(3.9), shows the typical velocity field in which the principal axes of stretching is along a nonaligned angle Φ . By applying the

diagonalization of this velocity field

$$\frac{\partial \mathbf{x}}{\partial t} = \mathbf{D} \mathbf{x}$$

$$\mathbf{D} = \Phi \dot{\epsilon}_0 \Phi^T \quad 3.38$$

and in terms of components

$$\mathbf{D} = \begin{vmatrix} \cos \Phi & -\sin \Phi \\ \sin \Phi & \cos \Phi \end{vmatrix} \begin{vmatrix} \dot{\epsilon}_0 & 0 \\ 0 & -\dot{\epsilon}_0 \end{vmatrix} \begin{vmatrix} \cos \Phi & \sin \Phi \\ -\sin \Phi & \cos \Phi \end{vmatrix} \quad 3.41a$$

or

$$\mathbf{D} = \begin{vmatrix} \dot{\epsilon}_0 \cos 2\Phi & \dot{\epsilon}_0 \sin 2\Phi \\ \dot{\epsilon}_0 \sin 2\Phi & \dot{\epsilon}_0 \cos 2\Phi \end{vmatrix} \quad 3.41b$$

The last matrix is the one which expresses the non-aligned pure shear velocity field.

3.4.5 General analysis of a velocity field

In a two dimensional homogeneous velocity field, owing to the incompressibility of the material, the diagonal elements of the matrix should be equal in magnitude. The velocity field matrix is

$$\mathbf{L} = \begin{vmatrix} L_{11} & L_{12} \\ L_{21} & -L_{11} \end{vmatrix} \quad 3.42$$

In section 3.4.2, it has been stated that any velocity field can be decomposed into the sum of ^{the} stretching field (\mathbf{D}) and a rotating field (\mathbf{W}). As we are considering the general case, the stretching field is taken as a non-aligned pure shear field. Therefore, according to the decomposition and diagonalization stages, the general velocity gradient will be split into

$$\mathbf{L} = \mathbf{W} + \mathbf{D} = \mathbf{W} + \dot{\Phi} \dot{\epsilon}_0 \Phi^T \quad 3.43a$$

in terms of components

$$\begin{vmatrix} L_{11} & L_{12} \\ L_{21} & L_{22} \end{vmatrix} = \begin{vmatrix} 0 & \frac{L_{12} - L_{21}}{2} \\ \frac{L_{21} - L_{12}}{2} & 0 \end{vmatrix} + \begin{vmatrix} L_{11} & \frac{L_{12} + L_{21}}{2} \\ \frac{L_{12} + L_{21}}{2} & -L_{11} \end{vmatrix} \quad 3.43b$$

or

$$\mathbf{L} = \begin{vmatrix} 0 & -\Omega \\ \Omega & 0 \end{vmatrix} + \begin{vmatrix} \dot{\epsilon}_0 \cos 2\Phi & \dot{\epsilon}_0 \sin 2\Phi \\ \dot{\epsilon}_0 \sin 2\Phi & \dot{\epsilon}_0 \cos 2\Phi \end{vmatrix} \quad 3.43c$$

By comparing each component of the matrices, we arrive at

$$\Omega = \frac{L_{21} - L_{12}}{2} \quad 3.44a$$

$$\dot{\epsilon}_0 = \pm \sqrt{L_{11}^2 + \left(\frac{L_{12} + L_{21}}{2}\right)^2} \quad \text{or} \quad \pm \sqrt{D_{11}^2 + D_{12}^2} \quad 3.44b$$

$$\Phi = \frac{1}{2} \tan^{-1} \left(\frac{L_{12} + L_{21}}{2L_{11}} \right) \quad \text{or} \quad \frac{1}{2} \tan^{-1} \left(\frac{D_{12}}{D_{11}} \right) \quad 3.44c$$

Therefore, if the velocity gradient matrix is found, the three parameters Ω (the spin rate) Φ (the principal stretching axis angle) and $\dot{\epsilon}_0$ (the principal stretching rate) can be computed.

3.5 Axisymmetrical deformation analysis

So far, we have confined our analysis to plane strain conditions. In practice, quite a few of the forgings are axially symmetrical products. So, the analysis of large deformation has to be extended to cover the axisymmetrical deformation processes.

3.5.1 Uniform dilation in two dimensions

Uniform dilation is one of the deformations in which the original square is uniformly expanded or contracted into a larger or smaller square

respectively as given in (fig.3.10). The deformation represented by the co-ordinate transformation equation is as follows : -

$$x = FX$$

where the deformation gradient matrix is represented in terms of components

$$F = \begin{vmatrix} m & 0 \\ 0 & m \end{vmatrix} \text{ or } = \begin{vmatrix} e^{\epsilon_m} & 0 \\ 0 & e^{\epsilon_m} \end{vmatrix}$$

Since uniform dilation is concerned with the increase or decrease in the area of the square and the determinant of the deformation gradient matrix F is equal to the area of the square, the component m is equal to

$$m = \sqrt{\det (F)}$$

and $\epsilon_m = \ln m$ 3.45

3.5.2 Axisymmetrical deformation

In this kind of deformation, the meridian plane remains plane hence it is convenient to measure the deformation in such a plane. On such a plane, (fig.3.11,) a square will be deformed into a parallelogram not necessarily of the same area due to the circumferential strain acting in the direction perpendicular to this plane which is perpendicular to the paper in (fig.3.11) and it is equal to

$$\epsilon_{\theta} = \ln \frac{2 \pi r}{2 \pi r_0} = \ln \frac{r}{r_0} \quad 3.46a$$

However, for each elemental volume, constancy of volume deformation must be satisfied,

therefore,

$$2 \pi r_0 \delta a_0 = 2 \pi r \delta a$$

$$\frac{r}{r_0} = \frac{\delta a_0}{\delta a}$$

or

$$e^{\epsilon_\theta} = \frac{\delta a_0}{\delta a} \quad 3.46b$$

In the analysis of large deformation, any uniform changes in the area of the assumed homogeneous field is called uniform dilatation as in section 3.5.1 and it is equal to

$$m = \frac{\delta a_0}{\delta a} = \frac{1}{e^{\epsilon_\theta}} \quad 3.47$$

Also, in section 3.5.1, the determinant of the deformation gradient matrix is equal to the proportional changes in the area of the deformation field.

In this axisymmetrical deformation, we can see that the deformation is taken in two steps, first, the square is deformed into a smaller one due to the circumferential strain. This is followed by the unaligned pure shear which transforms the square to a parallelogram. In other words, the whole deformation begins with a uniform dilatation and then follows by an unaligned pure shear of the square. The resultant deformation gradient matrix \mathbf{F}' representing the whole deformation can be firstly decomposed into another deformation field \mathbf{F} as follows : -

$$\mathbf{F}' = m \mathbf{F} \quad 3.48$$

and the second deformation field is then decomposed further

$$\mathbf{F} = \mathbf{R} \mathbf{U} = \mathbf{R} \mathbf{Q} \mathbf{e}_0 \mathbf{Q}^T$$

combining equation (3.48) and the above equation, equation (3.48) equal to

$$\mathbf{F}' = m \mathbf{R} \mathbf{\Theta} \mathbf{\epsilon}_0 \mathbf{\Theta}^T \quad 3.49$$

In this successive decomposition, the principal strains in this axisymmetrical deformation will be as follows : -

the principal stretching strain

$$\epsilon_r = \log m + \epsilon_0 \quad \text{or} \quad = \epsilon_0 - \frac{1}{2} \epsilon_\theta \quad 3.50a$$

the principal shrinkage strain

$$\epsilon_z = \log m - \epsilon_0 \quad \text{or} \quad = -(\epsilon_0 + \frac{1}{2} \epsilon_\theta) \quad 3.50b$$

and the circumferential strain

$$\epsilon_\theta = -2 \log m \quad 3.50c$$

3.5.3 Velocity field of a uniform dilation in two dimensions

In a uniformly dilating deformation field, the homogeneous deformation field represented by a unit square before deformation is being uniformly expanded or contracted into a larger or smaller square. The velocity field representing the motion is

$$\frac{\partial \mathbf{x}}{\partial t} = \mathbf{v} = \mathbf{L} \mathbf{x} \quad 3.35b$$

where \mathbf{x} is the current position vector of the particle

\mathbf{v} is the velocity vector

\mathbf{L} is the velocity gradient matrix

Since

$$\mathbf{x} = \mathbf{F} \mathbf{X}$$

by substituting this equation into equation (3.35b) and differentiating,

we get

$$\frac{\partial \mathbf{x}}{\partial t} = \dot{\mathbf{F}} \mathbf{X} = \dot{\mathbf{F}} \mathbf{F}^{-1} \mathbf{x} \quad 3.51$$

Equation (3.51) is equal to 3.35b and, therefore, the velocity field matrix L is equal to

$$L = \dot{F} F^{-1} \quad 3.52$$

In section 3.5.1, it can be seen that the deformation gradient matrix of a uniform dilation is equal to, in terms of components,

$$F = \begin{vmatrix} m & 0 \\ 0 & m \end{vmatrix} \text{ or } = \begin{vmatrix} e^{\epsilon_m} & 0 \\ 0 & e^{\epsilon_m} \end{vmatrix}$$

This is substituted into equation (3.52) and differentiating, we get

$$\dot{F} = \begin{vmatrix} \dot{m} & 0 \\ 0 & \dot{m} \end{vmatrix} \text{ or } = \begin{vmatrix} e^{\epsilon_m} \dot{\epsilon}_m & 0 \\ 0 & e^{\epsilon_m} \dot{\epsilon}_m \end{vmatrix}$$

and

$$F^{-1} = \begin{vmatrix} \frac{1}{m} & 0 \\ 0 & \frac{1}{m} \end{vmatrix} \text{ or } = \begin{vmatrix} \frac{1}{e^{\epsilon_m}} \text{ or } e^{-\epsilon_m} & 0 \\ 0 & \frac{1}{e^{\epsilon_m}} \text{ or } e^{-\epsilon_m} \end{vmatrix}$$

Therefore, we get the velocity field for a uniform dilation ~~is~~ as follow :-

$$L = \begin{vmatrix} \frac{\dot{m}}{m} & 0 \\ 0 & \frac{\dot{m}}{m} \end{vmatrix} \text{ or } = \begin{vmatrix} \dot{\epsilon}_m & 0 \\ 0 & \dot{\epsilon}_m \end{vmatrix}$$

3.5.4 Velocity field for an axisymmetrical deformation.

In section 3.5.2, the deformation on the meridian plane is taken in two steps. Similarly, the velocity field of the deformation is considered to involve three separate velocity fields. According to Euler and Stokes (85,86), any instantaneous state of motion may be resolved at each point into the sum of several fundamental fields. These are the uniformly

dilating field $\dot{\epsilon}_m$, the stretching or irrotational field D and the spin or the solenoidal field W . Therefore, the velocity field from an axisymmetrical deformation L can be decomposed into the following: -

$$L = \dot{\epsilon}_m + D + W \quad 3.52$$

Similar to the derivation in section 3.5.2, the various components of principal strain rates are as follows: -

the circumferential strain rate

$$\dot{\epsilon}_\theta = 2 \dot{\epsilon}_m \quad 3.53a$$

the fastest stretching strain rate

$$\dot{\epsilon}_r = \dot{\epsilon}_0 - \frac{1}{2} \dot{\epsilon}_\theta \quad 3.53b$$

the fastest shrinkage rate

$$\dot{\epsilon}_z = - \left(\dot{\epsilon}_0 + \frac{1}{2} \dot{\epsilon}_\theta \right) \quad 3.53c$$

where $\dot{\epsilon}_0$ is the principal strain rate.

CHAPTER FOUR

The Behaviour and the Distribution

of

Finite Deformation of Metal under Load

In recent years, considerable progress has been made in applying plasticity theories to practical metal working operations. Yet, the phenomenon connected with the flow and the failure of the metal under compression is still difficult to resolve. Therefore, this chapter is devoted to the basic understanding of the deformation and flow pattern of a bulk material under compressive load.

4.1 General Considerations

When a bulk of metal is compressed between two flat platens the free surfaces begin to bulge as in (fig.4.1). The degree of bulging of the specimen depends on the condition of the boundary constraints existing at that ~~moment~~ ~~instant~~ ~~time~~ and previously. This barrelling effect has been studied by several scientists (72,42,36,87) and they concluded that this is due to the frictional effects at the tool-work interface. Hsü (33,35) has developed a means of eliminating the barrelling by adding just enough lubricant at the interface. Furthermore, he found out that excessive lubricant will produce a bollard-shaped specimen as in (fig.4.2)

Cook, Jain and others (36,87,76) have also found out that the forming speed will affect the behaviour of the metal. There are others who suggested that the die geometry has an influential part in determining the deformation pattern. Therefore, the following sections will deal with the basic concept in the deformation pattern of the specimen.

4.2 Graphical representation of the extent of deformation.

In all manufacturing process such as forging of metal, deformation will depend not only on the current state of strains but also on the past

history of strain. The locus of the past history of strain (a measure of deformation) is called strain path or deformation path. A triangular co-ordinate system is proposed by Hsü (30) for recording the past state of strains.

4.2.1 The Triangular co-ordinate system

A state of strain is usually represented by its three principal natural strains, say $\epsilon_1, \epsilon_2, \epsilon_3$. In assuming that the metal is incompressible, we imply that the sum of the three principal natural strains will be equal to zero.

$$\epsilon_1 + \epsilon_2 + \epsilon_3 = 0$$

Three axes which are 120° apart in a plane can be used to record the varying state of natural strains, as in (fig.4.3). In the co-ordinate system, any point P in the plane which is located by the position vector OP can be referred to these three reference axes OI, OII, OIII as

$$\epsilon_1 = \bar{\epsilon} \cos \psi$$

$$\epsilon_2 = \bar{\epsilon} \cos (120 - \psi)$$

$$\epsilon_3 = \bar{\epsilon} \cos (240 - \psi)$$

where $\bar{\epsilon}$ is the effective strain of the state of strain and is the length of OP.

ψ is the angle between OP and OI.

In (fig.4.4), the three axes represent the uniaxial tension lines and their backward extensions show the uniaxial compression lines. There are lines in between each alternate tension and compression lines and they

represent pure shear. These twelve lines which are analogous to the clock face, can be used to represent the deformations and the clock numbers are used to represent the type of deformations such as pure tension and pure compression etc. The clock number is called the characteristic index of strain η in which the odd numbers mean pure shear and the even numbers mean either pure tension or compression. The index η is given by

$$\eta = \frac{6}{\pi} \psi$$

In this way, a state of strain can be represented as in the polar co-ordinate system by η and $\bar{\epsilon}$, as in (fig.4.3). The history of the state of strains recorded on this co-ordinate system will show the progress of a deformation and the scalar equation of this coaxial path is

$$\bar{\epsilon} = \bar{\epsilon}(\eta) \quad 4.2$$

4.2.2 Co-axial and non-coaxial path

Consider two deformations in which the particle P at position \mathbf{X} moves to \mathbf{x}_1 , and then to its final position \mathbf{x}_2 . These two transformations can be represented by the two deformation gradient matrices \mathbf{F}_1 & \mathbf{F}_2 . The resultant deformation will be \mathbf{F}_3 .

The definition of coaxiality: Two deformations are coaxial if and only if the principal directions of strain in the final resultant matrix \mathbf{F}_3 are equal to their initial principal directions of \mathbf{F}_1 . In other words, their principal stretching directions in successive deformations do not vary with respect to the material.

In mathematical terms, the two deformations are carried out by multiplying their deformation gradient matrices.

$$\mathbf{F}_3 = \mathbf{F}_2 \mathbf{F}_1 \quad 4.3$$

From Hsü's thorough investigations into the non-coaxiality problems (30,32) the coaxiality of deformations depends on the constancy of the principal axis angle of the first and the resultant deformation. If we take their components equations

$$\mathbf{F}_3 = \begin{vmatrix} \cos \omega'' & -\sin \omega'' \\ \sin \omega'' & \cos \omega'' \end{vmatrix} \begin{vmatrix} e^{\epsilon_0''} & 0 \\ 0 & e^{-\epsilon_0''} \end{vmatrix} \begin{vmatrix} \cos \theta'' & \sin \theta'' \\ -\sin \theta'' & \cos \theta'' \end{vmatrix} \quad 4.4a$$

$$\mathbf{F}_2 = \begin{vmatrix} \cos \omega' & -\sin \omega' \\ \sin \omega' & \cos \omega' \end{vmatrix} \begin{vmatrix} e^{\epsilon_0'} & 0 \\ 0 & e^{-\epsilon_0'} \end{vmatrix} \begin{vmatrix} \cos \theta' & \sin \theta' \\ -\sin \theta' & \cos \theta' \end{vmatrix} \quad 4.4b$$

$$\mathbf{F}_1 = \begin{vmatrix} \cos \omega & -\sin \omega \\ \sin \omega & \cos \omega \end{vmatrix} \begin{vmatrix} e^{\epsilon_0} & 0 \\ 0 & e^{-\epsilon_0} \end{vmatrix} \begin{vmatrix} \cos \theta & \sin \theta \\ -\sin \theta & \cos \theta \end{vmatrix} \quad 4.4c$$

By combining equations 4.4a, 4.4b, 4.4c, the coaxiality condition as stated in the above definition will require that the resultant principal angle θ'' equals to the initial principal angle θ .

$$\theta'' = \theta \quad 4.5a$$

Therefore, as further proved in Hsü's paper (30,32), a necessary and sufficient condition for coaxiality is that the above equation is satisfied. If the two angles θ and θ'' are not equal, the difference between them is called the non-coaxiality angle β and is equal to

$$\beta = \theta'' - \theta \quad 4.5b$$

4.2.3 Coaxial strain path

In section 4.2.1, a method has been devised to represent the triaxial coaxial strain path. We have seen that the path has the equation

$$\bar{\epsilon} = \bar{\epsilon}(\eta) \quad 4.2$$

Any finite deformation is just the current state of strain of the particle in question, represented by $\bar{\epsilon}$ and η .

Generally, most researchers (36,69,70,87,73) assume the ratio of the three principal strains i.e., η is constant throughout the deformation. This path is called the radial coaxial path, as path A in (fig.4.5). Naturally, most coaxial deformation processes such as sheet metal drawing and extrusion processes, etc., will not exhibit this kind of constancy except in certain well controlled experiments. Therefore, a curved path, as path B in (fig.4.5), will be the usual character in an ordinary coaxial deformation.

4.2.4 Non-coaxial path

In most manufacturing processes, the principal axes of stretching vary with respect to the material. This kind of deformation is called non-coaxial deformation and their degree of non-coaxiality can be found by the difference between θ'' and θ'' in section 4.2.2.

In triaxial conditions, the rotation of the principal axes can be expressed in terms of three angles, but in two dimensional cases, we can have a single angle β which is the non-coaxiality angle defined in equation

(4.5b). Therefore, the strain path in non-coaxial deformation can be represented by a space curve in terms of three parameters $\bar{\epsilon}$, η , and β as in (fig.4.6) and their equation,

$$\begin{aligned}\bar{\epsilon} &= \bar{\epsilon} (t) \\ \eta &= \eta (t) \\ \beta &= \beta (t)\end{aligned}\tag{4.6}$$

where t is the time or any other parameter which varies with the path.

4.2.5 Strain path in plane strain condition

For the study of deformation processes, three dimensional problems are difficult to solve practically, and most processes such as, plane strain extrusion or sheet drawing, strip forging etc., in which one of the principal axes is perpendicular to the plane of deformation, can be considered in two dimensional plane strain conditions. It is assumed that there is no deformation during the process along this direction under the plane strain assumption as in (fig.4.7).

$$\epsilon_3 = 0$$

Therefore, from the incompressibility of metal

$$\epsilon_1 = - \epsilon_2\tag{4.7}$$

A coaxial strain path will become, in this case, a radial path along the 5 o'clock direction of the triangular co-ordinate. Whereas, a non-coaxial path will be a curve plotted on a plane perpendicular to the clock face

and along the 5 to 11 o'clock line with the ordinate in terms of β (the non-coaxial angle) (fig.4.8). Throughout the thesis, as the deformation is limited to plane strain non-coaxial deformation, this strain path graph is adopted.

4.2.6 Finite deformation — its meaning and its measure

In a continuous deformation process, the configuration of the specimen keeps on changing plastically. A finite deformation is the end product of this continuous process. Consider a particle P in a continuous deformable medium. The minute area around P is assumed to be ~~in~~ a homogeneous field in which the configuration of that area at the vicinity of P is being deformed throughout the process. The end product of the deformation — the final configuration α will determine the finite deformation in (fig.4.9). In other words, the history of the deformation is excluded from the determination of the finite deformation.

The finite deformation is measured by the strains which can be found by comparing the terminal deformed configuration α with the undeformed configuration X in terms of the affine transformation. The finite strain can be obtained from the decomposition of the deformation gradient matrix as shown in sections 3.2.4 and 3.3.

4.3 Distribution of finite deformation of a workpiece in simple plane strain upsetting process

Simple upsetting, which is the beginning of most forging processes, is similar in nature to a compression experiment i.e., a bulk of metal is

compressed between two flat platens. Owing to the friction at the tool-
work^{piece} interface, the latter tends to bulge and ^{this} produces non-homogeneous
triaxial strains in part or whole of the work. This non-homogeneous
strain field is theoretically undesirable because differential material
properties will result.

4.3.1 Finite strain distribution of a deformed workpiece

In plane strain conditions, the deformation plane, as in (fig.4.11), is
printed with some minute square grids. This square is assumed to repre-
sent the vanishingly small homogeneous deformation field around the vic-
inities of its location in the workpiece. Applying the strain analysis
method shown in section 3.3.4, a finite strain for various points in the
plane can be determined and plotted on a contour map. (Fig.4.10) is a
typical example of a deformation contour map.

4.3.2 Finite strain distribution histogram

The contour map presented in the previous section shows the real finite
deformation pattern of a deformed workpiece. But, in the analysis of
deformation, ^{the} contour map alone presents a difficult task in further theo-
retical work. So, a graph with the finite strain plotted against their
respective percentage of area on the deformation plane is used. This
graph is called the strain distribution histogram and (fig.4.12) is a
typical example of a finite deformation.

4.3.3 Non-dimensional strain distribution histogram

In order to compare different deformation patterns, a dimensionless strain
distribution diagram is used in which the finite strain axis is replaced

by the percentage of strain. (Fig.4.13) shows the same deformation in the dimensionless diagram. The percentage of strain is equal to

$$\bar{\epsilon}_p = \frac{\bar{\epsilon}_a - \bar{\epsilon}_L}{\bar{\epsilon}_r - \bar{\epsilon}_L} \times 100 \% \quad 4.8$$

where $\bar{\epsilon}_L$ is the minimum effective strain

$\bar{\epsilon}_r$ is the maximum effective strain

$\bar{\epsilon}_a$ is the effective strain.

4.3.4 Homogeneous deformation

A homogeneous deformation of a specimen is defined as one in which the finite strains in the whole specimen are uniform. In another words, the current state of strains at various points of the specimen are the same.

4.4 Examples of deformation models in plane strain upsetting

4.4.1 Ideal reduction model

An ideal deformation of a workpiece is an efficient deformation process. In order to obtain this high efficiency within the deformation regions, the direction of the incremental strains should be coaxial with the direction of the maximum principal stress, and the resultant deformation will be a homogeneous one.

Siebel and Pomp (33) have developed a method to perform an ideal deformation by compressing the specimen between two conical dies. But they can obtain that within the elastic limit only. For cylindrical specimens, Hsü and Young (35), found out that if enough lubricant (PTFE) is placed between

the tool/work interface, an ideal plastic deformation can be obtained. The compression is a characteristic uniaxial one and its strain path is along 6 o'clock in the triangular co-ordinates. They also found a reverse of the barrel shaped specimen — a bollard shaped — if excessive lubricant (PTFE) is used. In plane strain extrusion, Richmond and others (66,14) have also developed a special die profile for extrusion processes so that a nearly ideal deformation is achieved.

In compression under plane strain conditions, an ideal deformation means that the frictional effects on the tool/work interface are negligible. The strain path will be radial along the 5 o'clock direction. All the finite deformation should be homogeneous and coaxial. This can be demonstrated by a specimen with square grids on its deformation plane as in (fig.4.14a). After deformation, the grids will be transformed into aligned rectangles as in (fig.4.14b).

The strain distribution graph, (fig.4.15), shows that the distribution for this type of deformation is just a horizontal straight line. The $\bar{\epsilon}$ intercept increases in proportion to the percentage of reduction in height of the specimen and the percentage of reduction in height is equal to

$$\Upsilon = \frac{h_0 - h}{h_0} \times 100\% \quad 4.9$$

where h_0 is the original height of the specimen;

h is the height of the deformed specimen.

If the reduction in height is used as an average reduction strain, then it is equal to

$$\bar{\gamma}_e = \frac{2}{\sqrt{3}} \ln \left(1 - \frac{\gamma}{100} \right) \quad 4.10$$

4.4.2 A theoretical zonal reduction model

Nadai, Hsü, Kobayashi etc. (61,29,41,78,32) have all reported that in an actual compression of metal, some parts of the specimen received more deformation than the other and the former parts are called shear bands as zone (1) in (fig.4.16). This means that the deformation is non-homogeneous and far from ideal. Therefore, a zonal model is proposed.

We realised that in most deformation processes, the distribution of deformation in the end product is usually non-homogeneous. So, we simplified the problem further by upsetting a ~~rectangular prism~~ as in (fig.4.11), in which the length is far longer than the width and height of its cross-section so that plane strain condition can be achieved. In the end product, a non-homogeneous finite deformation is assumed and the deformations are concentrated in certain regions (shear zones) only, leaving the rest of the regions undeformed (dead zones). (Fig.4.16) is the model itself with the undeformed and deformed grids showing the area of concentrated shearing. Zone (1) is the shear zone and (2) is the dead zone. The width of the zone (1), shear zone, increases as the reduction in height proceeds.

This zonal reduction model is proposed for theoretical comparison with the ideal model only because the mechanism in operating this model is kinematically inadmissible as it involves the opening and closing of metal

in the central region of the specimen when the specimen is being compressed.

Assuming that this model is possible, the deformation distribution curve will look like (fig.4.17). It will be a rectangular curve and the area enclosed will expand as ^{the} deformation progress. (i.e., γ increases)

4.4.3 Comparison of the two models

Theoretically, these two models are opposite ways of reducing a work-piece geometrically to the same level. The ideal model is feasible in practice and a homogeneous distribution is achieved by spreading the deformation evenly all through the product. Although the zonal model is practically impossible, yet, it shows in theory that by concentrating the deformation along certain zones, this extremely uneven distribution of strain can also produce the same degree of reduction.

Naturally, we can deduce from these two diagonally opposite models that an actual distribution will be one between these.

CHAPTER FIVE

The Incremental Theory
in Deformation Analysis

In finite deformation analysis, in the previous chapter, only the end product of a series of deformations was considered and from this finite configuration, we derived the finite strain. In other words, the strain path taken by the particle is neglected or assumed to be radial and coaxial and only the current state of strain is analysed. This approach when applied to the analysis of most manufacturing processes such as rolling, drawing, and strip forging are unrealistic because they involve the varying strain ratio η , or ^acurved strain path, and rotation of the principal axes. The extra work done due to the rotation of the principal axes, is neglected in the finite strain analysis. In order to avoid the discrepancies due to the neglect of extra work, ^{the} incremental strain path is considered.

5.1 Basic principles

5.1.1 The incremental strain

In section 3.4, the basic concept in deriving the incremental deformation is presented. A few examples of velocity fields and matrices representing rates of strain are also included and from that we can get the incremental strain.

$$d\mathbf{e} = \mathbf{D} dt \quad 5.1a$$

where \mathbf{D} is the rate of deformation matrix.

and the principal incremental strain in two dimensions is

$$d\epsilon_0 = \dot{\epsilon}_0 dt \quad 5.1b$$

where $\dot{\epsilon}_0$ is the strain rate.

5.1.2 Frame of reference

In general, a frame of reference means a set of co-ordinates system in which the fundamental measurable quantities in kinematics such as distance and time intervals of an event (\mathbf{X} , t) can be specified. Physically, it is a set of stationary reference objects which does not change in time and it is used to relate the physical phenomenon at a three dimensional space with a real time axis.

5.1.3 Change of frame and frame indifference

A change of frame is a one-to-one mapping of the point particle in space and time such that distances, time intervals and orders are preserved. An event under a change of frame will involve a rigid transformation and a shift in time. Therefore, the new position of the event will be

$$\mathbf{x}^* = \mathbf{R}(t) \mathbf{x} \text{ or } = \mathbf{x}^*(\mathbf{X}, t^*) \quad 5.1c$$

where $t^* = t - a$

$a = \text{constant}$

$\mathbf{R}(t)$ is the orthogonal matrix.

Under a change of frame, transformation will be induced for each time t , on scalar, vectors and tensors. In order to preserve the relationship among the different variables, the following transformation laws must be followed under a change of frame.

- (i) Scalars remain unchanged.
- (ii) A vector \mathbf{v} is transformed into another vector.

$$\mathbf{v}^* = \mathbf{R}(t) \mathbf{v} \quad 5.2a$$

(iii) A second order tensor or a matrix is transformed according to the following: -

$$\mathbf{\hat{S}}^* = \mathbf{R}(t) \mathbf{S} \mathbf{R}^T(t) \quad 5.2b$$

where \mathbf{S} is a second order tensor or matrix.

Function and field whose values are scalars, vectors or tensors matrices are called frame indifferent if both the dependent vectors and matrices transform according to the above laws. In other words, if the relationship among all the parameters of the event before the transformation is preserved after the transformation, then the transformation follows the above laws and the event is said to be frame indifferent.

5.1.4 Equivalent motion and equivalent deformation path (16,57,85,86)

Equation (3.8a) shows the motion of a body referred to some frame of reference as in the following : -

$$\mathbf{x} = \mathbf{x}(\mathbf{X}, t) \quad 3.8a$$

But, equation 5.1c described in the previous section, describes the same motion in a new frame.

$$\mathbf{\hat{x}}^* = \mathbf{R} \mathbf{x} \quad 5.1c$$

Physically, both equations express the same motion in the eyes of different observers and their frames are changed according to the transformation

laws in equation (5.2a,b) as stated in the last section. Their mathematical relationship is just a time-dependent rigid transformation and a time shift. Therefore, we can say that the motion is frame-indifferent, and the motions described by the two equations are called equivalent motion. Furthermore, any histories of motions which are transformed according to the above transformation laws are also called equivalent motions histories. Since deformation path is a function of ^{the} history of the motion, any two deformation paths whose histories of motion are related by the transformation laws are also called equivalent deformation paths.

5.2 Total deformation analysis

5.2.1 The extent of deformation and the curvature of the strain path

The significance of the curvature of a strain path can be elucidated by exploring the strain path of constant curvature. Such exploration will, in the following, be divided into (i) the coaxial case and (ii) the non-coaxial case with constant strain ratio (like the plane strain deformation).

(i) In the coaxial case, if a strain path of constant curvature starts from the origin, it will, obviously, return to the state of zero deformation represented by the origin. Such a circular path may be looked upon as generalized from a radial path starting from, and returning to the origin. In the circular path of this type, (fig.5.1) the effective strain $\bar{\epsilon}$ is related to the length of the path s , as follows

$$\bar{\epsilon} = 2 R \sin \frac{s}{2 R}$$

where R is the radius of curvature. Along such a path the effective strain $\bar{\epsilon}$ eventually (when s is $2\pi R$) returns to zero.

If a coaxial circular path is concentric to the origin, the fact that it adds nothing to the effective strain representing the apparent deformation is even more clearly seen. Along such a path, (fig.5.2) deformation ^{is} occurring continuously though the severity of deformation, represented by $\bar{\epsilon}$, apparently remains constant. The deformation that is added along such a path somehow fails to show.

(ii) To isolate the effect of non-coaxiality alone, it is desirable to illustrate the curvature due to non-coaxiality in a radial and non-coaxial path, in which the strain ratios remain constant (for instance, in plane strain deformation) and the principal axes of the incremental strains rotate with respect to the material.

In the second type of coaxial circular path shown in (fig.5.2) the radius of curvature is the effective strain itself. Although the severity of deformation remains constant here, the shape of the deformed body changes — as can be seen in (fig.4.4). In the corresponding circular path in the non-coaxial case, both the shape and the apparent severity of the deformation remain constant while the body is continuously being deformed. That such deformation is possible can be easily illustrated in (fig.5.3) where an ellipse is incrementally stretched and compressed along the arrow heads shown. Under such a non-coaxial deformation, the ellipse retains its shape, though its axes rotate slightly in the anti-clockwise direction.

(The mathematical treatment of this problem can be found in (30,32)). Thus, deformation can occur, and can continue, without change of shape, contrary to common sense expectations. The corresponding curve in (fig.5.4) is of course, a vertical line excluding the β -axis. In such a circular path (fig.5.5) the effective strain is also the radius of curvature, exactly as in the corresponding coaxial case.

Incidentally, there is also a circular non-coaxial path corresponding^{to} the circular coaxial one which starts from the origin. If Γ is the integral of the non-coaxial incremental strains, then for such a path

$$\bar{\epsilon} = 2 R \sin \frac{\Gamma}{2 R}$$

where R is the radius of curvature. Along such a path the shape of this specimen will, of course, change.

The above considerations are hardly applicable to forging in which such strange strain paths can hardly be expected. However, it is of theoretical interest and provides a clear illustration that total deformation and energy of deformation on the one hand, and effective strain based on the shape of the deformed body on the other are two different things. Problems in forging are related to the former, not to the latter.

5.2.2 Pure deformation

In section 3.3.1 a pure deformation in a body has been described and the motion is represented by equation (3.8b).

$$\mathbf{x} = \mathbf{F}\mathbf{X} \quad 3.8b$$

In this particular deformation, the deformation matrix \mathbf{F} is a symmetrical one and if it is decomposed, the matrix \mathbf{F} will be equal to \mathbf{U} , the right stretch matrix because there is no rigid body rotation, i.e., \mathbf{R} is equal to unit matrix.

5.2.3 Total deformation of a process

In a continuous deformation process, the total deformation of a particle in a deformable body is the accumulation of all the infinitesimal deformations along the strain path from the initial undeformed state to the final terminal state. In other words, the total deformation is a function of the history of deformation. Therefore, the total deformation intensity factor Γ in term of the deformation history will be : -

$$\Gamma = \Gamma(\mathbf{F}(\mathbf{X}, \tau)) \quad 5.3a$$

or the intensity value in two dimension equals

$$\Gamma = \sum_{i=0}^n (\dot{\epsilon}_i \delta t)_i \quad 5.3b$$

$$d\Gamma = \dot{\epsilon}_i dt \quad 5.3c$$

where $0 < \tau < t$

5.2.4 Total deformation with superimposed rigid body rotation

If we consider another deformation which differs from the one described in section 5.2.2 by superimposing a rigid body rotation on the pure deformation, the new position of the particle \mathbf{X} will be \mathbf{x}^* and the

motion will be : -

$$\dot{\mathbf{x}} = (\mathbf{R}) (\dot{\mathbf{F}}) \mathbf{X}$$

or
$$\dot{\mathbf{x}}^* = (\mathbf{R}) (\dot{\mathbf{x}})$$

The total deformation of this new deformation will be : -

$$\dot{\Gamma}^* = \dot{\Gamma} (\mathbf{R} (\tau) \mathbf{F} (\mathbf{X} , \tau))$$

or in two dimensions

$$\dot{\Gamma}^* = \sum_{i=0}^n (\mathbf{R} \dot{\epsilon}_0 \delta t)_i$$

According to the principle of frame indifference, the deformation in the above equation and the deformation in equation (5.3b) are equivalent and their scalar values, i.e. the total deformation, will be unchanged.

Therefore,

$$\dot{\Gamma} = \dot{\Gamma}^* \tag{5.4}$$

The above equation shows that in any equivalent deformation process, the total deformation $\dot{\Gamma}$ is the same.

5.3 The determination of the total deformation intensity $\dot{\Gamma}$ of a non-coaxial strain path factor

A finite deformation as analysed in Chapter four involves an initial angle, the deformation itself and the final rotated angle. A coaxial deformation will simply mean that the initial angle of the deformation is constant throughout the process as described in section 4.2.2. The total

deformation will be the sum of all the incremental deformations. This is also valid in calculating the total deformation of a non-coaxial path except in the determination of the incremental strain in which the rotation of the principal axes have to be considered.

5.3.1 An equivalent deformation path

According to the principle of equivalence in motion and deformation path, a history of motion with rigid body rotation elements superimposed is equivalent to a history of motion without that rigid body motion, provided that they are related by the transformation laws -- equation(5.2 a&b) in section 5.1.3. Therefore, a motion with rigid body rotation is the same as one without it. In other words, a deformation path with rigid body rotation is indifferent from a pure deformation path. For a pure deformation path, the history of the deformation will consist of the strain matrix only.

$$\text{i.e. } \mathbf{F}(\tau) = \mathbf{R}\mathbf{U}(\tau)$$

where $0 < \tau < t$

Here, the rigid body rotation is assumed to be equal to one, therefore,

$$\mathbf{F}(\tau) = \mathbf{U}(\tau) \qquad 5.5$$

5.3.2 The derivation of the incremental strain or rate of deformation matrix \mathbf{D} in terms of fixed configuration

In section 3.4, the incremental strain or the rate of deformation matrices referred to the current configuration is derived. It is impossible to

integrate all the incremental deformations if there is no fixed reference configuration. Thus, a fixed reference has to be used instead of the current configurations, and, in this case, the undeformed configuration is used.

A. The relationship between the derivatives of the deformation gradient matrix \mathbf{F} and the velocity field matrix \mathbf{L} .

The motion of a deformation is described by equation (3.8b) and if differentiated with respect to time t , the equation becomes : -

$$\frac{\partial \mathbf{x}}{\partial t} = \frac{\partial \tilde{\mathbf{F}}}{\partial t} \mathbf{X} + \mathbf{F} \frac{\partial \mathbf{X}}{\partial t}$$

Since the initial configuration is constant, therefore

$$\frac{\partial \mathbf{X}}{\partial t} = 0$$

$$\text{so, } \frac{\partial \mathbf{x}}{\partial t} = \dot{\tilde{\mathbf{F}}} \mathbf{X} \quad 5.6$$

whereas, the velocity field gradient matrix \mathbf{L} as defined in section 3.4 as : -

$$\mathbf{v} = \mathbf{L} \mathbf{x}$$

$$\text{or } \frac{\partial \mathbf{x}}{\partial t} = \mathbf{L} \mathbf{x} \quad 5.7$$

where \mathbf{v} is the velocity of the particle and is equal to $\frac{\partial \mathbf{x}}{\partial t}$

Equation (5.6&5.7) should be equal and if equation (3.8b) is substituted into the equations and we have

$$\mathbf{L} = \dot{\mathbf{F}} \mathbf{F}^{-1} \quad 5.8$$

B. The derivation of \mathbf{D} in terms of the stretch matrix \mathbf{U} .

Again, section 3.4 shows that a velocity gradient matrix can be decomposed into a stretching matrix \mathbf{D} and a spin matrix \mathbf{W} and is related to \mathbf{L} by the equation.

$$\mathbf{L} = \mathbf{W} + \mathbf{D} \quad 3.36$$

and

$$\mathbf{D} = \frac{1}{2} (\mathbf{L} + \mathbf{L}^T) = \frac{1}{2} \text{div } \mathbf{L}$$

$$\mathbf{W} = \frac{1}{2} (\mathbf{L} - \mathbf{L}^T) = \frac{1}{2} \text{curl } \mathbf{L}$$

3.37^a
b

Thus, by substituting equation (5.8) into the above equations, we get,

$$\mathbf{D} = \frac{1}{2} (\dot{\mathbf{F}} \mathbf{F}^{-1} + \mathbf{F}^{-T} \dot{\mathbf{F}}^T) \quad 5.9$$

In section 3.2.4, the deformation gradient can be decomposed into matrices \mathbf{R} and \mathbf{U} and its derivations will be :-

$$\dot{\mathbf{F}} = \dot{\mathbf{R}}\mathbf{U} + \mathbf{R}\dot{\mathbf{U}} \quad 5.10$$

also, the reciprocal of the deformation gradient matrix is :-

$$\mathbf{F}^{-1} = (\mathbf{R}\mathbf{U})^{-1} = \mathbf{U}^{-1} \mathbf{R}^{-1}$$

As \mathbf{R} is an orthogonal matrix $\mathbf{R}^{-1} = -\mathbf{R}^T$

Therefore

$$\mathbf{F}^{-1} = \mathbf{U}^{-1} \mathbf{R}^T \quad 5.11$$

Again

$$\mathbf{F}^{-1T} = \mathbf{R} \mathbf{U}^{-1} \quad 5.12$$

because

$$\mathbf{U} = \mathbf{U}^T \quad \text{symmetric matrix}$$

and

$$\dot{\mathbf{F}}^{-1T} = \mathbf{U}^T \dot{\mathbf{R}}^T + \dot{\mathbf{U}}^T \mathbf{R}^T \quad 5.13$$

Combining all the equations (5.13, 5.12, 5.11, 5.10) into equation (5.9), we have

$$\mathbf{D} = \frac{1}{2} \{ \dot{\mathbf{R}} \mathbf{U} \mathbf{U}^T \mathbf{R}^T + \mathbf{R} \dot{\mathbf{U}} \mathbf{U}^T \mathbf{R}^T + \mathbf{R} \mathbf{U} \dot{\mathbf{U}}^T \mathbf{R}^T + \mathbf{R} \mathbf{U} \mathbf{U}^T \dot{\mathbf{R}}^T \} \quad 5.14$$

Since, the matrix properties show that

$$\mathbf{U} \mathbf{U}^T = \mathbf{I}$$

$$\mathbf{R} \dot{\mathbf{R}}^T = -\dot{\mathbf{R}} \mathbf{R}^T$$

Equation (5.14) will be reduced to

$$\mathbf{D} = \frac{1}{2} \mathbf{R} (\dot{\mathbf{U}} \mathbf{U}^T + \mathbf{U}^T \dot{\mathbf{U}}) \mathbf{R}^T \quad 5.15$$

Similarly, we get the spin matrix

$$\mathbf{W} = \dot{\mathbf{R}} \mathbf{R}^T + \frac{1}{2} \mathbf{R} (\dot{\mathbf{U}} \mathbf{U}^T - \mathbf{U}^T \dot{\mathbf{U}}) \mathbf{R}^T$$

Equation (5.15 and 5.16) are important because they are referred to the fixed undeformed configuration and so their successive incremental strain can be summed to give the total deformation of the prescribed path. When

these equations are applied to analysing an equivalent deformation path, the equations are reduced to the equation below because in the equivalent path, the rigid body rotation element is assumed to be nil. Therefore, equation (5.15) becomes : -

$$\mathbf{D}_{eq} = \frac{1}{2} (\dot{\mathbf{U}} \mathbf{U}^{-1} + \mathbf{U}^{-1} \dot{\mathbf{U}}) \quad 5.17$$

5.3.3 The calculation of total deformation of this equivalent path

Equation (5.3b) expresses the total deformation in two dimensions, in terms of the principal rate of stretching and its time intervals. In order to calculate the principal rate of stretch $\dot{\epsilon}_o$, the rate of deformation matrix \mathbf{D} or in this case \mathbf{D}_{eq} have to be found and by applying equation (3.44b), $\dot{\epsilon}_o$ can be found for each incremental time interval t . The total deformation will be : -

$$\Gamma_{eq} = \sum_{\lambda=0}^n (\dot{\epsilon}_o \delta t)_{\lambda} \quad 5.3b$$

and from the frame indifference principle, section 5.1.3, this is equal to the actual total deformation.

CHAPTER SIX

Work, Path Characteristic and Redundant

Work of a Perfectly Plastic Body

6.1 Introduction

The derivation of the total deformation intensity Λ^{Γ} in the last chapter using the incremental theory is a step forward when the non-coaxiality of deformation is considered. Normally, the state of finite strain is understood to represent the degree of deformation and in such a representation, the non-coaxial effect on the path is neglected. So, the inclusion of the non-coaxial effect in the intensity factor Γ can be used as a measure of the deformation intensity of that particle. Later on in this chapter, the work done by this particle is derived, assuming the metal behaves perfectly plastically.

6.1.1 Work done by an element of a perfectly plastic deformable medium

Hill and Nadai and others (24,25,61) have made use of the incremental theory to obtain the incremental work done per unit volume by the element and it is equal to

$$dw = \text{tr} (\boldsymbol{\sigma} d\boldsymbol{\epsilon}) \tag{6.1a}$$

where $\boldsymbol{\sigma}$ is the stress matrix

$d\boldsymbol{\epsilon}$ is the incremental strain matrix

and the above equation is also equal to

$$dw = \bar{\sigma} d\bar{\epsilon} \tag{6.1b}$$

where $\bar{\sigma} = \sqrt{\frac{1}{2} ((\sigma_1 - \sigma_2)^2 + (\sigma_2 - \sigma_3)^2 + (\sigma_3 - \sigma_1)^2)}$

$$d\bar{\epsilon} = \sqrt{\frac{2}{9} ((d\epsilon_1 - d\epsilon_2)^2 + (d\epsilon_2 - d\epsilon_3)^2 + (d\epsilon_3 - d\epsilon_1)^2)}$$

For a perfectly plastic material, the effective stress will become the yield stress of the material σ_0 and equation (6.1b) will become

$$dw = \sigma_0 d\bar{\epsilon}$$

When the incremental work of the element is integrated along the strain path, we have

$$\int dw = \int \sigma_o d\bar{\epsilon}$$

and the total work done per unit volume is equal to

$$W = \sigma_o \int d\bar{\epsilon} \quad 6.2$$

The non-dimensional work done by the stress can be derived by dividing equation 6.2 by the yield stress to give

$$A = \frac{\sigma_o}{\sigma_o} \int d\bar{\epsilon} = \int d\bar{\epsilon} \quad 6.3$$

where A is the dimensionless work done per unit volume and is always greater than one if flow has occurred.

The incremental dimensionless work will be

$$dA = d\bar{\epsilon} \quad 6.4$$

Equation 6.4 shows that the incremental dimensionless work is equal to the incremental strain. In Chapter five, equation 5.1 relates the rate of the deformation matrix with the incremental strain matrix and when this equation is used, the incremental dimensionless work per unit volume is

$$dA = g(\dot{\epsilon}_o dt) \quad 6.5$$

where g represents a function.

Again, equation(5.3c) shows that the incremental total deformation intensity^{factor} $d\Gamma$ is the new parameter which we derived in the incremental analysis and it can be substituted into the above equation.

Hence,

$$dA = g(d\Gamma) \quad 6.6$$

and when the total work done per unit volume is considered, the dimensionless work of the element becomes

$$\int_0^A dA = \int_0^{\Gamma} g (d\Gamma)$$
$$A = g (\Gamma) \quad 6.7$$

The above equation means that the work of an element is a function of the total deformation that element has experienced.

6.1.2 Apparent work done by the element.

Apparent work is defined as the work required to deform an element plastically from its undeformed state to its final terminal configuration at constant strain ratio in a fixed principal direction. In other words, the path taken by the element from the initial position to the final position is a radial and coaxial strain path.

Similarly, we can quite easily have the same relation when perfect plastic material is considered. The dimensionless apparent work B

$$B = B (\bar{\epsilon}) \quad 6.8$$

where $\bar{\epsilon}$ is the effective strain.

We may conclude that the dimensionless apparent work is a function of the finite strain which derived from the deformation theory in Chapters three and four.

6.2 An ideal work path and the path characteristics of an element in a deformable body

6.2.1 An ideal deformation path of a particle in a deformable body

In this section, the meaning of an ideal deformation path is considered to

be one along which the work done by the particle is minimum. As stated in section 4.2.3 on the coaxial path and section 4.2.4 on the non-coaxial path, the minimum work path is the coaxial and radial path which connects the initial position O in (fig.6.1), to the current position P and is a straight line in the triaxial co-ordinates system i.e., path A. In Nadai's book (61), the minimum work path in terms of the deformation, is a hyperbolic curve as shown in (fig.6.2). Along this path, the work done which is derived from the incremental theory, will be equal to the apparent work done.

$$A_i = B_i = \text{minimum work done per unit volume.}$$

In all deformations, the apparent work done is the minimum work required in deforming the element into the current state.

6.2.2 Curved coaxial path

Following the above section, the minimum work path is an ideal path, and also the radial coaxial path. But in an actual coaxial deformation, a constant strain ratio η , is difficult to maintain and practically unrealistic. Therefore, a curved path such as path B in (fig.6.1), is a typical example in a coaxial deformation. Naturally, the work done along the curved path is more than the work done in the ideal path because the actual work done depends on the path length. The work done per unit volume of a curved coaxial path of a perfectly plastic element is equal to the following equation : -

$$W = \sigma_0 f \left(\frac{1}{\rho}, \bar{\epsilon} \right) \quad 6.9a$$

where σ_0 is a constant flow stress

$\bar{\epsilon}$ is the effective strain

f represents a function

ρ is the equivalent radius of curvature of the path.

The equivalent radius of curvature of this curved coaxial strain path can be derived by assuming that the length of the path equals the arc of a circle with radius ρ as in (fig.6.1).

When the coaxial path is radial, then the work will be : -

$$W = \sigma_0 \bar{\epsilon} \quad 6.9b$$

where the function is equal to the effective strain.

6.2.3 Path characteristic for non-coaxial plane strain deformation

In section 4.2.5, it has been shown that the non-coaxial path has its own special character and it is similar to a curved coaxial path. Firstly, an imaginary path is assumed to represent the deformation path in which the length of this path is equal to the extent of the deformation and measured by the deformation intensity factor Γ . In addition, the imaginary path is further assumed to be an arc of a circle of radius ρ , and the length of the arc equals the deformation intensity factor Γ . The effective strain $\bar{\epsilon}$ which represents the finite deformation, is just the chord inside the same circle joining the arc. The angle φ is half the angle sustained by the arc Γ of the circle. See (fig.6.3). Therefore, this particular path can be derived from the properties of circles and we get : -

$$\Gamma = 2\rho\varphi \quad 6.10a$$

and the effective strain is equal to

$$\bar{\epsilon} = 2\rho \sin \varphi \quad 6.10b$$

where φ is in radians.

If equation 6.10b is divided by equation 6.10a, the ratio between the effective strain and the deformation intensity will be : -

$$\frac{\bar{\epsilon}}{\Gamma} = \frac{\sin\varphi}{\varphi} \quad 6.10c$$

and this ratio can never be greater than one.

$$1 \geq \frac{\bar{\epsilon}}{\Gamma}$$

The radius of curvature ρ for this particular path can be determined from the measured value Γ , and the angle φ . It is equal to

$$\rho = \frac{\Gamma}{2\varphi} \quad 6.10d$$

For each instantaneous moment during the deforming process, the ratio of deformation, and the angle φ can be calculated. Then, an equivalent radius of curvature can be derived from the equation (6.10d). This radius ρ can also be determined graphically as in (fig.6.4). A radius of curvature of the path can be obtained by plotting the radius ρ against the reduction in height γ which is being used to describe the progress of a deformation acting on an element.

For a plane strain non-coaxial path, the work done per unit volume of a perfectly plastic element will be equal to : -

$$W = 2 \rho \sigma_0 \sin^{-1} \left(\frac{\bar{\epsilon}}{2\rho} \right) \quad 6.11$$

where σ_0 is the flow stress

ρ is the equivalent radius of curvature of the path.

The curvature of the path indicates the effect of the non-coaxiality existing during the deformation process. The final results are that a non-coaxial deformation consumes more work than the work consumed by a coaxial path.

6.3 Distribution of work done by a deformed body

6.3.1 Distribution pattern represented by means of a contour map

The distribution of work done on a specimen which is compressed in the plane strain condition is similarly plotted as in section 4.3.1, ^{Fig.(4.10).} The difference between the two is the use of two different theories in the determination of work in which the former leads to the calculation of apparent work and the actual work done for the latter.

6.3.2 Distribution pattern in term of a histogram

Again, this deformation pattern representation is similar to the finite strain representation in section 4.3.2 in which the work done replaces the finite strain $\bar{\epsilon}$ as shown in (fig.6.5).

6.4 Total work and redundant work for a simple reduction process

6.4.1 Total work done

In a simple upsetting, a block of metal is reduced to a lower height and the total work done is the summation of all the work done by each element of the whole cross-section of the specimen.

From the dimensionless work distribution graph as in section 6.3.2 and in (fig.6.5), the area beneath the curve is the total work done by the process on the whole surface area. Therefore, the total dimensionless work done per unit volume by the process is : -

$$A_T = \int_0^1 A d \left(\frac{a_a}{a} \right) \quad 6.12$$

where a is the total area of the cross-section

a_a is the actual area

A_T = total dimensionless work done per unit volume

A = dimensionless work per unit volume.

In order to calculate the total work done, the area beneath the curve in the work distribution histogram will be measured at different percentages of reduction of height, and their corresponding total works are plotted against the reduction in height.

6.4.2 Redundant work

An ideal reduction process is an efficient method in compressing a piece of metal from one configuration to the terminal one as explained in section 4.4.1. For a simple upsetting process, the ideal process is a uniaxial compression, in which the distribution of finite strain as well as the work done is homogeneous in every part of the body. Whereas, in actual upsetting, the distribution of strain is non-uniform and the total work done is usually found to be higher than the ideal process as shown in ^{the} extrusion process by Richmond (66) and Hill (27,25). So, Hill has proposed that this extra work required in deforming the block of metal to the same overall severity is called the redundant work A_R and is equal to : -

$$A_R = A_T - A_{iT} \quad 6.13$$

where A_{iT} is the ideal total work.

In fact, this redundant work is necessary in an actual process to overcome all the outside constraints such as the friction at the die/work interface and the geometry of the die. Furthermore, the redundant work can be used to determine the efficiency of the deforming process, as when the redundant work is near zero, the process will tend to be as efficient as the ideal case. Therefore, the efficiency ξ of deformation is equal to : -

$$\xi \% = \left(1 - \frac{A_R}{A_{iT}} \right) \times 100\% \quad 6.14$$

An efficient process will not just save energy, the wear of the die which is affected by the amount of load exerted on the die, is also reduced. Any excessive load usually distorts the alignment of the machine, but this is also minimised in an efficient process.

6.4.3 Apparent redundant work

From the finite deformation analysis, the total apparent work can also be determined from the strain distribution histogram and the apparent redundant work B_R is equal to : -

$$B_R = B_T - A_{iT} \quad 6.15$$

where B_T is the total apparent work.

The significance of this apparent redundant work is that it can be any value between a negative redundant work to a positive value. The variation means that if the metal is reduced non-homogeneously but coaxially as well as radially, the total work done may be less than the ideal process. The

above statement may be true theoretically as the total apparent work of an ideal reduction model is compared with the zonal model in (fig.6.6). The difference in the total apparent work can also be seen in Hsü's papers (33,35) and (fig.6.7) in which cylindrical specimens are compressed in an ideal and an ordinary test experiment. We can explain why the work consumed by the barrelled specimen is less than the ideal specimen, because we know that only the apparent work done and not the actual work, is considered. The difference between the redundant work and the apparent redundant work, i.e., $A_R - B_R$, is an indicator of how much work is consumed in rotating the principal directions in this non-coaxial process as compared to a stationary coaxial process.

CHAPTER SEVEN

The Filling and Spreading Characteristics

in a Closed Die Forging Process

7.1 The spreading of the metal

7.1.1 General considerations

A specimen under compression will either bulge outwards into a barrel shape or else take a bollard shape. Hill (26) has found out that this bulge profile can be represented by a spread coefficient. Baraya, Johnson, (5,38) and Tomlinson(83), followed Hill and applied approximately the same definition of spread by using the extreme condition such as sticking condition at the work/tool interface. But, Shabaik (72) traced the profile by recording the co-ordinates of the free boundary. In order to have a better quantitative understanding of the spreading mechanism, the following section is devoted to the study of the bulge and spread phenomenon.

7.1.2 An ideal spreading process

This ideal process is the resultant of the ideal reduction process proposed in Chapter four. Every stage will result in a homogeneous deformation and every particle will pursue a radial and coaxial strain path (in plane strain condition) or the minimum work path. Under this condition, the sideways spread of the metal will be the ideal one. In (fig. 7.1), the ideal sideways spread d_i of the particle P at the edge of the interface AP of the specimen will be : -

$$d_i = A' P' - AP = b' - b \quad 7.1a$$

when the specimen is under plane strain condition and the material is incompressible, equation (7.1a) will be equal to : -

$$d_i = \frac{b h}{h'} - b = \frac{\gamma b}{100 - \gamma} \quad 7.1b$$

where γ is the percentage of reduction in height.

In this ideal spreading process, every element will be displaced the same amount d_i along the free boundary thus forming a straight edged specimen.

7.1.3 Actual spreading of metal at the interface

Spreading of metal is the horizontal movement d of the edge of the interface before deformation from P to P'' in (fig.7.2). In fact, this edge displacement is of two phases. One is the sideways expansion of the original end face i.e. from P to P'' in (fig.7.3) and the other is the rotation or the folding process of the element on the free boundary on to the interface. (Fig.7.3) is showing the two processes in operation, the element Q which is at the free boundary before deformation is folded on the work/tool interface Q' . The existence of the folding process is due to the excessive frictional restraint and the high compressive pressure. So, an actual spreading will be a combination of the two with the folding of metal dominating the spreading process.

7.1.4 The spread coefficient

Hill and Johnson (26,5) have proposed a spread coefficient which is a function of the logarithm of spread ratio and reduction of height ratio. In compression, this index can hardly tell how much the spread is varied. Therefore, another spread coefficient is suggested which can show the

variation of the spread straight away. This coefficient is the ratio of the actual spread d over the ideal spread d_i for the same percentage reduction and the same width to length ratio. The spread coefficient S is equal to : -

$$S = \frac{d}{d_i} \quad 7.2$$

In the previous section, it has been explained that the spreading is composed of two processes. In order to distinguish the two, an expansion coefficient SD , of the original end face, and a folding coefficient, V , are used and their sum is equal to the spread coefficient.

$$S = SD + V \quad 7.3$$

where the sideways displacement coefficient SD is equal to

$$SD = \frac{\text{the actual horizontal displacement of the original end faces}}{\text{ideal spread } d_i} \quad 7.4$$

and the folding coefficient V is equal to

$$V = S - SD \quad 7.5$$

7.1.5 The bulge profile *

The spread coefficient discussed in the previous section concerned the horizontal displacement along the work tool interface which is directly influenced by the frictional condition. But the bulge profile can hardly be defined. It was found that if the spread coefficient at the

*Note: This analysis is only applicable to specimens with single barrel.

interface was less than the coefficient along the x-axis of symmetry, this difference means the bulge is a barrel shape, whereas if there is no difference, the spreading is near to the ideal case and also bulges do not exist.

$$(S_m - S_t) = +ve \quad \text{bulge shape, barrel}$$

$$(S_m - S_t) = 0 \quad \text{straight}$$

$$(S_m - S_t) = -ve \quad \text{bollard}$$

where S_m = spread coefficient along the equatorial axis

S_t = spread coefficient at the interface

7.2 Filling characteristic

7.2.1 General consideration

The success of the forming process does not depend on just the non-existence of cracks. The degree of the die cavity being filled is also another criterion for the success of the process. For a complete filling, the usual practice is to make the blank larger than required which results in a larger material wastage and forming energy. Naturally, an optimum size is ideally desirable but practically impossible to define. Up to now, there is no way to determine to what extent the die is filled, and the effect of blank size, frictional condition and excessive material in the filling process are all a mystery. In order to study these problems, the following is formulated for the investigation of the filling characteristic in a simple closed die forming process.

7.2.2 The filling coefficient

The filling of a die cavity can be simply described as the metal surface which is in contact with the surface of the die cavity.

Therefore, the coefficient is the ratio between the surface area of the workpiece in contact with the die cavity to the surface area of the die cavity. The filling coefficient is Λ .

$$\Lambda = \frac{\text{Surface area of specimen in contact with die}}{\text{Surface area of the die cavity}} \quad 7.6$$

This coefficient is an index to show whether the die is being filled completely, i.e., when $\Lambda = 1$, or else, i.e., when $\Lambda < 1$.

CHAPTER EIGHT

Experimental Equipment
and Technique

8.1 The experimental methods and data

The experiment consists of two parts; the first part is the investigation of the distribution of deformation in terms of the flow pattern and its complications such as the orientation of the plateau, rigid body rotation, bulge shape and homogeneity of deformation, and the latter part concentrates on the filling process of the die cavity. The experimental technique and equipment are described in separate sections in the following.

8.2 Experimental technique in the investigation of flow characteristic of metal under simple upsetting

8.2.1 Specimen data

After a series of tests for finding suitable material for the flow experiment in which solder, (lead and zinc) copper and pure aluminium have been tried, an aluminium alloy BS HE 30 is chosen so that this kind of extruded alloy commonly used by the forging firm, will provide a more realistic performance value. The composition of the alloy according to British Standard BS 1474 is :

H.E. 30	Al	Cu	Mg	Si	Fe	Mn	Zn	Cr	others
composition percentage	Rem.	0.1	0.5 _{1.2}	0.7 _{1.3}	0.5	0.4 _{1.0}	0.2	0.25	0.2

A preliminary metal testing program which involves the determination of (1) a suitable specimen size so that plane strain condition can be maintained, (2) the choice of suitable grid size, (3) the absence of any other

metallurgical side effects, is carried out. It was found that when the length to width ratio is over four, the longitudinal spreading of the metal in the centre section is negligible. When the capacity of the compression machine is considered, the specimen size chosen is of $\frac{1}{2}$ x $\frac{1}{2}$ inch (1.27 x 1.27 cm.), cross-section and 1 inch (2.54 cm.), long and two specimens are fixed together to form a specimen of $\frac{1}{2}$ by $\frac{1}{2}$ inch (1.27 x 1.27 cm.) in cross-section and 2 inch or (5.08cm.) long.

One major obstacle during the preparation of the specimen is the grain size of as-received Aluminium alloy. Because of the orange peel effect which adversely affects the accurate grid measurement, the alloy of the same material has to be cold worked (by compression) to over 50% in three principal directions so as to reduce the grain size. Standard annealing then follows in a salt bath maintained at 400°C for 20 minutes, and then the specimen is cooled slowly in the furnace. The metal is then machined to the required dimensions. The grain size is found to have greatly reduced to a workable size and the orange peel effect is minimised. The end faces are then polished ready for grid printing.

8.2.2 Preparation of the checker board (Master grid)

At the beginning of the project, a decision was made on the choice of experimental technique to measure the finite strain on the cross-section of the specimen. A checker board pattern with black and white squares is preferred to scribing grid lines. The reasons for the use of a checker board are that (1) the line of a grid line has a finite thickness and it may vanish after severe deformation and that may be detrimental to the

measurement, (2) the contrast of a black and white square gives a better and easier measuring alignment, (3) a more contrasted deformed print, (4) stress concentration is eliminated.

In order to make this kind of checker board grid, a master board was made. A piece of white formica was fixed onto a wooden board measuring $2\frac{1}{2}$ feet square. Then the white formica sheet was painted with a black ceramic paint. The choice of this paint is because of its brittleness when dried and the ease with which it can be scraped off. The painted formica board is cut with an extremely fine knife edge both horizontally and vertically making 100, $\frac{1}{4}$ inch (0.63cm.) squares on each side of the board and altogether 10,000 squares. Then the paint in alternative squares is peeled off with ^a fine chisel. This laboriously finished checker board is shown as in Plate P1. The master grid is taken to the university visual aid department for photographs. The final negatives are in five different square grid sizes : - (1) 0.026 in. (0.66m.m.), (2) 0.021 in. (0.53m.m.), (3) 0.016 in. (0.4m.m.), (4) 0.007 in. (0.17m.m.), (5) 0.004 in. (0.1m.m.), their variation in dimension is found to be less than 4% of the above mentioned value. After several preliminary experiments, the optimum size is chosen so that at over 60% reduction in height, the sides of the grid do not bend. In other words, if the sides of the grid become curved, it means that the square circumscribed by the sides can no longer represent a homogeneous deformation field and the deformation in this square is non-linear.

8.2.3 The printing technique

A. Equipment and chemicals.

- (1) A rig for the photographic printings is used for producing repeatable grids and for locating the specimen in close contact with the negative.
- (2) A centrifuge — An old record player with rotating speed at 120 r.p.m. is used to spread and dry the photo-resist evenly on the surface of the specimen.
- (3) Ultra-Violet lamp or U.V. lamp. A U.V. lamp with wave length 3650 Å supplied by Griffin Co., is connected with a choke to expose the undeveloped photo-resist.
- (4) Chemical used.
 - (a) Kodak printed circuit resist — a solution of resin in an organic solvent which becomes light sensitive when dried.
 - (b) Kodak printed circuit resist thinner — used to dilute the solution.
 - (c) Kodak printed circuit dye developer — for dissolving the unexposed area of the circuit resist and for colouring the exposed area.

B. Printing process.

The chosen grid size, 0.016 inch or (0.4m.m.) is printed on the polished surface of the specimen. The procedure of printing^{is} as follows : -

- (1) The surface of the specimen is cleaned with carbon tetrachloride.
- (2) The Kodak circuit resist and Kodak resist thinner is mixed in 4 to 1 ratio by volume. The mixture is spread on the specimen surface.
- (3) The coated specimen is placed in the centrifuge for drying.
- (4) The coated specimen is located onto the specially designed rig for printing.
- (5) S.A. weight is put on top of the specimen. This is to ensure that the coated face and negative are in direct contact so that a good sharp contrasting print can be obtained.

- (6) The specimen is exposed to the Ultra Violet light for about $4\frac{1}{2}$ minutes.
- (7) The exposed specimen is placed in a bath developer for about 60 seconds \pm 10 seconds during which time shaking of the specimen is desirable.
- (8) The specimen is taken out and carefully rinsed with water.
- (9) A fan blower is used to dry the specimen.

8.2.4 Experimental procedure

- (1) The testing machine -- A 50 tons (500 KN.) capacity Denison universal machine is used for loading the sub-press and a fixture is attached to raise or lower the sub-press.
- (2) The sub-press-- A cast steel sub-press made to specification by Colley Brothers (Tools) Ltd. The use of the sub-press is to ensure uniform and parallel travel of the two opposing platens. Plate P.2. Two pairs of dies were made. One pair is made to a ground smooth surface finish of (0.42 micron) so as to carry out lubricated experiments. The other pair is a machine-finished (4.5 micron) die to simulate rough sticking frictional conditions. Both of these dies are made of special tool steel and heat-treated.
- (3) Measuring microscope -- A travelling microscope is used which can measure down to \pm 0.0002 inch or (0.005m.m.) . The microscope is made by Scientific Instrument and the model is a Pye travelling microscope model no.6147.

- (4) Preliminary material test -- These tests involve the choice of a suitable ductile but commonly used metal, the optimum size of the grid squares and the die set alignment. The first and the second parts of these tests were described in the previous section 8.2.1 except the last test which is to test the alignment of the dies. Dial gauges were fixed on the die faces to check the parallelism between the two opposing faces during compression. See (fig.8.1). Again, dial gauges were fixed to the side faces of the moving die to ensure that lateral movements did not exist. These tests are essential as they may affect the deformation pattern in the final product.
- (5) The upsetting experiment --The experiment to investigate the metal flow consists of two parts, one is the upsetting of a **rectangular prismatic** specimen to 50% reduction in height with a rough die set. This is to simulate a rough frictional upsetting process and at every successive 10% reduction in height, the specimen is taken out and the changed co-ordinates of the grids are measured. The other series of experiment is to simulate lubricated conditions in which the machine ground die set is used. PTFE sheet is used as lubricant between the die and the work piece. At every stage, the same quarter section of the specimen is viewed under the microscope and the changes in co-ordinates with the reference axis (the reference face is the contact face of the specimen) are recorded. Owing to the large number of squares involved, it was decided that alternative squares only are measured.
- (6) Symmetry tests -- As there are nearly 1600 squares in the whole specimen and if only half of them are measured, the tedious measurement is too laborious, so a simplification is necessary. Since the specimen is

assumed to be symmetrical along the two axes, i.e., the x-axis and the y-axis, only a quarter of the original squares are required to be measured. So, there are about 1600 readings to be taken for each stage of reduction in height. In order to make sure this symmetry assumption is valid, several squares in each quadrant are measured and their calculated values are compared to check for symmetry. Their variations are found to be less than 5% in terms of strain at 50% reduction of height. But, for the lubricated series, the strain measured in each quadrant is found to have varied around 10% about the mean at 50% reduction in height.

8.2.5 Analysis of data

First, the co-ordinates of the grids are recorded on data cards and the state of strains, principal angle of the deformation the degree of rigid body rotation and the effective strain are computed by the digital computer. Since the specimen is deformed under the assumed plane strain condition, i.e. one of the three principal strains is zero and the absolute values of the other two are equal, the state of strain can be represented by one value. If this is a coaxial strain path, it will be a radial path at 5 o'clock on the triangular co-ordinate as explained in section 4.2.1. but, when all the history of the deformation is computed, it is found that the non-coaxial path is pre-dominant. The plane strain radial non-coaxial path can be plotted as in (fig.8.2) where β is the angle of non-coaxiality of a particle at different stages of reduction. The calculated state of strain and principal direction are plotted and the best fitted polynomial curve is chosen by means of the least square method. The curve fitting is carried out by a

HP 9830 desk mini-computer. For every square measured and their state of strain plotted, a polynomial curve is fitted and the coefficient for each strain path is punched on data cards. Another program is developed to calculate the velocity field, the rate of strain and its principal directions by the ICL 1905E digital computer. These computed results are used for further analysis and the graphs plotted are represented in later chapters.

8.3 Experimental method for the investigation of the filling characteristic

8.3.1 The specimen and its preparation

For this kind of investigation, a ductile metal, Aluminium, is chosen. The most convenient ductile Aluminium is E1C and its composition according to BS : 1474 standard is : -

E1C	Al	Cu	Si	Fe	Mn	Zn	Note
Composition percentage	99.0	0.1 max.	0.5 max.	0.7 max.	0.1 max.	0.1 max.	Cu + Si + Fe + Mn + Zn = 1%

Round bars of diameter $1\frac{1}{2}$ inch (3.81cm.) are bought from the retailer.

They are machined to the required dimensions of height to diameter ratio of 2.0, 1.8, 1.5. A centre hole is made for locating the specimen in the centre of the die cavity. The right location of the specimen in the centre of the die cavity is essential as a slight misalignment will make one side of the specimen touching the face of the cavity earlier than the other side of the specimen. The machined specimens are annealed by heating them to

360°C in a blow fan air furnace for 20 minutes and cooled in the furnace. They are marked and ready for testing.

8.3.2 Equipment (22)

- (i) Press and die set --The same Denison Universal testing machine is used as in the previous experiment.
- (ii) Sub-press -- A different sub-press is chosen for this particular purpose. Plate P.3, the press was purchased from an outside factory and machining was done to accommodate the dies. The ram with its hemispherical head, so as to provide a certain degree of self alignment, was connected to the top platen of the Denison machine.
- (iii) Dies -- All the dies and other equipment were made from a $5\frac{1}{4}$ inch (13.3cm.) diameter bar of high carbon-chromium steel supplied by Wrighton & Co. Ltd. of Birmingham. The dies were made to the dimensions of 1 inch (2.54cm.), $1\frac{1}{2}$ inch (3.81c m.) and $1\frac{3}{4}$ inch (4.45c m.) diameters. After machining, they were hardened by soaking in a furnace at 970°C for one hour and then oil quenched. Quenching was then followed by heating the dies up to 220°C for 30 minutes and cooled. The hardness achieved was around 60 Rockwell C. After heat treatment the parts were ground and polished to the finished dimensions as in plate P.3.

8.3.3 The forging procedure

The specimen is located in the centre of the die cavity by means of a location pin. A thin smear of carbon suspended grease is put between the die/specimen interface. The specimen is then compressed to the required height and taken out for measurement. Another specimen is similarly deformed but to a larger reduction in height. This is carried out until the die is

finally closed. Then, another series of experiment is repeated with different height to diameter ratios of the specimen.

8.3.4 The measuring procedure

The deformed specimen is degreased by means of carbon tetrachloride. The surfaces of the specimen which are in contact with the die face are traced onto a piece of paper by means of inking the contact area. This contact area is then measured with a planimeter and recorded.

8.3.5 Computation of data

This data is used for computing the filling coefficient and the spreading characteristic of a closed die forging process.

PART B

Discussion of Results

clan script

CHAPTER NINE

The Distribution of Deformation

under Continuous Loading

9.1 Introduction

Simple upsetting, which is the beginning of every forging process, has been studied closely in the past decade. Several theoretical predictions by Altan, Hill, Green, Lee, Kudo and Johnson (45,43,44,46,52,26) as well as experimental investigations such as those by Kudo, Lee and Kuhn, Thomason (47,54,81,72) have been carried out. The past investigations are either experimental studies concentrated on the deformation of the surface elements, neglecting the deformation pattern in the cross-section, or theoretical predictions based on simplified and unrealistic assumptions. Under this state of uncertainty and misunderstanding in the forging process, a better criterion has to be developed to represent and study the degree of deformation in the forging.

As has been explained in the introductory chapter, the representation of the degree of forging by reduction in height is both vague and unrealistic. Thus, the analysis of large deformation, developed in Part A of this thesis, is the proper tool to study the deformation in a specimen. With the recognition that the deformation in a specimen is a point function, it is more realistic to talk about a deformation field or distribution of deformation than to talk simply of deformation. Once deformation is analysed from point to point, a pattern of distribution of deformation will emerge. Every forging can be analysed in this way because in it there must be various points and at each point, there is a particular deformation, and their resultant deformations will collectively produce a pattern of distribution of deformation. This chapter is wholly devoted to the study of the various elemental deformations and their resulting pattern of deformation field.

9.2.1 The development of the pattern of distribution of deformation under continuous loading

Following the above argument that the deformation of a specimen is a point function, the resulting deformation pattern can be seen as a record of how the various elements are deformed during the process. Apart from the ideal reduction process in which every element is deformed similarly and coaxially, a specimen compressed between a pair of dies will have some portions of the specimen deformed more severely than others. This non-uniformity in the deformation of the various elements in the specimen will produce a non-homogeneous deformation pattern. In this project, in order to study the non-homogeneity of deformation in forging, square grids are printed on the cross-section of the ~~rectangular~~ ~~prismatic~~ specimen and these grids are used to analyse the deformation pattern on this plane. Since the deformation perpendicular to this plane is found to be negligible in our experiments, plane strain condition is assumed.

If the deformation is non-homogeneous under loading, the square grids printed on the cross-section of the specimen will display various degrees of distortion as shown in Plate P. 4 in which the specimen was compressed down to over 60% reduction in height and nonsymmetrical deformation to both x- and y-axes of the specimen appeared. Some squares will transform to rectangles or rotated parallelograms while the remaining squares maintain nearly their original shape -- squares. As a minute square is used to represent a small homogeneous deformation field in a particular position, the opposite sides of a deformed square should remain parallel. The development of the square

grids on the deformation plane can be seen from (fig.9.1 to 9.4) in which a specimen is reduced in height to different levels between a pair of unlubricated dies. The most severely distorted grids can be found to concentrate along the diagonal of the specimen. The flow lines of a few particular elements are shown in (fig.9.5).

Lubrication at the tool/work interface tends to reduce the shearing strain within the specimen. Thus, a set of less severely distorted grid patterns can be seen in (fig.9.6 to 9.9) when compared to those distorted grid patterns in (fig.9.1 to 9.4). Again, the flow of a few particular elements for this lubricated process are shown in (fig.9.10). A comparison of the distorted grids between the two processes can be seen in (fig.9.11^{a&b}). If enough lubricant is added at the tool/work interface, uniformly distorted grids will result. In other words, the deformation will be a homogeneous one.

9.2.2 The principal directions of the finite strains

In the past, deformation of a specimen ~~was~~ represented in general terms by the reduction in height. Apart from an ideal reduction process, this measure neither represents the real deformation within the specimen nor the nature of the directions of the deformations. The analysis of large deformation developed in Part A is, therefore, most suited to the study of deformation of a specimen in a thorough and realistic way.

Once the deformation is non-homogeneous, in other words, the deformation varies from point to point, the principal directions of deformation at

different points will not be in the same general direction. The non-alignments of principal directions are mainly caused by the fact that different elements pursue their own deformation paths. Owing to the fact that the deformation is non-uniform, some elements are deformed in a non-coaxial manner, i.e., the principal directions of deformation rotate with respect to the material during loading. The resulting principal directions of deformation of the various elements in the specimen will be as shown in (fig.9.12a and fig.9.12b).

9.2.3 The development of the zonal patterns

In pursuing the above argument that the deformation of a specimen is a point function, the state of deformations in any position should not be the same. By applying the analysis of large deformation developed in Part A of this thesis, the deformation, which is measured by the effective strain, along the tool/work interface of both a lubricated and unlubricated specimen are found to be unequal as given in (fig.9.13 and 9.14). The differences in deformation from point to point in the specimen show another defect in the representation of the degree of forging by the reduction in height, in which a homogeneous deformation is implied.

In proceeding further with the analysis, the deformation of the various points or elements in the specimen can be represented by the deformation intensity factor Γ , which is equal to the sum of all the incremental strains taken along the strain path. The detail definition of this quantity is given in section 5.3. The usefulness of this factor is shown by the fact that this scalar value is the measure of the extent of

deformation along the strain path taken by the element. In contrast, the effective strain, commonly used by other researchers to represent the deformation, is just the state of strain in which the history of deformation is neglected. With the effects of non-coax^aility and varying strain ratio taken into account, the actual deformation can only be measured by the intensity factor Γ in the analysis of large deformation.

Contour maps with lines of equal deformation intensity factor and plotted on the actual cross-section of the specimen can reveal the current deformation pattern. With the exception of the homogeneous deformation, actual deformation of a specimen will display a pattern in which some areas are deformed more than the others. If this pattern is drawn on a three dimensional diagram, it will look like a section of a geographical region which consists of mountains and valleys. Examples of these three dimensional deformation maps are shown in (fig.9.15 to 9.18). In terms of deformation, the appearance of plateaus and valleys will signify that the deformation is non-homogeneous and the plateaus represent severe deformation regions while the valleys show that the metal is hardly deformed. The plateau regions are commonly called the shear zones and the valleys are termed the dead metal zones. In fact, this is exactly what happened when a specimen was compressed between a pair of unlubricated dies as shown in (fig.9.19 to 9.22). Lubrication at the tool/work interface will just either shift the orientation of the plateau region or diffuse the distinction among the various zones as in (fig.9.23 to 9.26).

The two loading curves shown in (fig.9.27) can be seen to consist of three stages. These three stages are : -

- (i) metal deformed elastically,
- (ii) the establishment of plastic deformation sites and lastly
- (iii) the widening of the plateau regions.

9.3 The distinction of deformation zones in terms of the behaviour of the zonal elements

9.3.1 Introduction

The application of the analysis of large deformation in a compressed specimen has, so far, proved that an actual deformation field is a highly non-homogeneous one both in severity and in character. In addition, the deformation field is, in fact, divided broadly into two types of deformation zone — the shear and the dead metal zones. It can be seen immediately that the use of reduction in height as a measure of the degree of forging is far from being adequate.

The use of this analysis of large deformation is not for the purpose of showing simply that the deformation is non-uniform. The analysis is necessitated by the need for a thorough study in depth of the deformation process. Furthermore, this method of analysis reveals some aspects of the process that ~~no other~~ the researchers have ^{not} found. This is the individual behaviour of the zonal elements which collectively determine the pattern of the deformation field. Therefore, the following section is an extension of the analysis on the deformation field of a specimen.

9.3.2 The path characteristics.

A strain path is a record of deformations which a particular element has experienced. In section 4.2, the difference between a coaxial and a non-coaxial path has been explained. Under triaxial strain conditions, a non-coaxial path is a space curve as that in (fig.4.6). In our experiments, plane strain conditions are assumed and a two dimensional curve as in (fig. 4.8) can be used to represent the history of the deformation because one of the principal strains is equal to zero. With the exception of an ideal reduction process, any non-homogeneous deformation process will produce various individual strain paths according to their locality in the specimen.

9.3.3 The behaviour of strain paths in different deformation zones.

In the last section, two types of deformation zones have been established. They are (i) the shear zones and (ii) the dead zones. In fact, when the contour maps are looked into more closely, the two types of deformation zones can be seen to be located in five different areas. If the deformation of a typical element from each of these zones is studied by the method of large deformation analysis, the difference in the magnitude of deformation and the principal directions of deformation among the various zonal elements can confirm that the first type is the shearing zone and there are three areas in which this type occurs. The strain paths in zone (1) in (fig.9.28 and 9.29) are essentially nearly coaxial paths which means that the principal directions of deformation are fixed with respect to the material. Zone (2) is the corner zone in which the deformation is quite severe but the principal direction of deformation has been rotated through its history, sometimes in a positive and sometimes in a negative sense -- here positive means

anti-clockwise direction and vice versa. Zone (3) is the central shearing zone, and owing to the shearing process in this region, the path is characterised by a large deformation and the principal directions of deformation have been rotated during the process.

The second type is the dead metal zone. As the name implies, these regions are scarcely deformed. Zone (4) and (5) are regions belonging to these zones in which the strain paths are of low magnitude of deformation and their principal directions of deformation are only slightly rotated.

9.3.4 Curvature of the strain path

A. Co-axial path.

As suggested in section 6.2.2, the extent of deformation of a curved co-axial path B and the radial coaxial path A as shown in (fig.9.30), are quite different. Thus, the work done per unit volume for these paths are :-

for path A, the work per unit volume for a perfectly plastic material is equal to

$$W = \sigma_0 \bar{\epsilon}$$

and for path B, the work is equal to

$$W = \sigma_0 f \left(\frac{1}{\rho}, \bar{\epsilon} \right)$$

where σ_0 is the yield stress

$\bar{\epsilon}$ is the effective strain

ρ is the equivalent radius of curvature as defined in section 6.2.2.

f represents a function.

It can be seen that the work done by the curved coaxial path is a function of the curvature of path and the effective strain. When the path is radial as path A in (fig.9.30), the function $f\left(\frac{1}{\rho}, \bar{\epsilon}\right)$ will simply be equal to the effective strain $\bar{\epsilon}$.

B. The non-coaxial path

In the case of a non-coaxial path in the plane strain condition, a non-coaxial path can be represented on a two dimensional diagram as shown in (fig.4.8) and this non-coaxial path experiences more deformation than a coaxial path given the same finite deformation at the end. In contrast with the coaxial path in which the length of the path determines the extent of deformation, the length of the non-coaxial path as in (fig.4.8) does not represent the true extent of deformation because one of its axes, i.e., the non-coaxiality angle β ordinate, has no meaning in the extent of deformation. So, as explained in section 6.2.3, an imaginary path with its length equal to the extent of deformation which is represented by the deformation intensity value Γ , has been proposed. Furthermore, this path is assumed to be an arc of a circle with radius ρ and the length of the arc is equal to the deformation intensity value Γ . The effective strain $\bar{\epsilon}$ is equal to the chord inside the same circle joining the arc. Angle φ is equal to half the angle sustained by the arc of the circle. See (fig.9.31a). As derived in section 6.2.3, it can be seen that the radius of curvature ρ of this path is equal to

$$\rho = \frac{\Gamma}{2\varphi} \quad 6.10d$$

where Γ is the deformation intensity value

φ is half the angle sustained by the arc Γ .

Again, from section 6.2.3, the ratio of the effective strain $\bar{\epsilon}$ and the deformation intensity Γ is equal to the ratio of the sine of the angle φ and φ itself, i.e., equation (6.10).

$$\frac{\bar{\epsilon}}{\Gamma} = \frac{\sin\varphi}{\varphi} \quad 6.10c$$

where φ is in radians.

Therefore, if the ratio of the effective strain and intensity value is known, the angle φ can be computed from the upper curve in (fig.9.31b).

Thus, by projecting the known values of Γ and φ into the lower curves in (fig.9.31b), the intercept of these projections gives the radius of curvature of the path.

In ^{the} plane strain condition as in our experiments, a coaxial path is also a radial one and the curvature of the path is nil or in other words, the radius of curvature of the path is infinite. In contrast, the curvature of the non-coaxial path depends on the degree of non-coaxiality and it can never be equal to zero unless it is coaxial. So, in our results, a curved path will mean a non-coaxial path and the non-coaxiality is a function of the curvature of the path.

Fig.(9.32 and 9.33) show the radii of curvature of different strain paths in various zones as a function of the average reduction in height. It can be seen that all the non-coaxial paths have small radii of curvature. In contrast, the nearly coaxial paths have large radii of curvature.

9.3.5 Rigid body rotation of the zonal element

In section 3.2.4, it has been explained that deformation consists of a component of pure strain as well as a component of rigid body rotation (75). Both of these two components can be extracted from the deformation gradient \mathbf{F} of the deformation by polar decomposition as given in equation (3.23).

$$\mathbf{F} = \mathbf{R} \mathbf{U} \quad 3.23$$

where \mathbf{R} is the rigid body rotation matrix,
 \mathbf{U} is the right hand stretch matrix.

In fact, this rigid body rotation does not consume work and is a by-product of the neighbouring movements. The result of this bodily rotation of the element will affect not just the subsequent incremental strain directions, but also the spreading of the workpiece and the filling of the die cavity. Therefore, it is necessary to study the rigid rotation in a thorough way.

With an ideal reduction process, the various elements in the specimen will behave similarly so that a homogeneous deformation results. In contrast, a non-homogeneous deformation will produce zonal characteristics in rigid body rotation. In zones other than the corner zone and those near to the free boundary, the elements have rotated only moderately as can be seen in (fig. 9.34 and 9.35). In the corner zones, the elements are found to have rotated severely to more than 40° .

So, we can see that in a non-homogeneous deformation, the metal, encountering frictional constraint, will be forced to rotate bodily during

deformation instead of deforming uniformly. The degree of rotation in regions near to the free boundary and the corner zones depends on the frictional constraint at the work/tool interface.

In our experiments, with sufficient lubrication at the tool/work interface, the elements in the corner zones have rotated half the amount as compared with the same elements deformed without lubrication. In other words, friction existing along the interface will encourage the elements in the corner zones to rotate bodily, as shown in (fig.9.36).

The rigid body rotation of elements near to the free boundary have been found to have contributed to the barrelling of the specimen. With lubrication at the interface, the rotation is less severe than the specimen deformed without lubrication and thus, the bulge is less pronounced as given in (fig.9.37).

9.4 The effect of lubrication on the deformation distribution pattern.

In the previous sections, it has been shown that the general patterns of deformation on the cross-section of the specimen are affected by the application of lubricant. In the following section, the effect of lubrication will be further explained in terms of the orientation of the deformation plateau, the deformation pattern and the behaviour of various zonal elements.

9.4.1 The zonal pattern and the orientation of the plateau.

When a specimen is compressed between a pair of lubricated dies, the friction at the tool/work interface will be reduced and thus the deformation will be

more homogeneous than the specimen compressed between unlubricated dies. Consequently, the increase in homogeneity of deformation will dilute the deformation and diffuse the zonal distinction up to the stage when there is no difference in deformation among the various zones, in other words, the deformation is homogeneous. The difference between the lubricated and unlubricated processes can be seen clearly when the two contour maps are compared for the same reduction in height as in (fig.9.46^{ab}).

Sometimes, lubrication will also delay or re-orientate the development of the deformation plateau. As far as the analysis has indicated, the deformation of a specimen compressed between unlubricated dies is concentrated on the same elements from the beginning of the forging process. The lubrication in the process dilutes the concentration of deformation into a wider area so that the difference between the peak and the lowest deformation is only half of the difference between the peak and the lowest deformation of the unlubricated specimen. Owing to the efficient dispersion of deformation in the lubricated process, ^a deformation plateau does not appear until lubrication breaks down. The plateau at this time emerges in a different position. These can be seen in the contour maps (fig.9.38 to 9.45) which are plotted on the original undeformed grid position. The deformation plateaus are shown on these coloured portions.

9.4.2 The effect of lubrication on the behaviour of the zonal elements

As in the previous section, the analysis has shown that lubrication diffuses the distinction of various zonal appearance. Any diffusion of the zonal

distinction means that the various zonal elements behave nearly similarly. In another sense, the path histories, the curvature of the paths and the rigid body rotations of the various zonal elements will tend to be similar, consequently, a nearly homogeneous deformation pattern will result. In our experiments, this is exactly what happens when sufficient lubrication is added at the tool/work interface. The paths are similar as in (fig.9.29) and the same for the rigid body rotation and the curvature of the paths. These similarities begin to change when lubrication breaks down.

9.5 Concluding Remarks

On the whole, this chapter gives a general description of what the reaction of the material is towards external forces. Apart from the ideal reduction process, two types of deformation zones can be distinguished in both the lubricated and unlubricated specimens tested in this project. In each type of deformation, further differences can be observed in the characteristics of the strain paths, the differences being related to the locality of the sites analysed. If distribution is made on the basis of these differences, then five sub-types of deformation can be observed. Thus, of the two main types, the 1st type is the shear zone, with three sub-types and the second is the dead zone with two sub-types.

Under continuous loading, the metal flow is mainly controlled by the outside boundary condition. Thus, as in the lubricated process, the dispersion of deformation is so efficient that concentration of deformation, which gives rise to the formation of deformation plateaus, does not appear until the lubrication has broken down. In contrast, the reverse will happen if

the outside constraint exists right at the beginning of the process. Some regions will be clearly underdeformed and an ever increasing portion is deformed further away from the average level. The existence of this rising plateau, if concentrated along a narrow band only, will be fatal to the success of the process as ~~cracks~~ cracks may appear in these regions. Unless a carefully lubricated process is devised so that the plateau is re-oriented to areas which can subsequently be machined away, concentration of plateau range is inevitable.

The inclination of the principal directions of deformation in each element which is determined by the lubrication existing along the work/tool interface, signifies whether or not the deformation is homogeneous.

The difference in the behaviour of elements in various zones in terms of path history, curvature of path and rigid body rotation are summarised in the following table 9. 1.

Table 9.1

Zone	Grouping	Path History	Radii of Curvature	Rigid Body Rotation	Principal strain direction
(1) Central zone	shearing zone	(i) Near coaxial (ii) Large magnitude of deformation.	(i) Large radii of curvature	(i) do not rotate	aligned with the x,y-axes of the specimen
(2) Corner zone	shearing zone	(i) Non-coaxial path	(i) small radii of curvature	(i) rotate vigorously during the process	have been rotated vigorously during deformation
(3) Central shear zone	shearing zone	(i) Non-coaxial path (ii) large magnitude of deformation	(i) small radii of curvature	(i) rotate moderately during the process	have been moderately rotated during process
(4) Right hand dead zone	dead zone	(i) Non-coaxial (ii) Small magnitude of deformation	(i) small radii of curvature	(i) rotate slightly	slightly nonaligned to the x,y-axes of the specimen
(5) Left hand dead zone	dead zone	(i) Non-coaxial (ii) Small magnitude of deformation	(i) small radii of curvature	(i) rotate slightly	aligned with the x,y-axes of the specimen

CHAPTER TEN

The Homogeneity of Deformation

10.1 General introduction

In the last chapter, the zonal development of a deformed specimen has been discussed initially, followed by a detailed analysis of the individual behaviour of elements in the various zones. Apart from being more precise and widely applicable, the analysis of large deformation has, so far, been demonstrated to be the proper tool to study forgeability. As argued in the introductory chapter of this thesis, the whole idea of forgeability hinges on the damage in strength through deformation. Since deformation is seldom homogeneous, the damage to the strength of the forging is also seldom uniformly distributed. So, the use of reduction in height as a measure to record the degree of forging by some researchers (58,68) can be seen at once to be unrealistic.

In the results presented so far, it can be seen that an actual deformation is non-homogeneous. In fact, the more the deformation deviates from a homogeneous one, — the more severe the differential is between the peak and the lowest deformation and the damage to the strength is further away from being homogeneous, so, the extent of the distribution of deformation or the homogeneity of deformation should be included in the consideration of the degree of forging.

In the following section, the homogeneity of deformation will be discussed. An idea will be proposed to quantify the deformation distribution in terms of a characteristic equation of homogeneity.

10.2.1 The criteria of homogeneity in deformation process

The distribution of deformation is found to be a continuous process in which the degree of homogeneity is varying. The changing homogeneity is governed by the following two criteria : -

- (i) The initial external condition will determine the initial homogeneity value.
- (ii) The continuously changing outside constraints coupled with the internally developed pattern, will determine the resulting homogeneity of deformations.

It can be seen that the formation of a non-homogeneous deformation pattern is a continuous process in which the deformation pattern, determined by the outside constraint, keeps on changing with the varying outside environment till its final terminal pattern is established.

10.2.2 The meaning of homogeneity

In order to study the deformation pattern on a comparable basis, the dimensionless deformation distribution histogram developed in Chapter five is applied. In a homogeneously distributed deformation, every elements in the specimen attains the same degree of deformation and the distribution curve of the deformation is a horizontal curve at the top of the dimensionless histogram. Thus, any non-homogeneous deformation will change the curve into one below that horizontal line. So, the homogeneity value can be defined as the ratio between the total actual deformation W_a and the total peak homogeneous deformation W_T and is equal to

$$\xi = \frac{W_a}{W_T} = \int_0^1 \left(\frac{\Gamma_a}{\Gamma_T} \right) d \left(\frac{a_a}{a} \right) \quad 10.1$$

where Γ_a is the actual deformation intensity

Γ_T is the peak deformation intensity

a_a is the actual area

a is the total area.

Therefore, the homogeneity value will be equal to one for a homogeneous deformation and less than one for a non-homogeneous deformation.

10.2.3 The characteristic equation of homogeneity

In section 10.2.1, it has been suggested that every upsetting process has its own characteristic distribution of deformation which is conditioned by its own initial stage and varies according to the changing external environment. Thus, the homogeneity of deformation is a function of the process parameter $\bar{\gamma}_e$ which is the reduction in height and is equal to

$$\xi = \xi_0 + f(\bar{\gamma}_e) \quad 10.2$$

where ξ_0 is the initial homogeneity value,

f is a function.

The first term on the right hand side in the above equation (10.2) is the initial homogeneity value. It is the projected homogeneity value for a particular process in which the pattern of distribution of deformation is assumed to have been established right at the beginning of the deformation by the outside environment. This projected value is a constant in a

particular deformation process. So, for a virgin material, when the load acts on the specimen, the initial homogeneity value can be any value depending on both the initial frictional condition at the tool/work interface and the subsequent deformation patterns. For a pre-forged specimen, the new initial homogeneity value for re-forging will be the previous final homogeneity value plus the effect of the new initial deformation. The new value can never be equal to one unless both the previous pre-forging and the new deformation are homogeneous. The second term is a function of the process parameter $\bar{\gamma}_e$ and by differentiating the equation, we can get the following : -

$$\frac{d\zeta}{d\bar{\gamma}_e} = \frac{df}{d\bar{\gamma}_e} \quad 10.3$$

The differential of the homogeneity equation indicates the trend of the deformation distribution of the process.

10.2.4 Some aspects of the homogeneity of deformation

Apart from upsetting between flat and parallel platens, absolutely homogeneous deformation is not even geometrically possible. In any actual forging process it is, for obvious reasons, advantageous to achieve as nearly homogeneous deformation as possible. It is, therefore, interesting to investigate the factors which favour homogeneity of deformation.

If the stress is always homogeneous throughout the workpiece, the deformation must be homogeneous. Friction causes non-homogeneity of stress, hence, the higher the friction, the less homogeneous the deformation.

On the other hand, the non-uniform distribution of the flow stress in the material due to work-hardening improves homogeneous deformation distribution. Take an example of two materials, A and B, subjected to the same forging process, where A is very highly work-hardening and B is hardly work-hardening at all. When non-uniform strains are developed in B, the flow stress remains constant, so that non-uniform deformation continues to develop under the heterogeneous stress conditions. In contrast, as soon as non-homogeneous strain develops in material A, the flow stress becomes very uneven so that the deformed parts require much higher stresses for further deformation and the relatively undeformed parts will flow much more easily. Thus, even under non-homogeneous stress conditions, the deformed parts will cease to flow until the relatively undeformed parts are also work-hardened to somewhere near the same level of hardness as the parts already deformed. In other words, deformation will tend to be dispersed.

10.2.5 The homogeneity of deformation in upsetting processes

The dimensionless deformation distribution curves are used to show the distribution of deformation at various reductions in height on a comparable basis. When the deformation is nearly homogeneous, the distribution curve will be a curve near to the straight horizontal line of the homogeneous deformation. The dimensionless distribution curves for the deformations with or without lubrication are shown in (fig.10.2 and 10.1) respectively. It can be seen immediately that there are two distinctive trends in the changes in shape of the distribution curves under continuous reduction in height.

In the first diagram, (fig.10.1), the area beneath the curve increases with the reduction in height. On the other hand, the latter graph, (fig.10.2), shows the reverse trend, i.e., the area decreases with the increase in reduction in height. Since, the area beneath the distribution curve indicates the degree of homogeneity, the unlubricated process as shown in (fig.10.1), shows that the deformation starts off with a low homogeneity value, in other words, the deformation is severely non-homogeneous. But, as the deformation proceeds, the degree of homogeneity improves. On the contrary, lubrication at the tool/work interface produces a high initial homogeneity value. But, the gradual decrease in the value indicates that the deformation becomes less homogeneous than before. This reduction in the degree of homogeneity also coincides with emergence of the deformation zones as shown in (fig.9.18). The two different trends for the two deformation processes are summarised in (fig.10.3) which shows the homogeneity value as a function of the reduction in height.

10.3 Concluding remarks

All throughout the chapter, it has been demonstrated that an actual deformation can hardly be homogeneous and so is the damage to the strength of the forging. Therefore, the distribution of deformation in the specimen has to be included when considering the degree of forging. The distribution of deformation in a specimen was represented by the homogeneity value suggested in the last section. This homogeneity value is a function of the process parameter $\bar{\gamma}_e$. Apart from the ideal homogeneous deformation in which the homogeneity value is equal to one, all the other

deformations will have the homogeneity value of less than one. It can be seen that the smaller the homogeneity value, the larger the differential between the peak and the lowest deformation in the specimen and the zonal development is more distinct than the deformation with a larger homogeneity value. So, more severe damage to the strength of the forging will result with a low homogeneity value of deformation than the one with a high homogeneity value.

A work-hardened material by theory tends to improve the homogeneity of deformation under continuous loading even though the stress distribution is non-uniform. On the contrary, the flow stress of the non-work-hardened material remains constant, so that, non-uniform deformation continues to develop under the heterogeneous stress condition.

CHAPTER ELEVEN

Redundant Work and Redundant Deformation
of a Perfectly Plastic Medium

11.1 Introduction

Engineers have, hitherto, talked about forgeability of metals in terms of fracture due to deformation, but, in fact, forgeability cannot be quantified by just looking for the appearance of cracks, as they may exist in areas which are inaccessible to all optical means^{of observation.} So, a new idea has to be found to relate the forgeability with the damage to the strength of metal through deformation. Again, damage is hard to detect and there are so many types of damage to the metal that none can be used alone in defining forgeability. Therefore, the logical step is to find the deformation that the specimen has experienced. Actual deformation has been found to be non-uniform and so is the damage to the strength of the forging.

The old idea of representing the degree of forging by the reduction in height has to be dropped because of the non-homogeneity of deformation existing in most forgings. The analysis of small strains has also to be abandoned because the magnitude and directions of deformation in forging are of such a nature that the superposition of strains is impossible. So, the only proper route to the study of forgeability, via the damage to the strength by deformation, is by the analysis of large deformation.

With the application of the analysis of large deformation developed in Part A of this thesis, the deformation phenomena in the upsetting process have been studied thoroughly as given in the previous two chapters. Not only two types of deformation zones have been found; there are, in fact, five various zones and the zonal elements behave quite differently. So, it can be seen that the study of forgeability cannot do without the analysis of deformation zones which, in turn, determine the homogeneity of deformation

in a specimen. The latter is essential in representing the degree of forging, because any average value, such as the reduction in height, is a poor measure. The distribution of deformation represented by the homogeneity value of the deformation is important in the consideration of the degree of forging because a deformation with a low homogeneity value is bound to be more damaging to the strength of the forging than the one with a high homogeneity value, other things being equal. This is true because a low homogeneity value means that the deformation of a specimen is severely non-homogeneous and this extreme concentration of deformation encourages crack growth (65,69).

If the upsetting process is looked at from the point of view of work consumption, it can be seen that any extra work required to reduce the specimen to a lower level will produce one with more deformation than theoretically necessary. This extra amount of work may either be directed to deform those scarcely deformed elements in the specimen or to encourage crack growth in those already highly deformed elements. The former will cause the distribution of deformation to become more uniform while the latter is fatal to the forging. Therefore, the following chapter is devoted to the analysis of work done, the redundant work and the deformation dispersal efficiency of the processes.

11.2 The total work done in upsetting process

11.2.1 Deformation distribution curves

Many engineers (70,^{51,87,58}5) assume that the work consumed in deforming a specimen is a simple function of the reduction in height. Since an actual deformation

is found to be never homogeneous, the total work done can never be a simple function of the reduction in height alone. It should be, in fact, equal to the sum of all the work done by every element in the specimen, in which the individual degree of deformation is not the same. In our analysis as suggested in Part A, the extent of deformation of an element can be represented by the scalar value called the deformation intensity factor Γ and it is used extensively in the last two chapters. For a perfectly plastic material, the dimensionless work is equal to the deformation intensity factor Γ , assuming the constant flow stress to be unity. When all the deformations of every element are plotted against the percentage of area occupied, a deformation-distribution-histogram can be derived. It can be seen immediately that any non-uniformity in deformation will change the shape of the deformation distribution histogram. A homogeneous deformation means that, the deformations of every element are the same and on the histogram, the distribution curves will be just horizontal straight lines. Any non-uniformity in the deformation of the specimen will be reflected as a change of shape of the distribution curve from horizontal lines. Figs(11.1 and 11.2) are deformation distribution curves of the lubricated and unlubricated processes. It can be seen that the lubricated process produces a flatter distribution curve than the unlubricated process.

11.2.2 The work done on a perfectly plastic body

By what is said in the above paragraph, deformation intensity varies from point to point and can be plotted in a histogram. Since the work done on a perfectly plastic material, as developed in section 6.1.1 is equal to

$$W = \sigma_0 \int d\Gamma$$

the dimensionless work done per unit volume, A , is then equal to

$$\begin{aligned} A &= \frac{\overline{\sigma}_0}{\sigma_0} \int d\Gamma \\ &= \int d\Gamma \end{aligned}$$

where $\overline{\sigma}_0$ = yield stress

Γ = deformation intensity

and it means that the dimensionless work done per unit volume will vary according to the deformation intensity value. Therefore, the total dimensionless work will be equal to the area beneath the deformation distribution curve. It can be noticed that every process will consume a certain amount of energy and, for the same reduction in height, different processes will consume different amounts of energy. Again, here, the use of the reduction in height as the sole representation of the degree of forging can be seen to be inadequate. For the work done by different processes, represented by the reduction in height in which homogeneous deformation is implied, will be the same. The limitation in using a poor measure to represent the degree of forging, which leads to the subsequent wrong conclusion in work consumption, has been perpetuated in the past. In fact, the old idea of relating the reduction in height with forgeability is very much vulnerable to the change in shape of the deformation-distribution curve. As given in (fig.11.3), it can be found that the work done for the same reduction in height depends on the outside constraints that the specimen has experienced. The discrepancies in work consumption from the homogeneous deformation depend on the nature of the distribution curves. In (fig. 11.3), one thing stands out in that the work done by a piece of perfectly plastic metal, compressed between a pair of lubricated dies, has been found to be less than the work consumed by the homogeneous deformation.

This observation is found to have contradicted the general belief that the ideal process is the most efficient process and consumes the least amount of work. But, these apparent discrepancies may be due to the following two reasons. The first reason is what most researchers did in concluding that the ideal process is the most efficient, is that the processes they have investigated are deformation processes in which deformations are restricted in all directions, such as the extrusion process. Whereas, in ^{the} free upsetting process, the restriction is one degree only. So, an ideal upsetting process, in which every element is deformed similarly, may not be as efficient as the lubricated process in which some elements take most of the load and the remaining regions are deformed less than the average deformation. The second reason is the hypothesis made in assuming that the metal behaves in a perfectly plastic manner and this theme is explained in more detail in the following section.

11.2.3 The effect of strain hardening on the total work done

In Chapter six, we assumed that the metal behaves as a perfectly-plastic body and with that assumption, a dimensionless work can be derived. If, however, strain hardening is taken as the actual behaviour of the metal, then the effective stress will be equal to : -

$$\bar{\sigma} = g (\bar{\epsilon}) \quad 11.1$$

where $\bar{\sigma}$ = effective stress,

$\bar{\epsilon}$ = effective strain,

g is a function,

and the work done per unit volume of an element will be : -

$$W = \int g (\bar{\epsilon}) d\bar{\epsilon} \quad 11.2$$

As shown in (fig.11.4), the work done on a perfectly-plastic-element, equal to area A, is less than the work done on a strain hardened element (A+B).

So, if the strain hardening effect is taken into the consideration of the work distribution histogram, the total work done will be higher than the work done by the perfect plastic material as given in (fig.11.5).

11.3 Redundant deformation and redundant work in a perfectly plastic body

Hill (27,25) and Richmond (14,66) have proposed the concept of redundant work by comparing the work done in the actual process with that in the ideal process. In the upsetting process, it can be seen that there are several ways to reduce the specimen to the same level of reduction in height, disregarding the shape of the side faces.

As suggested in section (11.1), any extra amount of work required to reduce the specimen to a lower height may be diverted either to act on those scarcely deformed elements thus improving the homogeneity of deformation, or to further the concentration of deformation which may lead to crack growth. So, the following section is the analysis of redundancy in both deformation and work and lastly of the deformation dispersion efficiency.

11.3.1 The redundant deformation and redundant work

As suggested in the above paragraph, there are several ways to reduce a specimen to the same level of reduction in height. So, the difference between the ideal total work and the actual total work is called the redundant work of the process.

The dimensionless redundant work for the perfectly plastic body is given by equation (6.13),

$$A_R = A_T - A_{iT} \quad 6.13$$

or

$$A_R = \int \Gamma_a d \left(\frac{a_a}{a_T} \right) - \int \Gamma_i d \left(\frac{a_a}{a_T} \right)$$

where A_R = redundant work,

A_T = actual total work,

A_{iT} = total ideal work,

Γ_a = actual deformation,

Γ_i = ideal deformation,

a_a = actual area occupied by the actual deformation,

a_T = total area.

In overcoming the outside constraints such as friction at the tool/work interface, more work is needed and so is the redundant work required. This is shown to be the case in (fig.11.6). As the ideal reduction process consumes more work than the process with lubricated dies, the redundant work so defined, is negative. See (fig.11.6). But, this trend tends to reverse at higher reduction in height which coincides with the emergence of the deformation plateau as in (fig.9.25 and 9.26).

The difference between the average total deformation and the ideal deformation is called the redundant deformation. Equation (6.13) gives the difference of the two amounts of work done in the process. Since the ideal deformation and the average total deformation Γ_{av} are constant, equation (6.13) can be replaced by

$$A_R = ((\Gamma_{av}) - \Gamma_i) \int d \left(\frac{a_a}{a_T} \right) \quad 11.3$$

where Γ_i is the ideal deformation

and the term inside the bracket $((\Gamma_{av}) - \Gamma_i)$ is the redundant deformation Γ_R .

Then equation (11.3) becomes

$$A_R = \Gamma_R \int d \left(\frac{a_a}{a_T} \right) \quad 11.4$$

and the redundant deformation is similar to the redundant work of the process. Fig.(11.6) shows the same curves as the redundant work but with a different ordinate. It can be seen that in order to reduce the specimens to the same height, some processes deform the specimen more than the other processes.

11.3.2 The efficiency of deformation dispersion

In Chapter six, it has been shown that the success of a process depends partly on how efficiently the deformation is dispersed throughout the whole body of the specimen. Hill, Richmond and Davernport (27,66,14) in analysing extrusion processes, have stated that the most efficient reduction process is the one in which the deformation is uniformly distributed, or the ideal process. The higher the efficiency of deformation dispersal, the better the process is in terms of work consumption. The lesser the work consumed, the less the likelihood of crack appearance, so that, severe concentration of deformation will be reduced. The efficiency of deformation dispersion developed in section 6.4.2 is repeated here, and the efficiency equation is

$$\eta = \left(1 - \frac{A_R}{A_{iT}} \right) \times 100\% \quad 6.14$$

where A_R = redundant work,

A_{iT} = total ideal work.

Fig.(11.7) shows the efficiency of the unlubricated and lubricated processes. It can be seen that the lower the efficiency; the higher the work consumed and the lubricated process is the most efficient process in achieving the same overall reduction in height.

11.4 Concluding Remarks

Once again, it has been demonstrated all throughout this chapter that the forgeability of metal or process is not a simple matter that can be handled by a single factor such as the maximum reduction in height. The use of this factor is fundamentally based on the tacit implication that the deformation is homogeneous.

In the last two chapters we have already concluded that an actual deformation can hardly be homogeneous. Zonal developments, their distinctive zonal behaviours and their resulting deformation patterns measured by a homogeneity value, are all parts of the natural phenomena revealed in our study. So, it can be seen that the work consumption of various processes can never be the same and the differences in work depend on the shapes of the deformation-distribution curves.

In our upsetting experiment, it has been found that the total work consumption is greatly influenced by the nature of the deformation distribution curve. The old concept of work consumption is related to the reduction in

height alone, is proved to be extremely vulnerable to the change in the shape of the deformation-distribution curves, or in other words, the homogeneity of deformation. For the same reduction in height, the work consumed by the unlubricated process is far in excess of the ideal as well as lubricated processes. In fact, it is the lubricated process which consumes the least amount of work.

The difference in work consumption for the same reduction in height by different extrusion processes have been suggested by Hill (27) and Richmond (66,14) and they are called the redundant work. In the upsetting process, the same term can be applied. It is found that a negative redundant work exists in the lubricated process in which the deformation is not uniform. In other words, a lubricated process produces a slightly non-homogeneous deformation and consumes an amount of work less than both the unlubricated and homogeneous deformation processes. The subsequent deformation dispersal efficiency which is the ratio of the amounts of redundant work to the ideal work, has also confirmed that the lubricated process is the most efficient one. This is contrary to the concept suggested by the above two pioneers, that the ideal homogeneous process should be the most efficient one. But, as we can see in ^{the} upsetting process, the boundary constraint is one degree only, (i.e. the reduction in height). Unless the deformation is restricted in every direction such as the extrusion process, in an ideal upsetting process, every element is deformed in the specimen and may not be the most efficient process in reducing the specimen to the same height. The amount of redundant work in the free upsetting process such as ours, may have caused the same **serious** side effects in the forging or the process

itself. Since an actual deformation can seldom be a homogeneous one, the extra work or redundant work, is most likely used in creating a severely concentrated deformation pattern as in the unlubricated process in our experiments. Any highly concentrated deformation regions are usually sites for crack propagation. In another words, the extra work consumed is used for encouraging the crack growth which can be seen in several research papers (69,65).

Die wear is another problem related to this redundant work. As suggested by some researchers (39,80,71) extra work required to overcome the friction at the tool/work interface must contribute to the abrasive wear of the forging dies. Since the work used to overcome the friction causes a considerable rise in ^{the} temperature of the dies and enhances the weakening of the surface material, the die life is reduced. So, redundant work is most undesirable because it shortens die life.

CHAPTER TWELVE

The Spreading and Filling

Characteristics

of the Forming Process

12.1 General considerations

Up to this chapter, we have discussed the significance of forgeability by means of studying the damage to the strength through deformation, in other words, the study of the distribution of deformation so that a degree of forging can be properly established. It has been demonstrated throughout every chapter so far that the searching **for** cracks is outdated and unrealistic and that the old idea of relating the degree of forging to the reduction in height leads very much to fallacy. On the contrary, actual deformations can hardly be homogeneous and the total work consumed by the deformation is never the same. In other words, processes conditioned by different environments such as friction at the tool/work interface, consume different amounts of energy and produce various deformation patterns.

One thing has been neglected in our discussion so far, and it is that the success of a forging process also depends on the successes of ^{the} spreading and filling of the die cavity. The modes of the changing outside boundaries of the workpiece to suit the rigid shape of the die cavity are the aspects that most researchers have missed in the study of forging. Neither an incompletely filled forging nor ^abadly filled forging with a lot of laps (folding holes) can be claimed to be a success. Since the aim of the project is to analyse the forging process in a thorough way, the mechanisms behind the success of a forging process and a better forgeability criteria, such as spreading and filling characteristics, have to be included in our investigation. Therefore, this chapter is totally devoted to the study of these two mechanisms.

12.2.1 The spreading phenomenon and the bulge profile of the specimen under continuous loading

Fig.(12.1) shows the spreading coefficient, as defined in Chapter seven , of the lubricated and unlubricated processes, as a function of average reduction strain $\bar{\gamma}_e$. This coefficient derived in section 7.1, is an indicator of how much the end face of the specimen has expanded as compared with the ideal spreading. It can be seen that lubrication at the tool/work interface has improved the sideways spreading of the metal initially, but the coefficient drops and settles at around 0.25 at higher reductions in height. In our results, the lubricant used has been exhausted early in the deformation process and this lack of further lubricant reduces the metal movement. In contrast, in the unlubricated process, the metal spreads nearer to the ideal spreading as described in section 7.1.2 when initial spreading restriction is overcome. This high spreading value is essential for the die designer who likes to have a quickly spread product without resorting to elaborate lubricating equipment.

It has been explained in section 7.1.5 that the bulge profile is influenced by the differences between the spreading of metal in the middle section of the specimen and the spread at the tool/work interface, provided the height to diameter ratio (H/D) of the specimen is less than two. (if $H/D > 2$, double barrelling will occur) If the difference in spread between the middle section and the top is positive, then the profile is barrel shaped and if it is negative, the bulge is in bollard shaped. The curves in (fig.12.1) have shown that the differences in the spread in

both processes are positive and thus the bulge profile is barrel shaped as shown in (fig.9.37).

12.2.2 The relationship between the two spreading mechanisms

In the past, it was assumed that the spreading process consists of sideways expansion of the end faces of the specimen only. Schey (87) and others (49) have found that spreading is not just the expansion of the end faces of the specimen. It also includes the folding of metal from the side face of the specimen.

In section 7.1.4, the spreading of the metal by the two mechanisms has been explained. These are the sideways expansion of the original end faces of the specimen and the folding of the side metal onto the contact faces. Their relative percentage magnitudes can be derived from the following equation : -

the percentage of sideways expansion of the original end faces, N, is equal to

$$N = \left(\frac{s - \mathcal{V}}{s} \right) \times 100\%$$

where s is the total spread coefficient defined in section 7.1.4.

\mathcal{V} is the folding coefficient defined in section 7.1.4.

Since the total spread of metal is made up of two processes, the percentage of folding M is then equal to : -

$$M = 100 - N$$

From the results obtained in our experiments, in an unlubricated process, the total spread of metal at the interface is caused mostly by the folding

of metal while the folding is less in the lubricated process. Fig.(12.2) shows the proportion of folding against the reduction in height of both the lubricated and unlubricated processes and it can be seen that at high reduction, over half of the spread is due to the folding of metal from the side face.

12.2.3 The effect of rigid body rotation on folding

In Chapter nine, it has been suggested that rigid body rotation of the elements in the corner regions has contributed to the folding of metal from the free boundary surface to the tool/work interface. It is anticipated that a vigorous rigid body rotation of those elements near to the free boundary and the corner zone will result in a high percentage of metal being folded onto the contact face. Thus, a smaller degree of rotation will produce a lower percentage of folding in the spread of metal at the interface. Fig.(12.3) shows the rigid body rotation of one particular element in the corner zone against the percentage of folding. It can be seen that a high rigid body rotation correlates well with a high percentage of folding in the frictional process.

12.3 The filling of the die cavity

In place of the reduction in height, it has been proposed to use the analysis of large deformation. The reduction in height has, as explained before, been thought of both as a strain and as a general measure of the degree of forging for the whole specimen. In the former sense, namely, a strain measure, it is now replaced by the analysis of large deformations. It is also necessary to find a more significant measure of the degree of forging for the workpiece as a whole. The measure proposed for this purpose

is the filling coefficient. If a forging is incompletely filled, it is treated as scrap and the process has failed. The coefficient is, thus, developed to indicate how near a forging is to its completion and how the various parameters influence the filling process.

For the sake of simplicity, an axisymmetrical, cylindrical forging is chosen for the investigation of the filling processes. As there are so many parameters affecting the process, some of them are isolated so that the effect of the others can be analysed more precisely.

12.3.1 The height to diameter ratio (H/D) of the specimen

The relationship between the H/D ratio of the specimen and the H/D ratio of the die cavity is essential in determining the spread of the filling process. As our experiment is concerned with ^{the} filling of a die of simple shape, cylindrical dies are used throughout the experiments. When the H/D ratio for the die cavity is one, the cavity will be filled quickly provided the H/D ratio for the specimen is near to one as in (fig.12.4).

In the figures (12.4 to 12.6), it can be seen that there are different rates of filling throughout the process. Before the specimen touches the side face of the die, the rate of filling is rather low and consists mainly of the spreading of the end faces of the specimen. But, after the specimen touches the side face, the rate increases quickly and the H/D ratio of the specimen plays an essential part in the speed of filling. So, it can be derived from these two distinctive rates of filling that if the die profiles as shown in (fig.12.7a and b) are to be filled by the same size specimen,

the one in (fig.12.7b) will be filled faster than the one in (fig.12.7a).

12.3.2 The effect of extra volume of metal

In all the results mentioned so far, the volume of metal of the specimens are within one or two percent of the exact volume of the die cavity. But any extra volume of metal has been found to have great influence on the filling process. Fig.(12.8 and fig.12.9) show the filling characteristic of specimens which have excess metal. It can be seen that the speed of filling **increases with** the amount of extra volume of metal in the specimen.

In(fig.12.10) are curves for the effect of any extra volume of metal in the specimen. Increase in the volume of metal has quickened the filling process irrespective of changes in H/D ratio of the specimen.

Therefore, if the amount of energy consumption of a forging is neglected, it can be said that an increase in the volume of the specimen will result in a quickly filled cavity.

12.3.3 The loading factor in the filling process

The load situation has not so far been discussed in the previous arguments. Nowadays, load required is one of the essential considerations which every die-designer has to consider. As the press capacity is equal to the peak load required to deform the specimen, any saving in maximum load requirement will mean the same amount of saving in press capacity. If the press has to provide more load than the forging required, then

the excessive load, according to several research papers e.g. (39,80), may contribute to ~~the~~ serious die wear problems. Therefore, a proper design of the forging will reduce the die wear problems and the choice of the right press size will provide an optimum usage of machines. Fig.(12.11 and 12.12) show curves of load against the filling coefficient of the forging process. It can be seen that a specimen with the same volume as the die cavity consumes the least amount of load in filling the die cavity. Practically, specimen with the exact volume as the die cavity is difficult to produce a completely filled forging. So some extra amount of volume is desirable.

It is shown in (fig.12.11 and 12.12), that the load rises slowly when the die is nearly filled, especially after the specimen touches the side of the cavity, but relatively rapidly in the early stages. (But the load rises sharply when the die is nearly closed.) The filling process consists of two stages, one, the spreading of the metal on the end faces and the other, the complete filling of the side of the cavity. As the load increases more rapidly in the early stage, and the early stage is just the filling of the end faces, it can be seen that more load is required to fill just the end faces than the filling of the sides of the cavity. See (fig.12.11 and 12.12). In addition, after the specimen touches the side of the cavity, the specimen with more metal will fill the die quicker than the one with the lesser amount of metal. Fig,(12.13) shows the summary of curves with the load plotted against the extra volume of metal with the H/D ratio of specimen varying from 1.5 to 2.0.

When complete die filling is not the principal criterion in selecting a process then ^aspecimen with the exact volume is ideal for minimizing the load.

12.4 Concluding remarks

Throughout this chapter, we have discussed the two essential phenomena in forging processes. The spreading of metal at the end face of the specimen is presented separately from the filling characteristic of a closed die forming process. The spreading has been found to consist of two separate processes. These are the folding of metal and the sideways expansion of the original end faces. The folding process has been seen to be the dominating mechanism in the spreading process. Lubrication reduces the proportion of folding in the spreading process, but over half of the spreading of metal in this lubricated process is due to the folding process. Rigid body rotation of elements near to the corner zone and the free boundary have been found to influence the folding process. Since friction encourages the rigid body rotation of elements in those regions, folding is also very severe in the unlubricated process.

The filling process which is the essential criteria in forging has also been studied with the aim of a better understanding of the process. The various effects of the process parameters are summarised in the following table (2.1).

Table 12. 1

SPECIMEN	EXTRA VOLUME	LOAD	FILLING COEFFICIENT
H/D Ratio			
constant	increasing	-----	quicker to fill the cavity
decrease	increase	-----	slow to fill
increase	-----	increase	for the same degree of filling
constant	increase	increase	for the same degree of filling
increasing	increase	-----	for the same degree of filling

NOTE : The H/D ratio of the die cavity is maintained constant.

CHAPTER THIRTEEN

Conclusions

CIEN SCRIPT

In the past, the use of the appearance of cracks on the surface of the forging was the sole criterion of forgeability. As described throughout the thesis the concept of forgeability is not as simple as is generally thought to be. This is because visible cracks in a forging are both misleading and difficult to define. It is misleading because cracks may have initiated from the inside of the specimen and those areas are usually inaccessible to optical means or observation. By the time cracks appear on the face of the forging, it may be already too late, as the visible cracks indicate that the forging is falling apart rather than that it has started to crack. It is difficult to define because the size of the visible cracks is hard to define, as cracks visible by eyes are different from those visible through the use of a microscope. So, the inaccuracy of the method coupled with the unsuitability of the appearance of cracks for defining the failure of a forging requires the development of other more widely applicable criteria.

The idea of relating the forgeability to the loss of strength through deformation is more realistic than that of standardising the means of detecting cracks. Since the loss of strength is a continuous and gradual process, a point must be chosen for any particular forging process beyond which a forging must not be deformed. This end point is determined by the minimum acceptable strength rather than by the crack size.

The end point defined by the limiting reduction in height is very unrealistic. To represent the degree of forging by the reduction in height has been proved throughout the past chapters to be inadequate. The use of this

measure implies that the deformation of the specimen is homogeneous. As revealed in Chapter nine, actual deformation can hardly be homogeneous, and ^{can} neither [^] the loss of strength. This non-homogeneity of deformation will affect the forgeability of metal in such a way that a highly non-homogeneous deformation will fail **more** easily than a homogeneous one, other things being equal. For the former represents a severely concentrated deformation in which crack growth and exhaustion of ductility happen simultaneously. Therefore, the use of reduction in height as a measure of the degree of forging is erroneous.

We have indicated, so far, that a deformation can hardly be uniform, in other words, it is a point function. Deforming a specimen produces a deformation distribution pattern and this pattern varies according to the outside environment such as friction at the tool/work interface. In order to study this deformation in a thorough way, analysis of large deformation has been developed as in Part A of this thesis so that the limitation of both the reduction in height which implies a homogeneous deformation, and the small strain analysis in which elastic deformation is assumed, are eliminated. The development of this analysis came out of the necessity in the forgeability study rather than its elegant mathematical display. In fact, with the application of this analysis, the derivation of the deformation intensity factor Γ , which is used to measure the extent of deformation of an element, is an essential tool in the analysis of large deformation. The zonal pattern of the deformation and the spreading mechanism are also revealed.

As a consequence of this analysis, the homogeneity value of the deformation of a specimen is also derived. With it, it is possible to overcome the inability, by the use of ^{an} average value such as the reduction in height, to represent the degree of forging of a non-homogeneously deformed specimen. In other words, a low homogeneity value means a deformation with very severe concentration of deformation and consequently, any further deformation may have exhausted the ductility of metal in the already highly deformed region and work the metal beyond its acceptable strength level.

In this thesis, forgeability is based on the deterioration of strength through deformation. Of course, forgeability is only a particular manner in which the ductility of the material manifests itself, the manner being determined by a practical forming process, namely, forging. It is, therefore, also reasonable to extend this point of view to the concept of ductility itself, and generalize the usual idea of ductility to mean the deterioration of strength through deformation in general, whether it is induced by forging, or drawing, or extrusion, or biaxial stretching.

It has long been recognized that ductility depends on both the hydrostatic compression and the deformation (12,13,67,68). For the present purpose, it is convenient to refer to the criterion proposed by Cockcroft, namely, that fracture will occur when

$$\int_0^{\bar{\epsilon}_f} \bar{\sigma} \left(\frac{\sigma^* - p}{\bar{\sigma}} \right) d\bar{\epsilon} = C$$

where p is the hydrostatic stress,

$\bar{\sigma}, \bar{\epsilon}$ are effective stress, strain,

σ^* is the local maximum principal tensile stress,

$\bar{\epsilon}_f$ effective strain at fracture.

Although the function $\int_0^{\bar{\epsilon}_f} \bar{\sigma} \left(\frac{\bar{\sigma}^* - p}{\bar{\sigma}} \right) d\bar{\epsilon}$ in Cockcroft's formula is unknown, theoretical considerations suggest and experimental results on crack formation in different forming processes confirm that the strength of metals in general is damaged by deformation, but the damage is mitigated by the hydrostatic compression accompanying the deformation. Hence, for a radial coaxial strain path, the exhaustion of ductility increases with the deviatoric stress (OA in fig.13.1) and decreases with the hydrostatic stress (OB in fig.13.1), in other words, for the same stress vector, $(\bar{OA} + \bar{OB})^{\frac{1}{2}}$, the larger the angle, ψ , the better for the engineer. Both the deviatoric component \bar{OA} and the hydrostatic component \bar{OB} are dealt with in this thesis from the point of view of forgeability.

With regard to the deviatoric stress component \bar{OA} , as was explained in Chapter five, the true amount of deformation is the length of the strain path Γ , rather than the finite strain as determined from the deformed grid. Of even greater importance, however, is the distribution of the total deformation. Apart from the hydrostatic pressure, the total deformation at a point in the product represents the damage to the strength at that point. Thus, a contour diagram like (fig.9.19 to 9.26) shows the variations of the damage, without taking the effect of the hydrostatic pressure into account. Such a contour diagram is of fundamental importance in the study of forgeability, defined with regard to the damage to the material strength. Forging is used for parts which have to be strong, otherwise it is cheaper to cast or fabricate the part. Therefore, when a forged product is in service it is highly stressed. We can consider, as the designer does, the stress distribution in the part under service conditions. At every point in the part there are three principal stresses and of these principal stresses, the part

to cause flow or fracture is the deviatoric component. Thus, if the effective stress, or the magnitude of the deviatoric stress component is plotted throughout the product under service conditions, we will get another contour diagram showing how much each part of the product is endangered. The contour diagram in (fig.9.19 to 9.26) shows, as explained before, the degree the product is weakened. Forgeability as conceived in this project goes beyond a test for some characteristics of the material or the process to determine how far the forging process can proceed without "fracture", whatever that means. The study of forgeability as conceived here aims at the design of the forging process to maximize its effectiveness, and a forging process is considered to be effective if it causes little damage to the strength of the product. When metals are deformed, some damage is bound to be done to the strength of the material, especially when the deformation is non-uniformly distributed, as in forging. The distinction between the strength of the material and the strength of the product opens up the possibility of rational design of the forging. The contour diagrams like (fig. 9.19 to 9.26) which show the distribution of the weakness of the material in different parts of the product may also be seen in reverse as showing the distribution of the strength of the product. Now, a forging process well designed from the point of view of forgeability (as conceived here) requires a matching of (i) the contour diagram showing the distribution of the weakness, to the drawing showing which parts are subsequently machined away, so that the weak regions, which are inevitable, can be designed to take the positions of what is to be machined away; and (ii) the contour diagram showing the distribution of the strength, to that showing the effective stress in the product under service, so that the strongest part (or at least not the weakest part) can coincide with the part that is most endangered.

In this conception of forgeability, a process of high forgeability is not even one with relatively little damage to the strength of the material; rather it is one in which severe damage can occur, but only in regions to be machined away, and some damage occurs, as it always does in forging, but only where the stress in service is low. In other words, no engineering material is perfectly forgeable, and in so far as all of them are not perfectly forgeable, they suffer some loss of strength when forged. The present study of forgeability proposes that the inevitable loss of strength should be placed where it does not matter or, to be more precise, the weaker material should be where it matters less, the most weakened where it matters least and the hopelessly weakened part where it does not matter at all. Improving forgeability is then not merely a matter of finding a more forgeable material or a set of more forgeable conditions (such as hot forging), but also a matter of using an imperfectly forgeable material to its best forging potentiality.

The application of such a concept of forgeability will lead to totally new avenues of design principles. Instead of designing the shape of a forging for the function of the product, the shape and size should also be designed with due regard to its forgeability -- as it is conceived here. For example, by the criterion of forgeability proposed here, a forging may take a particular shape because of the advantageous re-positioning of the most severely deformed zones. Machining may be done on the forged product for no functional reason, but in order to remove weakened material. Or else, some bulk may be added in the design to certain parts of the forging to gain a more suitable distribution of the deformation. Indeed, it is not altogether inconceivable that some bulk may be added in a sophisticated design, so that it takes the greatest deformation from other more essential parts of

the product and then the added bulk is machined to strengthen effectively the product. Such applications to forging design would not be possible without a valid analysis of the non-homogeneous deformation as is proposed in this thesis.

As it is, the soundness of forgings are at present often judged by what are called "flow lines" -- which neither are lines nor represent any flow, being streaks formed by the elongated grains and revealed by etching. Needless to say, "soundness", itself an ill-defined concept, is somehow or other guessed from the appearance of these "flow lines" in some intuitive manner, at its best of a hit -and miss nature and its worst, pure magic. That such ^{an} inspection technique is still widely used is a symptom of the real need for a strain analysis that is related to forgeability. Indeed, "flow lines" may be considered to be a kind of primitive strain analysis based mostly on artistic imagination. What is achieved in this project is the lifting of the strain analysis from the intuitive level, at which elongation of grains get confused with flow, to a scientific and rigorous level, at which large deformations are properly split into their essential components. An incidental and curious consequence of the mathematical analysis practised here is the revelation of the home-spun character of the evaluation of forgings by "flow lines". In that method, the acute need for some analysis or other had overwhelmed even the demand for clarity and **rigorous** in the technologists, to make them resort to a vague method suggested by imagination and supported by the half-obscure patterns of fictitious "flows".

As suggested by Siebel and confirmed in our ~~experiments~~, different degrees of deformation exist in a zonal manner when a metal body is compressed. In

fact, two main groups are found, which are (A) the active or shear zones, and (B) the passive or dead zones; as shown in (fig.9.15 to 9.18).

These groups are further divided into five different zones as shown in (fig. 9.28) namely, the central uniaxial zone (1) the corner zone, (2) the shearing zone, (3) and the two dead metal zones, (4) and (5) as shown in (fig. 9.28).

The history of deformation is recorded in the strain path. In a deformable medium, the various elements will have their own local behaviour which may or may not conform to the overall bulk behaviour. In terms of strain paths, different zones will have dissimilar paths in magnitude, and in non-coaxiality. In general, we can say that the paths in the shearing zones are characterised by their large magnitudes in deformation. The curvatures of strain paths reflect the non-coaxiality and the changing strain ratio of the deformable elements. The curvature of the paths is found to be quite similar except for the one in the central zone. This means that the larger the radii, the more nearly coaxial the path will be and this is reflected in the strain path plot for the central zone.

Rigid body rotation of the deformable element is usually neglected in the deformation analysis. In fact, it influences not just the principal directions of the incremental stresses, but also the physical shape of the whole specimen. All the other zones exhibit a small degree of rigid body rotation except ⁱⁿ the corner region and those along the free boundary. Friction encourages the rigid body rotation of these elements in the unlubricated process to rotate to twice that amount achieved in the lubricated specimen. Furthermore, this bodily rotation has been found to be the main

mechanism in the folding of the metal.

Previously, the work done by various upsetting processes was assumed to be a function of the amount of reduction in height. Owing to the fact that deformation is hardly homogeneous, work consumed by the various processes should be different and should depend on the outside constraints such as friction existing at the tool/work interface. In fact, for the same reduction in height in upsetting processes, the work done has been found to be not the same for the same material and the difference between the work required by the ideal process and the work done by the actual process is called the redundant work. Naturally, the redundant work means more work consumed than required and this extra amount of work may induce further concentration of deformation, crack growth, die wear problems and the usage of press capacity.

It is also necessary to find a more significant measure of the degree of forging for the specimen as a whole. So, the measure proposed for this representation is the filling coefficient. In the forging studies, the filling process is seldom investigated because of its complexity. But, an incompletely filled forging is usually treated as scrap. So, the degree of forging has to include the consideration of whether or not the specimen is near to its completion by means of the filling coefficient developed in Chapter seven.

It has been found that when the height-to-diameter ratio H/D of the die cavity is unity, any increase in H/D ratio of the specimen will slow down the filling process. As can be expected, this filling process will be

speeded up when the H/D ratio of the die is less than 1. Extra volume of metal added will generally speed up the filling process irrespective of the specimen H/D ratio.

The stress component \overline{OB} , in (fig.13.1), does not, of course, contribute to the tendency towards deformation but only adds to the load on the forging. In the chapter on the filling characteristics (Chapter twelve), it is shown how the load increases rapidly when the die is nearly closed, especially after the work has touched the sides of the cavity, but, it is relatively low in the early part of the forging process. The forging load is bound to increase in any forging process, owing to strain-hardening and to the hydrostatic stress in the later part of the stroke. Nevertheless, from the point of view of damage to the strength, the ideal forging load is one which is relatively high at the beginning and increases little during the stroke. In such a process, the hydrostatic compression is high throughout the process, so as to mitigate the damage to the strength of the material and the load is not increased very much, so that the capacity of the press is not wasted in most parts of the stroke. As it is, the natural tendency of the forging process is such that in the major part of the stroke the material is deformed without high hydrostatic compression, causing damage to the strength of the product, and towards the end of the stroke, the hydrostatic pressure is greatly increased but the amount of deformation then is very small, that is, the protective influence against damage is ineffective.

The abrupt increase in the forging load at the end of the stroke is undesirable in practical terms for several reasons. In the first place, a

large capacity of the press is needed for only a small part of the process. In the second place, the high load towards the end of the stroke endangers the die, especially since it is almost an impact load. Even if the die does not break, it is likely to be deformed and worn after long use.

The individual behaviour of various elements in the whole body of the metal will collectively determine the bulk reaction towards external conditions. A similar performance for each individual element will result in a homogeneous deformation, a zoneless distribution pattern, a uniform spreading at the free boundary, and in fact, an ideal deformation. Apparently, in actual processes, this ideal situation is far from the truth and various elements will behave according to their "locality" which result in a non-homogeneous deformation pattern. In forging practice, a non-homogeneous deformation is the result of both the metal and the process being unable to disperse the deformation. This concentration of deformation and the subsequent building up of strain gradient between the shear zones and the dead zones are found to have encouraged the growth of hair cracks internally which are undetectable from the surface, as shown in papers on fractures (65,69). Unless subsequent machining is aimed at removing the severely deformed area leaving those dead or less deformed metal as the finished product, non-homogeneous deformation is undesirable.

Rigid body rotation provides the folding mechanism and friction encourages the rotation. Furthermore, friction produces a quicker spread of metal than the lubricated process which is contrary to what is generally believed to be the case. Again, in forging practice and design, it has been

suggested that spreading in a form of folding has speeded up the filling of the end face of the die cavity. But, in closed die forming processes, this folding of metal from the side face of the specimen may be prevented, by the contact of the specimen with the sides of the die, thereby, making filling corners much more difficult. Furthermore, forging defects such as laps which are formed whenever metal folds over itself will be found owing to the folding of metal. In the design of forging dies, the ability for the metal to flow easily determine the choice of the corner radii, fillet radii and sometimes the draft angles. Take an example of comparing the corner radii of aluminium and tungsten (70) forgings. We anticipated that aluminium can flow and rotate more freely than tungsten, and the result is that the corner radii for tungsten must be at least twice that of aluminium.

In practice, when complete die filling is not the principal criterion in selecting a process, the minimization of load may assume considerable importance.

CHAPTER FOURTEEN

Future Work

Like the study of formability and drawability in sheet metal forming or the machinability in metal cutting, the forgeability of metal involves a wide range of material as well as process parameters that the present knowledge is outdated and overstretched. A more precise understanding of the forging mechanism and consequently forgeability, is much needed in securing a better competition with the other processes. The concept of forgeability as conceived here as the deterioration of strength in the forging, is of such an important and wide application in the forging industry that only a part of its implication can be dealt with within the scope of the present study and many other investigations immediately suggest themselves. But, there are only a few which stand out and warrant further study. The first one concerns the improvement in the experimental technique much used throughout the present project. The others are more fundamental in the study of forgeability problems in forming processes, that is, the detection of structural damages. The last area worth further investigation is the flash behaviour in the closed die forming which determines the filling process of each forging.

14.1 The improvement in experimental technique

In this project, the essential bottlenecks, if it can be called that, are the co-ordinates measurements of the distorted grids. As there are more than four thousand readings at each stage of reduction, the time consumed for this laborious and eye tiring, manual job is relatively large (around two to four weeks). Furthermore, another problem arises from this lengthy process in that ageing of the material will occur and thus, when it is

compressed further, ^{the} properties of the material may have already changed. In order to eliminate this side effect and speed up the measurement, a mechanised equipment has to be used. It is found that the distorted grids can be accurately photographed and subsequently, the specimen will be deformed without further delay. This will minimise the ageing effects. The negative of the photograph after development will be enlarged by projecting onto the measuring table which is connected to a mechanised co-ordinate punching machine commonly used in the physics department for measuring the elementary particles paths and radii of curvature etc. Therefore, by locating a grid point on the projection table and pressing a button, this particular co-ordinate will be automatically recorded and punched onto a computer card. This data will be analysed by the computer. This method has been estimated to have saved around 70% of the original time.

14.2 The detection of structural failure

From our understanding so far, part of the forgeability criteria is the structural failure of the forgings such as cracks appearance etc. There are two ways to determine the damage. The first one is the detection of growth and initiation of cracks. As cracks are, strictly speaking, not initiated but only grow, so some scales have to be found to record their growth. Density is one of this scale and worth further work. The next method is the static and fatigue strength of the forging according to its function in use.

14.2.1 The density evaluation method

Following the above argument, density can be used as one of the standard

scales to record the growth of cracks. In fact, quite a few researchers have employed this tool in the studies of structural damage and the leading ones are Rogers, Horon, Garofalo and Wriedt (67,68,70,88,28,19). All of them have found that density does decrease when deformation increases. Their various views and methods are summarised in table 14.1 and also their respective results presented in (fig.14.1). The decrease in density from their results cannot be said to be related to the state of strain of the particle directly because it is only the average reduction in area of the whole specimen that they are considering. With the use of our strain analysis method, a direct relationship between the state of strain and the density variation can be found.

The density evaluation can be carried out simply by using ^rAchimedes principle. To detect the growth of cracks, the density has to be measured up to an accuracy of 10^{-4} . This accuracy can be achieved as most chemical balances can easily measure down to a tenth of a milligram.

A. Temperature effect

The variation in temperature of the measuring media and the specimen have been one of the major obstacles in the design of this experiment. This is important because a difference in temperature will affect the density calculation, which is undesirable. Therefore, a constant temperature environment has to be maintained between the measuring media, the deformed specimen and the undeformed specimen. A temperature controlled room with variation in temperature of 1°C is desirable for the site of the equipment. If hydrostatic weighing method is used, then, a constant temperature bath

with a thick copper calorimeter immersed in it is most suitable. The temperature of the bath is controlled by a temperature gauge and compensated by the ultra violet light source. The ultra violet light is used because its radiation can heat up a large volume of the circulating medium. This bath should be ideally kept within a variation of less than $\pm 0.01^{\circ}\text{C}$ and constantly stirred. The measuring media is kept in the thick wall calorimeter so that the good conductivity of copper and its thickness will balance out any minor fluctuation in temperature of the media. The liquid used in the constant temperature bath is pure water but the choice of the measuring media depends on other factors (i) economic reason, and (ii) side effects such as bubble-formation and corrosive action. The temperature inside the measuring media should be maintained ^{at} around $\pm 0.005^{\circ}\text{C}$. It was found that changes in the density of the measuring media, in this case water, due to the changes in temperature of 0.1°C at the nominal temperature of 24°C , is around 0.03%.

In the course of finding a better and accurate means to control the temperature variation within the measuring media, several researchers (88,6) have derived some specific method such as the differential weighing method in which both a deformed specimen and undeformed specimen of the same metal are hung on both sides of the chemical balance and the changes in density can be derived. But, this method requires similarly complicated temperature control equipment. So a new method is desirable so that complicated instrumentation can be eliminated. By extending Bell's mathematical approaches (6), the ratio of changes in density of the specimen can be found to be equal to

$$\frac{\Delta \rho_s}{\rho_{s0}} = 1 - \frac{W_{an} (W_{a0} - W_{l0})}{W_{a0} (W_{an} - W'_{ln})} R \quad 14.1$$

where $\Delta \rho_s$ is the change in density of the specimen

ρ_{s0} is the density of the undeformed specimen

W_{a0} is the weight of undeformed specimen in air

W_{l0} is the weight of undeformed specimen in liquid

W_{an} is the weight of the deformed specimen in air

W'_{ln} is the weight of the deformed specimen in liquid.

R is the temperature correction factor and it is equal to

$$R = \left(1 + \frac{\Delta \rho}{\rho} + \beta t \right) \quad 14.2$$

where $\Delta \rho$ is the change in density of the measuring media

ρ is the original density of the measuring media

β is the coefficient of cubical expansion of the measuring media.

With the use of the above equations, the changes in density of the deformed specimen can be evaluated, provided that accurate measurement of temperature and elimination of all damaging factors such as bubbles and surface tension etc. can be achieved.

B. Bubble formation

Bubbles^{are} usually formed when a rough surfaced metal body is immersed into a liquid from air. These bubbles will adhere onto the rough surfaces and increase the buoyancy of the specimen which is detrimental to the density measurement. They can be reduced either by physically shaking the specimen until all the visible ones have disappeared or by choosing a high viscosity

liquid. In fact, the latter is more effective in tackling the formation of bubbles and one example of the liquid used is diethylphalate.

C. Corrosive effects

Some measuring media will react to the metal specimen which is no good for density measurement. So a medium has to be chosen which is inert towards the specimen.

D. Surface tension

The capillary action of the liquid molecules of the measuring media exerting on the suspension wire is a headache in the precision density measurement. Although, the force acting on the wire is minute in the weighing of the whole specimen, yet, the changes in density of the deformed specimen are so small that this pulling force cannot be neglected. For an ordinary wire, the pulling force is estimated to be around 11 mg . Therefore, in order to maintain the pulling force constant in every measurement, the meniscus of the liquid to wire interface should be kept to the same shape so that in calculating the ratio $\frac{\Delta \rho}{\rho}$, in the changes in density of the specimen, the error caused by the surface tension can be eliminated.

E. Measuring liquid level

The level of the measuring medium is essential because any decrease or increase in the liquid level means a corresponding decrease or increase in the total immersed length of the suspension wire which, in turn, affects the minute changes in the density of the deformed specimen. So the liquid level has to be checked and maintained at the same height in every experiment.

A typical layout of the equipment is shown in (fig.14.2), and from our tests, this method is found to be most promising in evaluating the damages of a metal after cold working.

14.2.2 Fatigue test

In the service function of a forging, the static or the fatigue strength of it is more fundamental in the determination of a structural failure. As we all realise, the more similar the testing method to its real serving situation, the more realistic the testing results. Most of the forging used in industry are under constant dynamic stress such as a connecting-rod or crank shaft in the motor engine, which are different to the conditions in static testing method. Therefore, it is better to know the fatigue strength of the forged parts than the likely appearance of cracks etc., as the fatigue tests simulate closely the actual condition that the forging will experience. Naturally, again, with the use of our strain analysis method, a direct relation will be found between the fatigue strength and the state of strain of the specimen.

14.3 The flash behaviour and its effects

Flash which is a form of extra volume of metal in the forging will usually speed up the filling process as shown in our filling experiments but also it consumes more energy. In order to achieve a fully filled forging, a considerable amount of extra volume of metal in the form of flash has to be used. Firstly a series of experiments to study the flash formation mechanism has to be designed. It will consist of a standard die shape and a varying flash geometry. The resultant flow characteristic and distribution

of deformation will determine the mechanism of its formation. The next set of experiments will involve the study of the effects of flash on the filling characteristic of the forming process. A completely filled forging is always a necessity in most closed die forging, but there are several parameters which have to be considered such as the specimen size, shape, the die cavity shape and the flash geometry. Their inter-relationship is so complex that their effects on the filling process due to the flash formation can only be studied by carefully isolating some of them.

Table 14.1

Author and Source	MATERIAL PROPERTY			DENSITY MEASUREMENT				DEFORMATION		
	material	Density g/c.c.	Method	Balance Accuracy	Liquid media	Temp. control	Overall Accuracy	Reduction	Density change	Process used
Rogers 67,68 (1967)	Al. Alloy 6060	2.7072	H.S.	10^{-5} gm.	Diethylphtha- late	$\pm 0.003^{\circ}\text{C}$		7070 10%	0.34%	Sheet drawing
Hordon 28 (1961)	Pure Al.		D.H.S.	10^{-5} gm.	Dibromopro- pane	$\pm 0.01^{\circ}\text{C}$ 25 $^{\circ}\text{C}$	$\pm 1 \times 10^{-5}$	30%	0.01%	shear
Rogers 67,68 (1967)	OFHC Tough pitch	8.929 8.904	H.S.	10^{-5} gm.	Diethylphtha- late	$\pm 0.003^{\circ}\text{C}$		80% 70%	0.056% 0.255%	drawing
Hordon 28 (1961)	Pure Cu.		D.H.S.	10^{-5} gm.	Dibromopro- pane	$\pm 0.01^{\circ}\text{C}$ 25 $^{\circ}\text{C}$		30%	0.01%	shear
Maier 56 (1936)	Com. Cu.	8.92426	H.S.	10^{-4} gm.	CCl_4	20 $^{\circ}\text{C}$ $\pm 0.01^{\circ}\text{C}$	5 in 10^6	75%	0.25%	drawing
Smart 79 (1941)	Com. Cu. OF Cu.	8.9581 8.9314	H.S.	10^{-4} gm.	CCl_4	20 $^{\circ}\text{C}$ $\pm 0.05^{\circ}\text{C}$	5 in 10^5 1 in 10^4	90% 70%	0.037% 0.153%	drawing
Garofalo 19 (1962)	Stainless steel 316	8.0	H.S.	10^{-5} x 5gm.	Bromoben- zene	$\pm 0.02^{\circ}\text{C}$ $\pm 0.0006\text{g/c.c.}$	$\pm 0.0010\text{g/c.c.}$ $\pm 0.0006\text{g/c.c.}$	50%	0.08%	Compress- ion

Table 14.1 (continued)

MATERIAL PROPERTY		DENSITY MEASUREMENT				DEFORMATION				
Author and Source	Material	Density g/c.c.	Method	Balance Accuracy	Liquid Media	Temp. Control	Overall Accuracy	Reduction	Density Change	Process Used
Keeler 40 (1953)	Pure Fe Steel SAE 1020	7.8549 7.8538	H.S.		Monobromobenzene		± 0.00056 g/c.c.	60%	0.194% 0.115%	Cold Rolling
Andrew 3 (1950)	Fe Steel	7.865 7.8395		10^{-4} gm.	Paraffin	$\pm 0.04^\circ\text{C}$	$\pm 0.01\%$	80% 60%	0.262% 0.275%	Drawing
Maier 56 (1936)	Fe	7.862				20°C		87%	0.98%	Torsion
Wriedt 88 (1970)	Steel AISI.1086							85%	0.3%	Wire Drawing

H.S. = Hydrostatic weighing

D.H.S. = Differential H.S.

APPENDIX I

Diagonalization of a positive definite and real symmetric matrix*

In order to show that a general real symmetric matrix can be reduced to diagonal form by means of an orthogonal transformation, a real symmetric

A is assumed to have distinct characteristic roots $\gamma_1, \gamma_2, \dots, \gamma_n$. Let x^1, x^2, \dots, x^n be an associated set of characteristic vectors normalized by the condition that

$$(x^i, x^i) = 1$$

$$i = 1, 2, \dots, n$$

Consider the matrix **T** formed upon using the vectors x^i as columns.

Schematically,

$$\mathbf{T} = (x^1, x^2, \dots, x^n)$$

Then \mathbf{T}^T is the matrix obtained using the x^i as rows,

$$\mathbf{T}^T = \begin{vmatrix} x^1 \\ x^2 \\ \vdots \\ x^n \end{vmatrix}$$

and is called the transpose of **T**.

Since

$$\mathbf{T}^T \mathbf{T} = ((x^i, x^j)) = \delta_{ij}$$

where δ is the Kronecker delta

it can be seen that **T** is an orthogonal matrix.

* NOTE : refer to Bellman, R., Introduction to Matrix Analysis, McGraw-Hill, 1970.

It follows that

$$\mathbf{T}^T \mathbf{A} \mathbf{T} = (\gamma_i (x^i, x^j)) = (\gamma_i \delta_{ij})$$

or in terms of components

$$\mathbf{T}^T \mathbf{A} \mathbf{T} = \begin{vmatrix} \gamma_1 & & & 0 \\ & \gamma_2 & & \\ & & \dots & \\ 0 & & & \gamma_n \end{vmatrix}$$

The matrix on the right hand side has its main diagonal the characteristic values ($\gamma_1, \gamma_2, \dots, \gamma_n$) and zeros every place else. A matrix of this type is called a diagonal matrix. This process of reducing a real symmetric matrix to a diagonal matrix by orthogonal transformation is called the diagonalization and is represented by the above equation.

ACKNOWLEDGEMENTS

The author of this thesis gratefully acknowledges all who have offered their assistance towards the project, especially to his Supervisor, Professor T. C. Hsü, for the valuable guidance and advice. The author is also grateful to Professor A. J. Ede, Head of the Department of Mechanical Engineering, for permitting the use of the equipment and least of all, the assistance of all the technicians in both the department of Production Engineering and Mechanical Engineering.

The author is greatly indebted to his wife for the typing of the manuscript and also grateful to Mrs. C. Watkinson for checking the manuscript.

BIBLIOGRAPHY.

- (1) Alexander, J. M., "The Effect of Coulomb Friction in the Plane Strain Compression of a Plastic Rigid Material", *Journal of Mechanics and Physics of Solids*, 3, 1954, 233-245.
- (2) Altan, T., Gerds, A. F., Nichols, D. E., Henning, H. J., and Fiorentino, R. J., A Study of Mechanics of Closed-Die Forging, Final Report for Army Material and Mechanics Research Center, Battelle Memorial Institute, Ohio, Contract no. DAAG 46-68-C-0111, D/A Project 6331.
- (3) Andrew, J. H., Lee, H., Chiang, P. I., Fang, B., and Guenot, R., "Effect of Cold-Work on Steel", *Journal of Iron and Steel Institute*, 165(II), 1950, 145-166.
- (4) Avitzur, B., Metal Forming: Processes and Analysis, McGraw Hill, New York, 1968.
- (5) Baraya, G. L., and Johnson, W., "Flat Bar Forging", *Advances in Machine Tools Design and Research*, Birmingham, 1964, 449-469.
- (6) Bell, G. A., "The Measurement of Small Changes in Density in Large Specimen", *Australian Journal of Applied Sciences*, 9, 1958, 236-244.
- (7) Biswas, S. K., and Rooks, B. W., "Application of a Computer Simulation Technique to estimate Load and Energy in Axisymmetrical Closed Die Forging", *Advances in Machine Tools Design and Research*, Birmingham, 1972, 371-382.
- (8) Bridgeman, P. W., Studies in Large Plastic Flow and Fracture, Harward Press, 1964.
- (9) Bühler, H., and Bobbert, D., "The Distribution of Deformation after Pressing", *Industrie-Anzeiger*, 8(100), 1966, 309-312.

- (10) Al-Chalabi, M., McCormick, F. J., and Huang, C. L., "Strain Distribution within Compressed Circular Cylinders", *Experimental Mechanics*, 14(12), 1974, 497-501.
- (11) Clough, R. W., "Use of Modern Computer in Structural Analysis", *Journal of Structural Division, Proceeding of the American Society of Civil Engineering*, 84, ST3, paper no. 1636, May 1958.
- (12) Cockcroft, M. G., "Ductile fracture in Cold Working Operations", *Ductility*, American Society for Metal, 1967, 199-225.
- (13) Cockcroft, M.G., and Latham, D.J., "A Simple Criterion of Fracture for Ductile Metals", National Engineering Laboratory, NEL report no. 240, July 1966.
- (14) Devenpeck, M. L., and Richmond, O., "Strip-Drawing Experiments with a Sigmoidal Die Profile", *Transaction of American Society of Mechanical Engineers*, paper no. 64-WA/Prod-17.
- (15) Dewhurst, P., and Collins I. F., "A Matrix Technique for constructing Slip-line Field solutions to a class of Plane Strain Plasticity Problems", *International Journal for Numerical Methods in Engineering*, 7, 1973, 357-378.
- (16) Eringen, A. C., Mechanics of Continua, John Wiley and Sons Press, 1967, chapter one and two.
- (17) Freudenthal, A. M., Introduction to the Mechanics of Solids, Wiley, New York, 1966.
- (18) Fung, Y. C., Foundation of Solide Mechanics, Prentice Hall, 1965.
- (19) Garofalo, F., and Wriedt, H. A., "Density change in an Austenitic Stainless Steel deformed in Tension or Compression", *Acta Metallurgia*, 10, November 1962, 1007-1012.

- (20) Geiringer, H., Proceeding of the 3rd International Conference of Applied Mechanics II, Stockholm, 2, 1930, 185-190.
- (21) Green, A. P., "A Theoretical Investigation of the compression of a Ductile Material between Smooth Flat Dies", Philosophical Magazine, 42, 1951, 900-918.
- (22) Harris, A., A Study of Combined Extrusion and Upsetting, Msc Dissertation, University of Aston, 1969.
- (23) Hencky, H., Zeits. Angew Math. Mech., 3, 1923, 241-251.
- (24) Hill, R., "On the problem of uniqueness in the Theory of a Rigid Plastic Solid I", Journal of Mechanics and Physics of Solids, 4(4), 1955, 247-255.
- (25) Hill, R., Mathematical Theory of Plasticity, Oxford Press, London, 1950.
- (26) Hill, R., "A General Method of Analysis for Metal Working Processes", Journal of the Mechanics and Physics of Solids, 11, 1963, 305-326.
- (27) Hill, R., "A Remark on Diagonal Str^aming in Plane Plastic Strain", Journal of the Mechanics and Physics of Solids, 14, 1966, 245-248.
- (28) Hordon, M. J., and Averbach, B. L., "Precision Density Measurement on Deformed Copper and Aluminium Single Crystals", Acta Metallurgia, 9, March 1961, 247-249.
- (29) Hsü, T. C., "A Study of Large Deformations by Matrix Algebra", Journal of Strain Analysis, 1(4), 1966, 313-320.
- (30) Hsü, T. C., "The Characteristics of Coaxial and Non-Coaxial Paths", Journal of Strain Analysis, 1(3), 1966, 216-222.
- (31) Hsü, T. C., "Velocity Field and Strain Rates in Plastic Deformation", Journal of Strain Analysis, 2(3), 1967, 196-206.

- (32) Hsü, T. C., "Some Implications of Non-Coaxiality in Finite Deformations", *Journal of Engineering Material and Technology, Trans. of A.S.M.E.*, 95, 1973, 87-93.
- (33) Hsü, T. C., "A Study of the Compression Test for Ductile Materials", *Material Research and Standard*, 9(12), 1969, 20-53.
- (34) Hsü T. C., and Choi C. Y., "Mohr Circles for Large and Small Strains in Two-Dimensional Deformations", *Journal of Strain Analysis*, 6(1), 1971, 62-70.
- (35) Hsü T. C., and Young A. J., "Plastic Deformation in the Compression Test of pure Copper", *Journal of Strain Analysis*, 2(2), 1967, 159-170.
- (36) Jain, S. C., and Bramley, A. N., "Speed and Frictional Effects in Hot Forging", *Proceeding of the Institution of Mechanical Engineers*, 182 Pt 1 no.39, 1967-68, 783-798.
- (37) Johnson, W., and Mellor, P. B., Plasticity for Mechanical Engineers, Van Nostrand, 1962.
- (38) Johnson, W., Sowerly, R., and Haddow, J.B., Plane-Strain Slip Line Fields : Theory and Bibliography, Edward Arnold, London, 1970.
- (39) Kannappan, A., "Wear in Forging Dies", *Metal forming*, Dec., 1969, Jan., 1970, 335-343, 6-21.
- (40) Keeler J. H., and Davis, H. M., "Density and Hydrogen Occlusion of some Ferrous Metals", *Journal of Metals, Trans. A.I.M.E.*, Jan., 1953, 44-48.
- (41) Kobayashi, S., "Deformation Characteristics and Ductile Fracture of 1040 Steel in Simple Upsetting of Cylinders and Rings", *Journal of Engineering for Industry, Trans. A.S.M.E.*, May 1970, 391-399.
- (42) Kobayashi, S., "Theories and Experiments on Friction, Deformation and Fracture in Plastic Deformation Processes", *Proceeding Symposium on the Relation Between Theory and Practice of Metal Forming, Ohio*, editor Hoffmanner, A.L., Oct., 1970. 325-347.

- (43) Kobayashi S., and Thomsen E. G., "Approximate Solutions to a problems of Press Forging", Transaction of the American Society of Mechanical Engineers, Paper no. 58-A-140.
- (44) Kobayashi S., and Thomsen, E. G., "Upper and Lower-Bound Solutions to Axisymmetrical Compression and Extrusion Problems", International Journal of Mechanical Science , 7 , 1965, 127-143.
- (45) Kudo, H., "An Upper-Bound Approach to Plane Strain Forging and Extrusion", International Journal of Mechanical Science, 1, 1960, 57-83, 229-252, 366-368.
- (46) Kudo, H., "Some Analytical Analysis of Extrusion and Cold Forging", International Journal of Mechanical Science, 2, 1960, 102-127.
- (47) Kudo, H., and Aoi, K., "The Effect of Compression Test Conditions on the Fracturing of a Medium Carbon Steel II a Study of Cold Forgeability Steel", Sosei-to-Kako, 8(72), 1967, 17-27.
- (48) Kudo, H., Sato, K., and Aoi, K., "On Cold Forgeability Test", Annals C.I.R.P., 17, 1968, 309-318.
- (49) Kudo, H., and Nagahama, T., "Experimental Results for Upsetting Pressure and Material Spreading", Journal of Japan Society of Technology in Plasticity, 10(106), 1969-11, 827-846.
- (50) Kuhn, H. A., Lee, P.W., and Erturk T., "A Fracture Criterion for Cold Forming, Journal of Engineering for Industry, Trans. A.S.M.E., Oct., 1973, 213-218.
- (51) Lange, K., "Theory and basic Principles of Drop Forging", Metal Treatment and Drop Forging, May 1965, 184-195, June 1965, 210-230, July 1965, 264-270.
- (52) Lee, C. H., Numerical analysis of the Mechanics of Plastic Deformation Problems, PHD Thesis, University of California, Berkeley, 1970.

- (53) Lee, C. H., and Kobayashi S., "Analysis of Axisymmetrical Upsetting and Plane-Strain Side-Pressing of Solid Cylinders by the Finite Element Method", Journal of Engineering for Industry, Trans.A.S.M.E., May 1971, 445-454.
- (54) Lee, P. W., and Kuhn H. A., "Fracture in Cold Upset Forging -- a Criterion and Model", Metallurgical Transaction, 4, April 1973, 969-974.
- (55) Lippmann, H., "Elementary Methods for the Analysis of certain Forging Processes", International Journal of Mechanical Science, 1, 1960, 109-120.
- (56) Maier, C.G., "Theory of Metallic Crystal Aggregates", Transaction of A.I.M.E., 122, 1936, 121-175.
- (57) Malvern, L. E., Introduction to the Mechanics of a Continuous Medium, Prentice-Hall, 1969, chapters 4,5,6.
- (58) McClintock F. A., "On the Mechanics of Fracture from Inclusions", Ductility, American Society for Metal, Ohio, 1967, 255-277.
- (59) Medrano R. E., Gillis P., Hinesley, C. P., and Conrad, H., "Application of Visioplasticity Technique to Axisymmetrical Extrusions", Proceedings of a symposium on the relation between theory and practice of metal forming, Ohio, Edited by Hoffmanner, A. L., Oct. 1970, 85-114.
- (60) Murnaghan, F. D., Finite Deformation on an Elastic Solid, Wiley, New York, 1951, chapter 1 and 2.
- (61) Nadai, A., Theory of Flow and Fracture of Solid, Volume II, McGraw Hill, New York, 1963, chapter 11, 12, 13, 14.
- (62) Nagamatsu, A., Murota, T., and Jimma, T., "On the Non-Uniform Deformation of Material in Axially Symmetrical Compression caused by Friction", Bulletin of the Japan Society Mechanical Engineering, 14(70), 1971, 331-347, 14(70), 1971, 314-330.

- (63) Nebe, G., "Über die Spannungs -- und Formänderungsverteilung beim Stanzen", Doktor-Ingenieurs Dissertation, Technischen Hochschule Aachen, 1965.
- (64) Noll, W., "A Mathematical Theory of the Mechanical Behaviour of Continuous Media", *Archive for Rational Mechanics and Analysis* 2, 1958-59, 197-226.
- (65) Palmer, I. G., Smith, G. C., and Warda, R. D., Conference on Physical basis of Yield and Fracture, Institute of Physics and Physical Society, London, 1967, page 53.
- (66) Richmond, O., and Devenpeck, M. L., "A Die Profile for Maximum Efficiency in Strip Drawing", *Proceeding of the 4th U.S. National Congress of Applied Mechanics*, 2, 1962. 1053-1057.
- (67) Rogers, H. C., and Coffin L, "An Analysis of the Effect of Friction on Sheet Drawing", *International Journal of Mechanical Science*, 13, 1971, 141-155.
- (68) Rogers, H. C., and Coffin, L., "Investigation of the Nature of Structural Damages in Metal Deformation Process", General Electric Co., Research and Development Center, Final report NOW 660546, June, 1967.
- (69) Rogers, H. C., "Effect of Material Variables on Ductility", Ductility, American Society for Metal, Ohio, 1967, 31-61.
- (70) Sabroff, A.M., Boulger, F. W., Henning, H. J., and Spretnak, J. M., "A Manual on Fundamentals of Forging Practice", Battelle Memorial Institute, Ohio, Contract no. AF 33(600)-42963.
- (71) Scott, D., "Metallurgical Aspects of Wear", National Engineering Laboratory, NEL report no. 316.

- (72) Shabaik, A. H. , "Prediction of the Geometry Changes of the free boundary during Upsetting by the Slip-Line Theory", Transaction of the American Society of Mechanical Engineers, paper no.70-WA/Prod-17.
- (73) Shabaik, A. H. , "Theoretical Methods for Analysis of Metal Deformation Problems", Ph.D. Thesis, University of California, Berkeley.
- (74) Shabaik, A. H. , and Thomsen, E. G. , "Computer Aided Visioplasticity Solution of some Deformation Problems", International Symposium on the Foundation of Plasticity, Warsaw, Editor Sawczuk, A. , Aug. 1972, 177-200.
- (75) Shield, R. T. , "The Rotation associated with Large Strains", S.I.A.M. Journal of Applied Mathematics, 25(3), Nov. , 1973, 483-491.
- (76) Schroeder, W. , and Webster, D. A. , "Press-Forging thin sections: Effect of Friction, Area and Thickness on Pressure Required", Journal Applied Mechanics, Trans.A.S.M.E. , Sept. 1949, 289-294.
- (77) Siebel, E. , "Kräfte und Materialfluz bei der bildsamen Formänderung", Stahl und Eisen, 45, 1925, 1563.
- (78) Siebel, E. , "Grundlagen zur Berechnung des Kraft -- und Arbeitshedarfs beim Schmieden und Walzen", Walzwerksaussch-Berick Nr. 28, 1923,S, 1/19.
- (79) Smart, J. S. , Smith, A. A. , and Philips, A. J. , "Preparation and some Properties of High Purity Copper", Transaction of A.I.M.E. , 143, 1941, 272-286.
- (80) Thomas, A. , "Wear of Drop Forging Dies", Proceeding Mechanical Conference in Tribology in Iron and Steel work, London, 1969,135-145.
- (81) Thomason, P. F. , "The Use of pure Aluminium as an Analogue for the History of Plastic Flow, in Studies of Ductile Fracture Criteria in Steel Compression Specimens", International Journal of Mechanical Science, 10, 1968, 501-518.

- (82) THOMSEN, E. G., Yang, C. T., and Kobayashi, S., Mechanics of Plastic Deformation in Metal Processing, Collier-Macmillan, 1965.
- (83) Tomlinson, A., and Stringer, J. D., "Spread and Elongation in Flat Tool Forging", *Journal of the Iron and Steel Institute*, Oct.1959, 157-162.
- (84) Truesdell, C., The element of Continuum Mechanics, Gordon and Breach, 1966, chapter2.
- (85) Truesdell C., and Toupin, R., "The Classical Field Theories", *Handbuch der Physik*, Volume III, Part I.
- (86) Truesdell C., and Noll, W., "Non-linear Field Theories of Mechanics", *Handbuch der Physik*, Volume III, Part 3, section 15-25.
- (87) Wallace, P. W., and Schey, J. A., "Metal Flow in Forging : A Practical Study", *Advances in Machine Tools Design and Research*, Manchester, 1969, 525-536.
- (88) Wriedt, A., and Hughes, H. A., "The Density Variation of a High-Carbon Steel Wire with Wire Drawing Strain", *Metallurgical Transaction*, 1, Dec. 1970, 3457-3458.
- (89) Yamada, Y., Yoshimura, N., and Sakurai, T., "Plastic Stress-Strain Matrix and its Application for the Solution of Elastic-Plastic Problems by the Finite Element Method", *International Journal of Mechanical Science*, 10, 1968, 343-354.

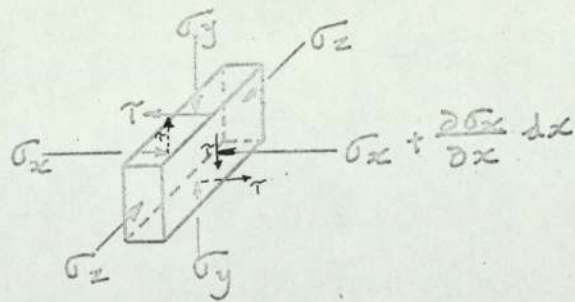
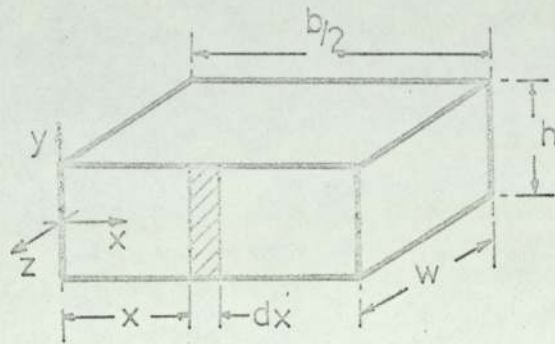
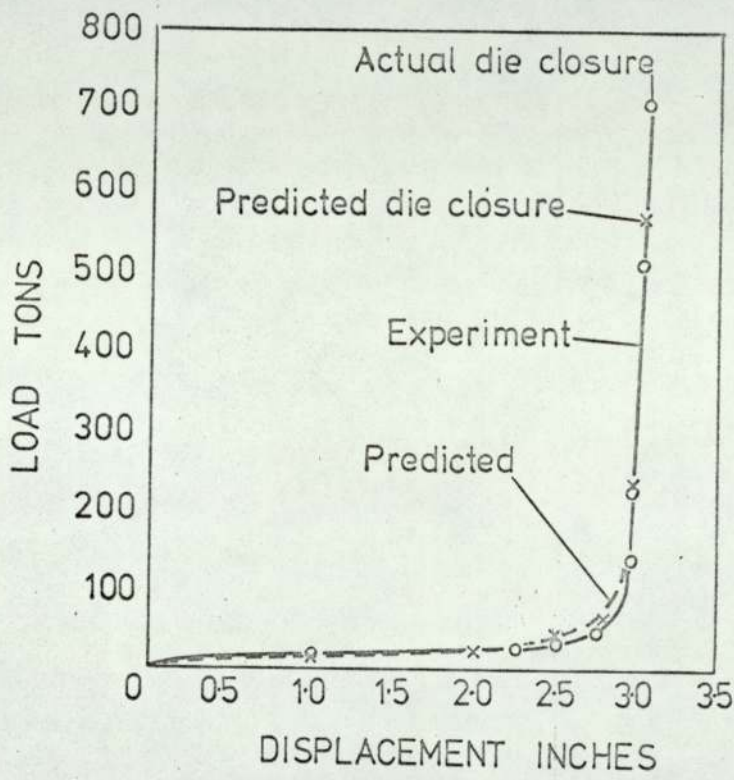
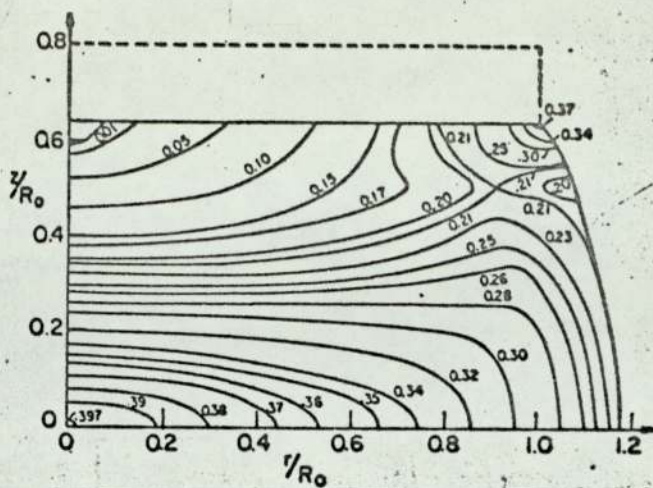


FIG. 2.1

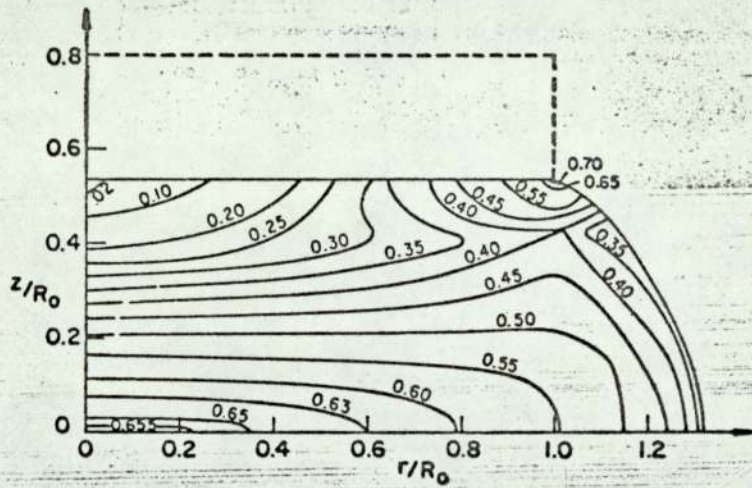


AFTER (2)

FIG. 2.2



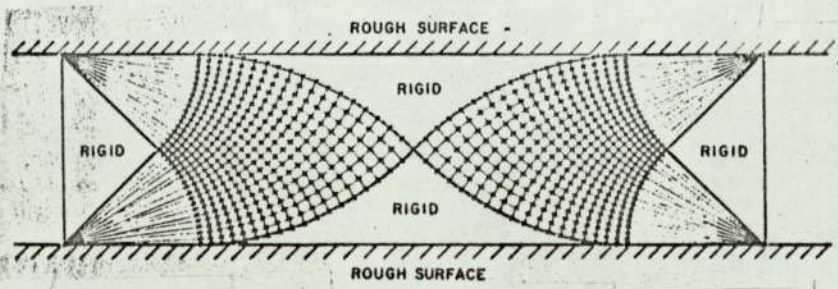
20%
RED.in HEIGHT



33 %
RED. in HEIGHT

AFTER [52]

FIG. 2.3



AFTER [72]

FIG. 2.4

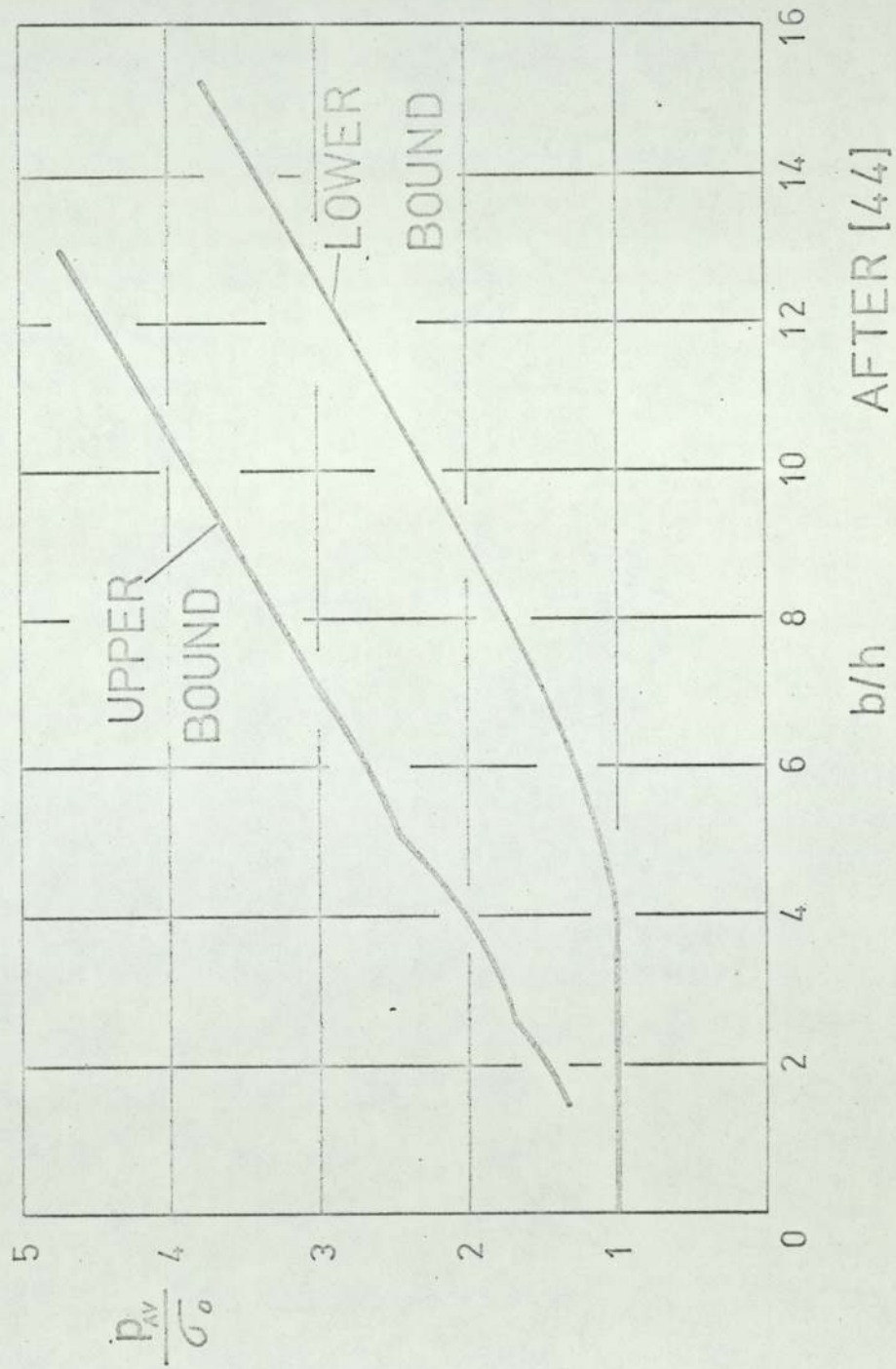
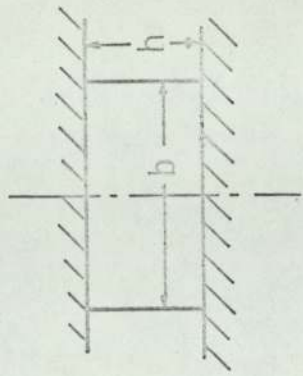


FIG. 2.5 AFTER [44]

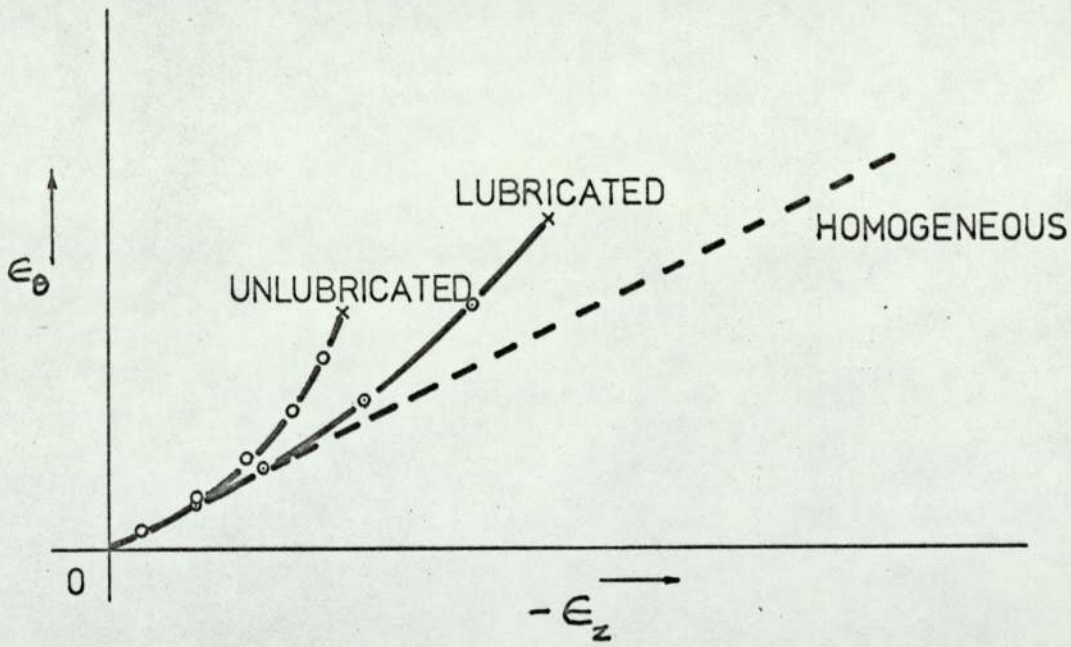
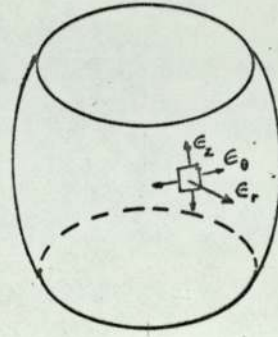


FIG. 2.6 AFTER [47,48]

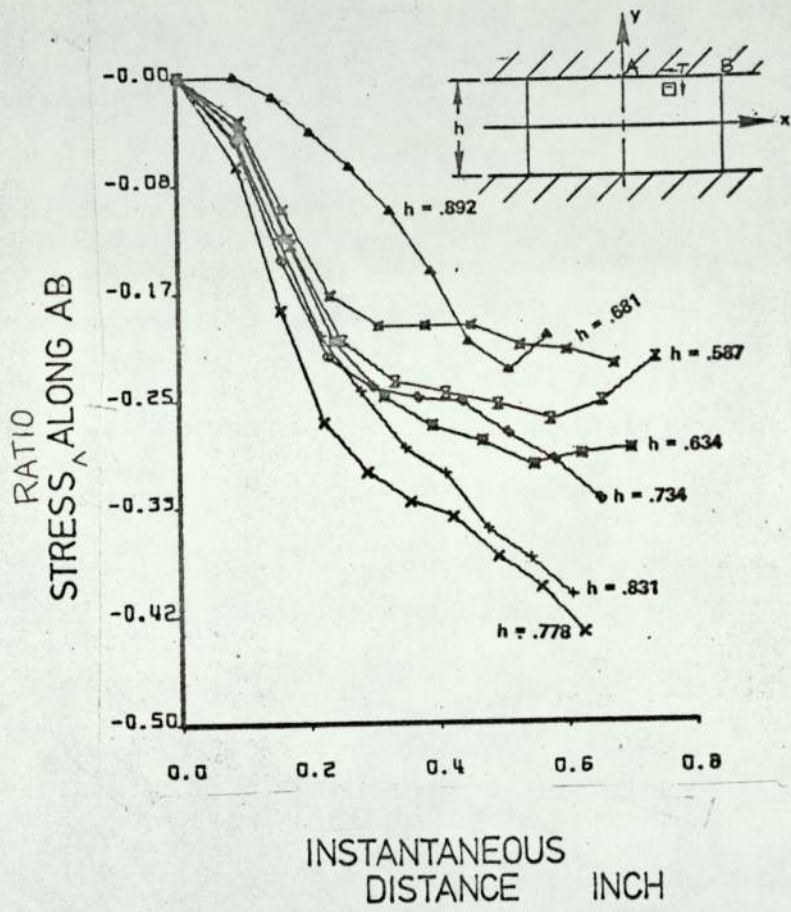
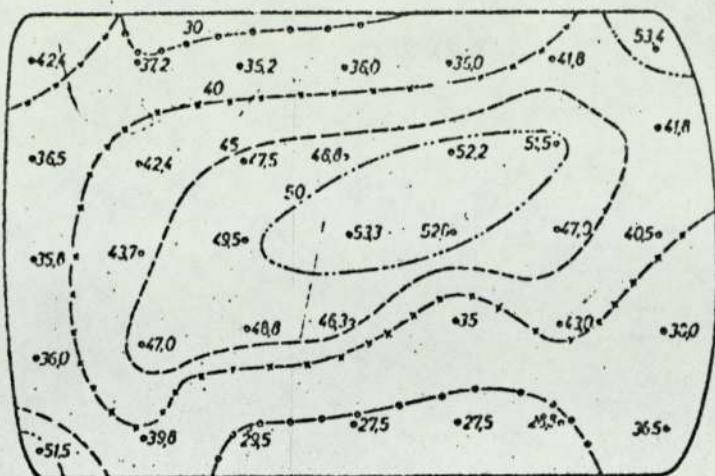
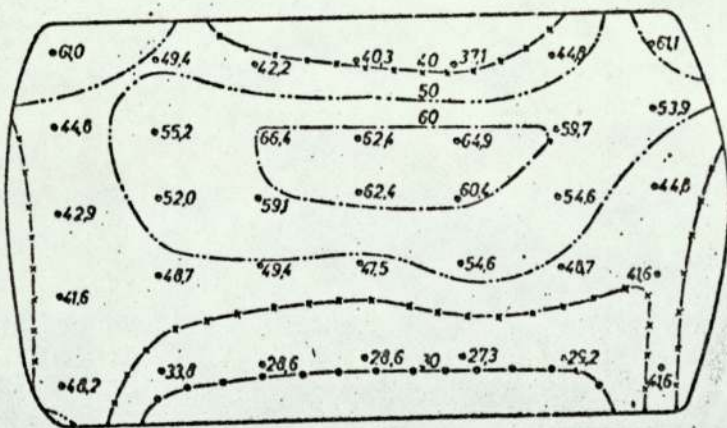


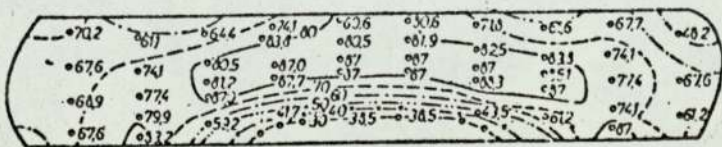
FIG. 2,7 AFTER [72]



42%
RED. in HEIGHT



48%
RED. in HEIGHT



72%
RED. in HEIGHT

AFTER [9] FIG. 2.8

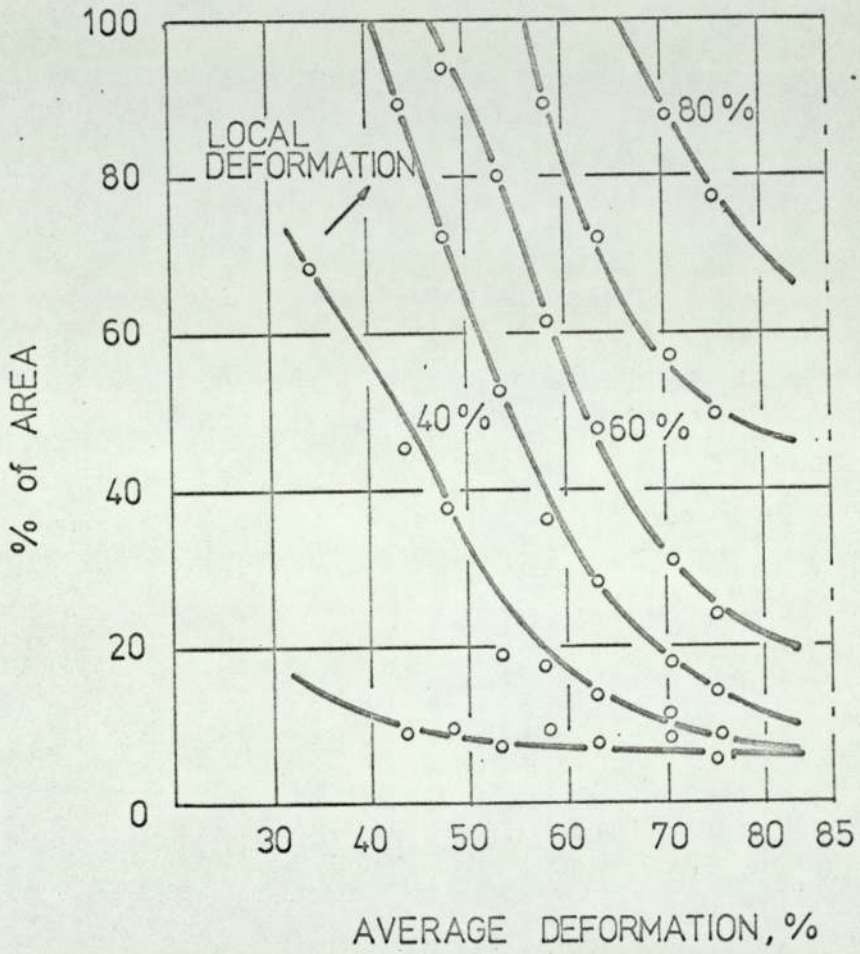


FIG. 2.9 AFTER [9]

P	SLAB METHOD
Q	UPPER BOUND
R	SLIP LINE
S	LOWER BOUND

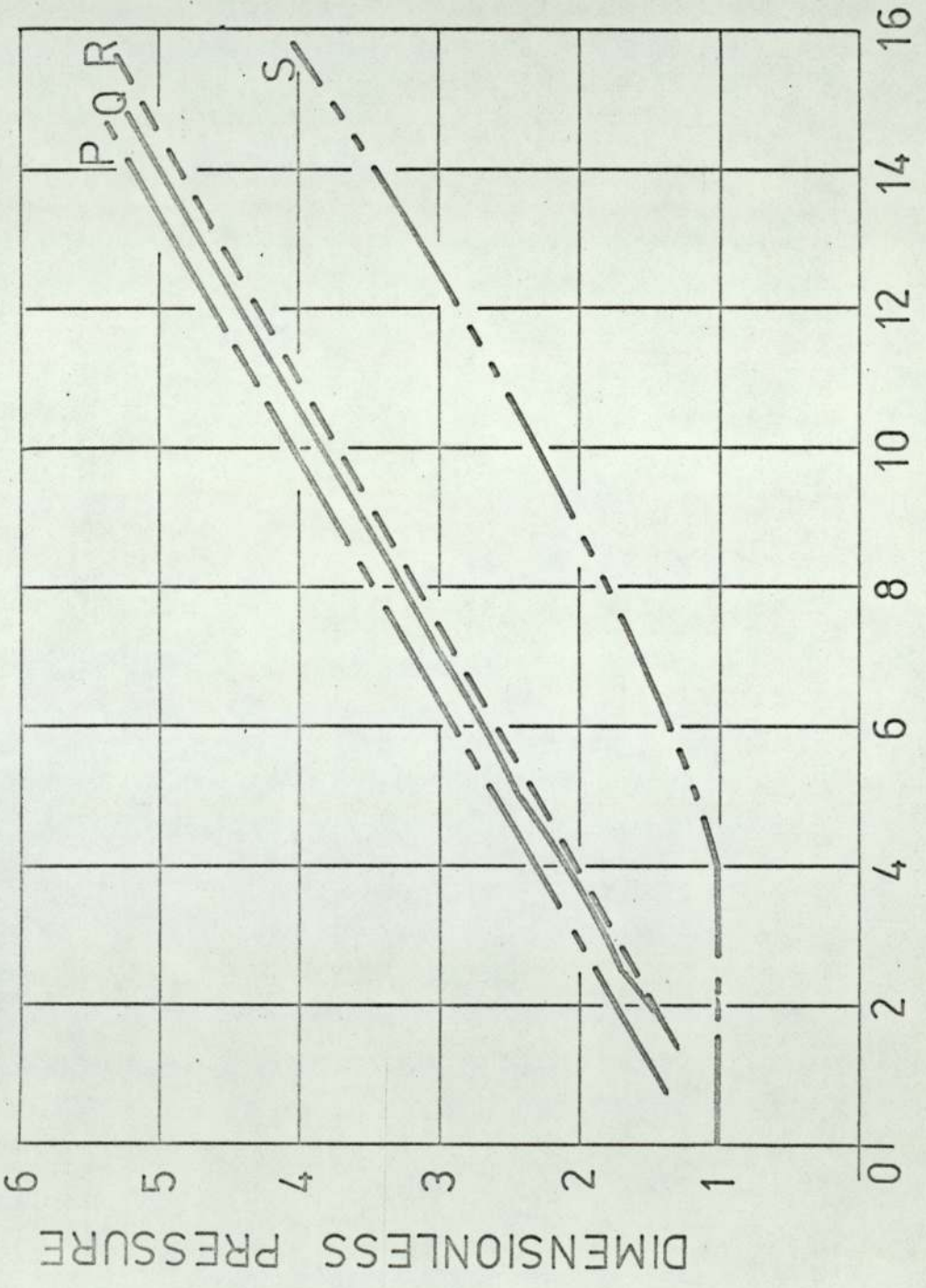
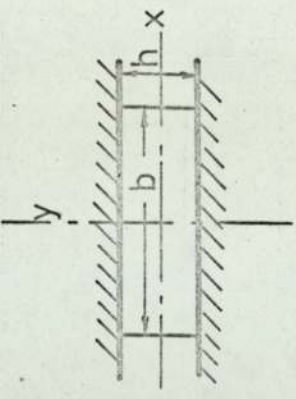


FIG. 2.10 WIDTH TO HEIGHT RATIO b/h

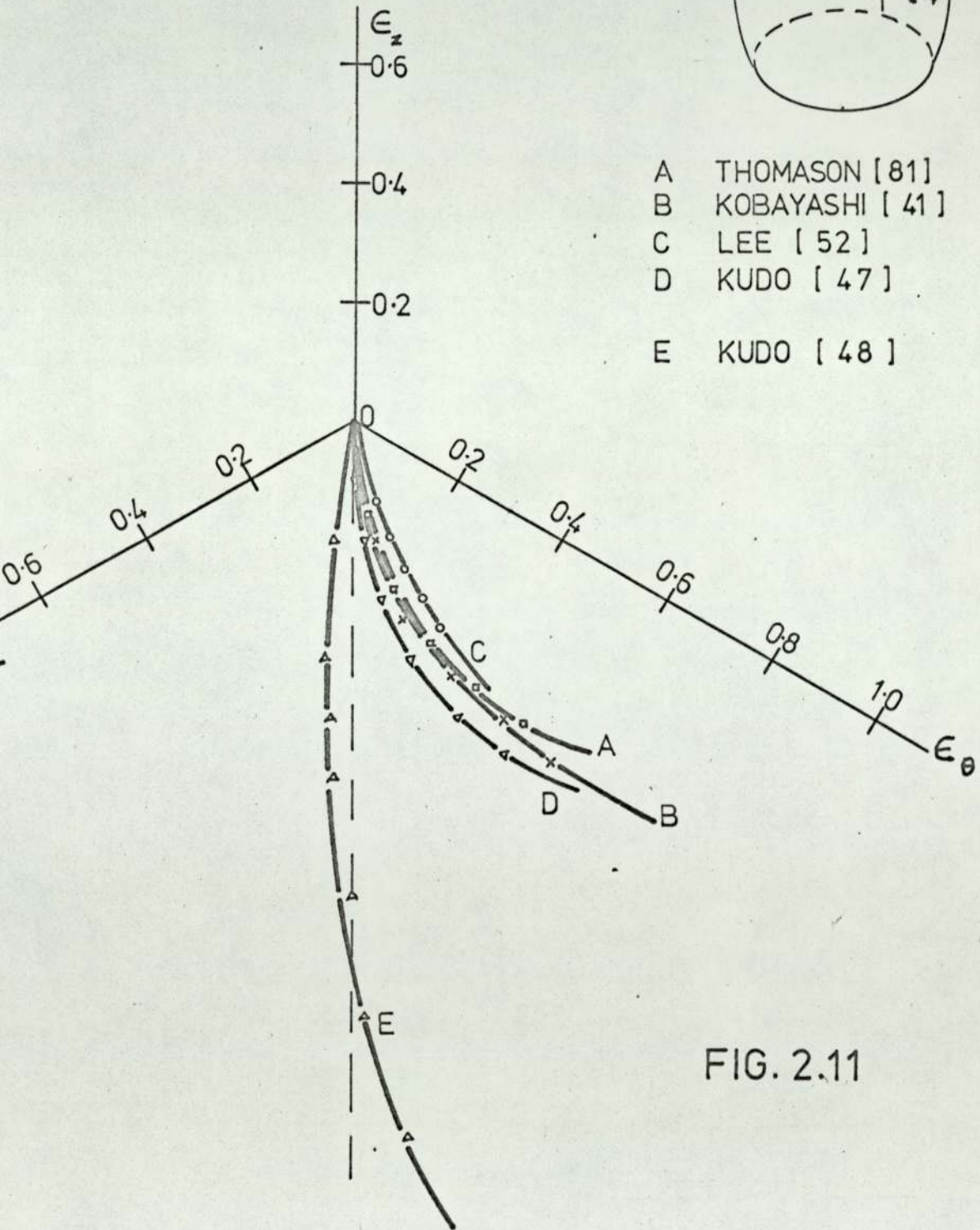
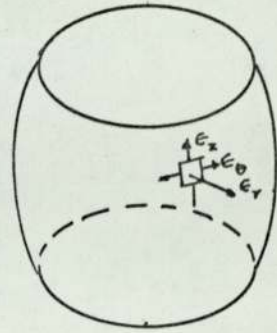


FIG. 2.11

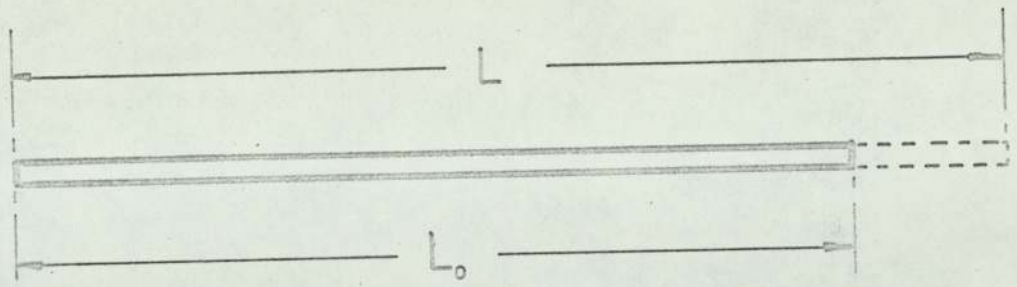


FIG. 3.1

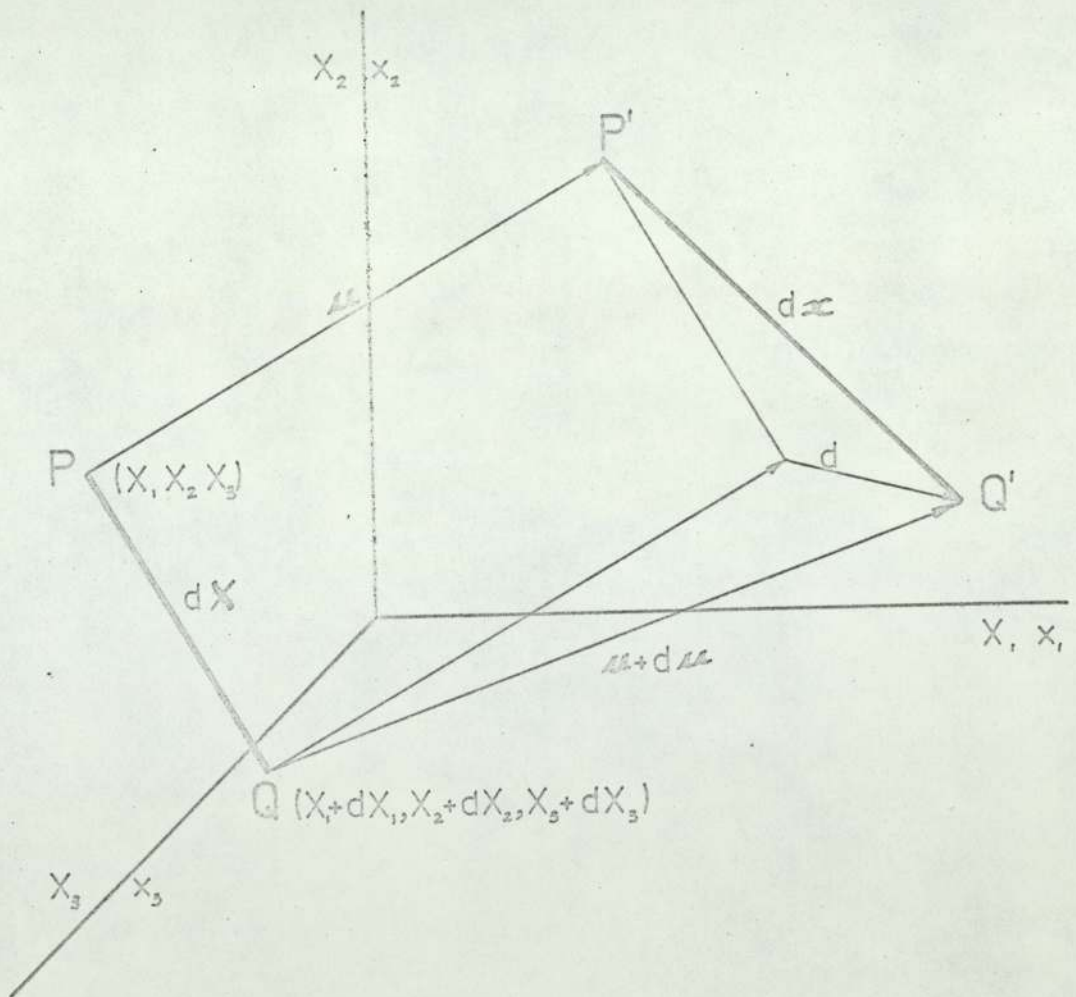


FIG. 3.2

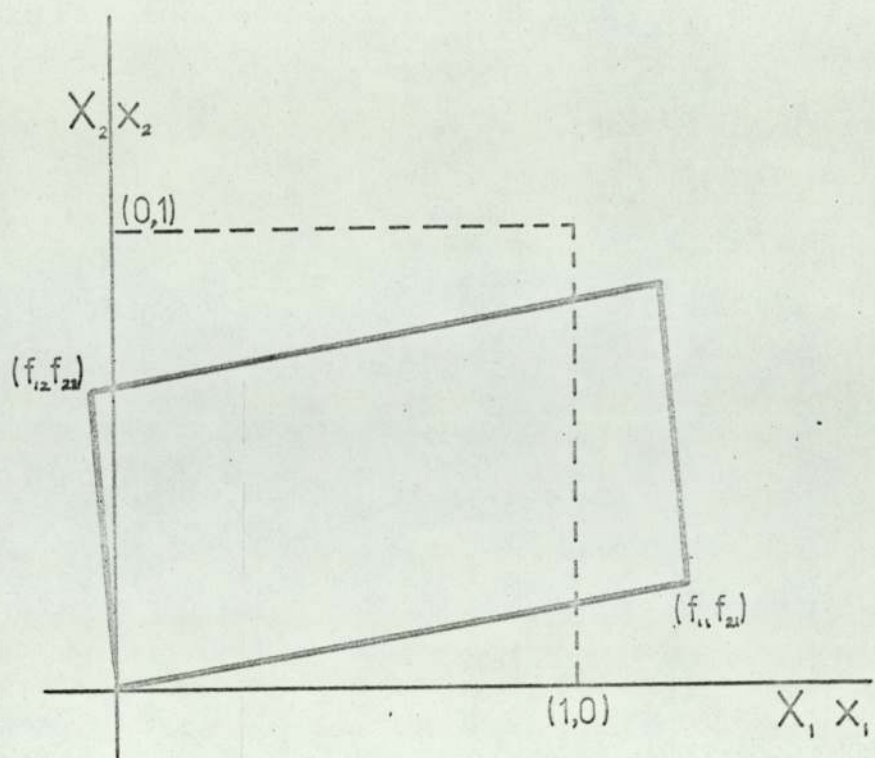


FIG. 3.3

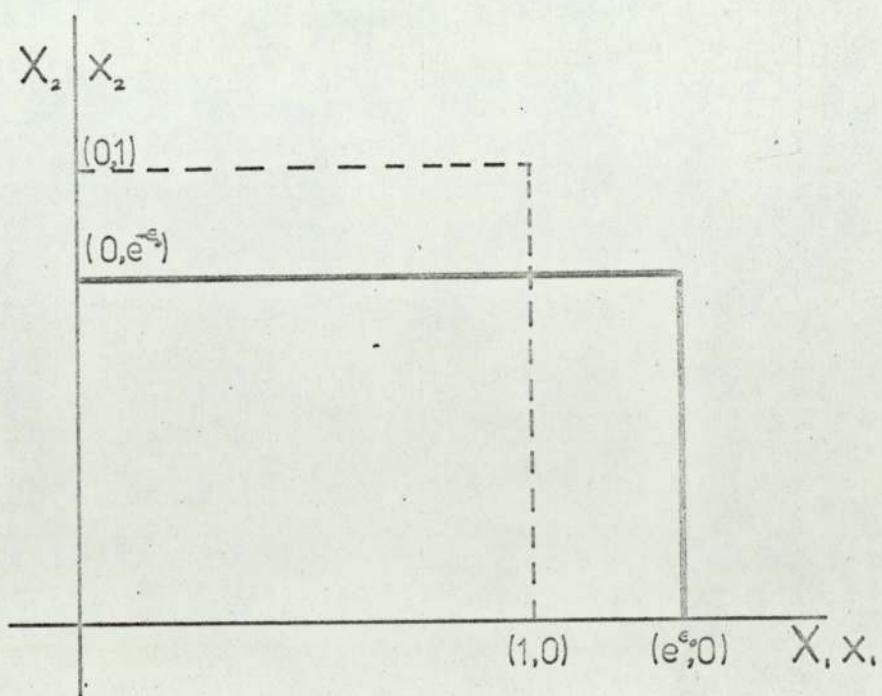


FIG. 3.4

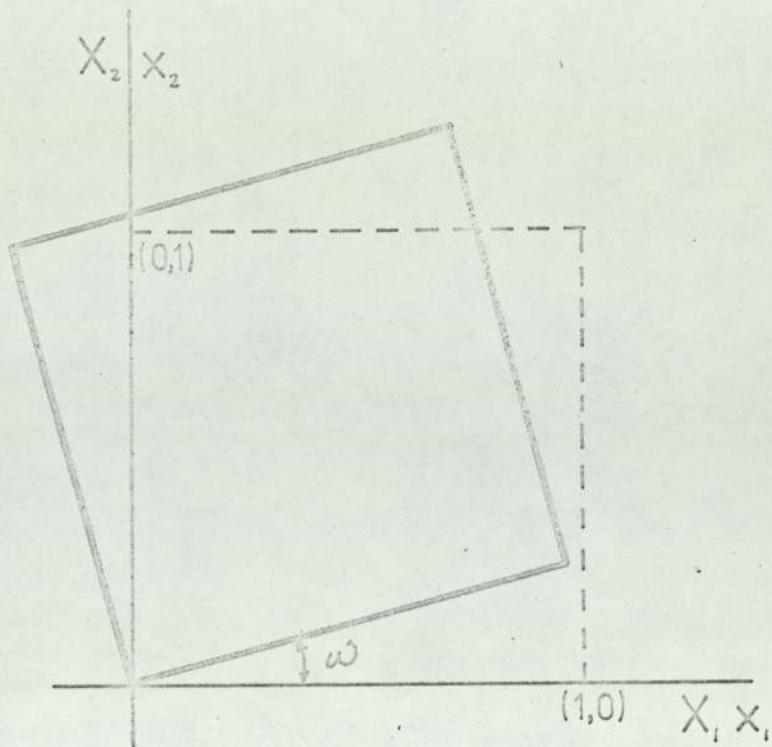


FIG. 3.5

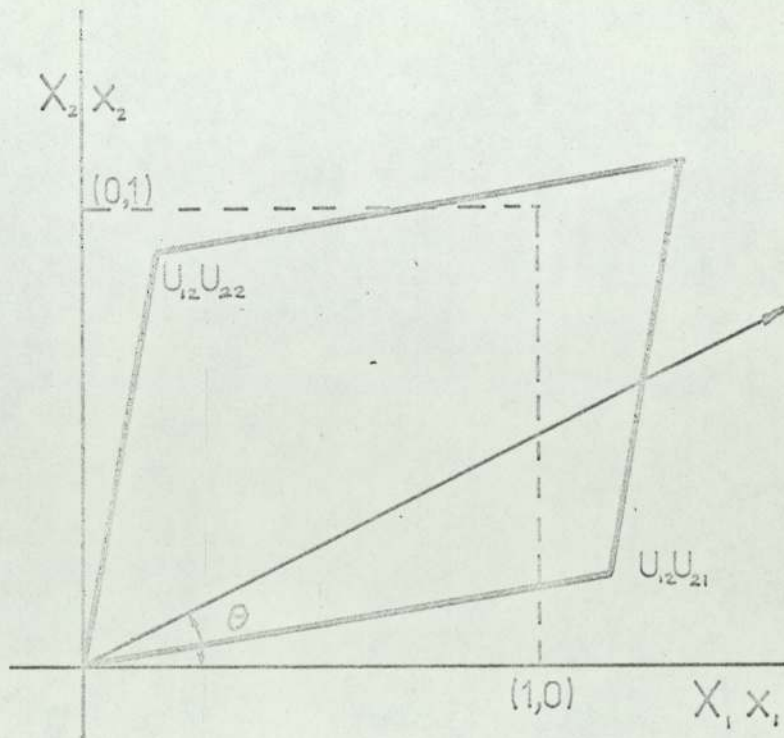


FIG. 3.6

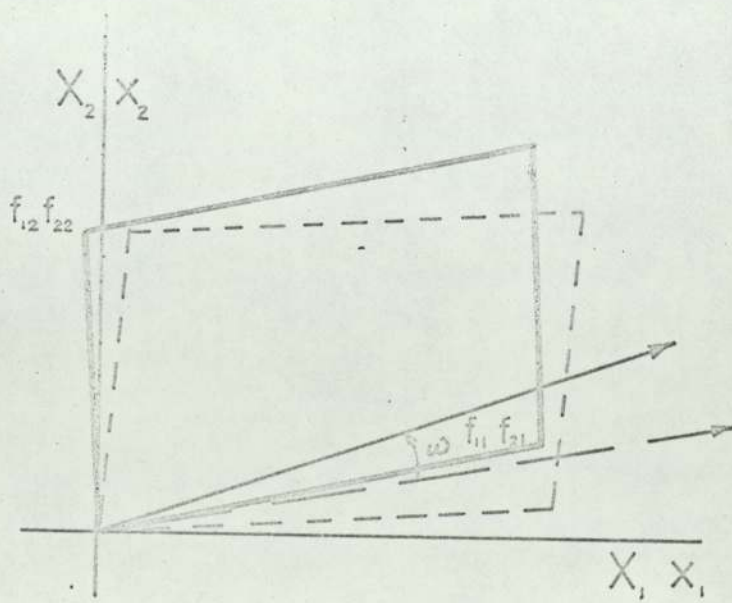
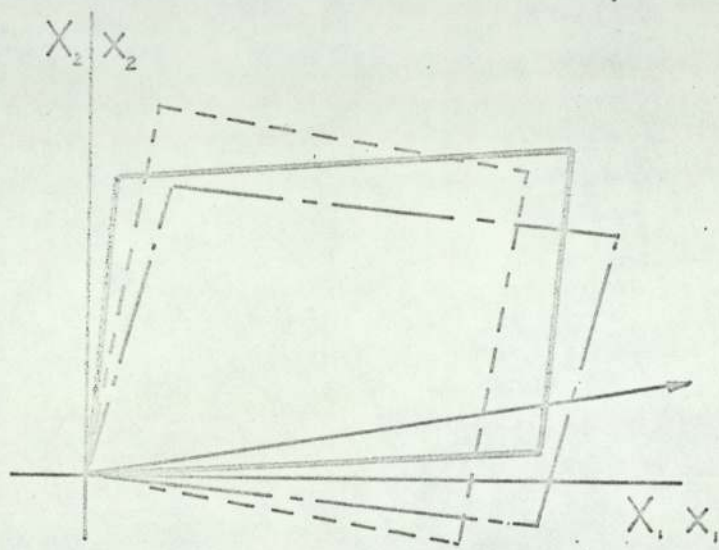
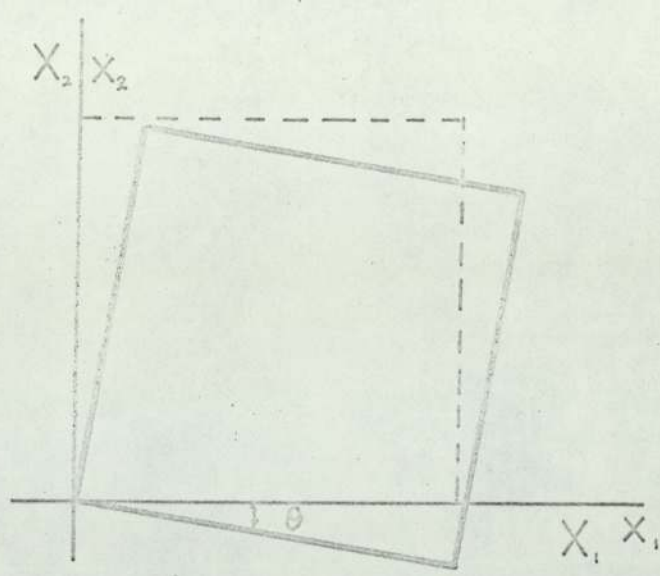


FIG. 3.7

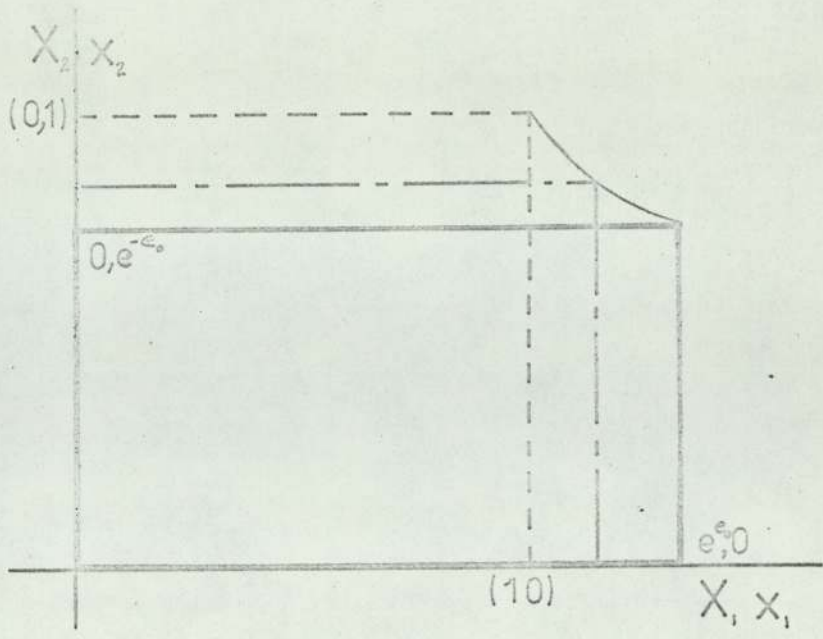


FIG. 3.8

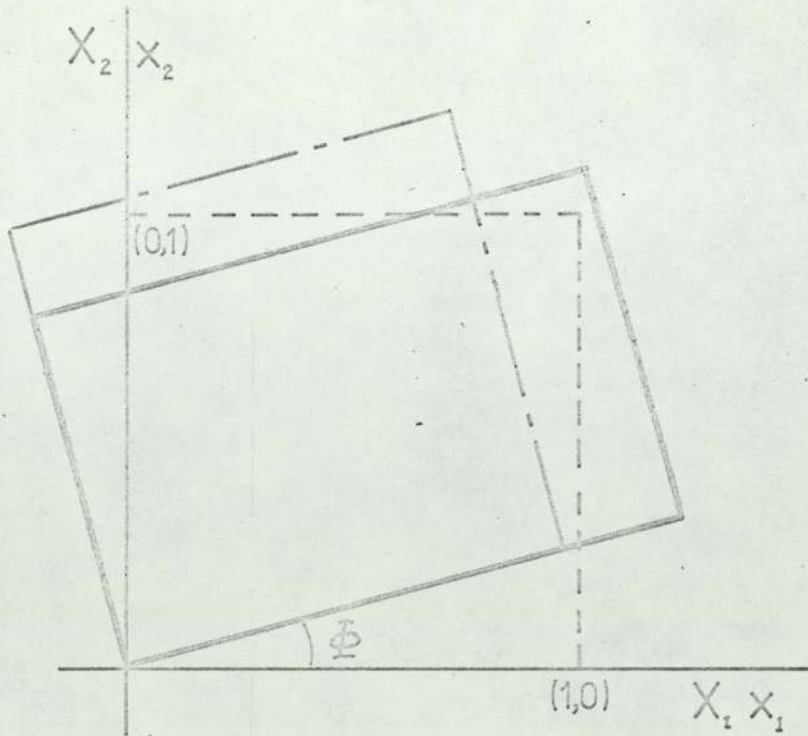


FIG. 3.9

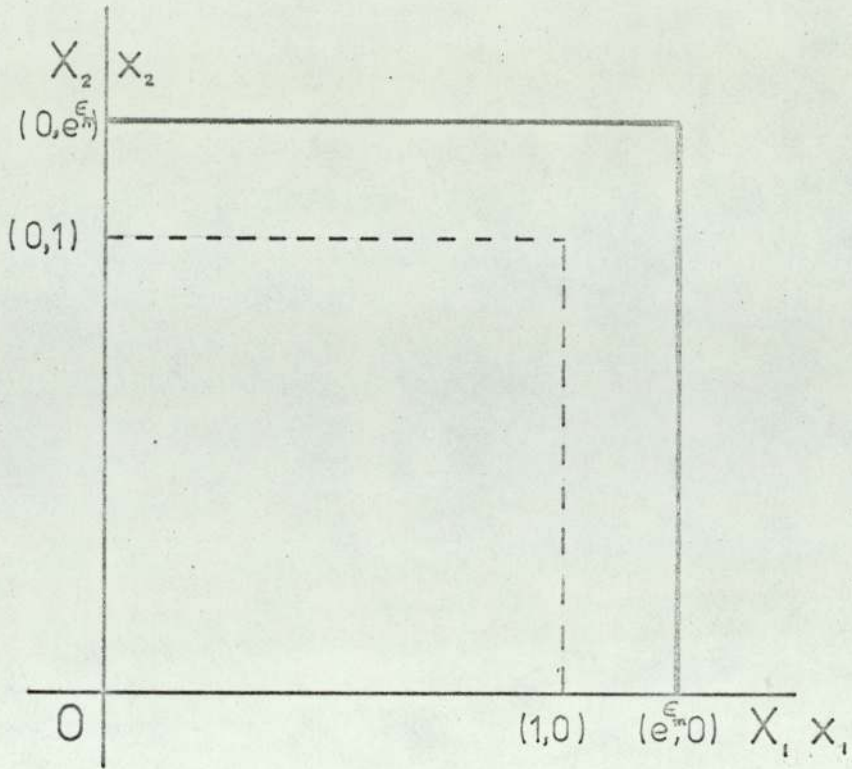


FIG. 3.10

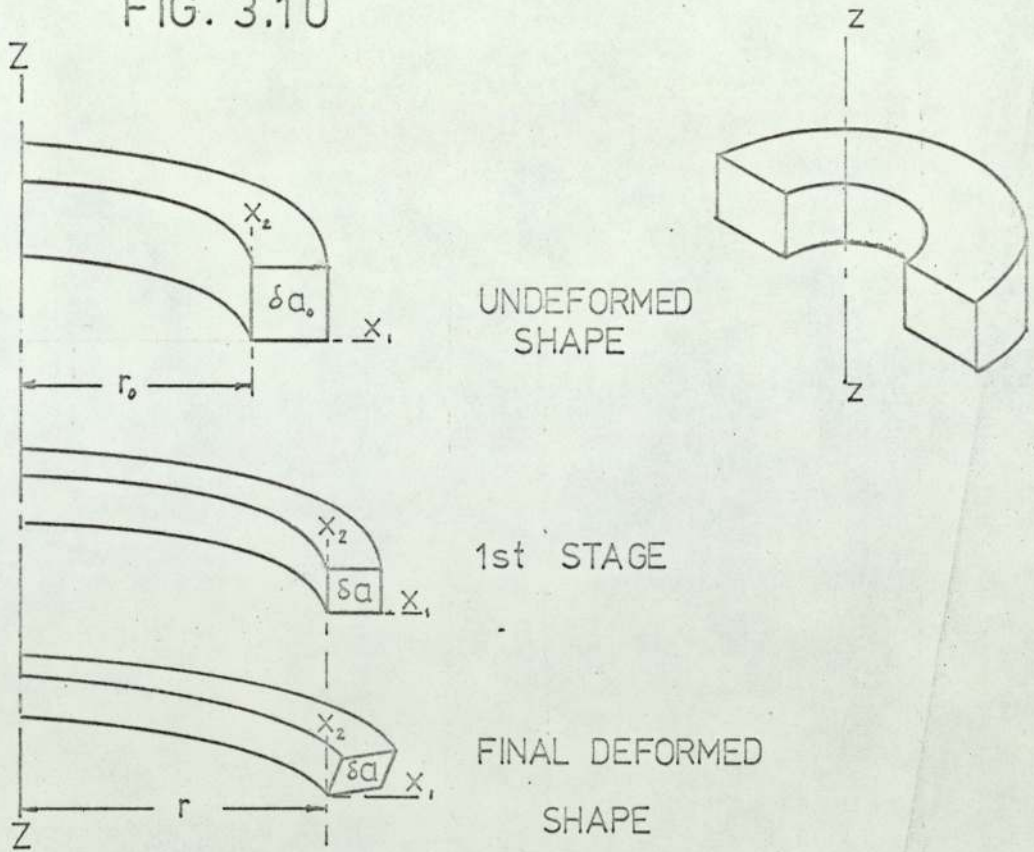


FIG. 3.11

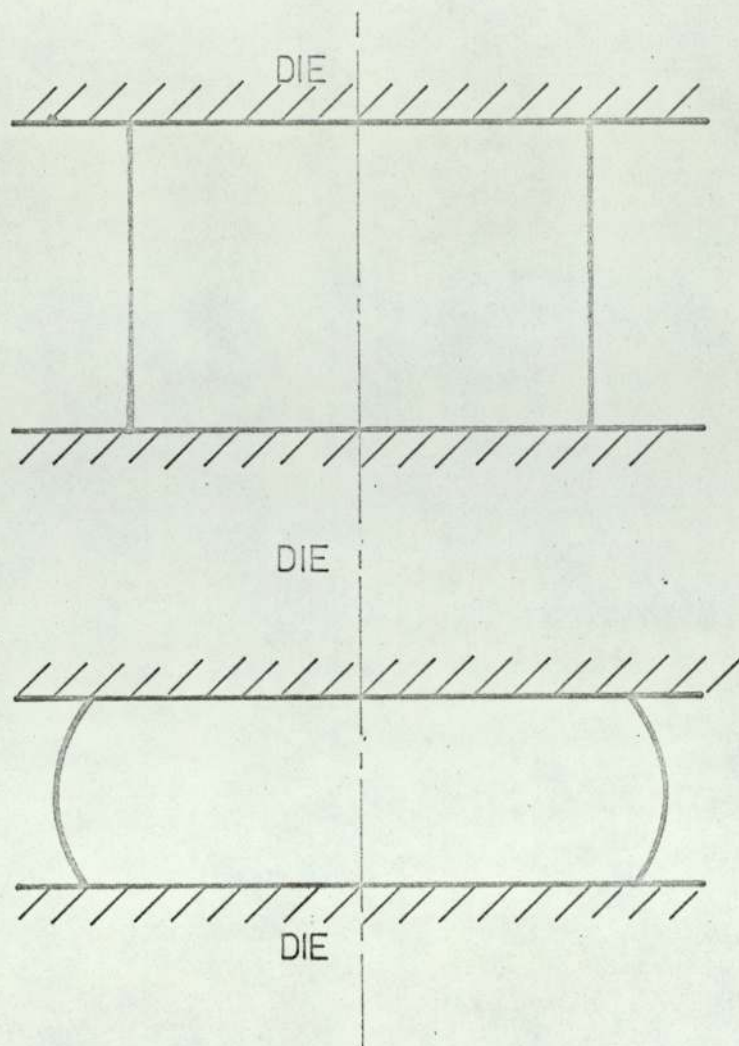


FIG. 4.1

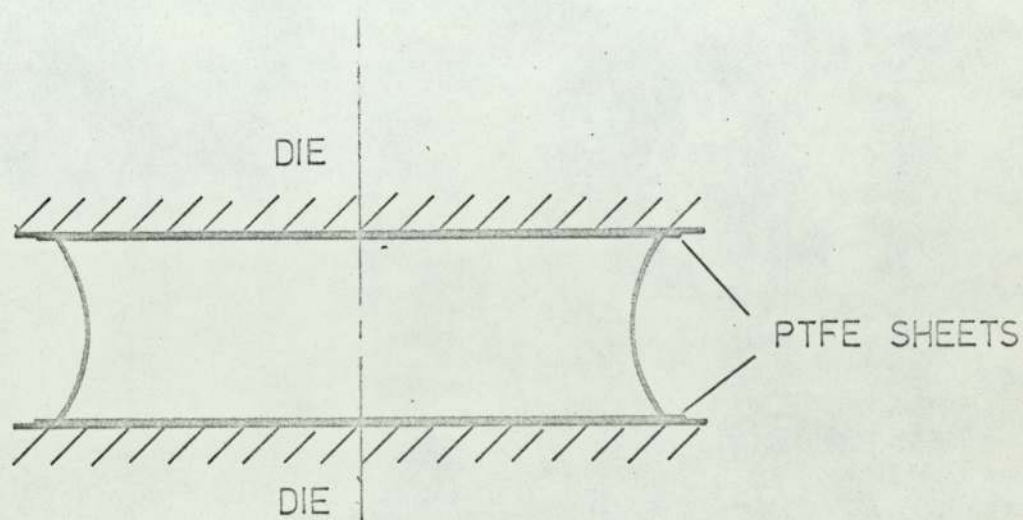


FIG. 4.2

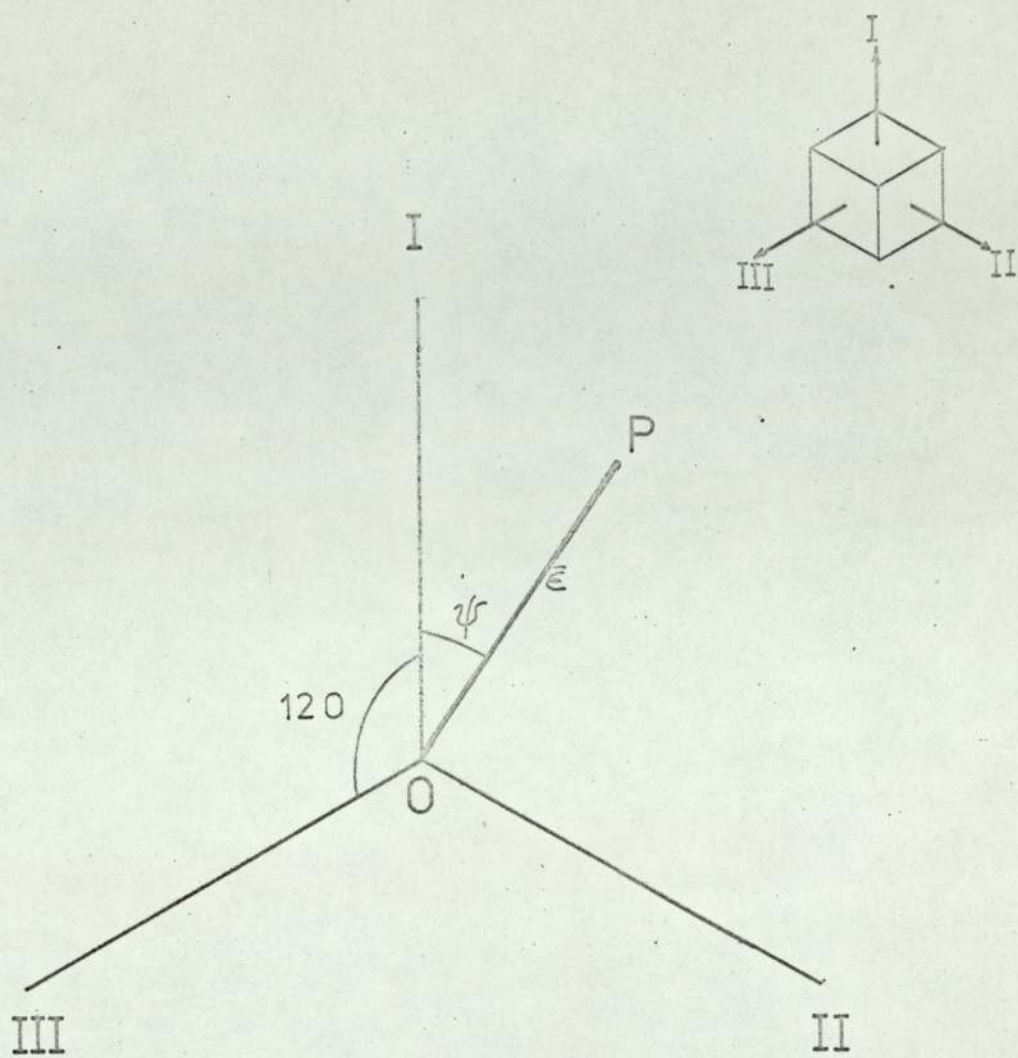


FIG. 4.3

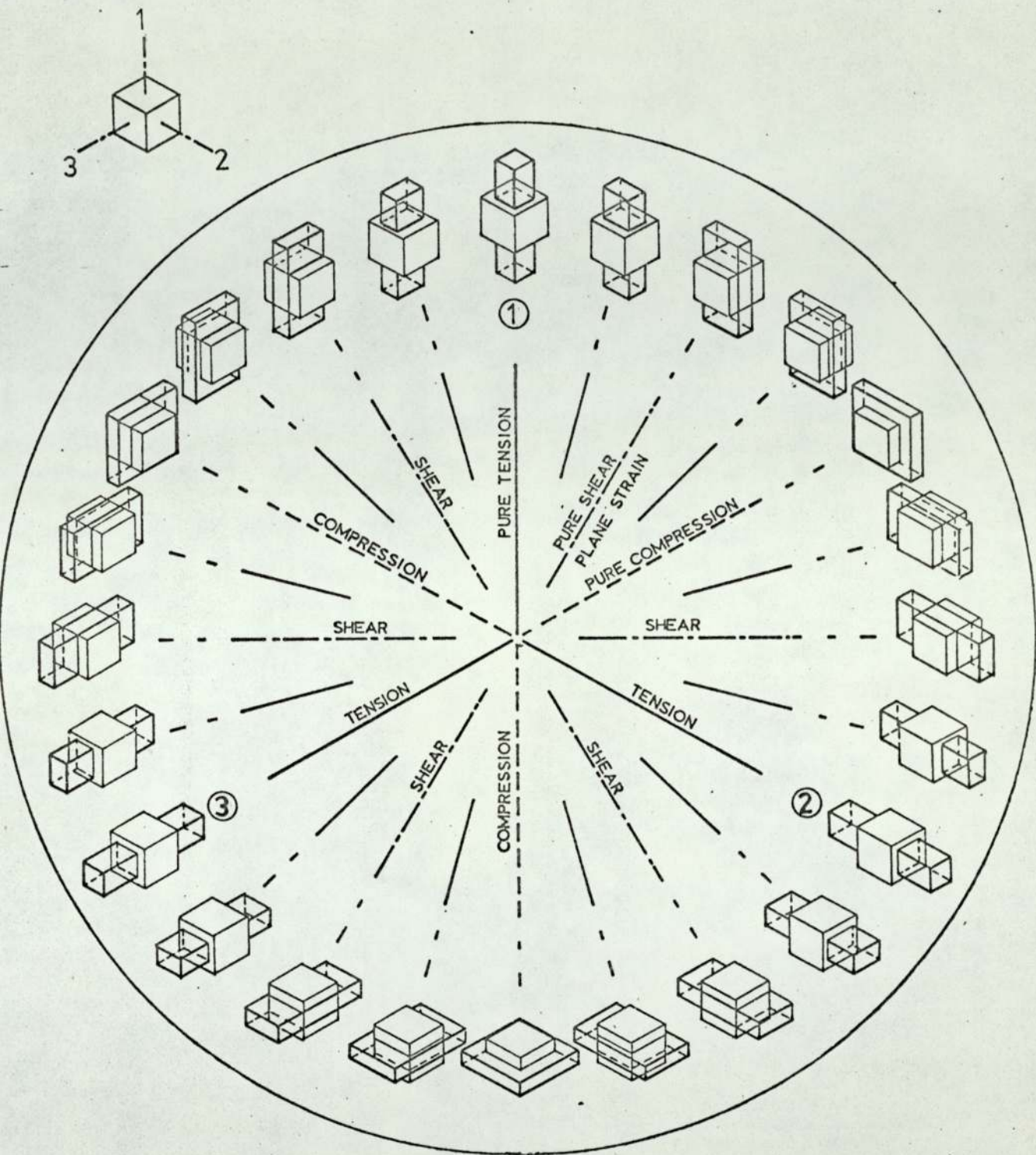


FIG. 4.4

After T.C. Hsu, 'The Characteristics of Coaxial and Non-coaxial Strain Paths,' *Journal of Strain Analysis*, 1966, 1(3), 218

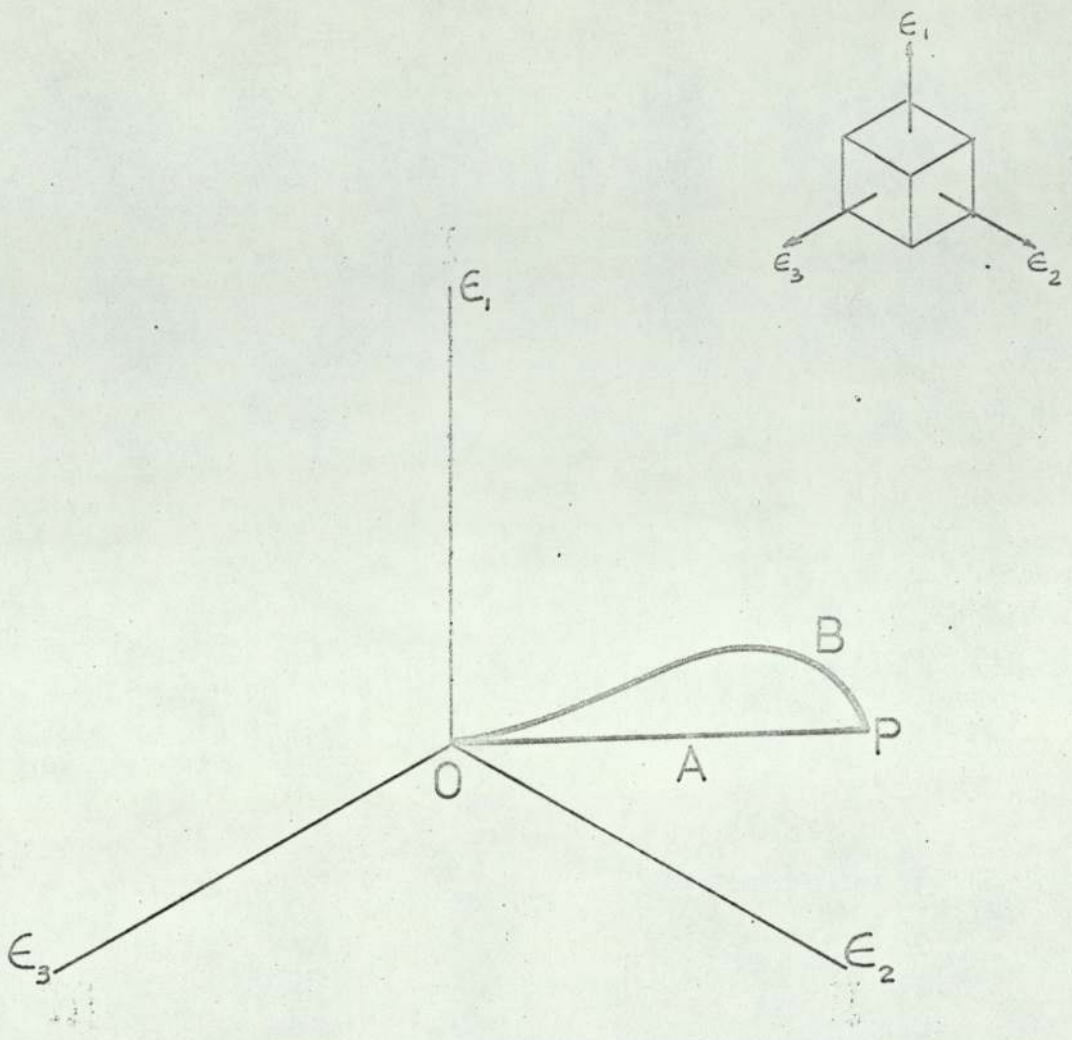


FIG. 4.5 .

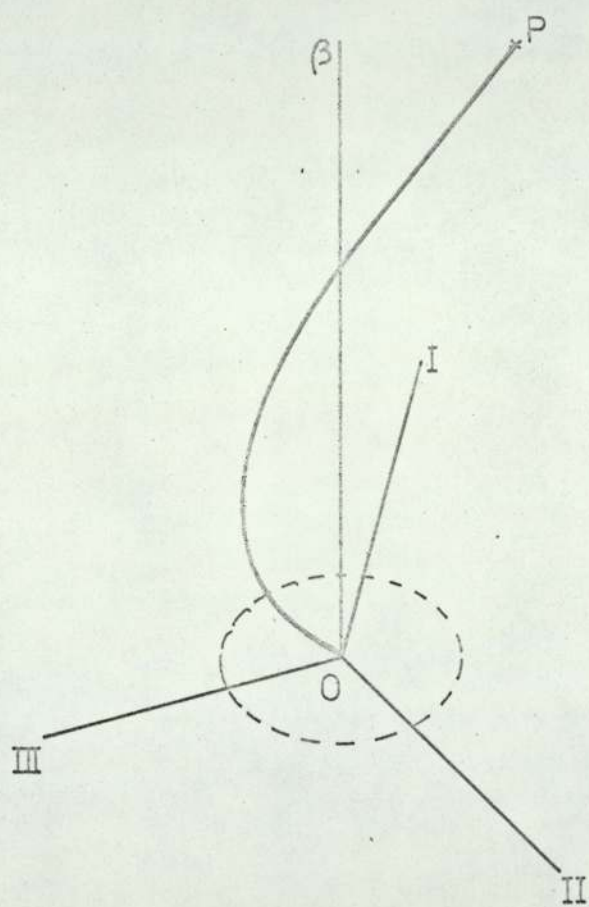
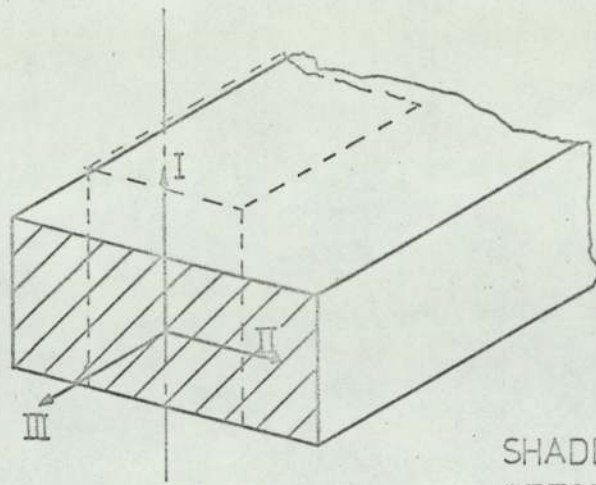


FIG. 4.6



SHADED AREA IS THE DEFORMATION PLANE

FIG. 4.7

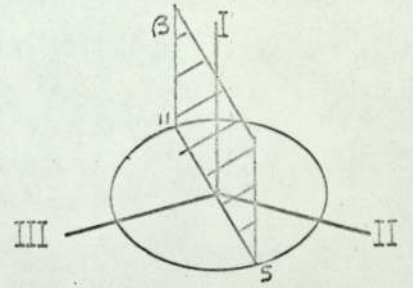
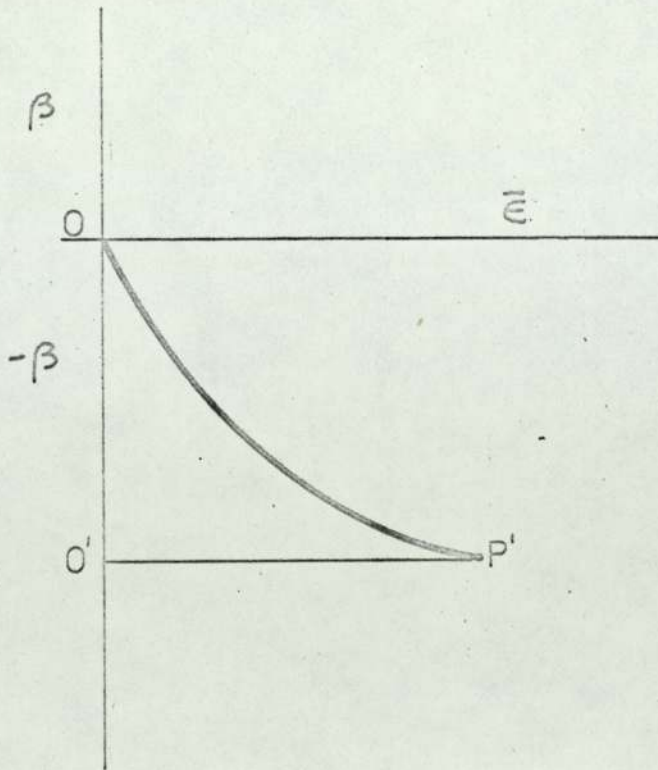


FIG. 4.8

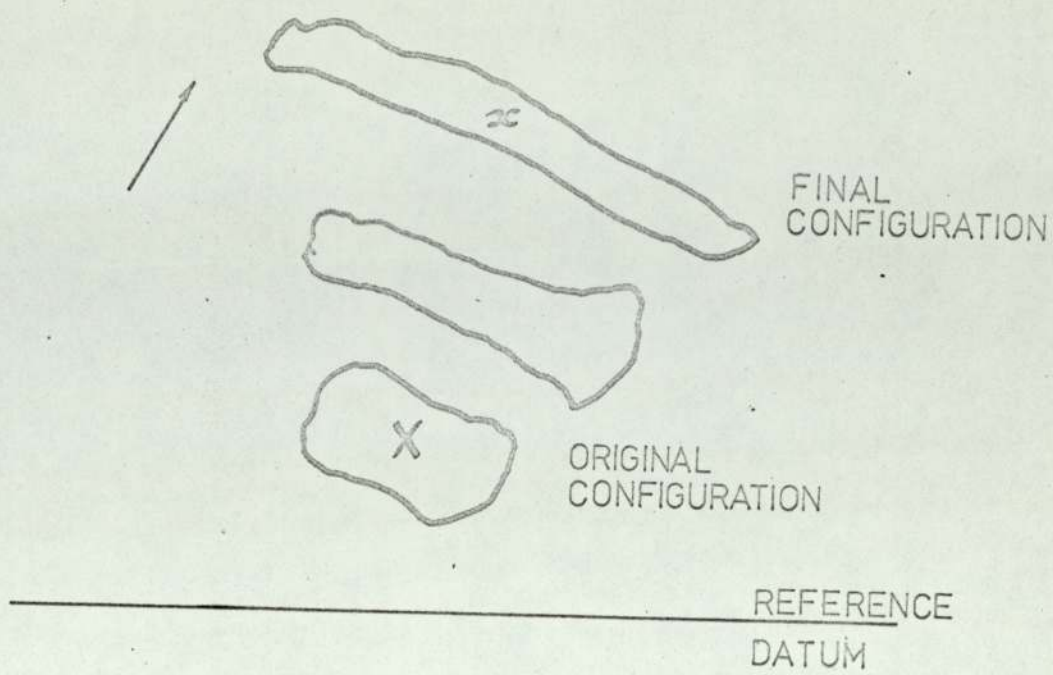


FIG. 4.9

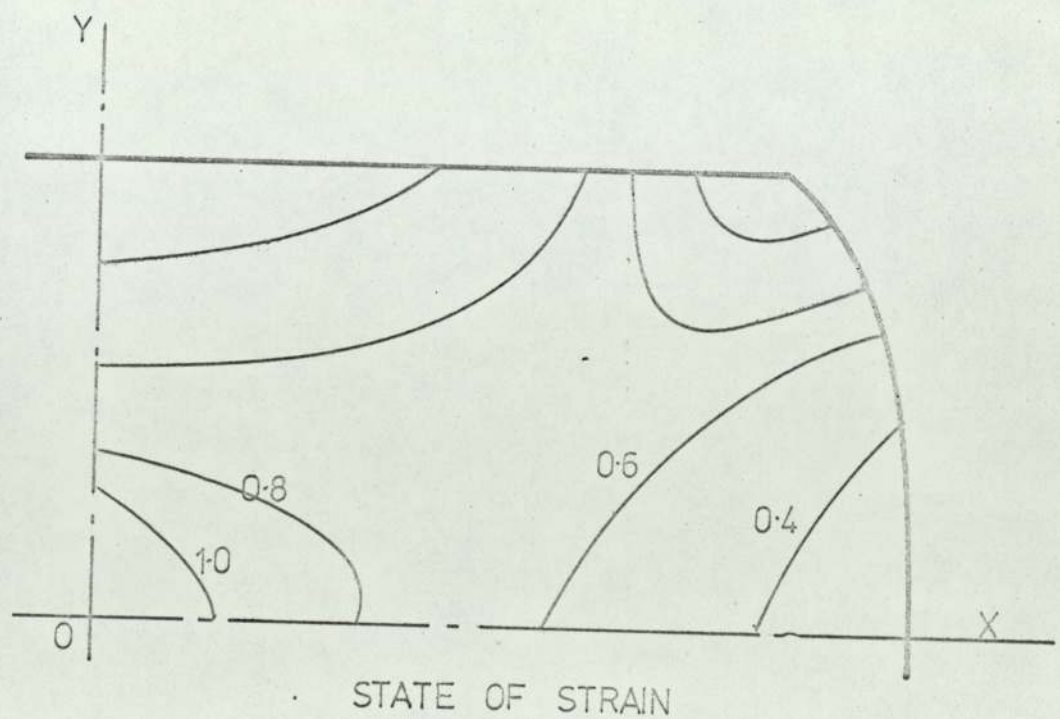


FIG. 4.10

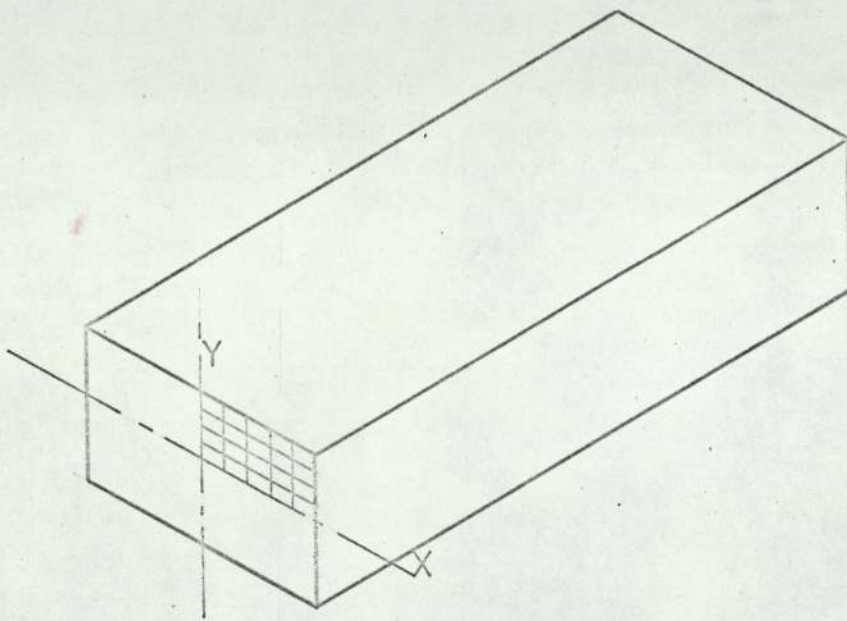


FIG. 4.11

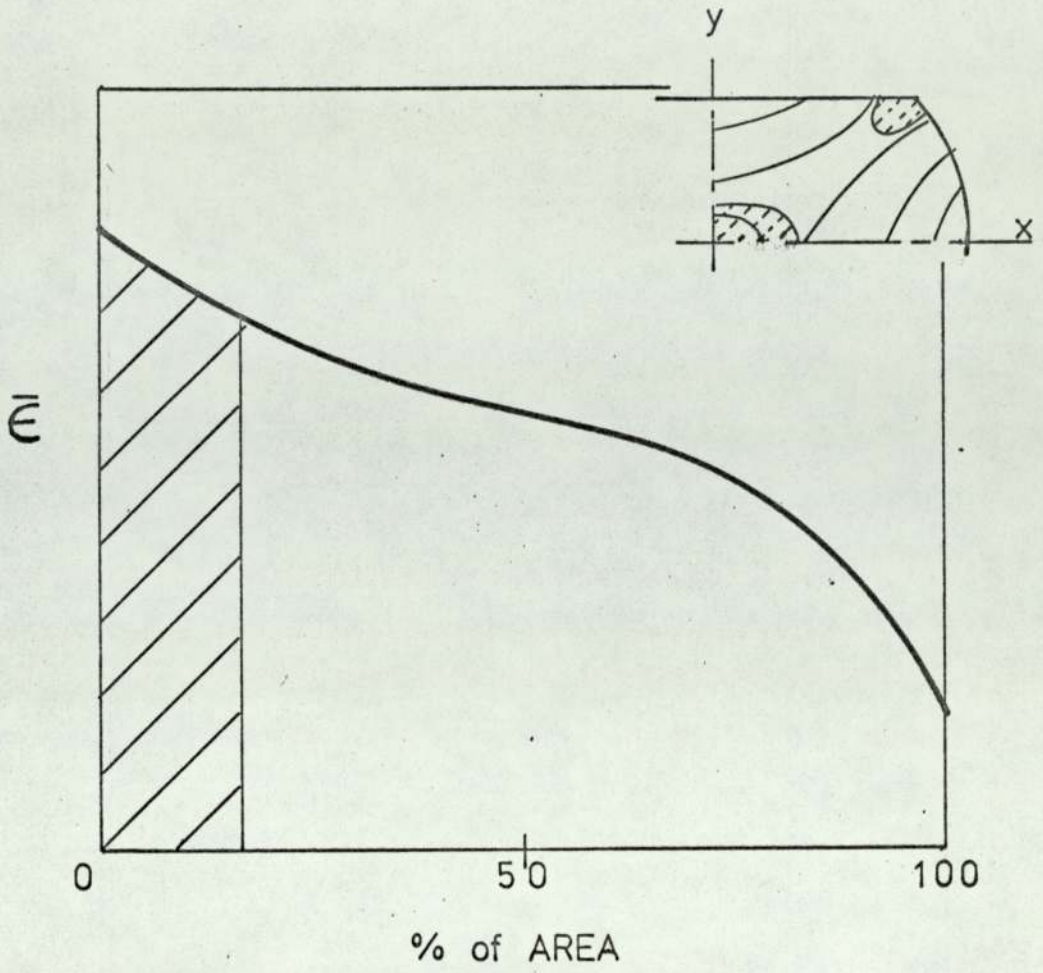


FIG. 4.12

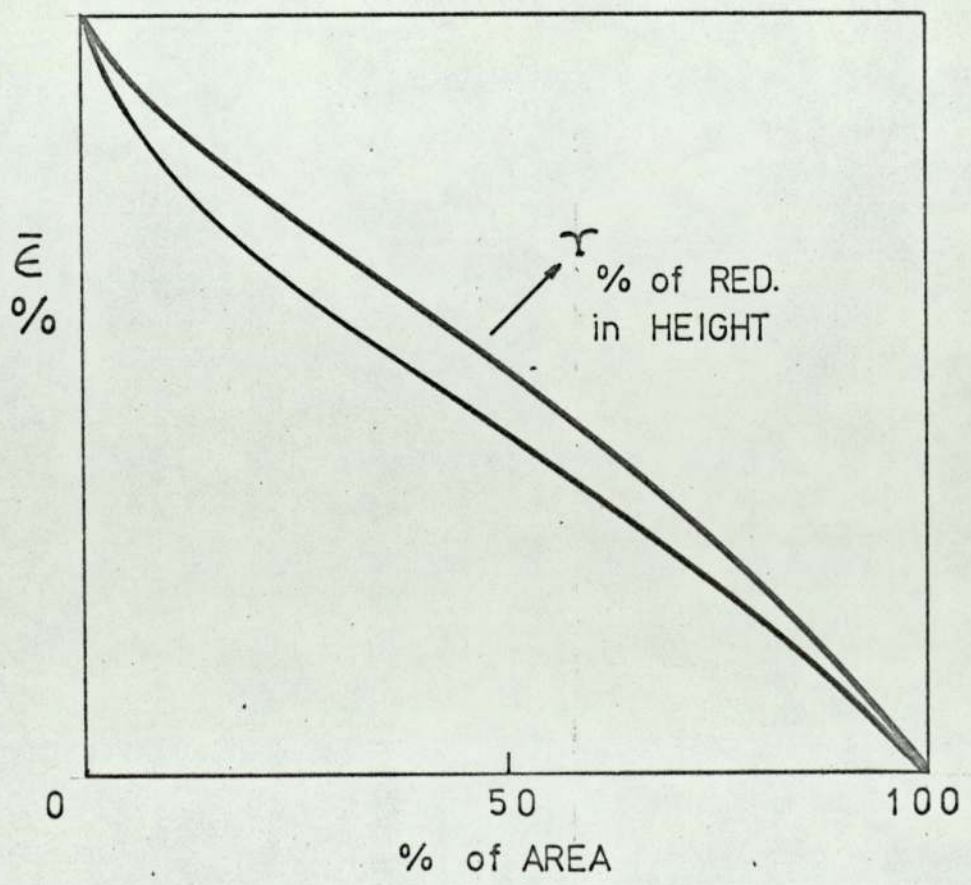


FIG. 4.13

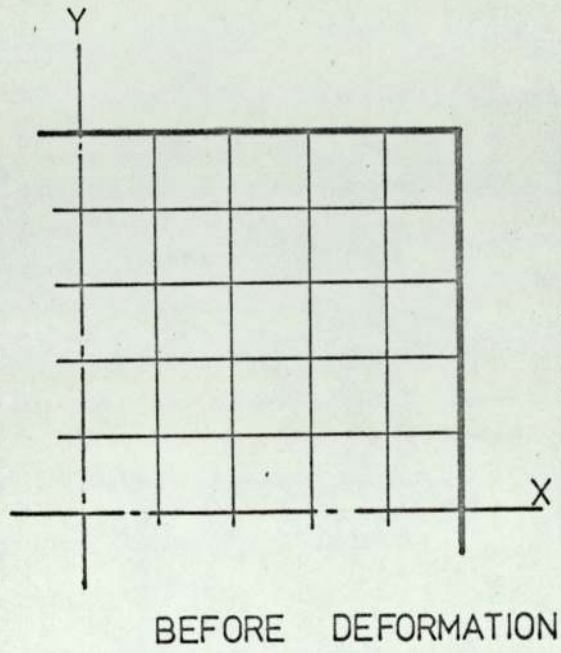


FIG. 4.14a

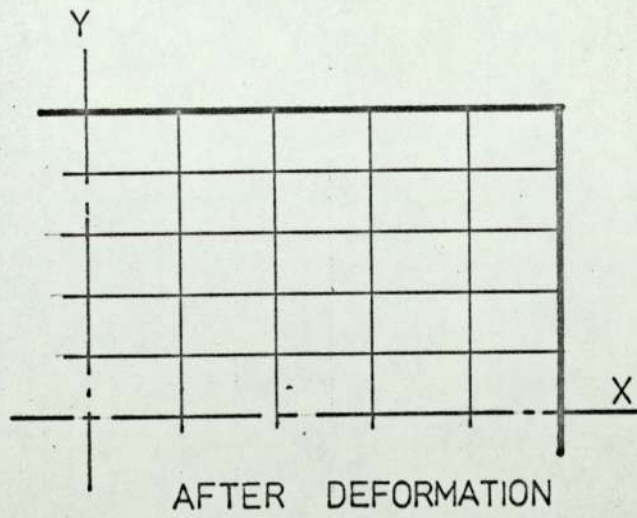


FIG. 4.14b

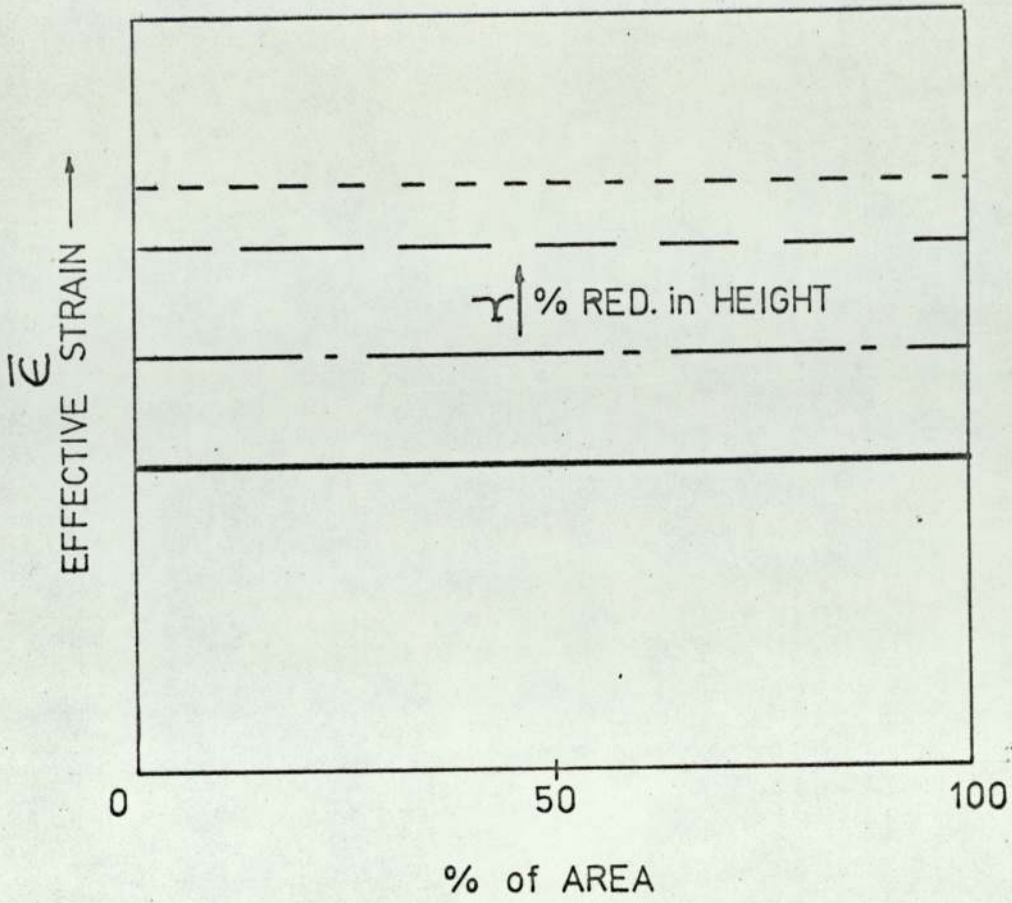


FIG. 4.15

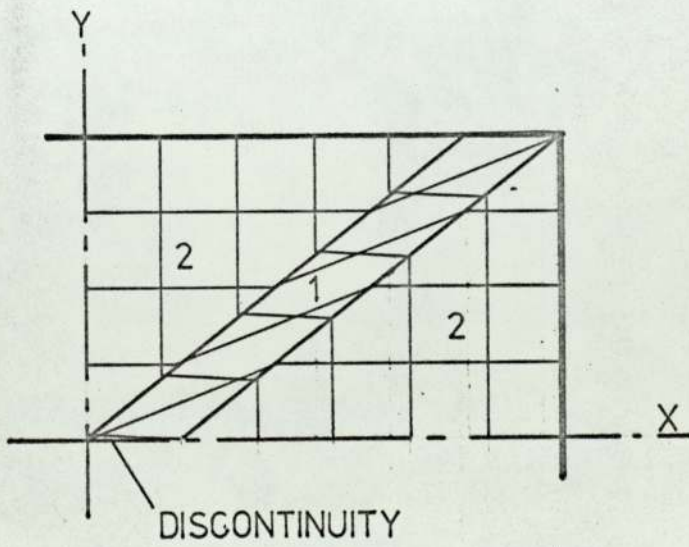


FIG. 4.16

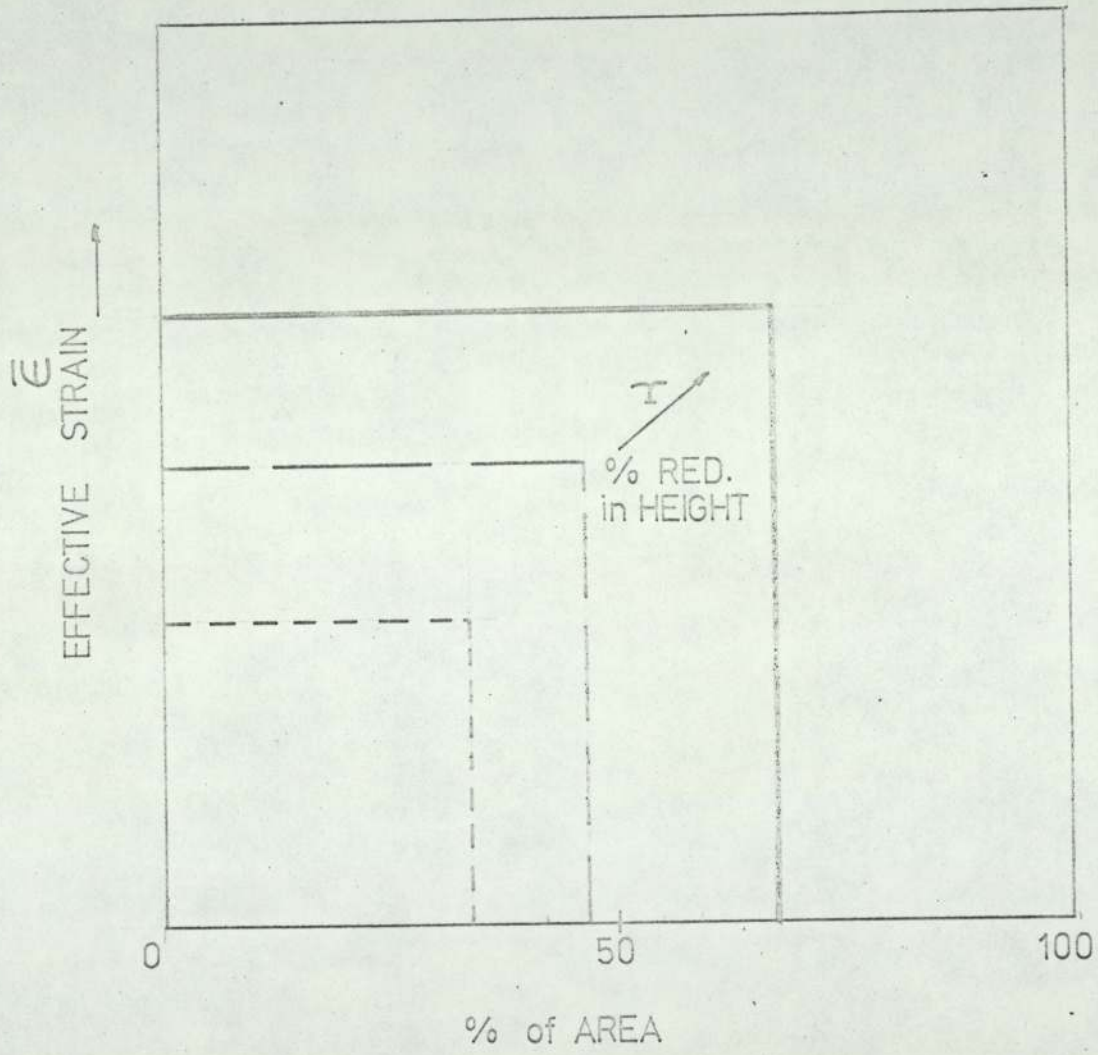


FIG. 4.17

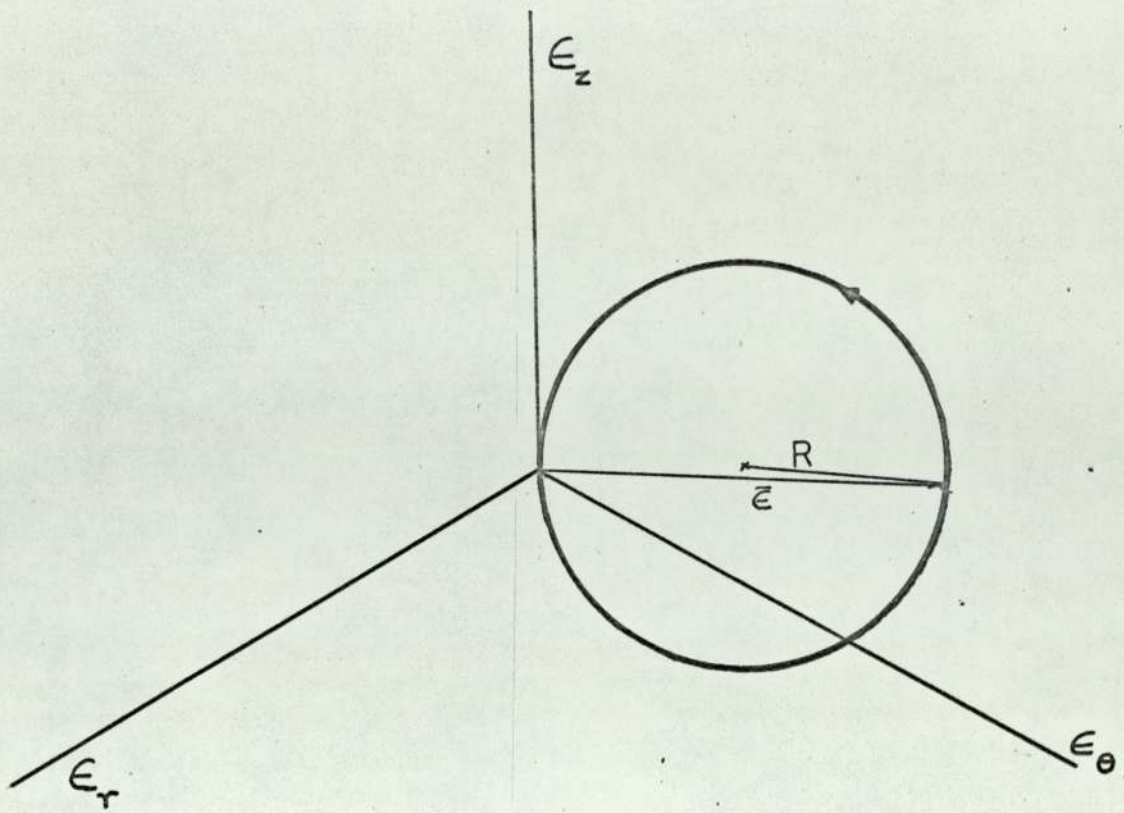


FIG. 5.1

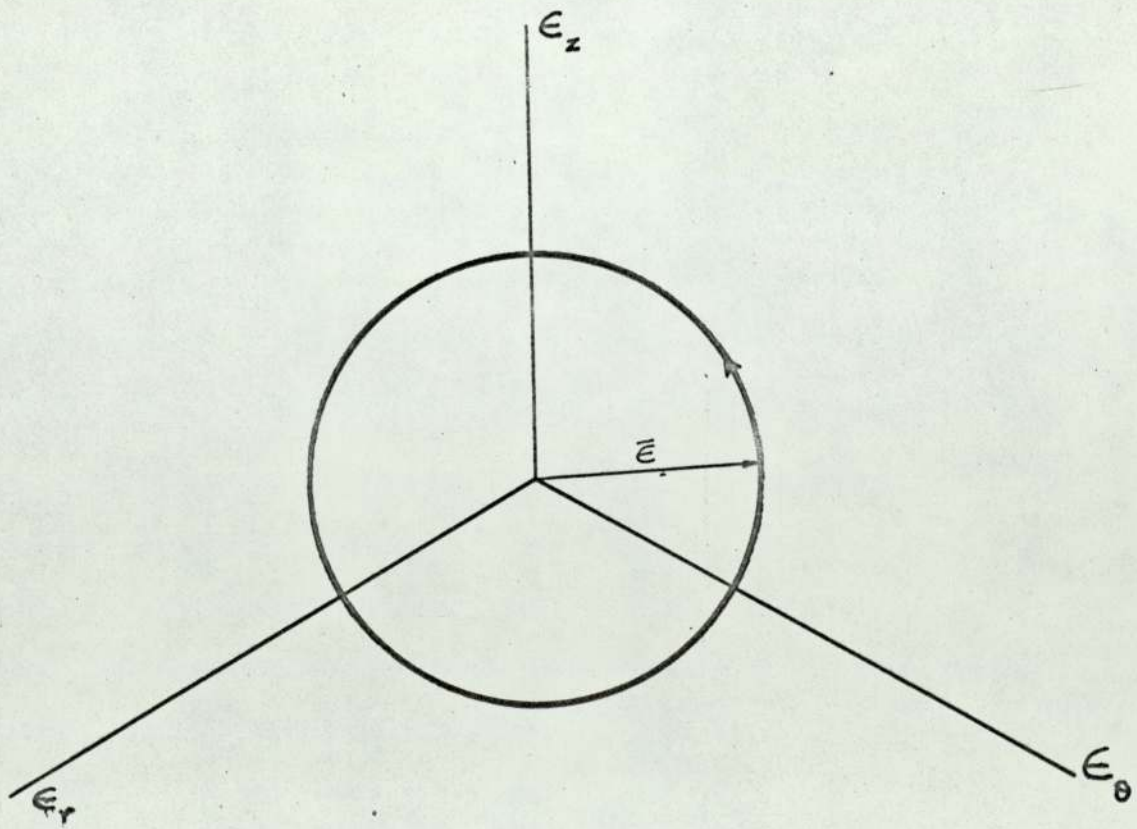


FIG. 5.2

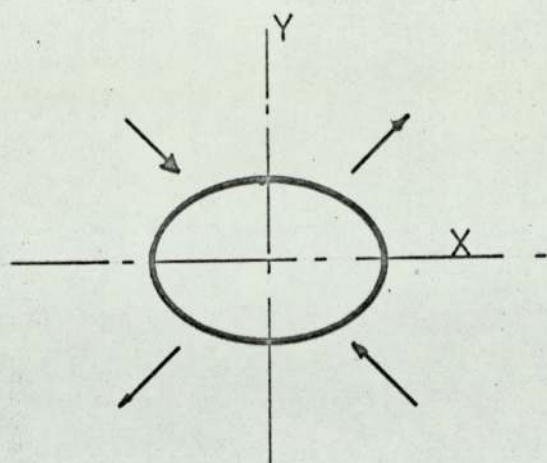


FIG. 5.3.

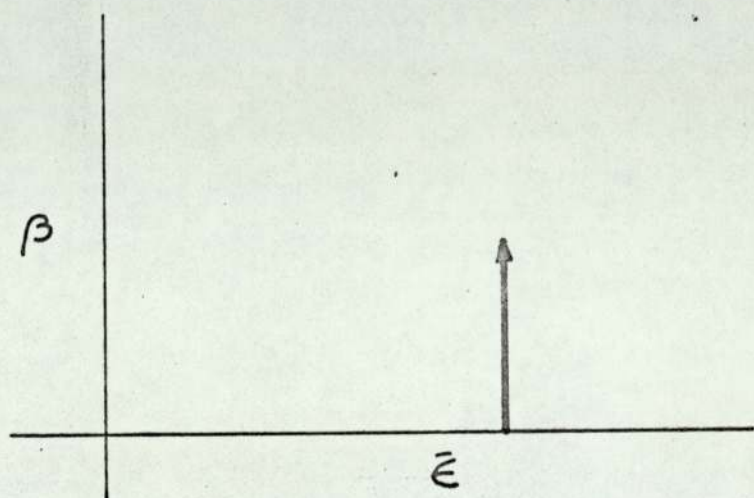


FIG. 5.4

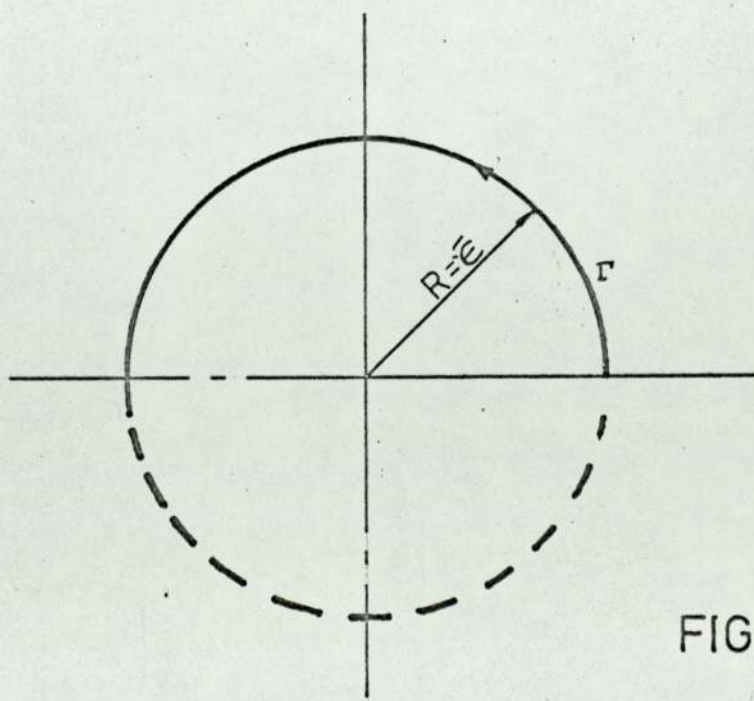


FIG. 5.5

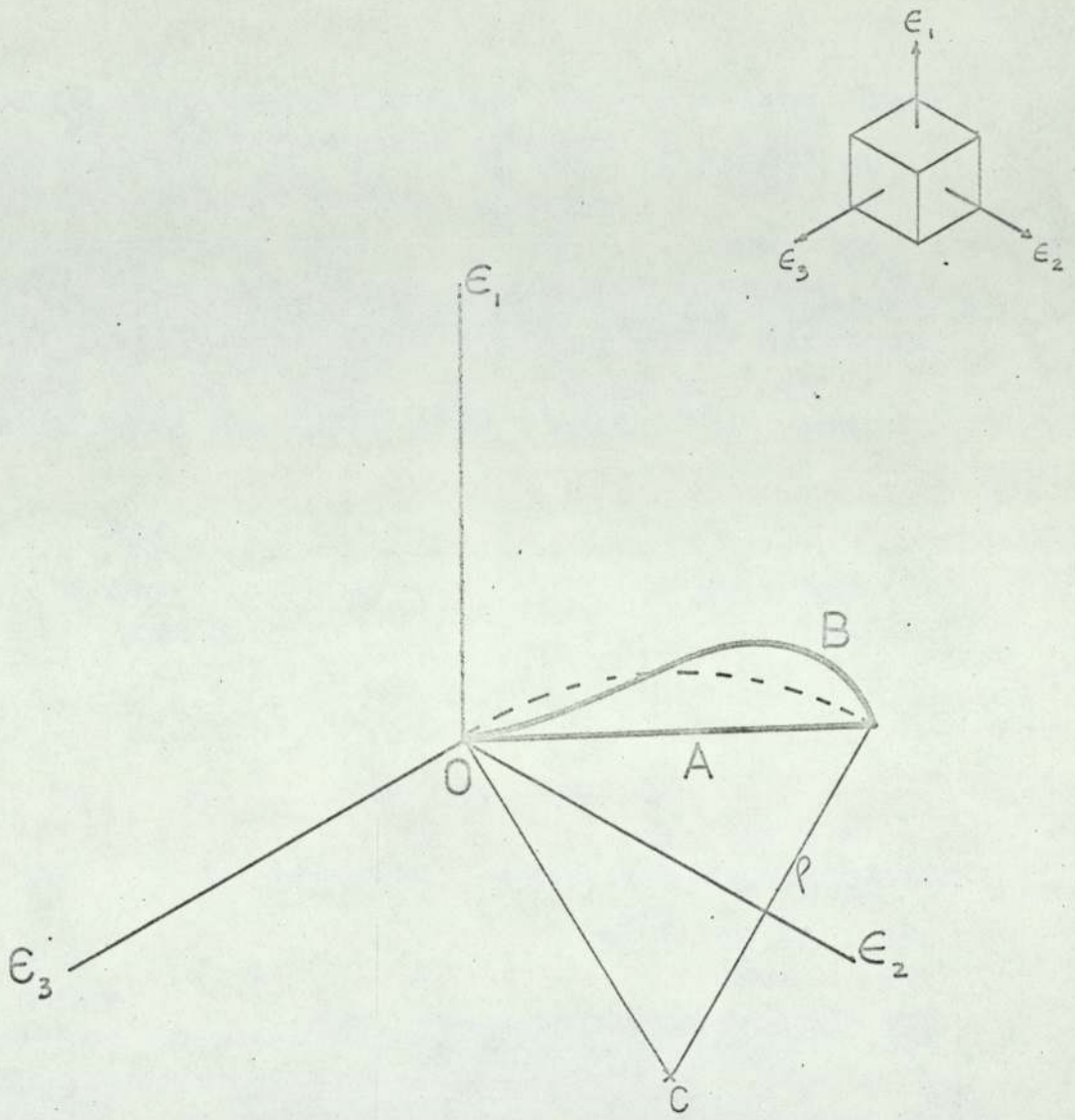


FIG. 6.1.

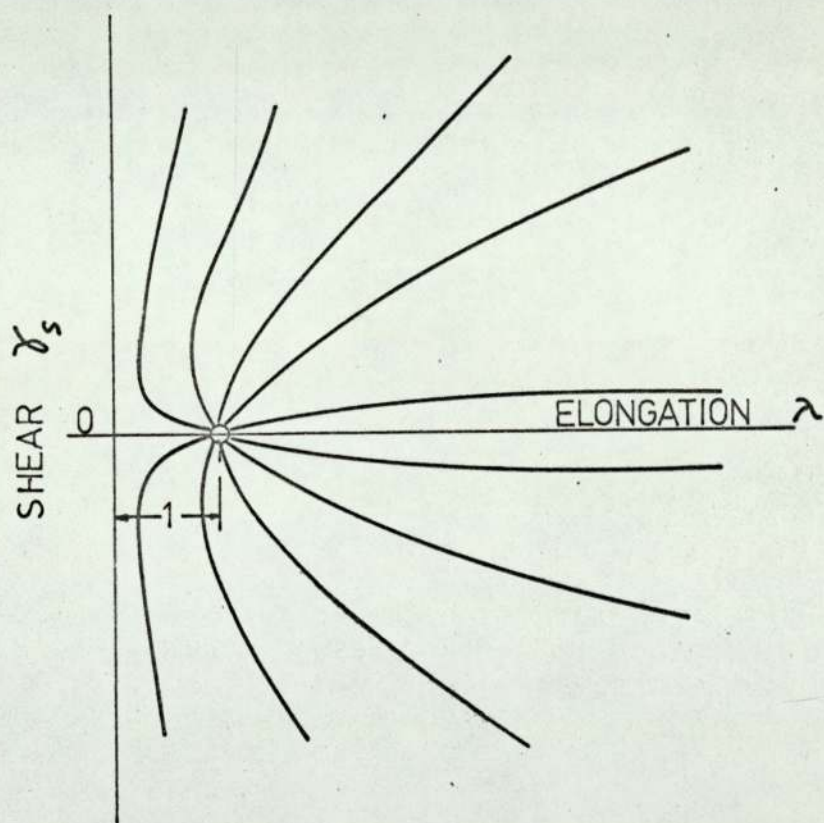


FIG. 6.2 AFTER [61]

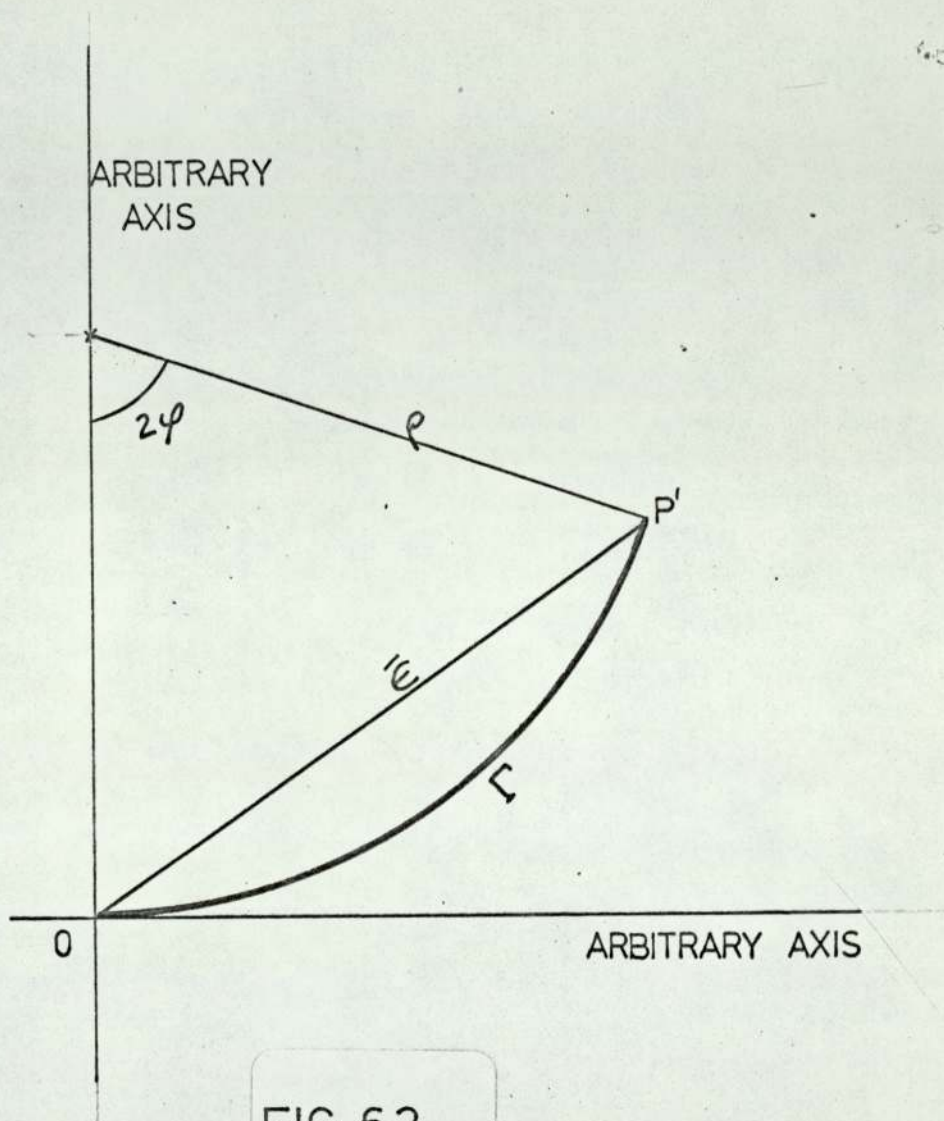


FIG. 6.3

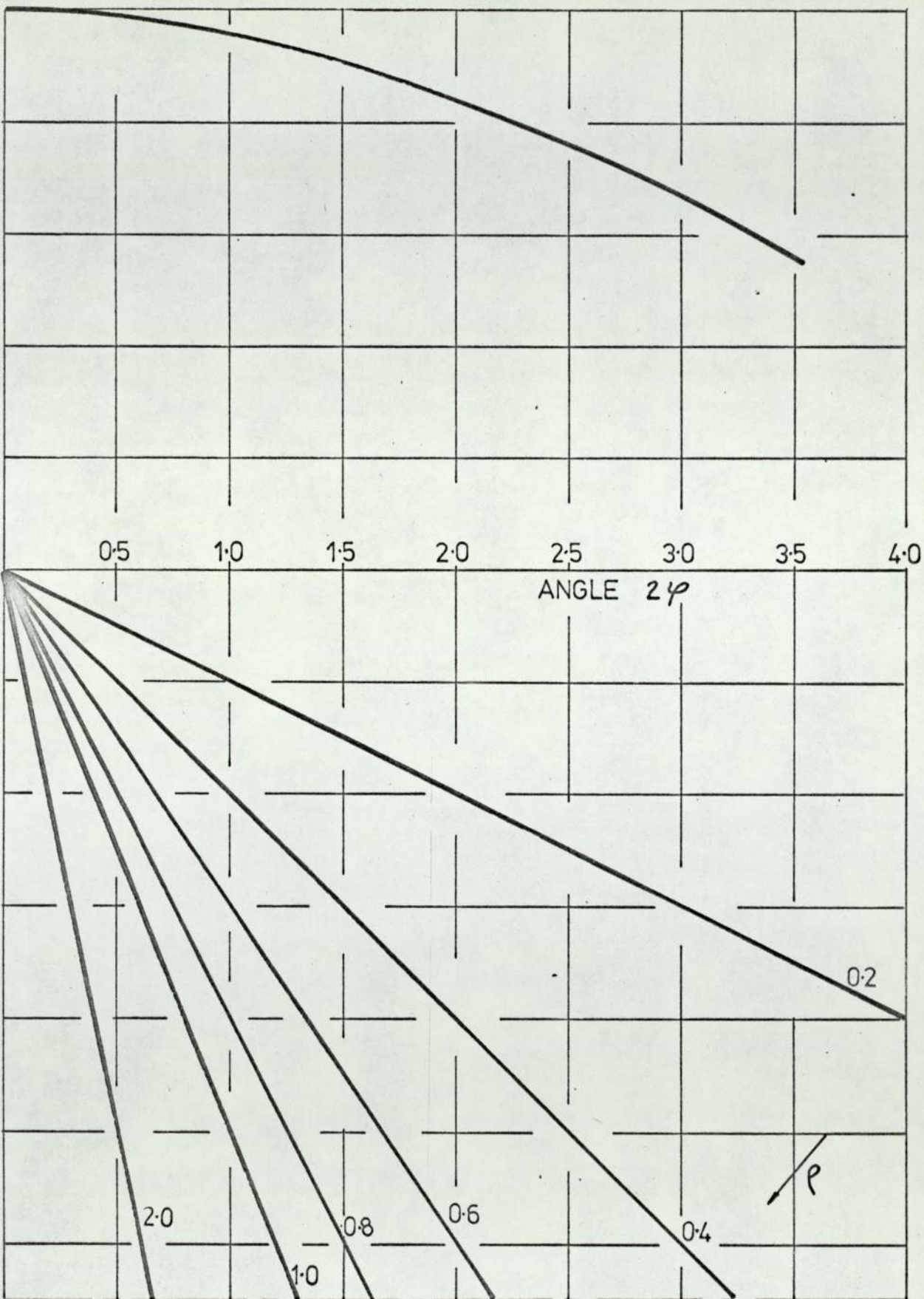


FIG. 6.4

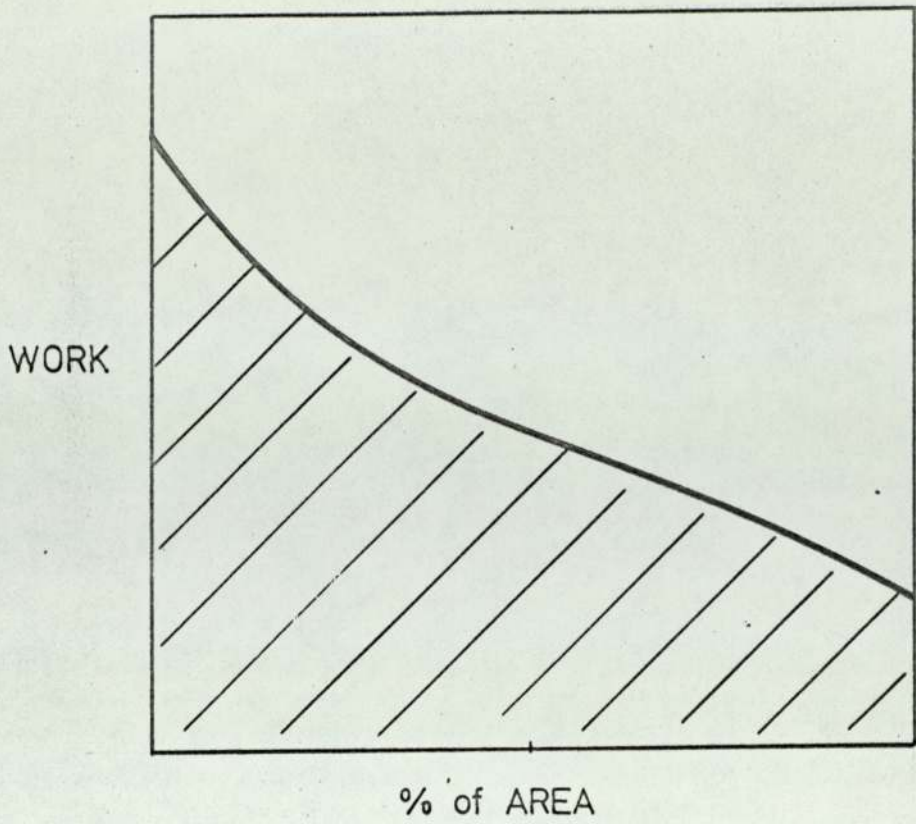


FIG. 6.5

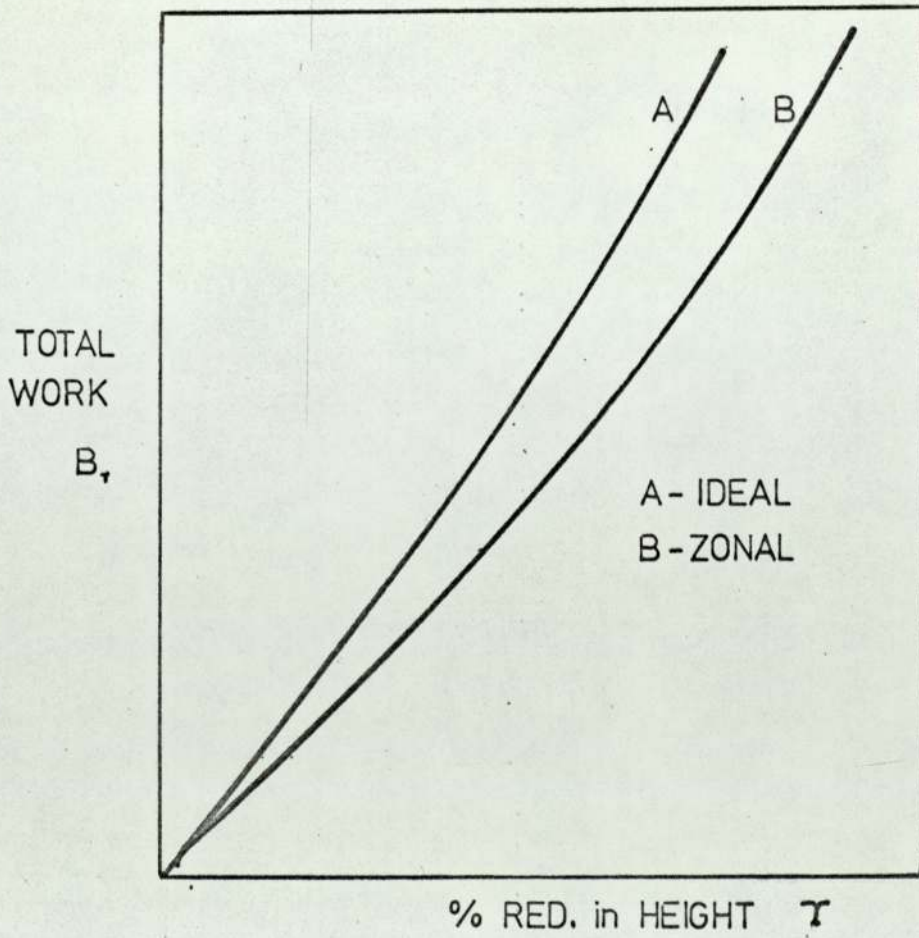
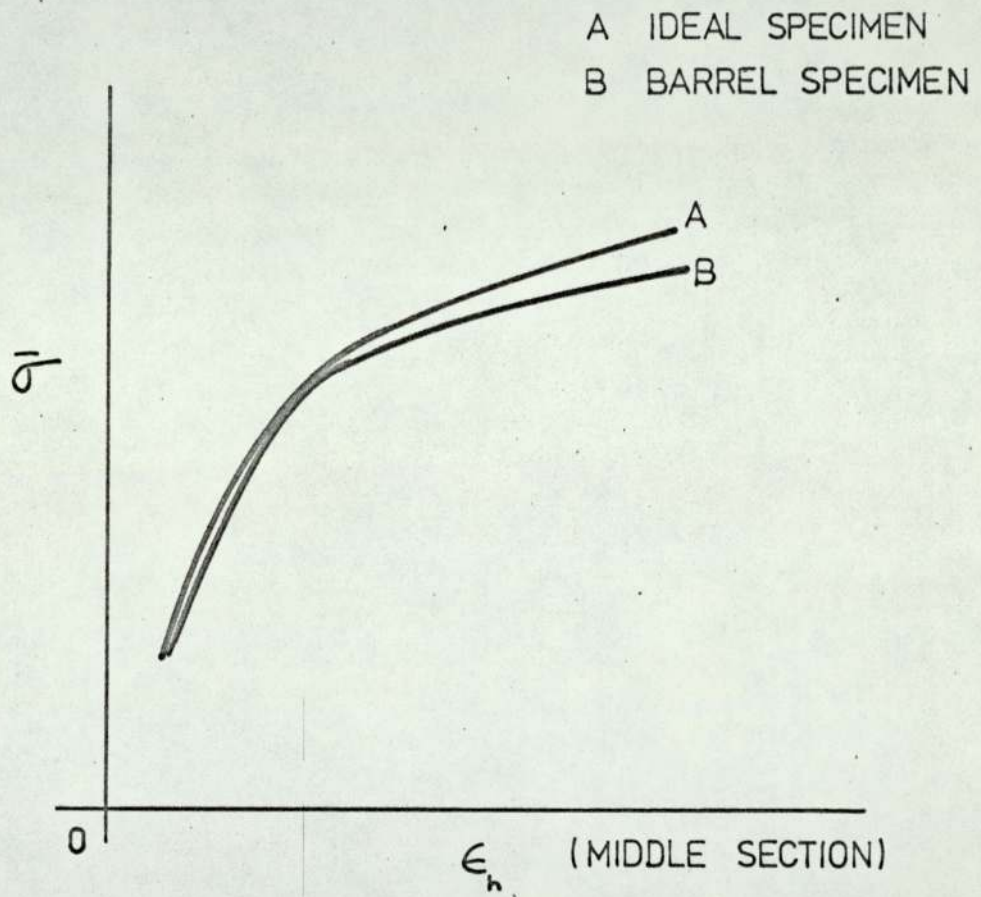


FIG. 6.6



AFTER HSÜ [33 35]

FIG. 6.7

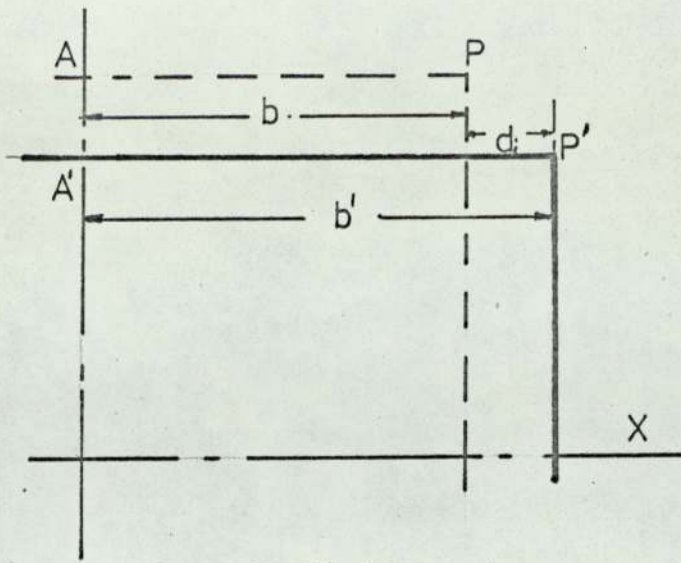


FIG. 7.1

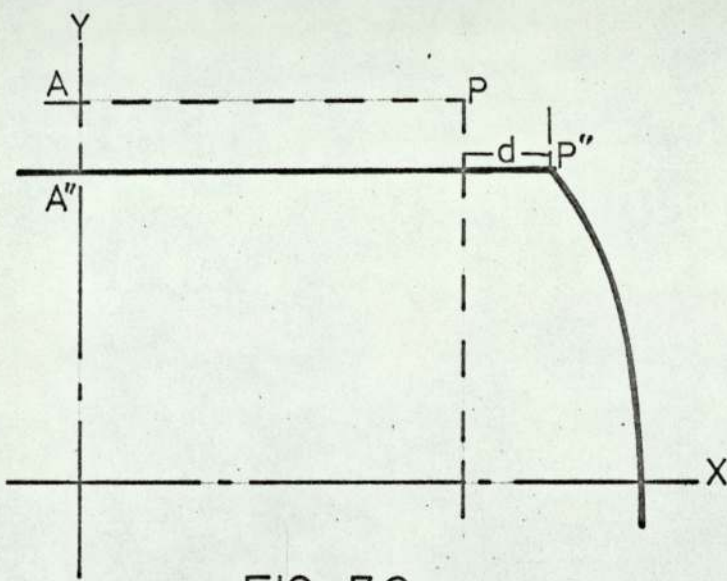


FIG. 7.2

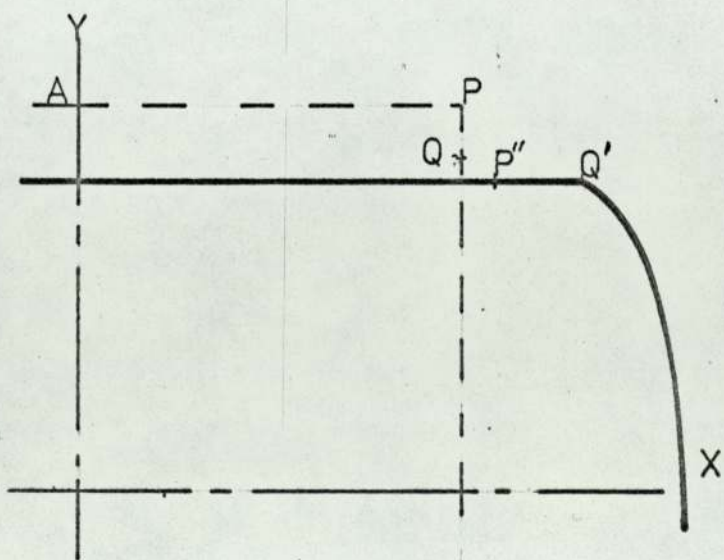


FIG. 7.3

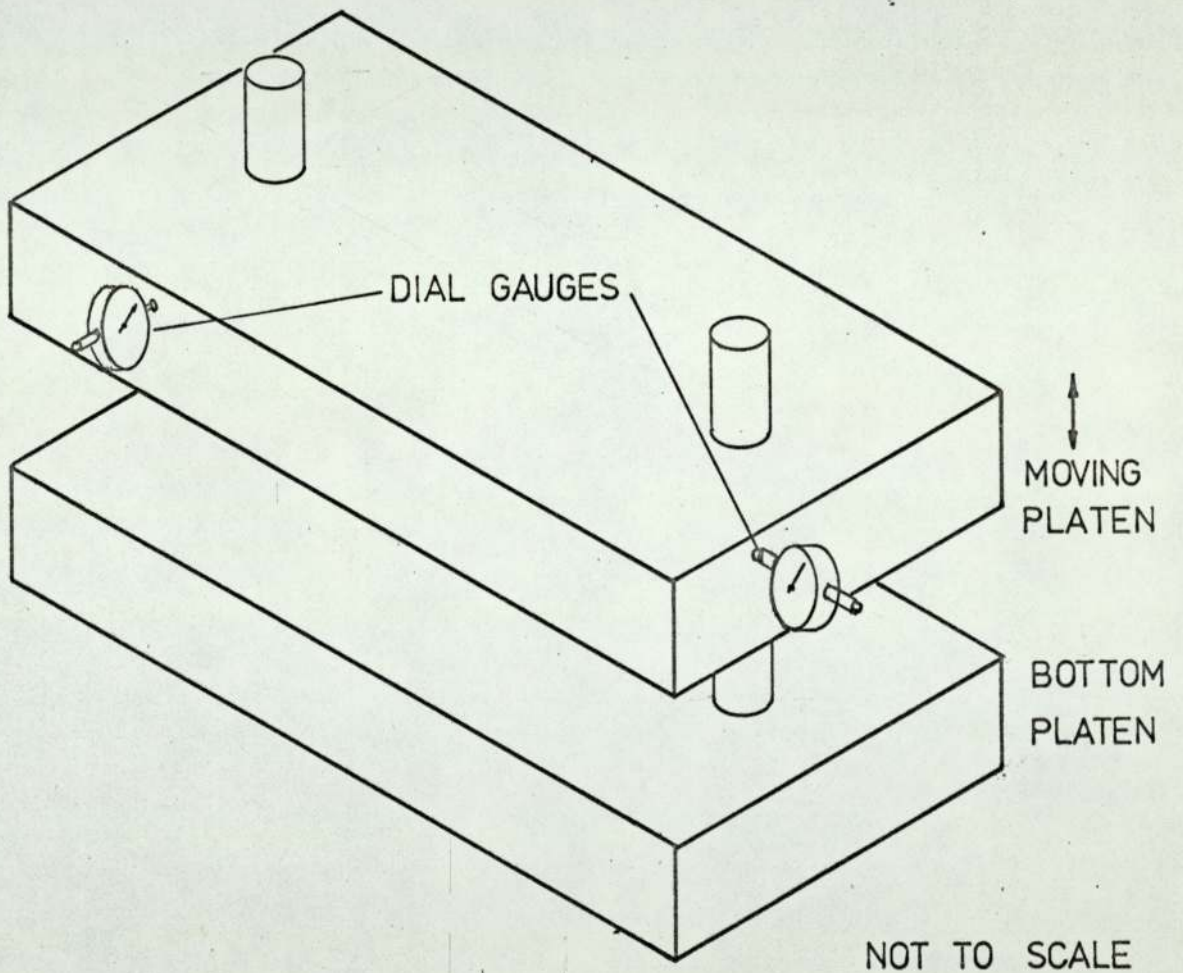


FIG. 8.1

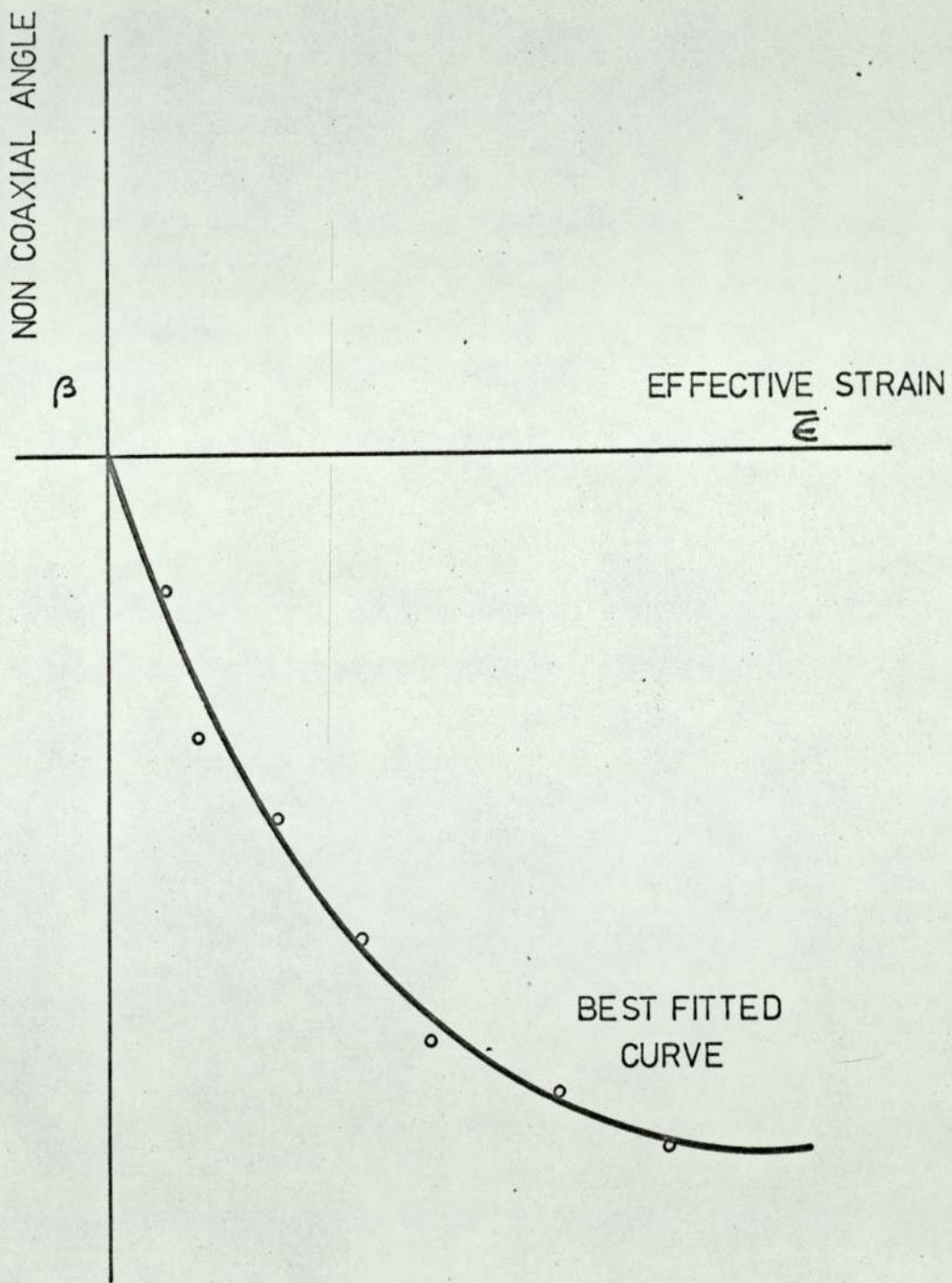
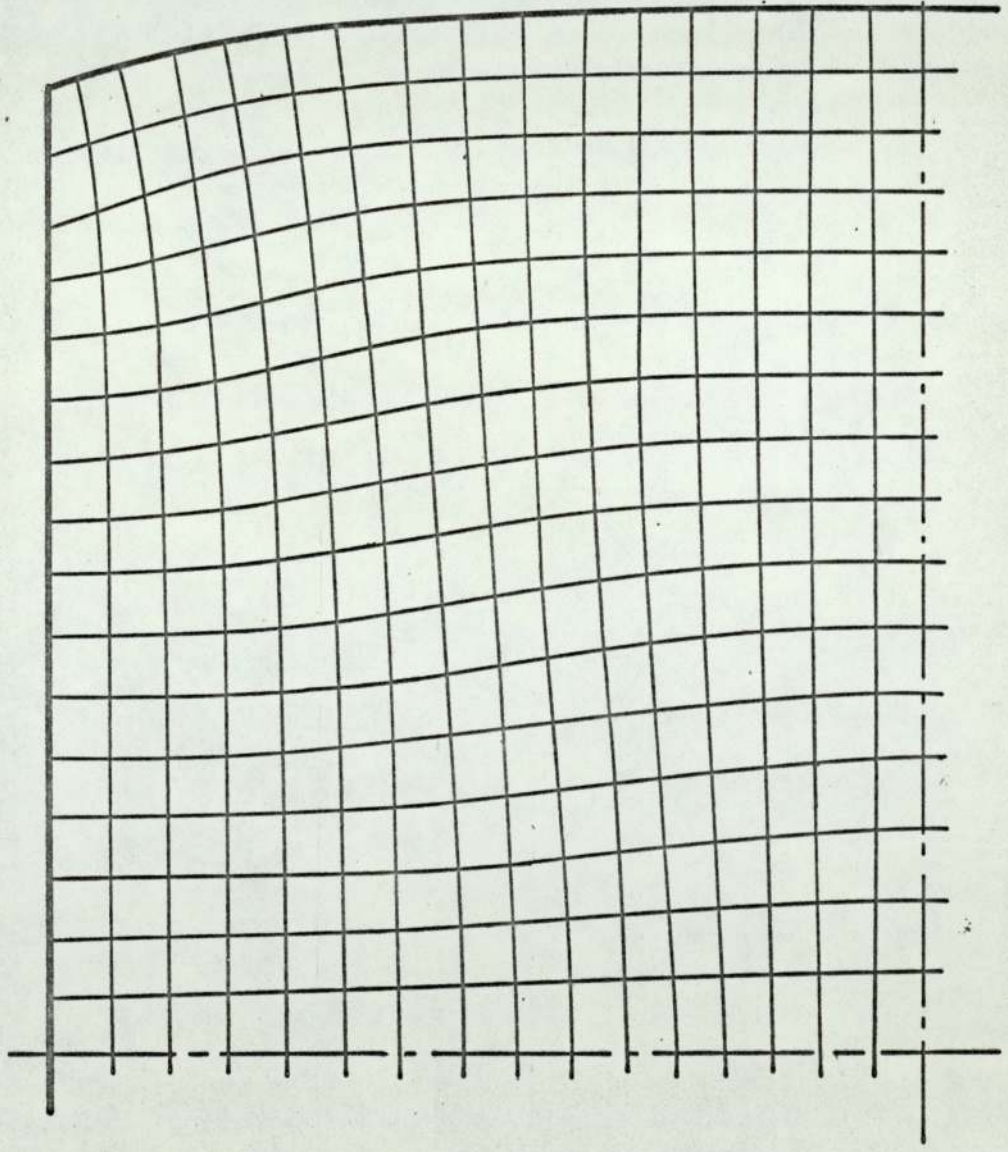


FIG. 8.2

Y-AXIS



9% RED. in HEIGHT
UNLUBRICATED DIE

FIG. 9.1

X-AXIS

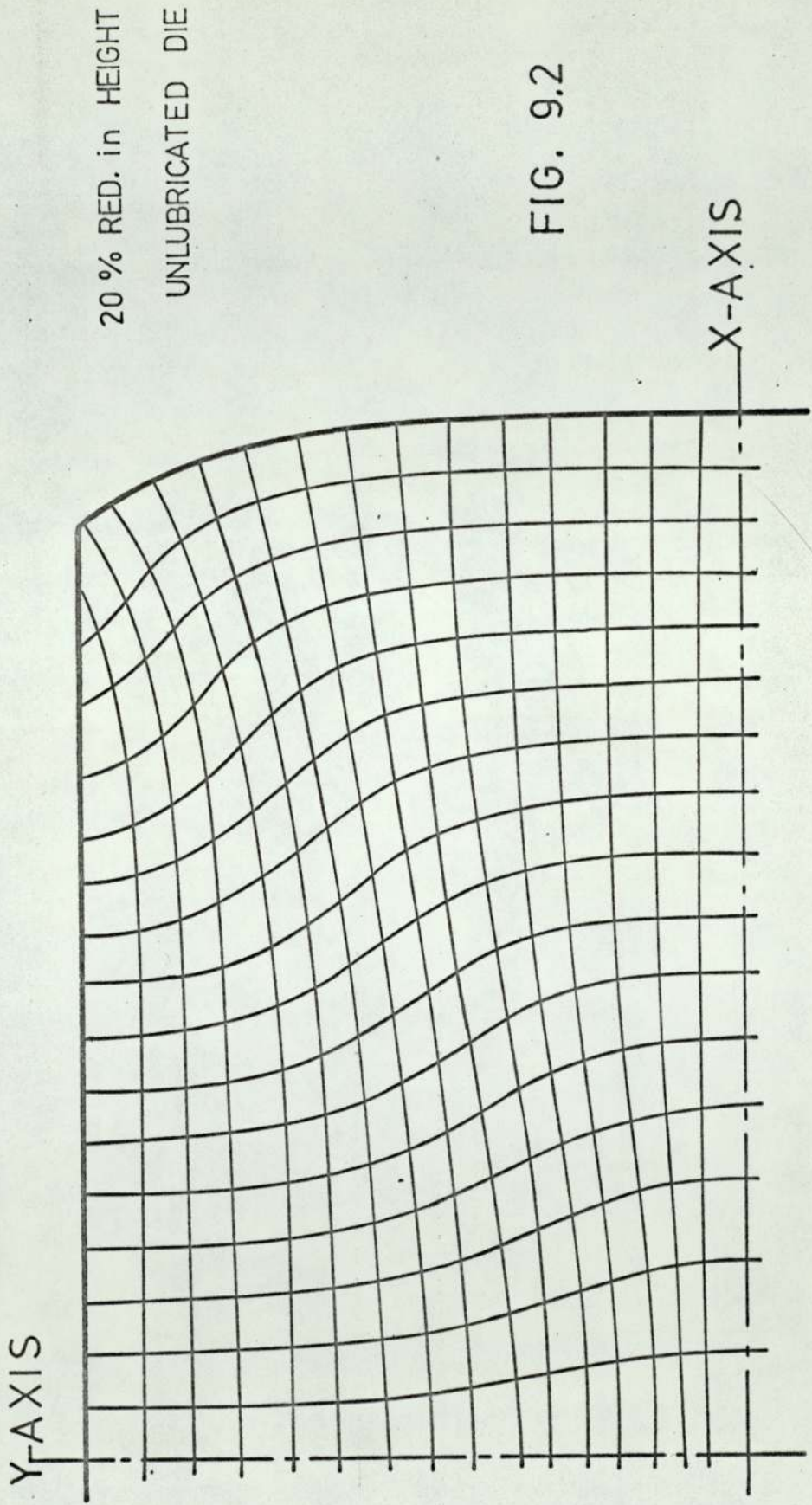


FIG. 9.2

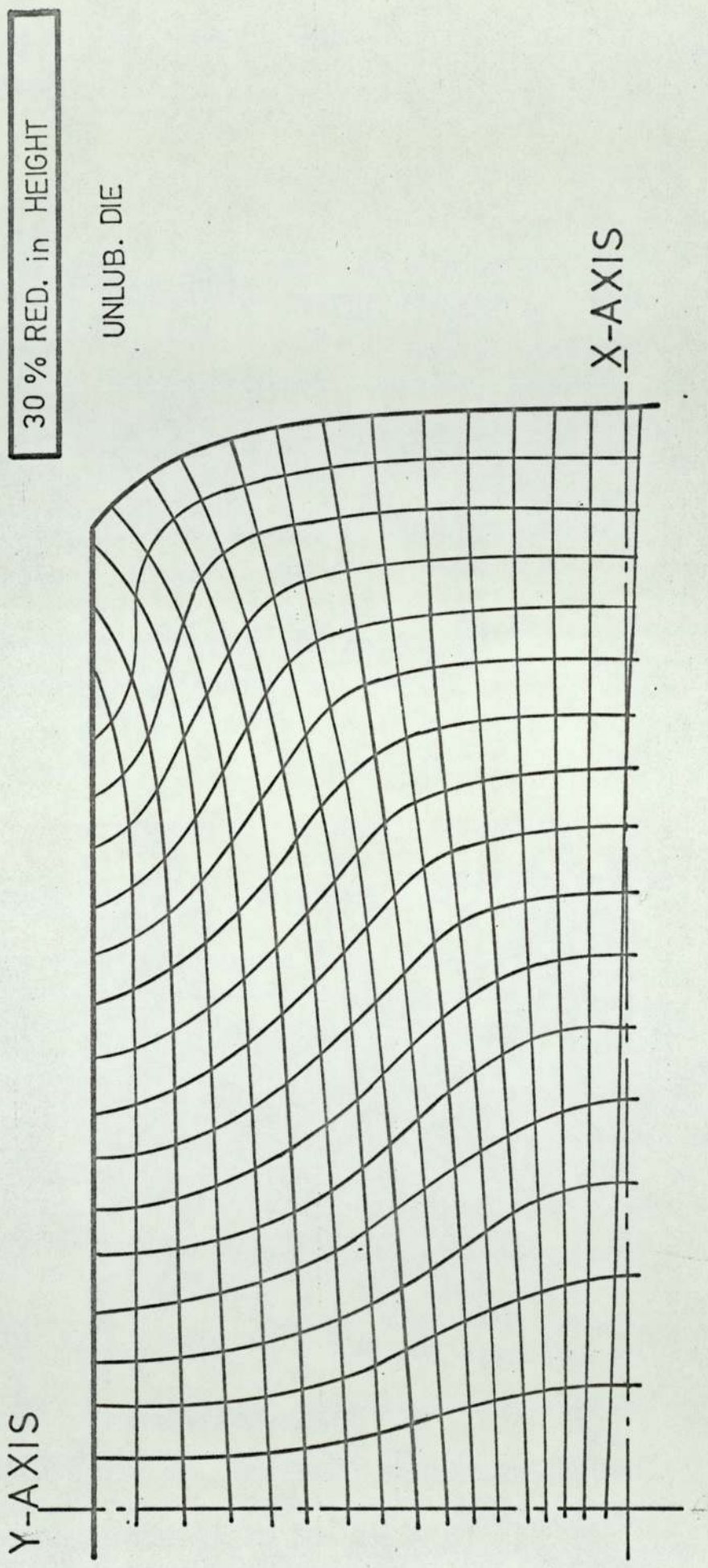


FIG. 9.3

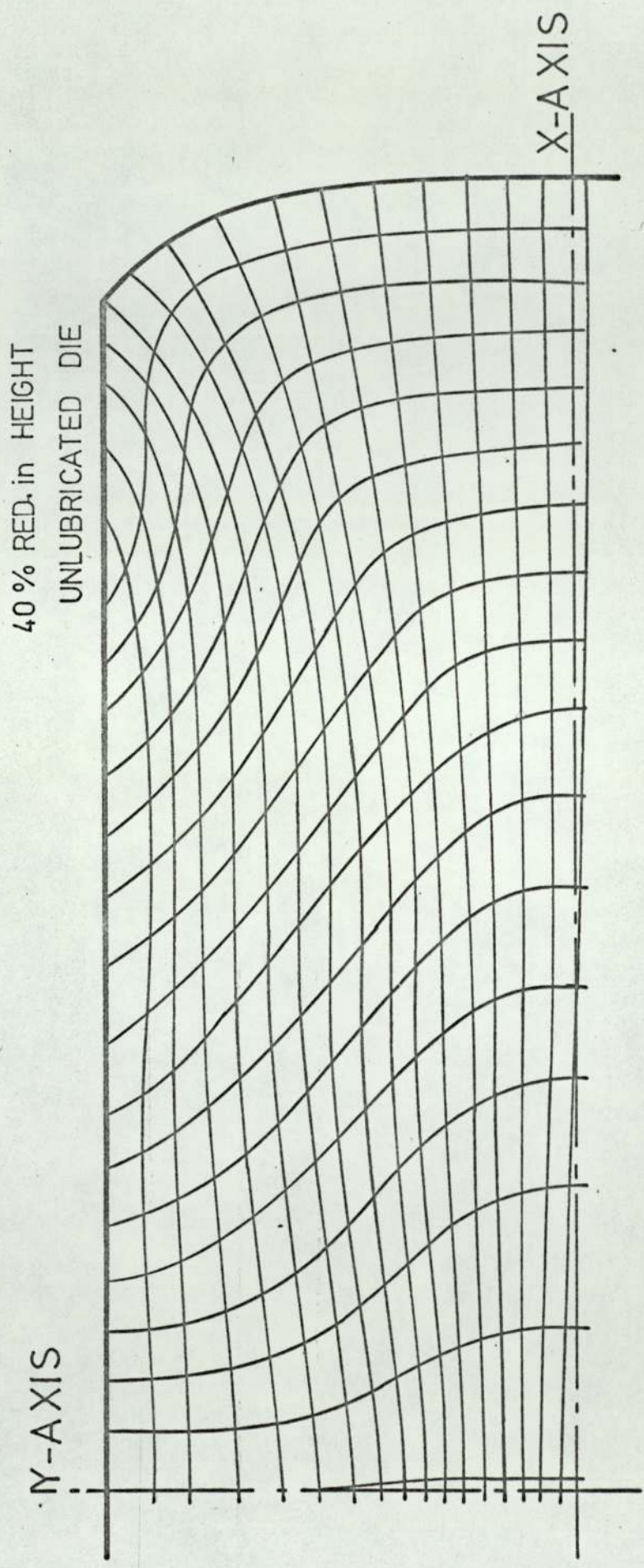
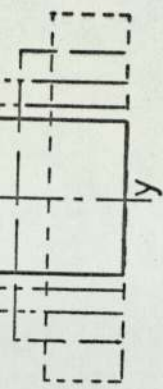


FIG. 9.4



	% of RED. in HEIGHT	MEAN STRAIN
A	8.7	0.11
B	20.2	0.26
C	30.3	0.42
D	40.3	0.60

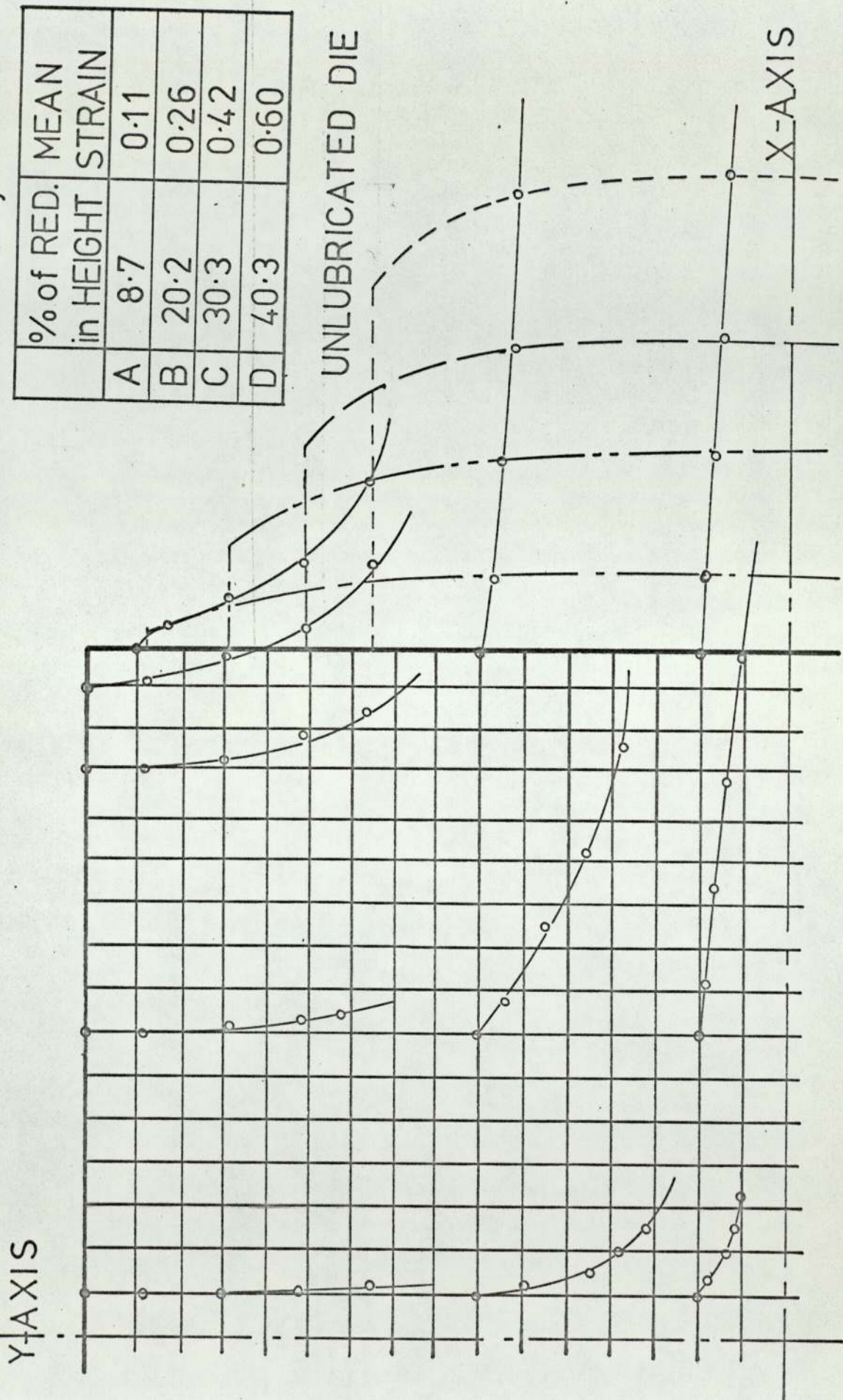
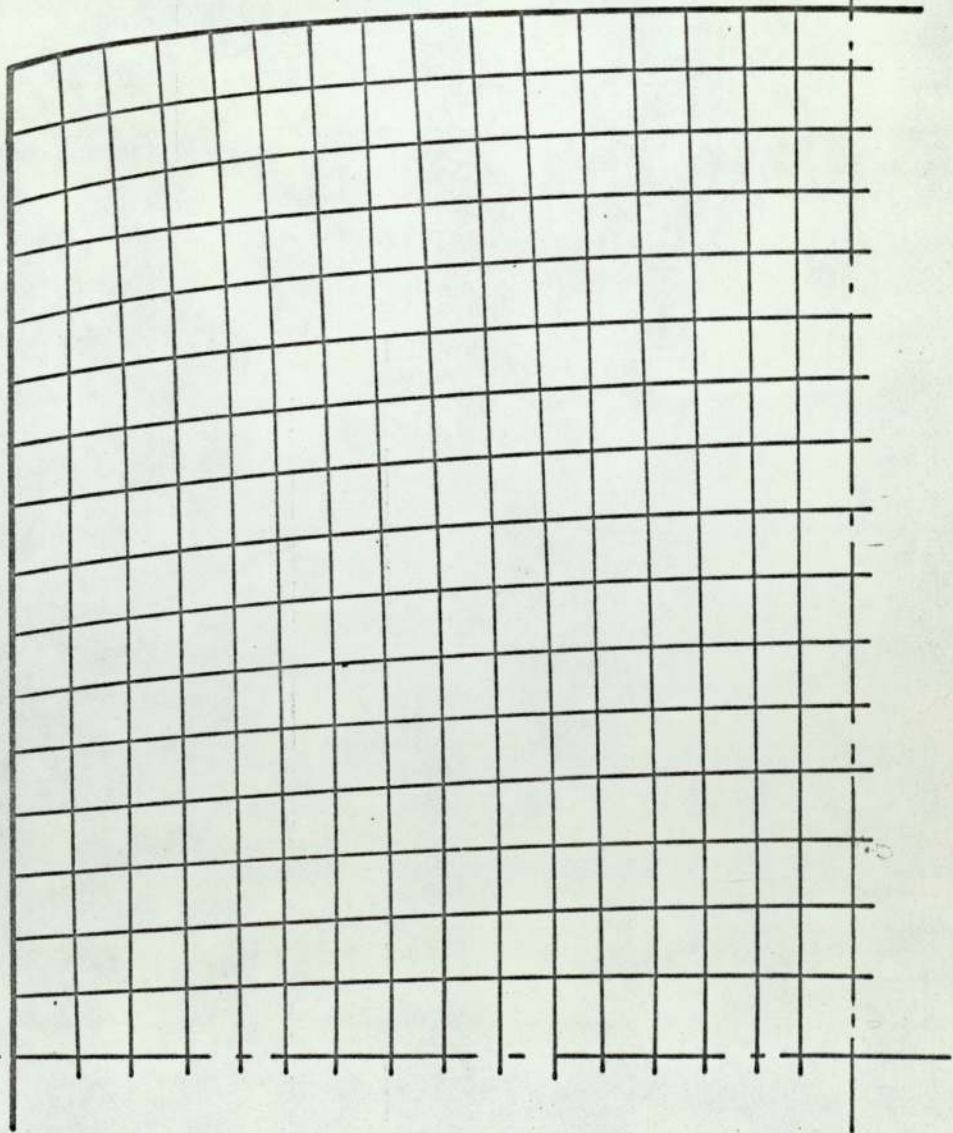


FIG. 9.5

Y-AXIS



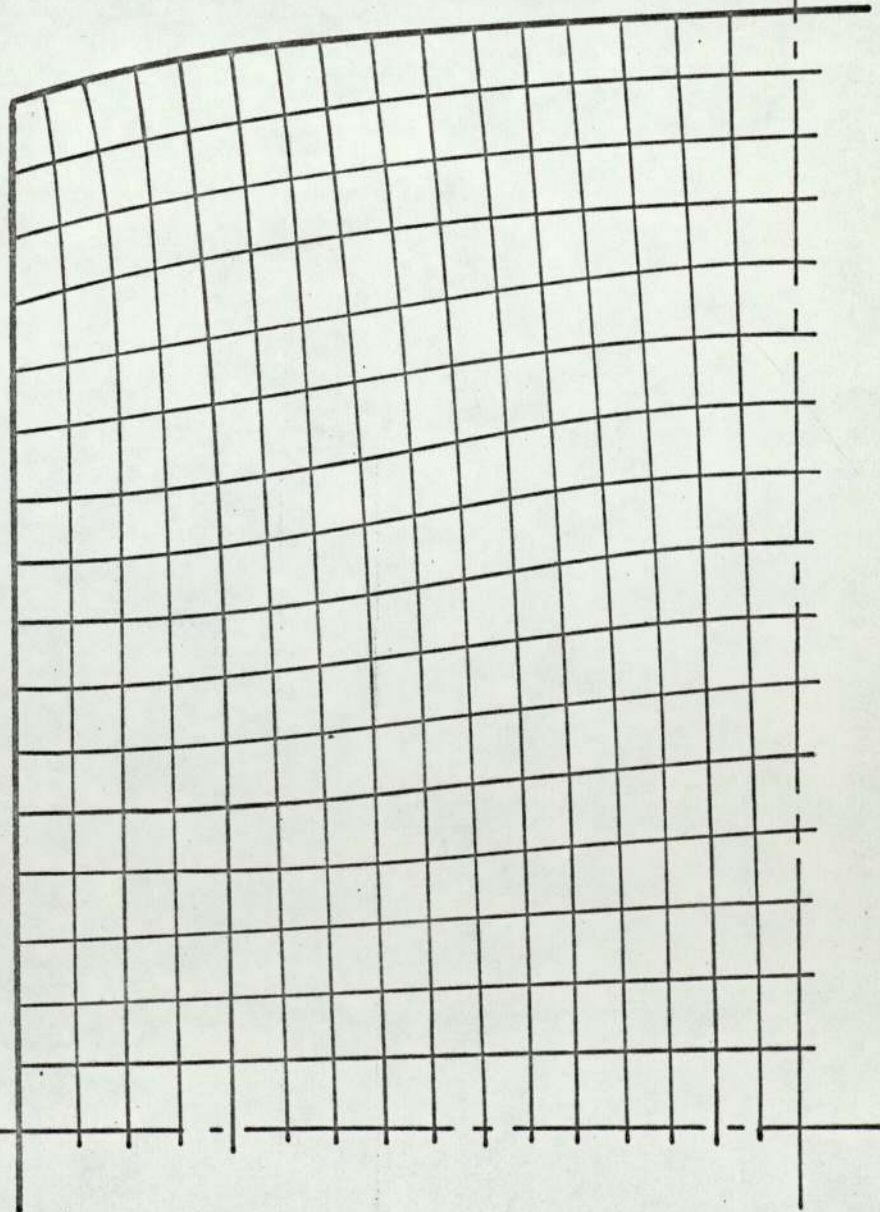
11% RED. in HEIGHT

LUBRICATED DIE

FIG. 9.6

X-AXIS

Y-AXIS



20% RED. in HEIGHT
LUBRICATED DIE

X-AXIS

FIG. 9.7

Y-AXIS

30% RED. in HEIGHT

LUB. DIE

X-AXIS

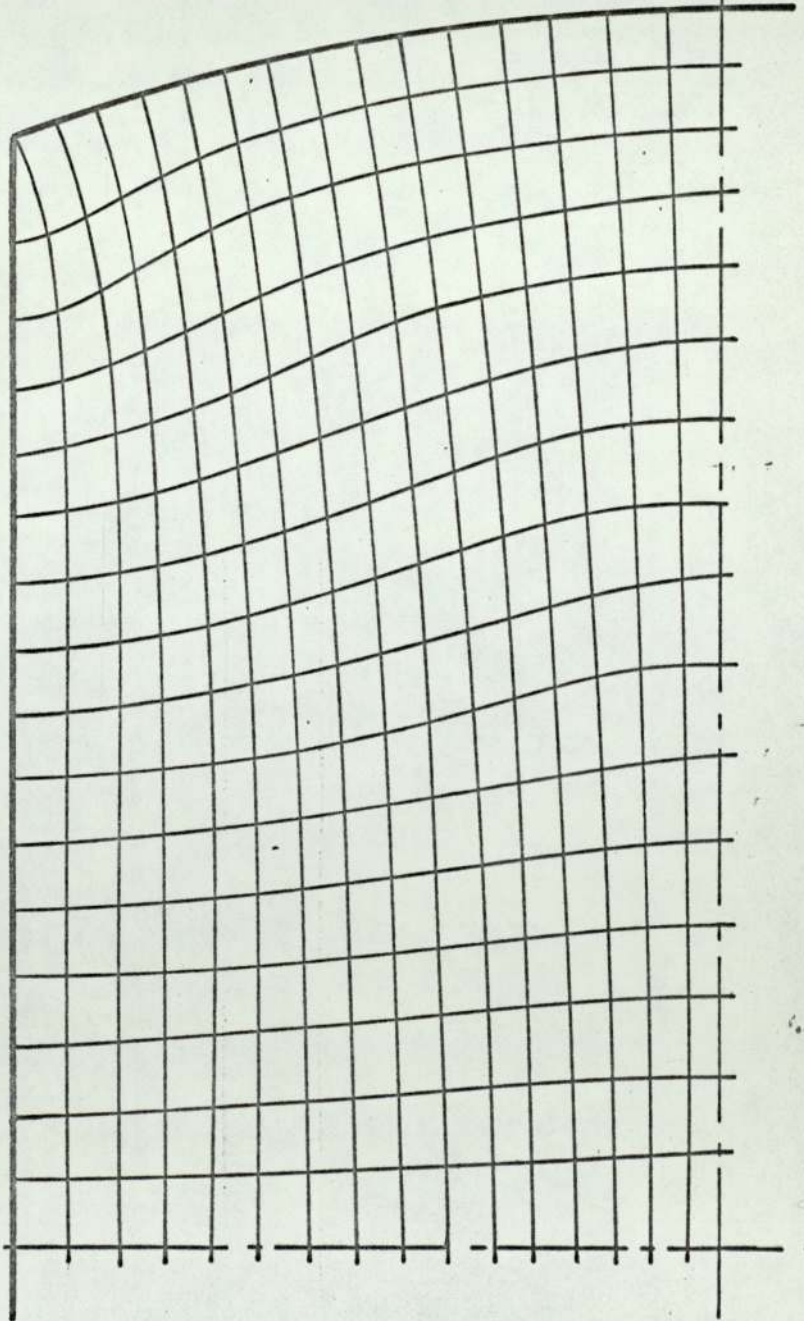


FIG. 9.8

T63

40% RED. in HEIGHT
LUBRICATED DIE

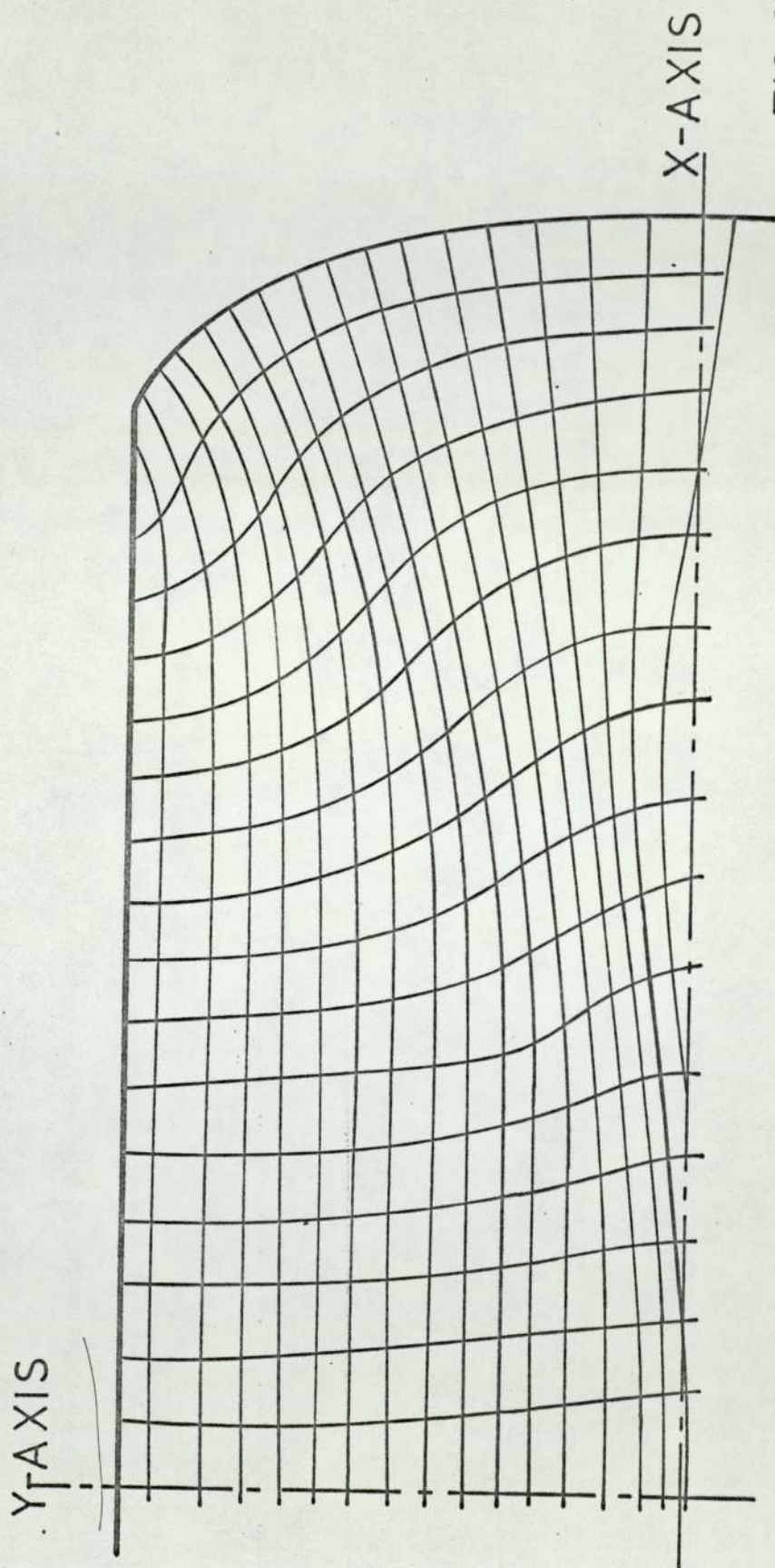
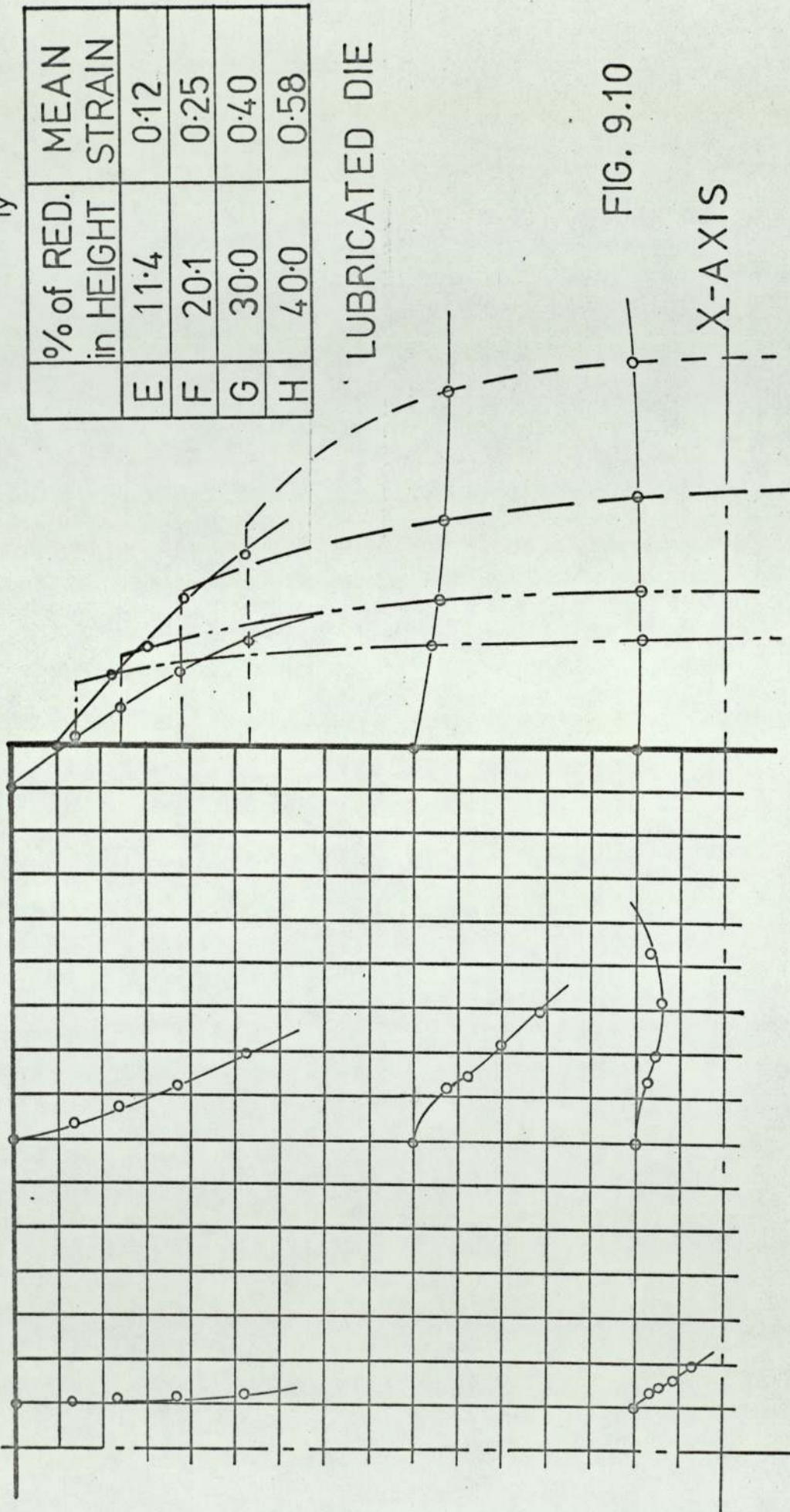
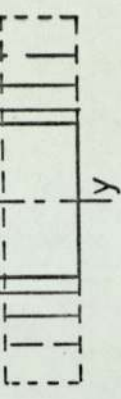


FIG. 9.9

Y-AXIS



LUBRICATED DIE

	% of RED. in HEIGHT	MEAN STRAIN
E	11.4	0.12
F	20.1	0.25
G	30.0	0.40
H	40.0	0.58

FIG. 9.10

X-AXIS

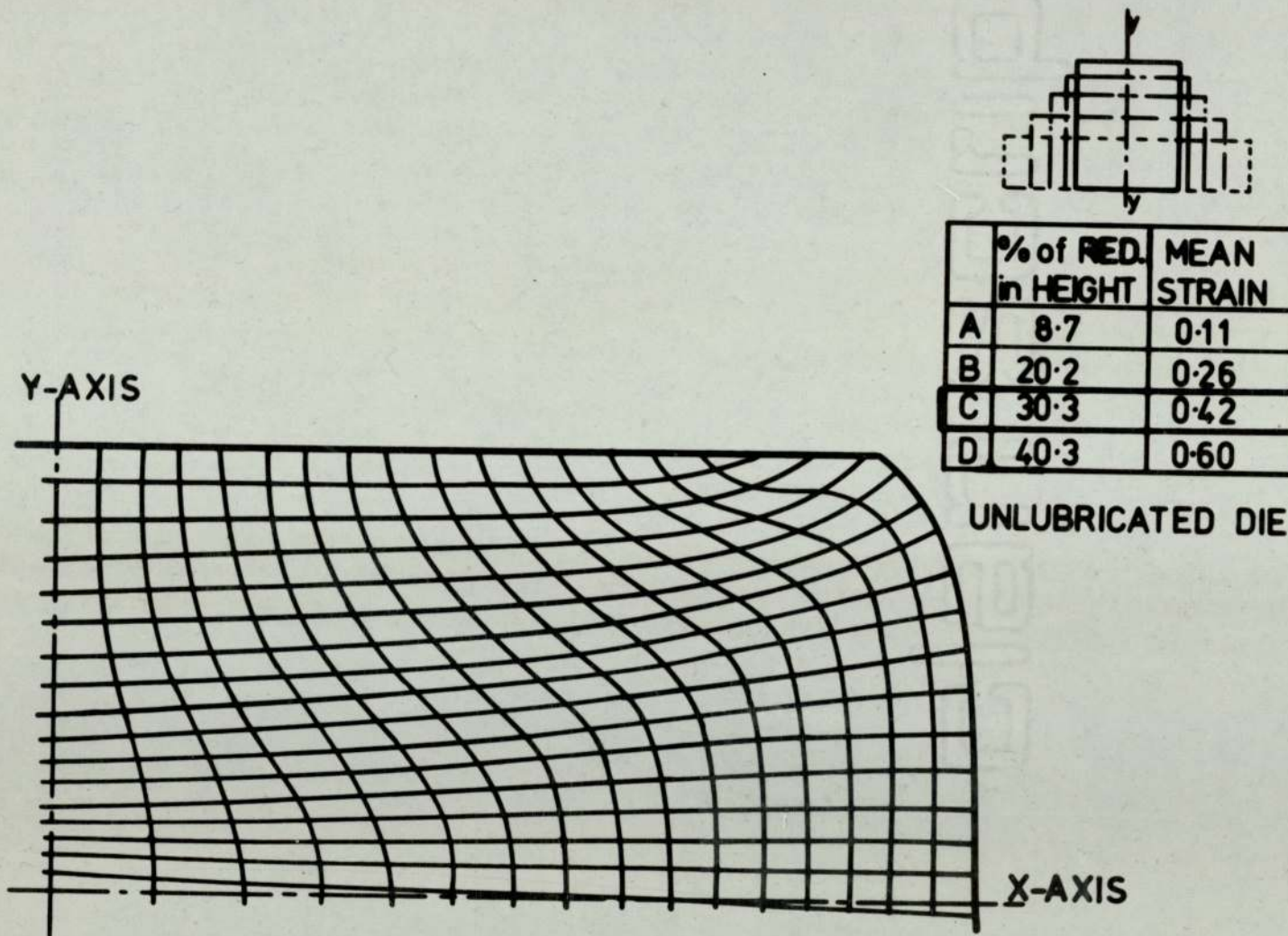
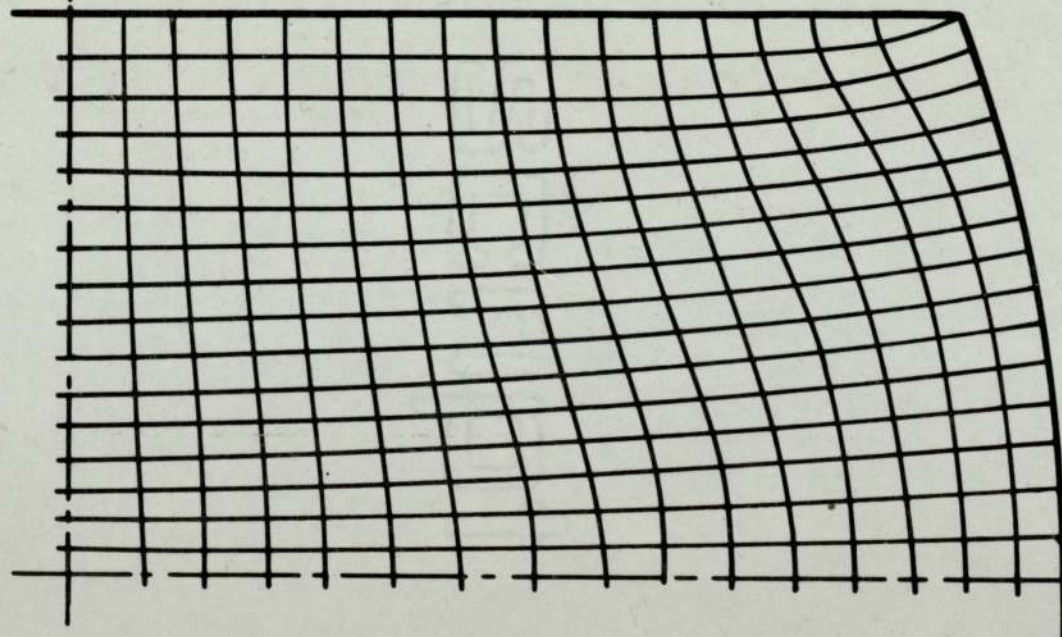
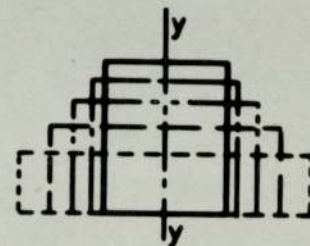


FIG. 9.11a

Y-AXIS



X-AXIS



	% of RED. in HEIGHT	MEAN STRAIN
E	11.4	0.12
F	20.1	0.25
G	30.0	0.40
H	40.0	0.58

LUBRICATED DIE

FIG. 9.11b

UNLUBRICATED SPECIMEN

40 % RED. in HEIGHT

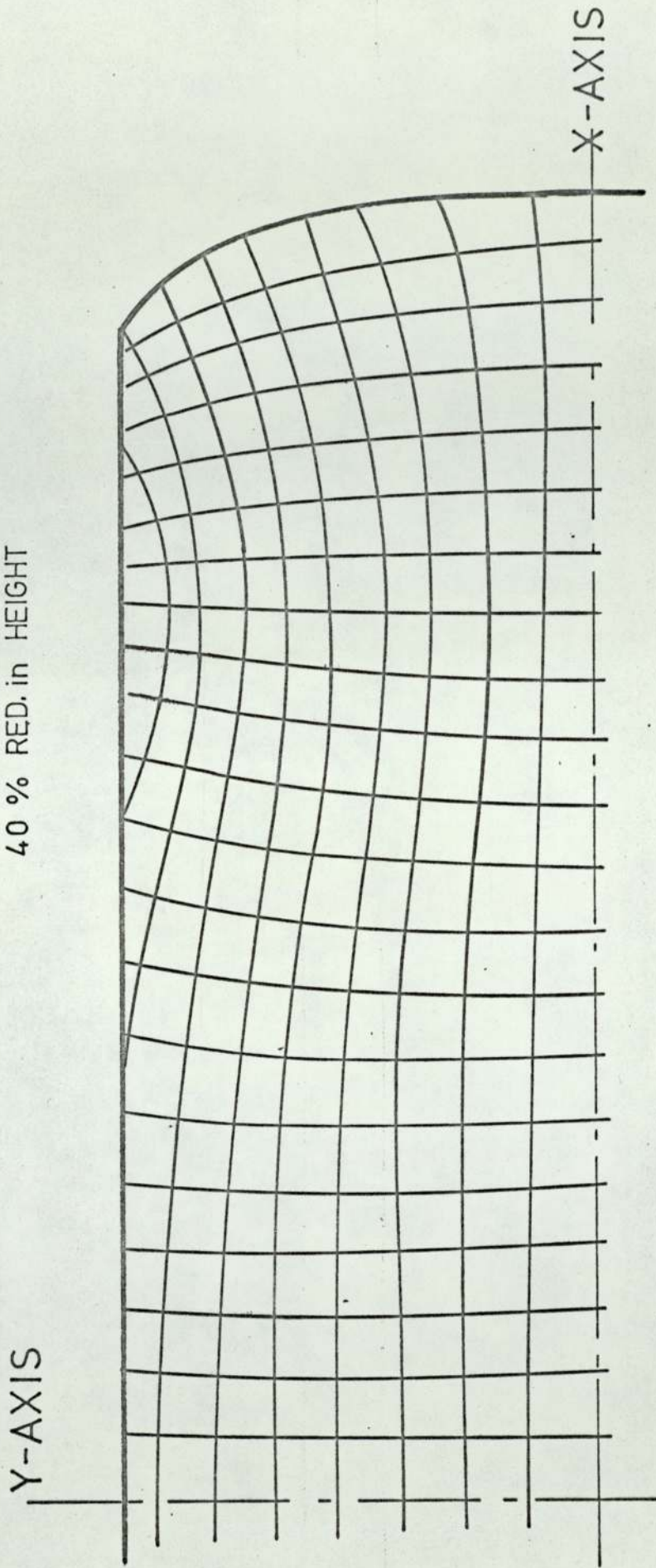


FIG. 9.12 a

LUBRICATED SPECIMEN

40% RED. in HEIGHT

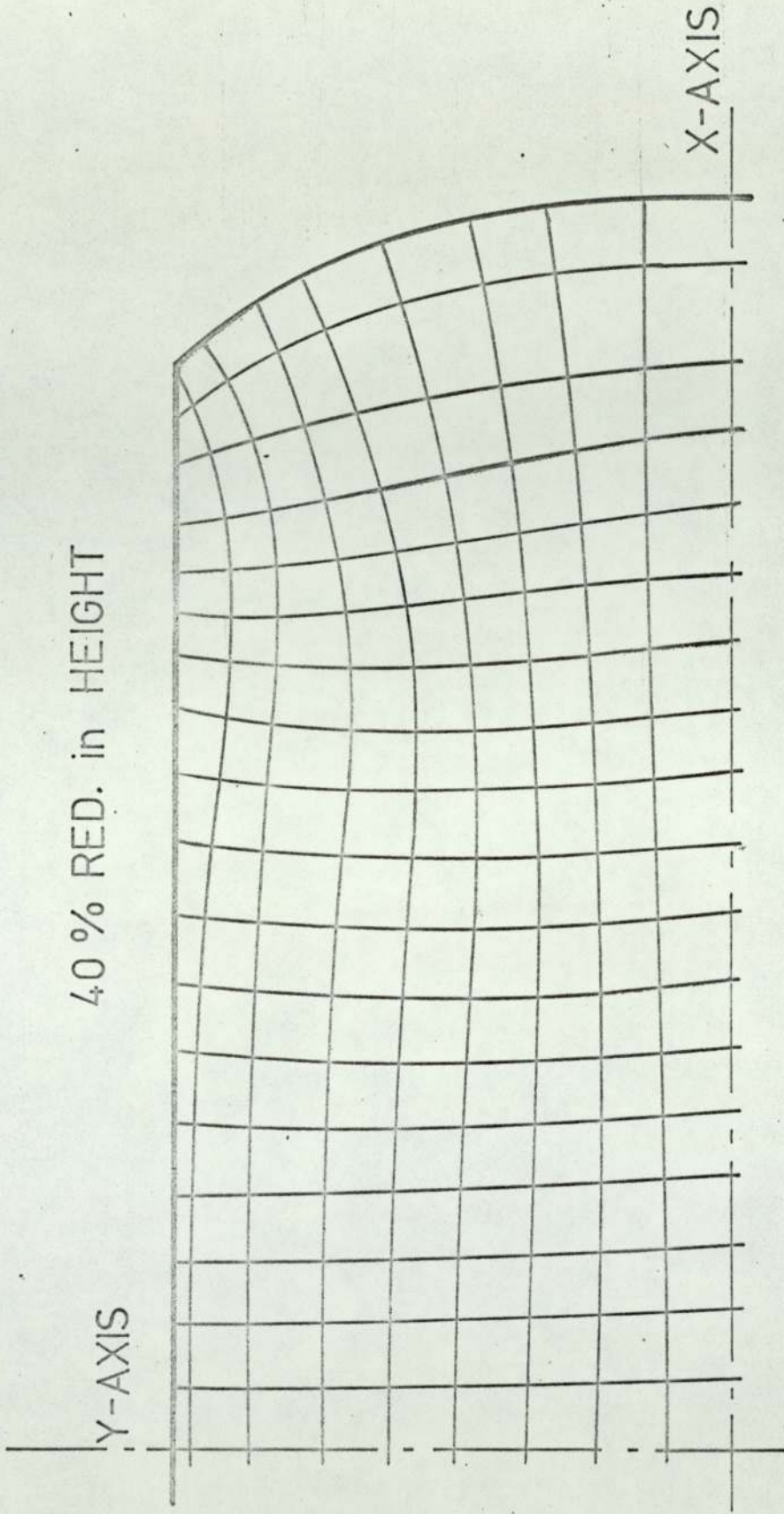


FIG. 9.12b

	% OF RED. in HEIGHT	MEAN STRAIN
A	8.7	0.11
B	20.2	0.26
C	30.3	0.42
D	40.3	0.60

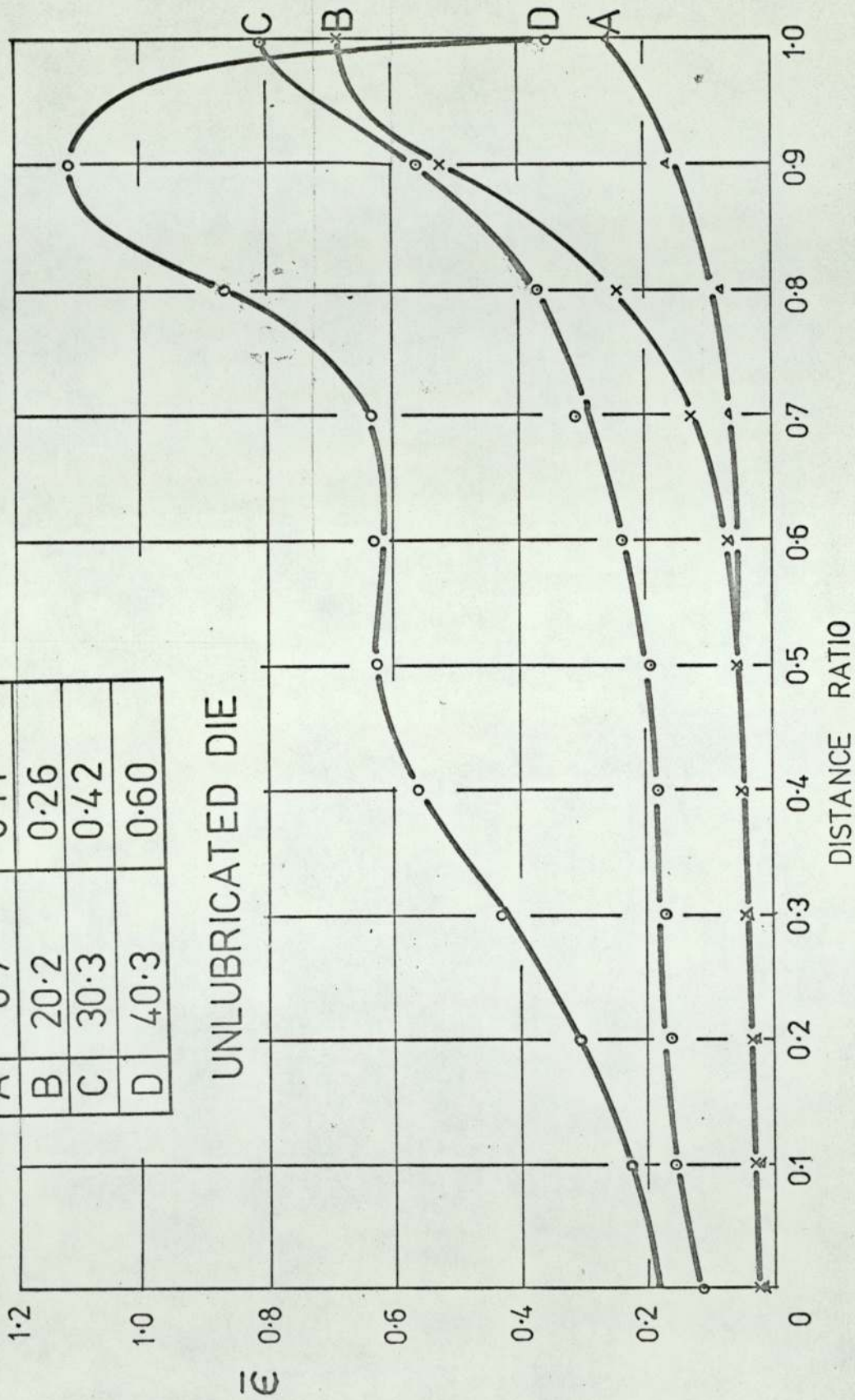
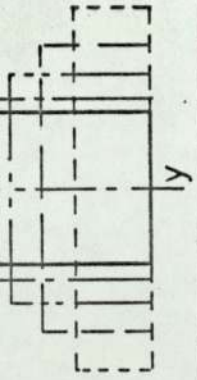


FIG. 9.13



	% of RED. in HEIGHT	MEAN STRAIN
E	11.4	0.12
F	20.1	0.25
G	30.0	0.40
H	40.0	0.58

LUBRICATED DIE

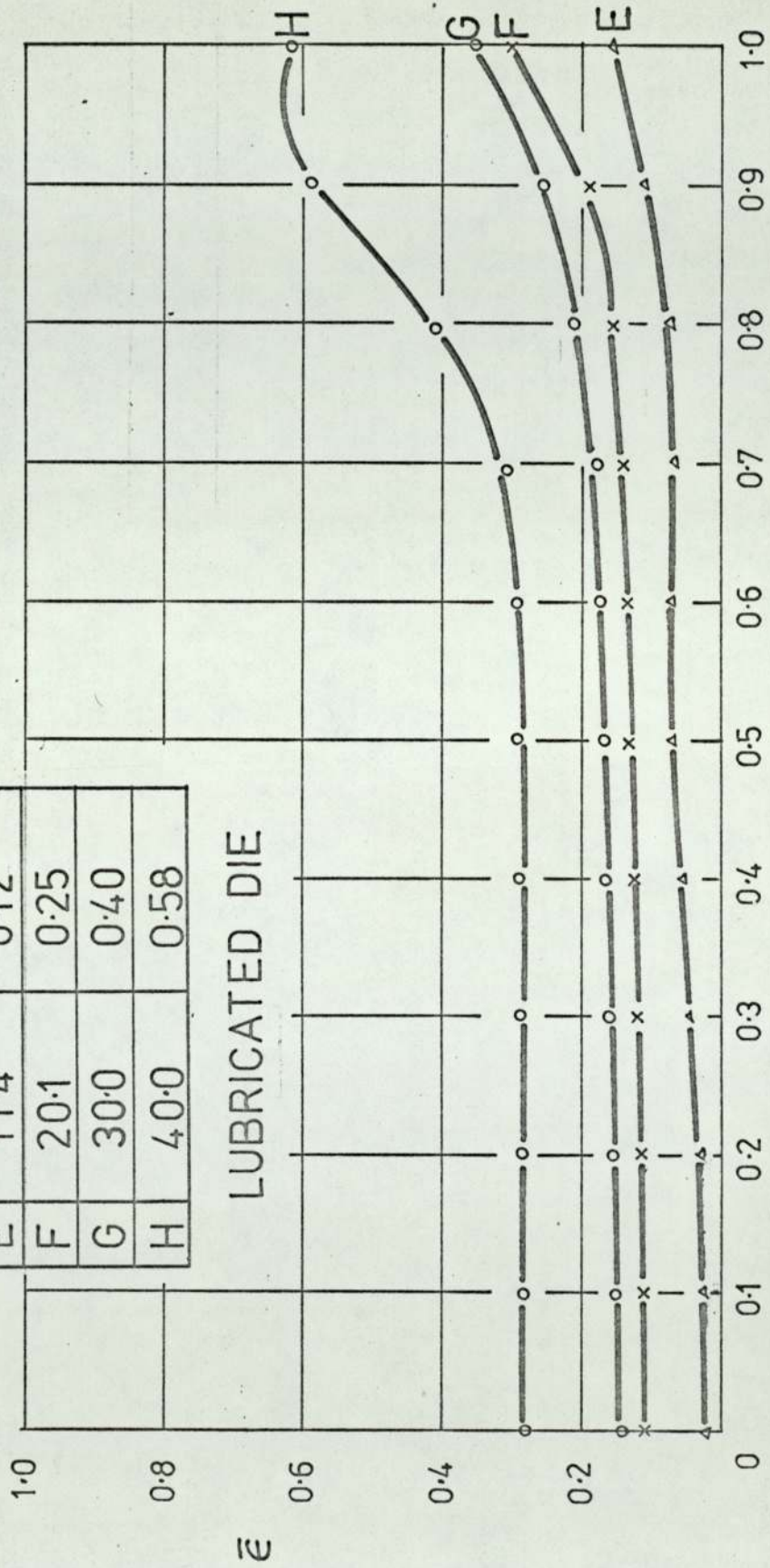


FIG. 9.14

UNLUBRICATED DIE
20% RED. in HEIGHT

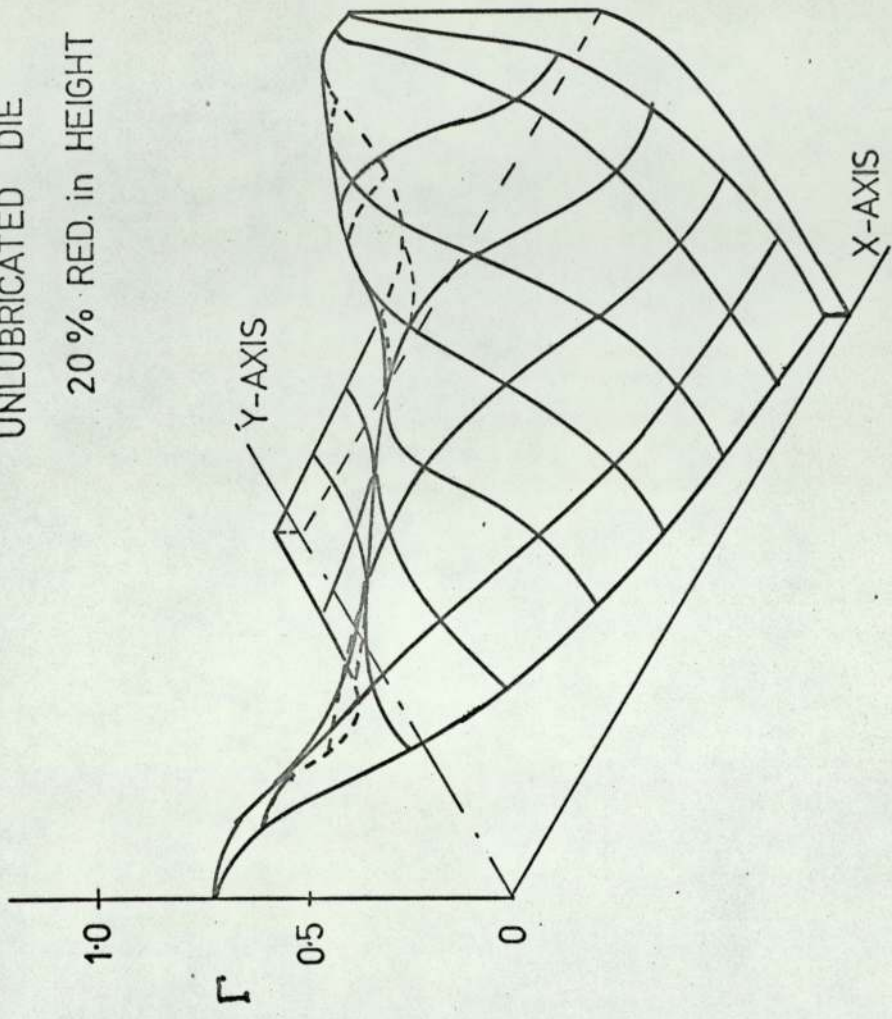


FIG. 9.15

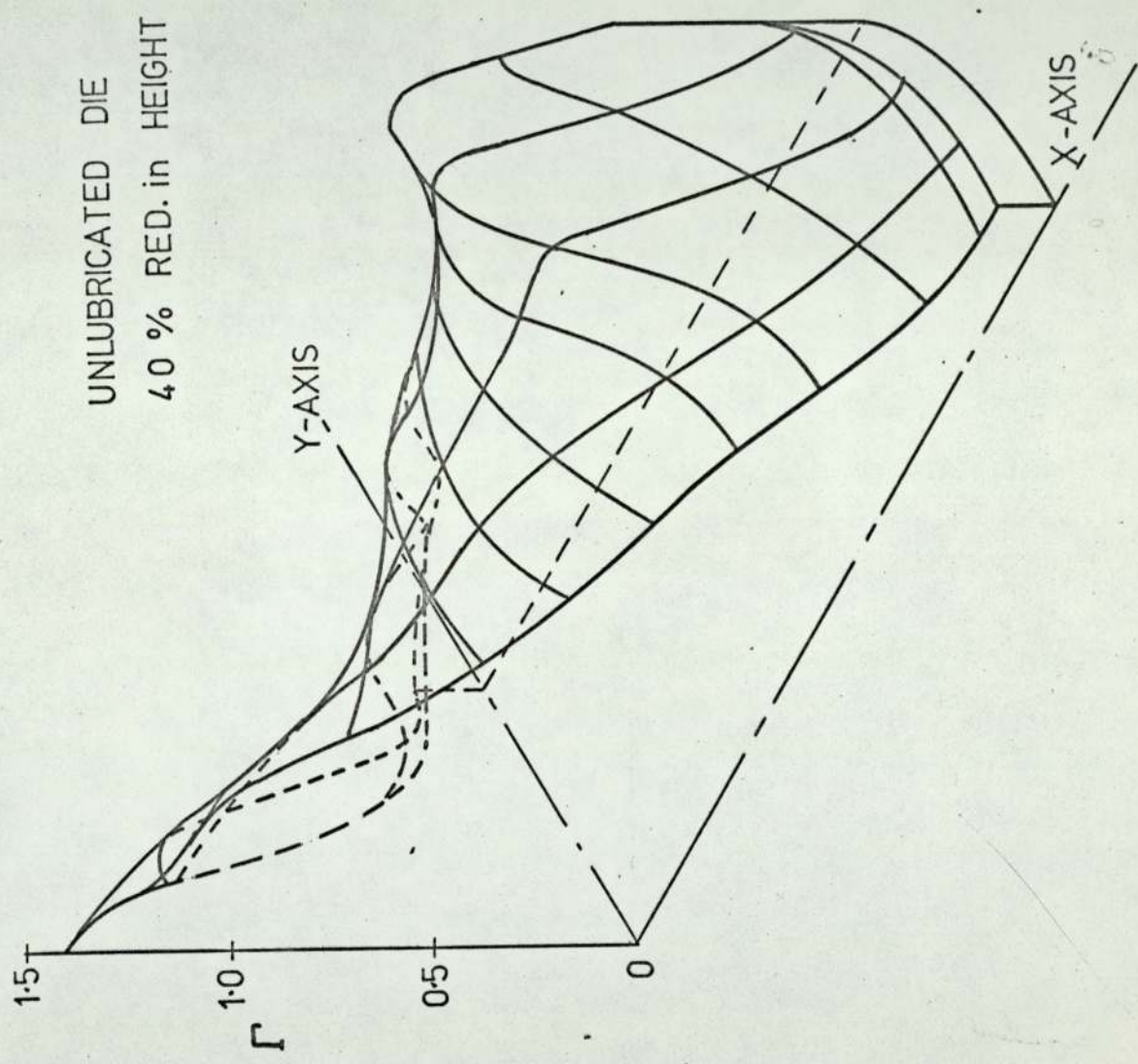


FIG. 9.16

LUBRICATED DIE
20 % RED. in HEIGHT

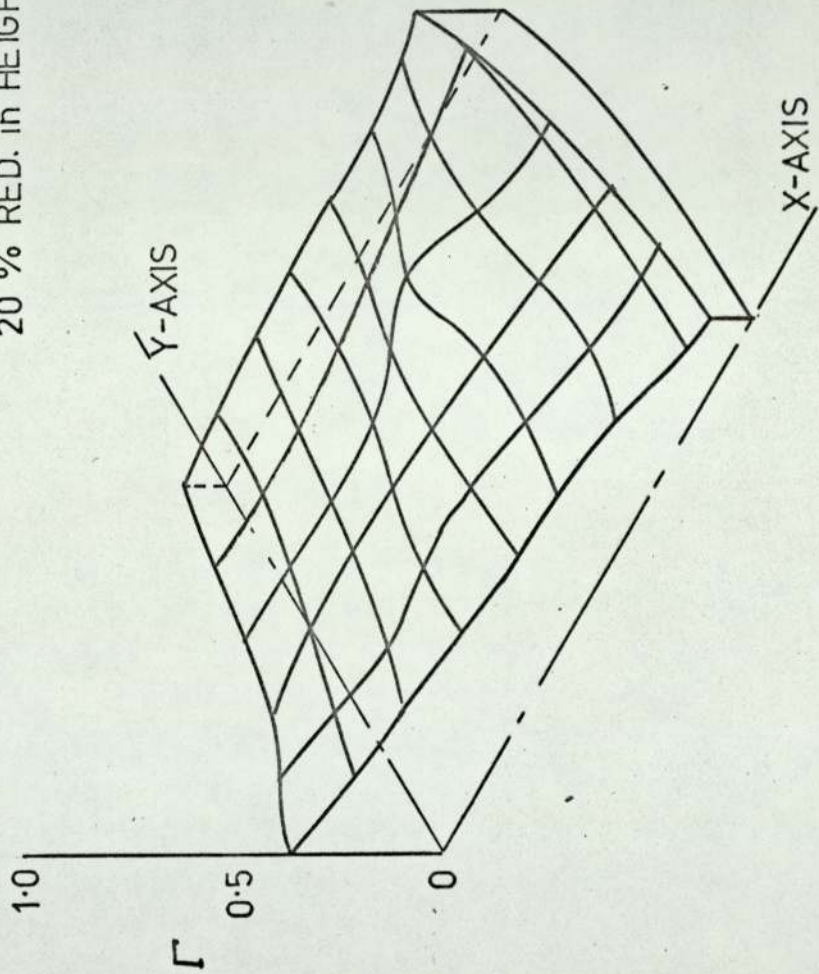


FIG. 9.17

LUBRICATED DIE
40% RED. in HEIGHT

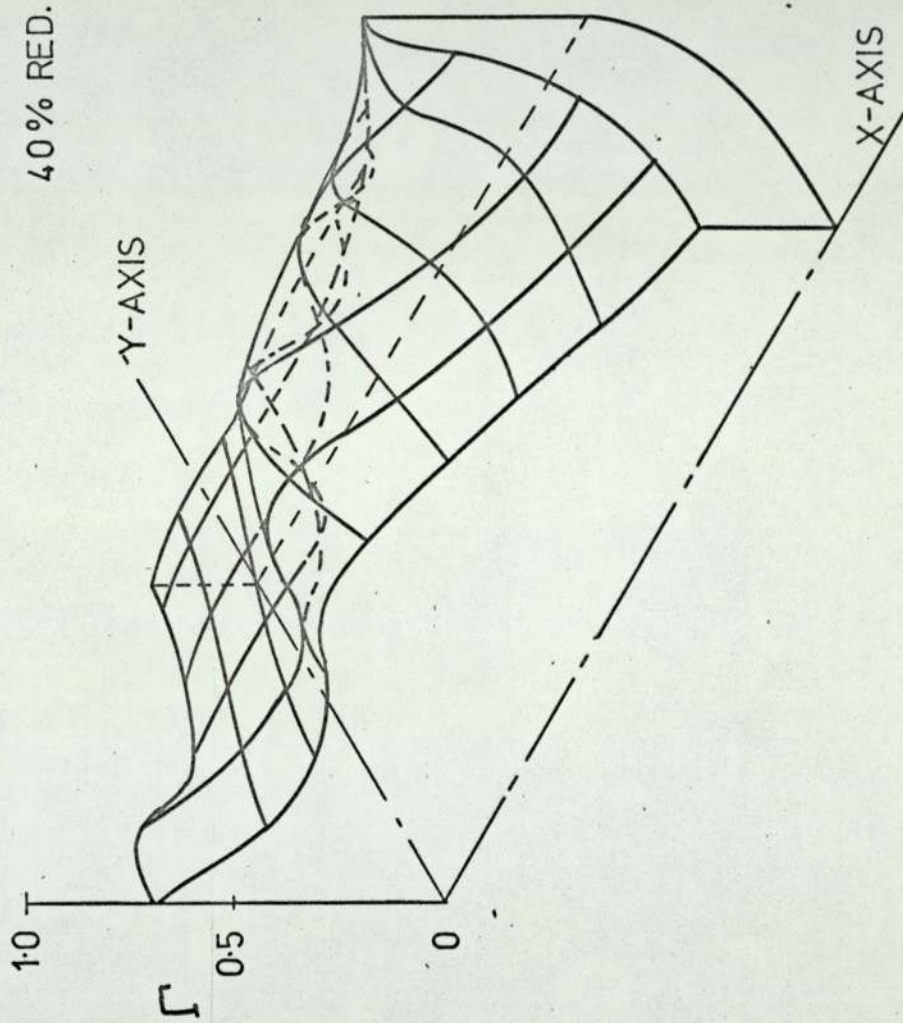


FIG. 9.18

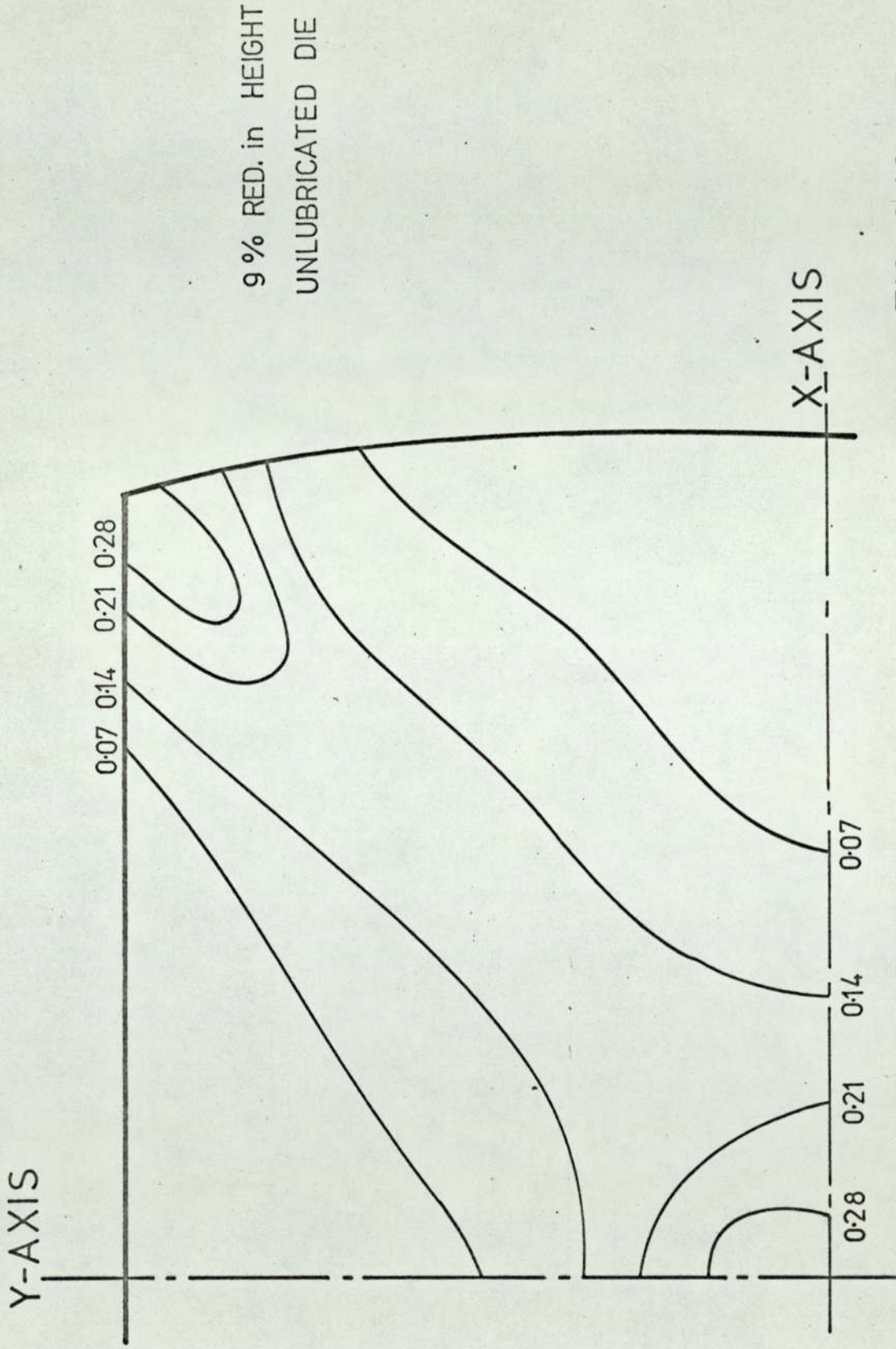


FIG. 9.19

20% RED. in HEIGHT
UNLUBRICATED DIE

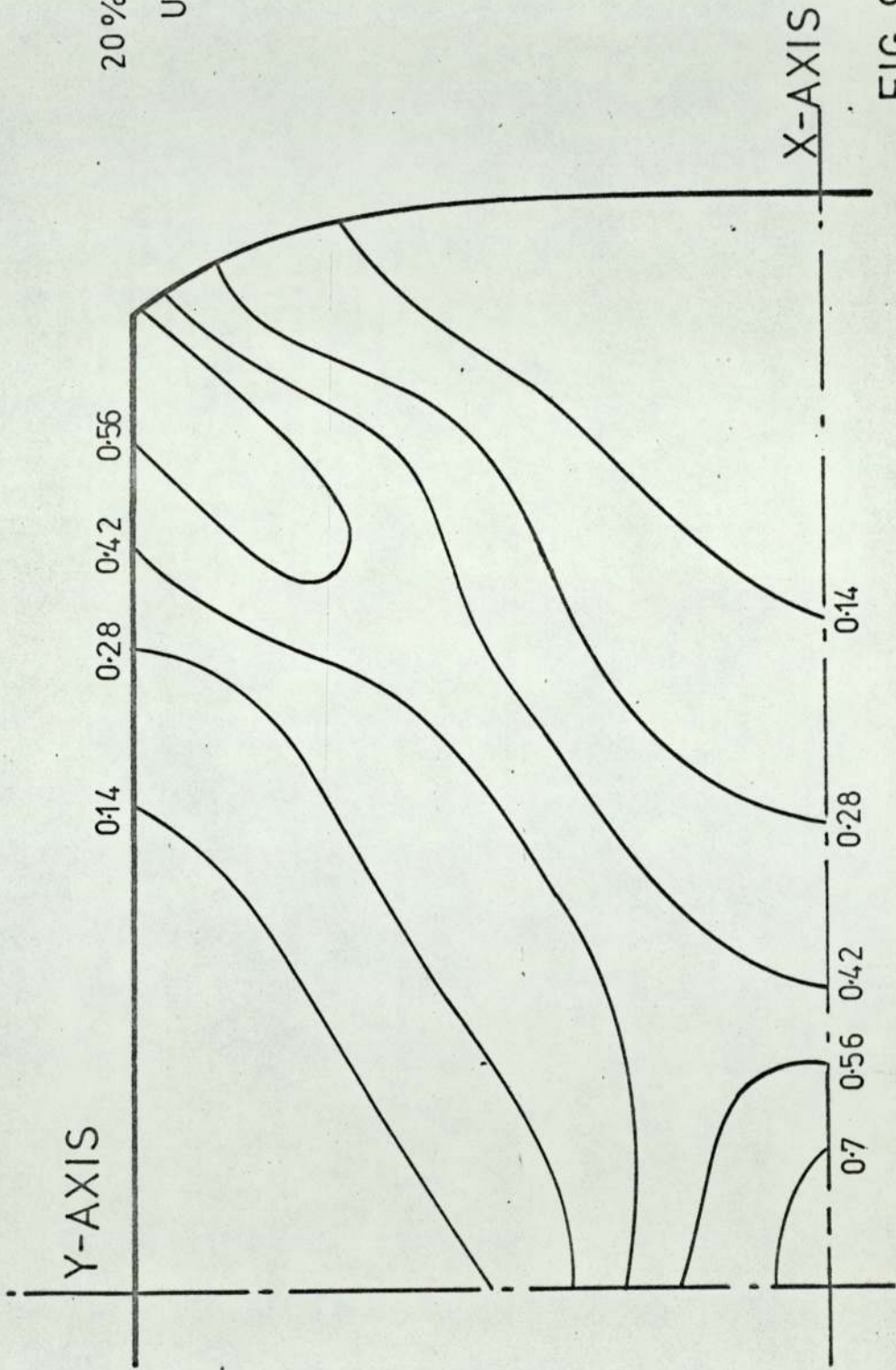


FIG. 9.20

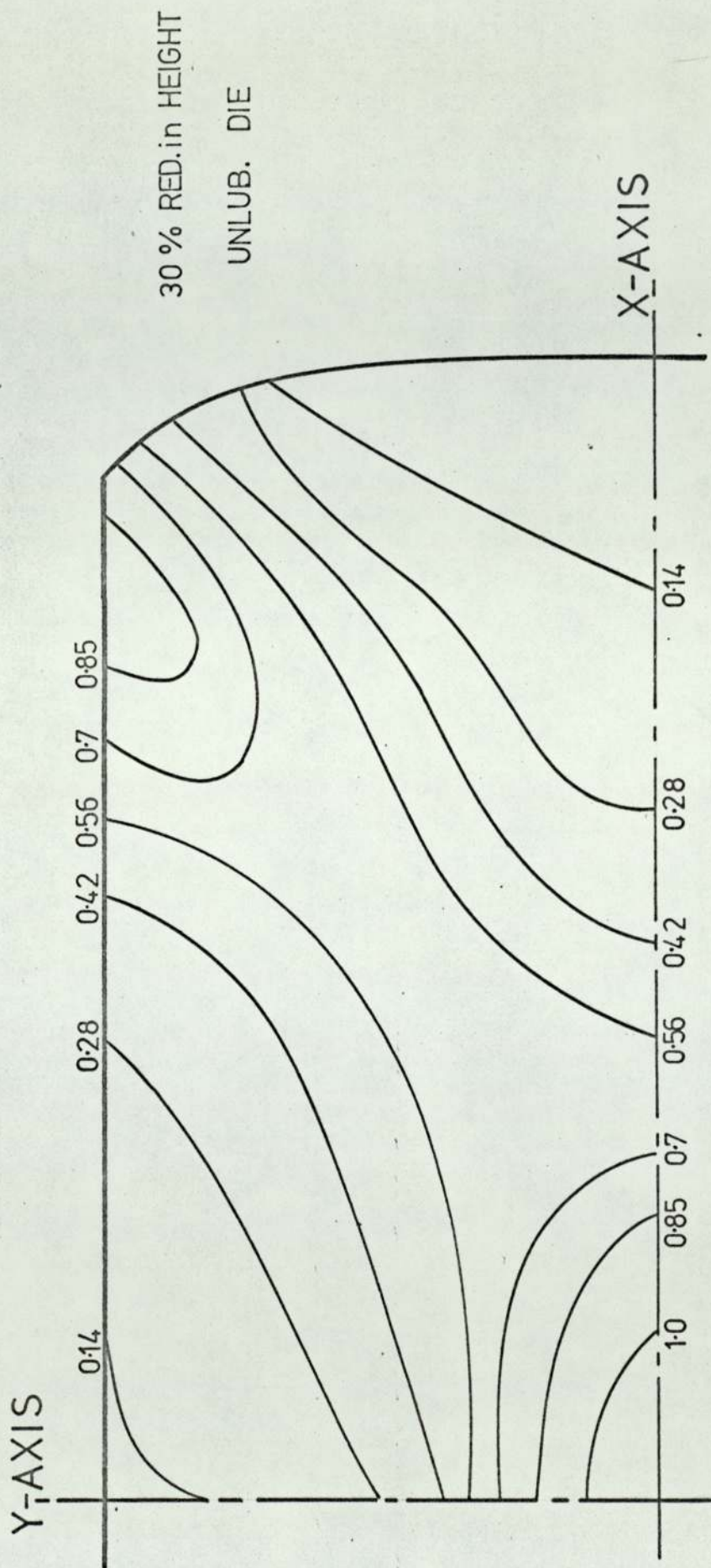


FIG. 9.21

STATE OF DEFORMATION

40 % RED. in HEIGHT
UNLUBRICATED

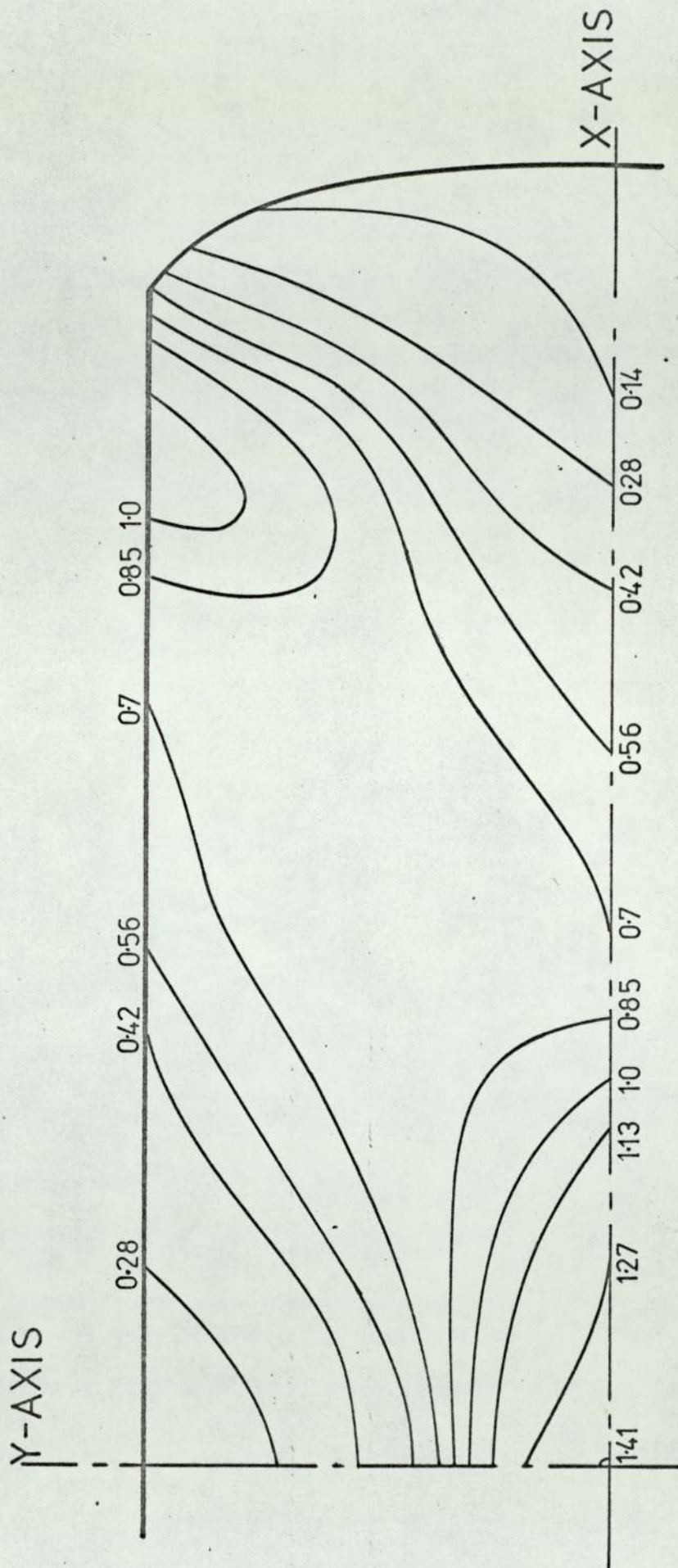
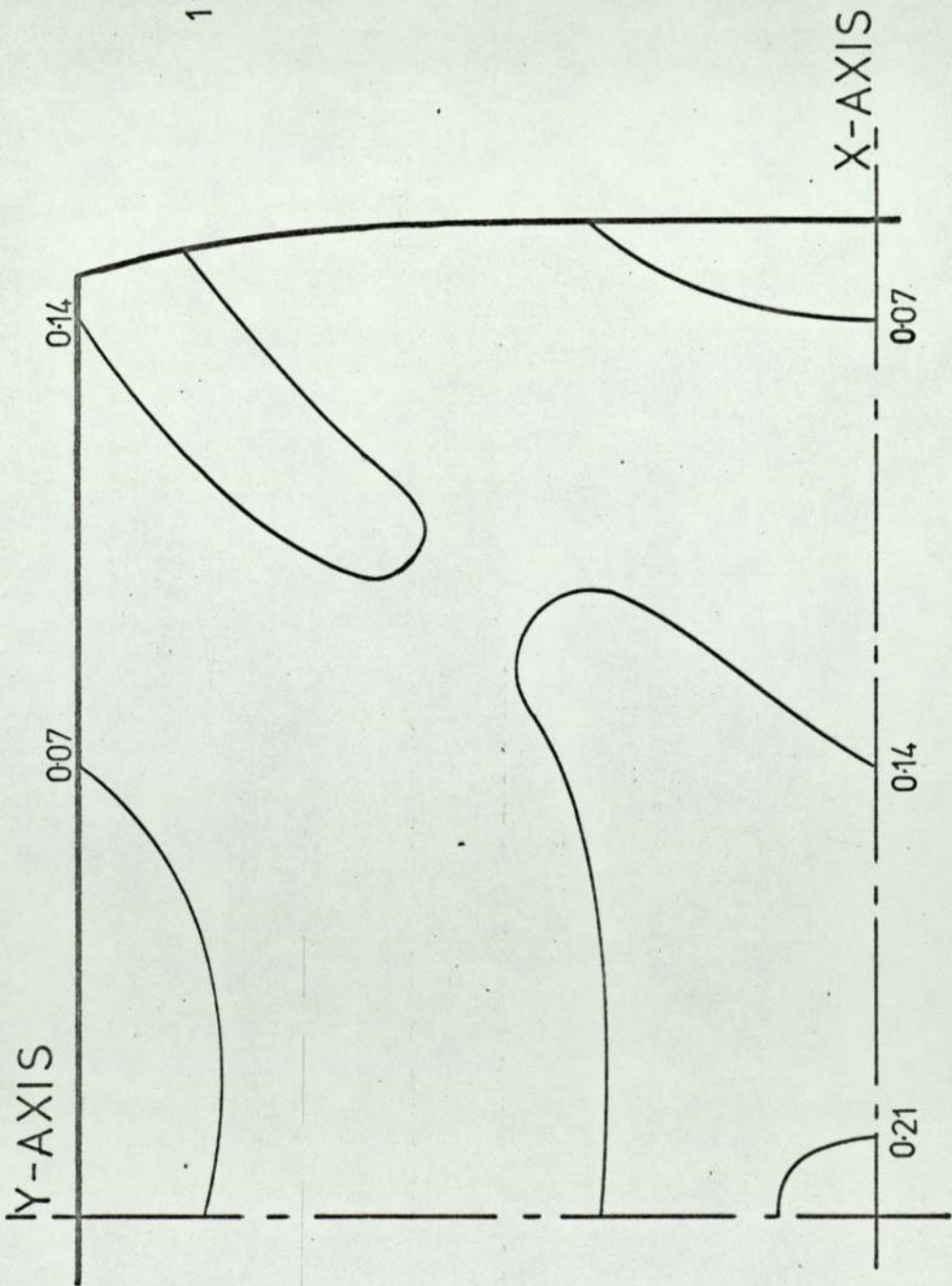


FIG. 9.22



11% RED. in HEIGHT
LUBRICATED DIE

FIG. 9.23

20% RED. in HEIGHT
LUBRICATED DIE

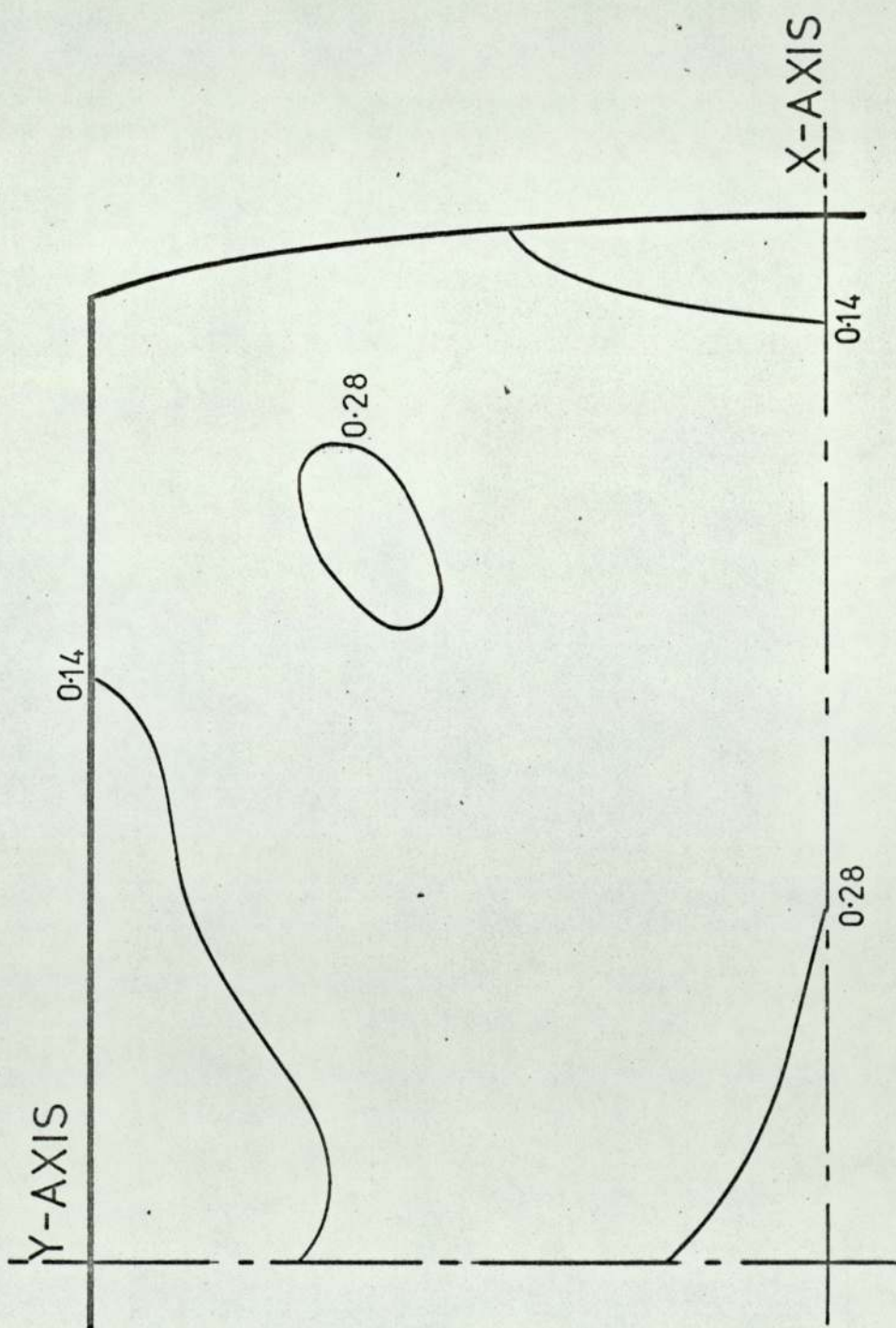
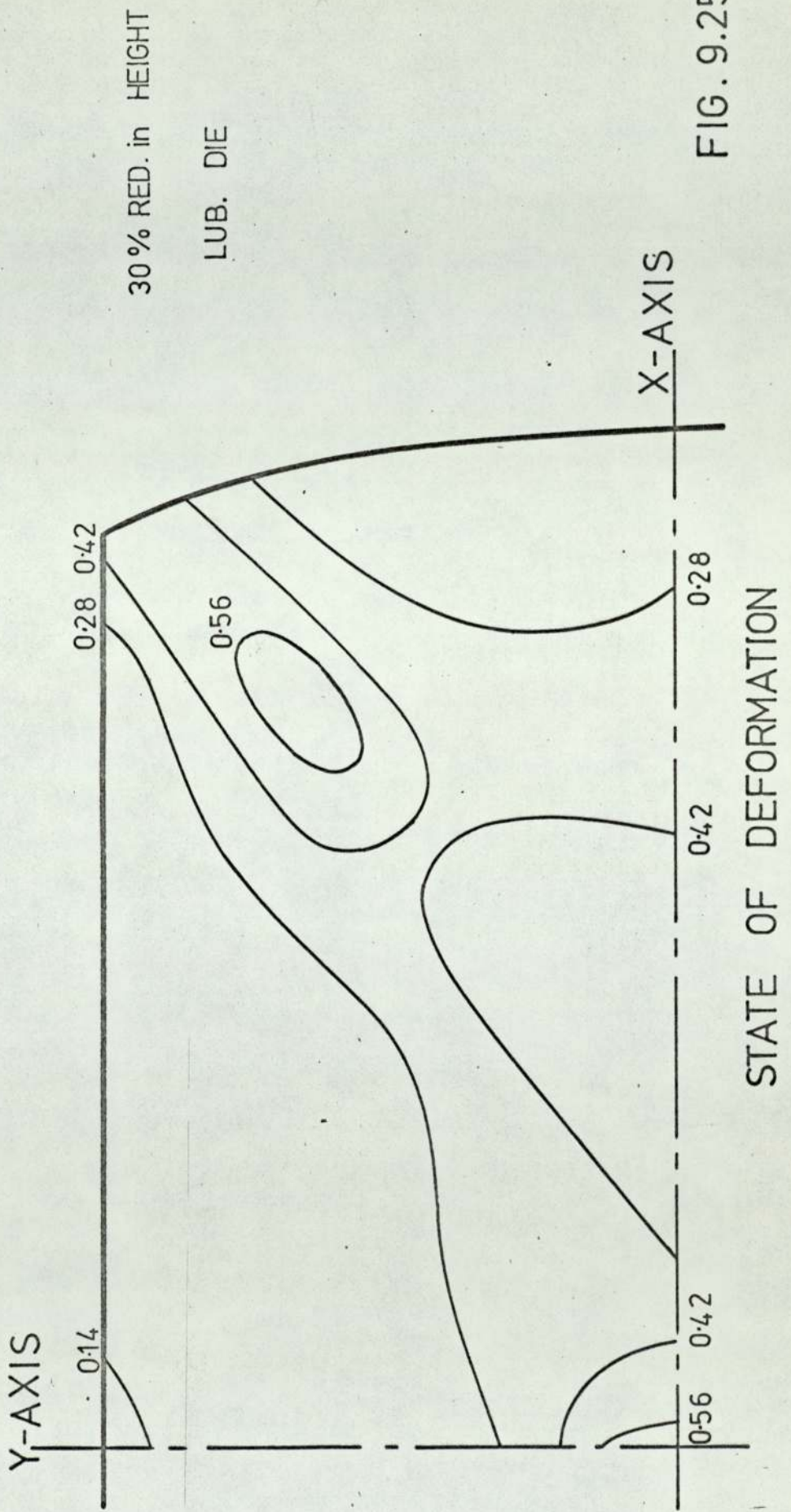


FIG. 9.24



40 % RED. in HEIGHT
LUBRICATED DIE

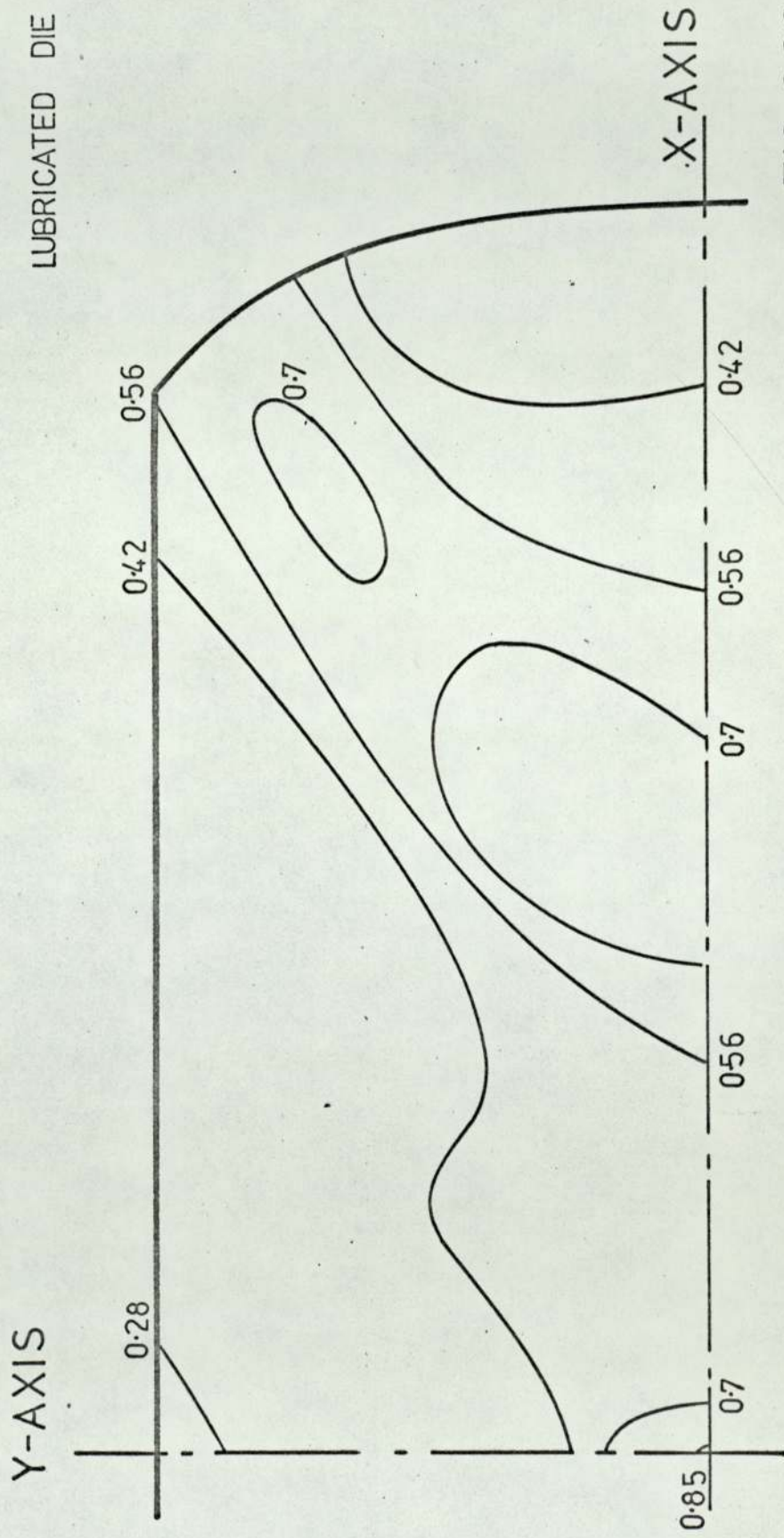


FIG. 9.26

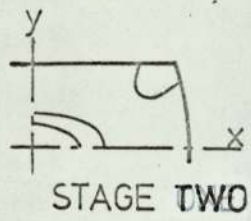
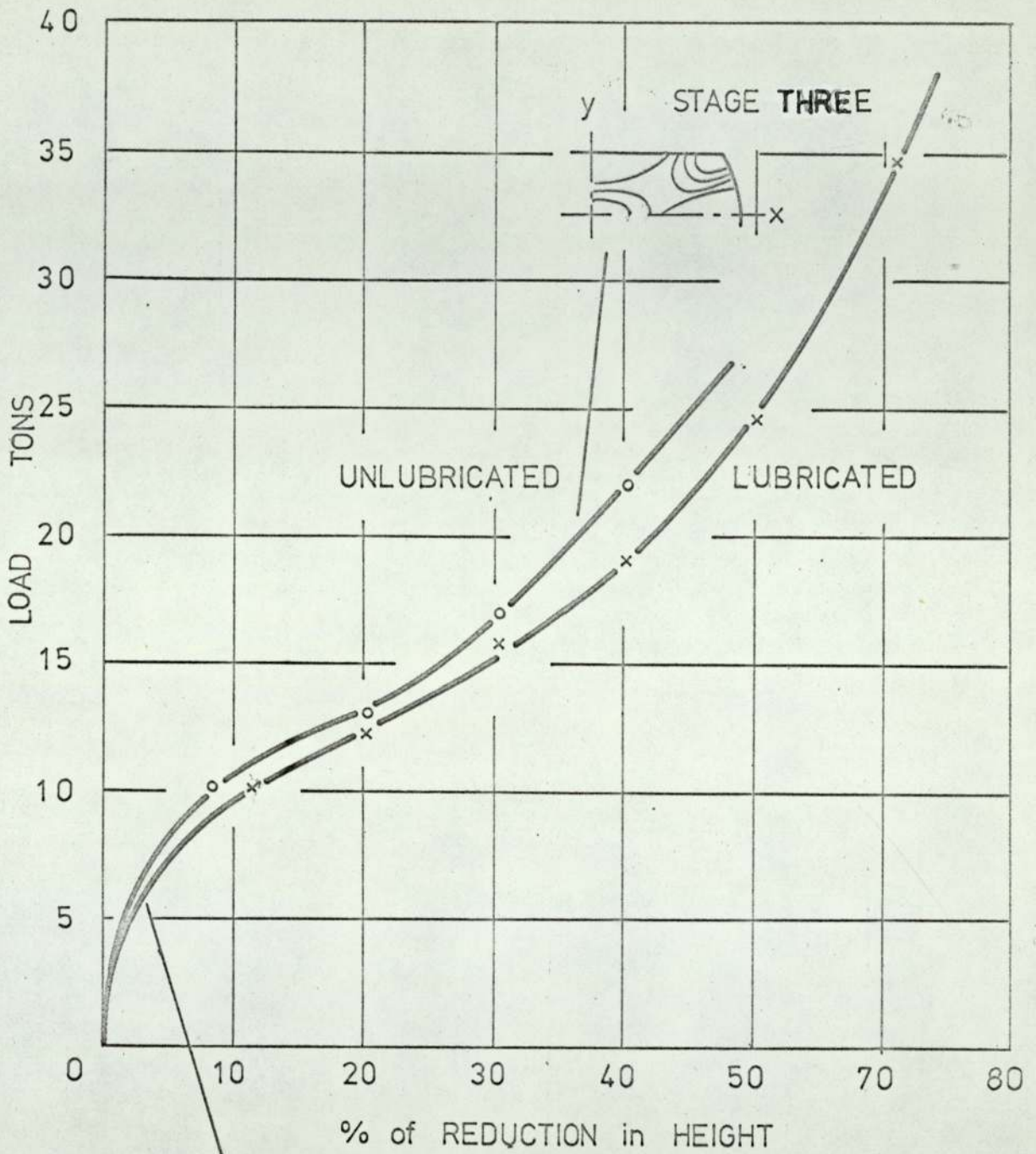


FIG. 9.27

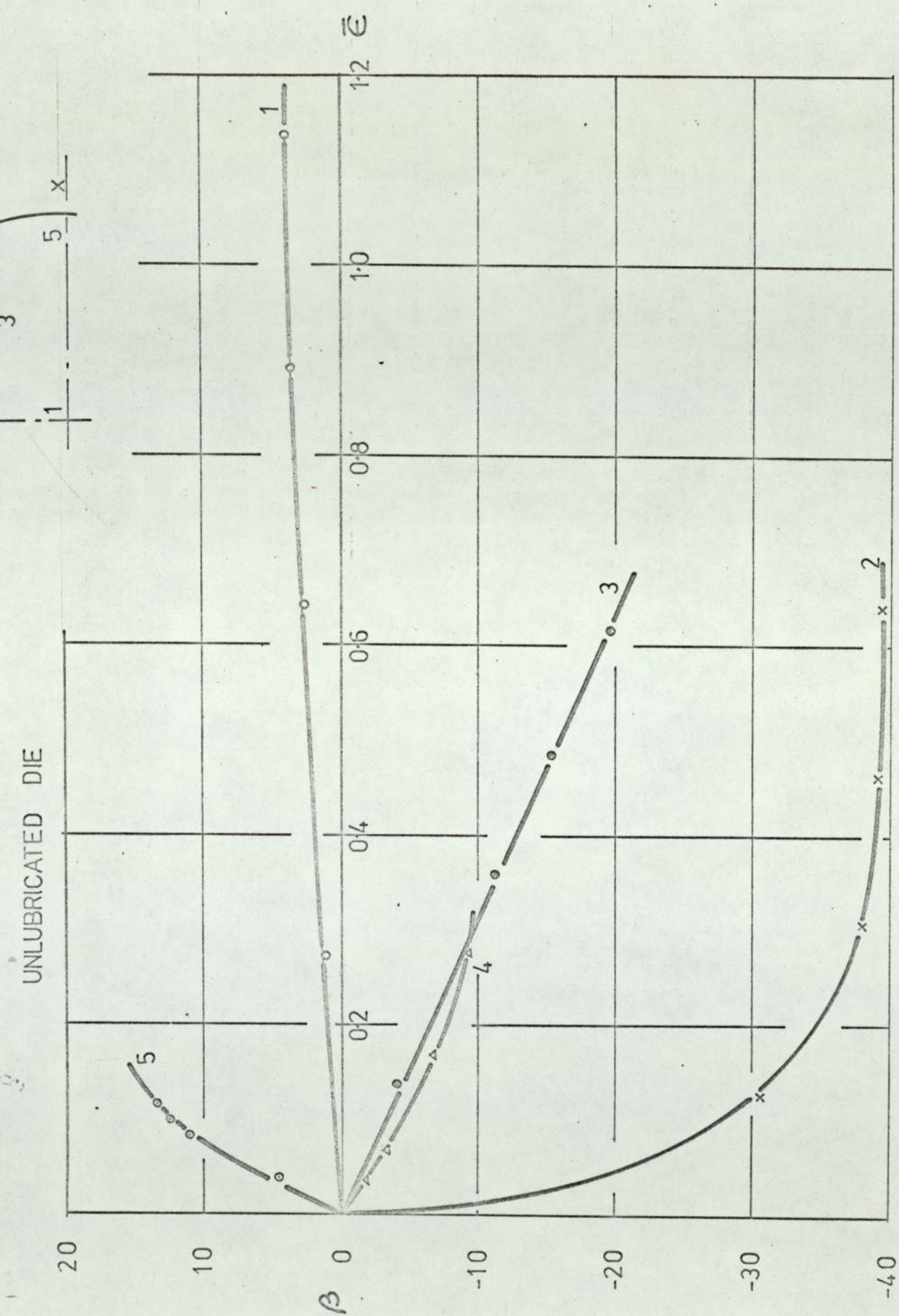


FIG. 9.28

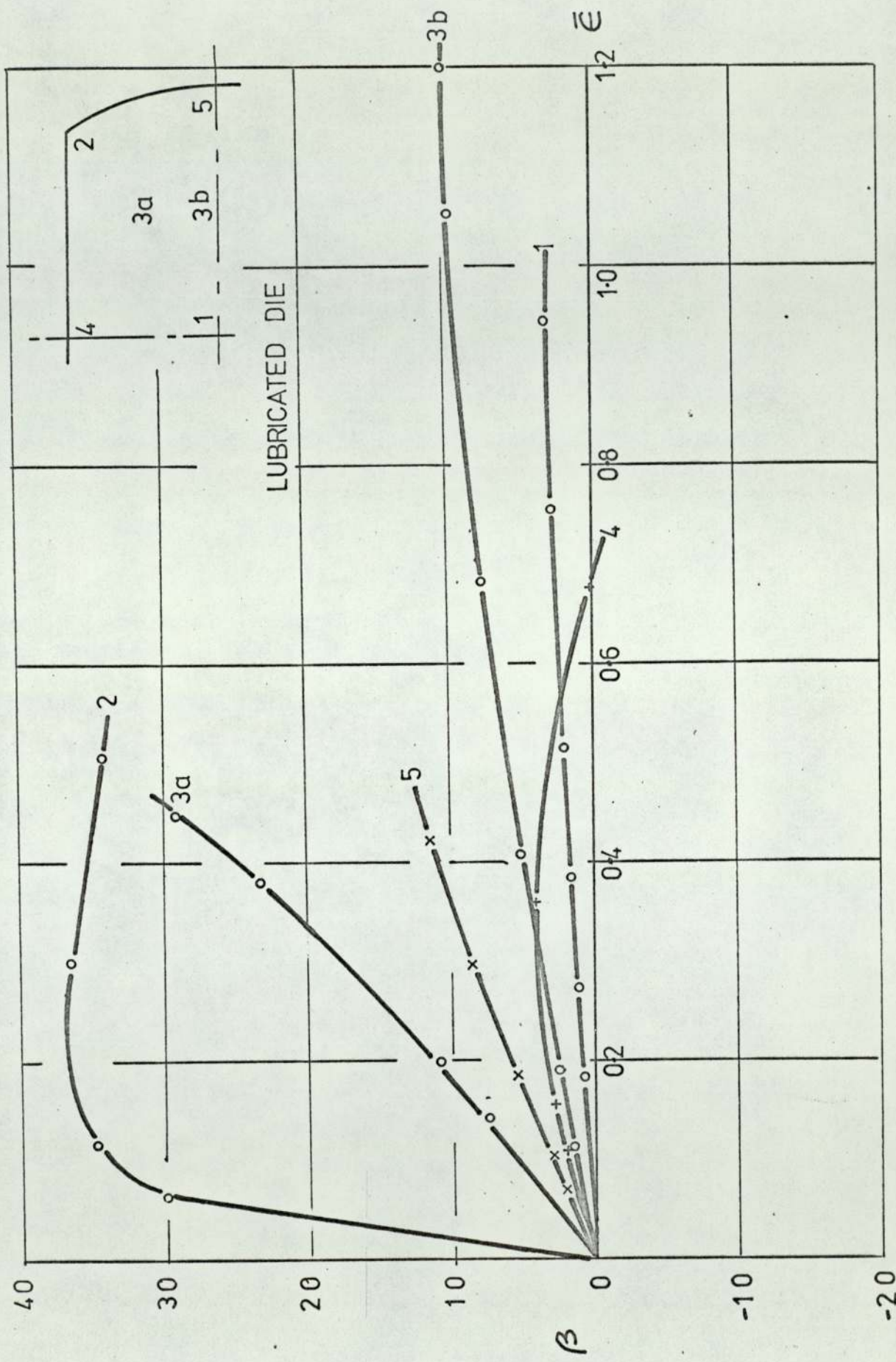


FIG. 9.29

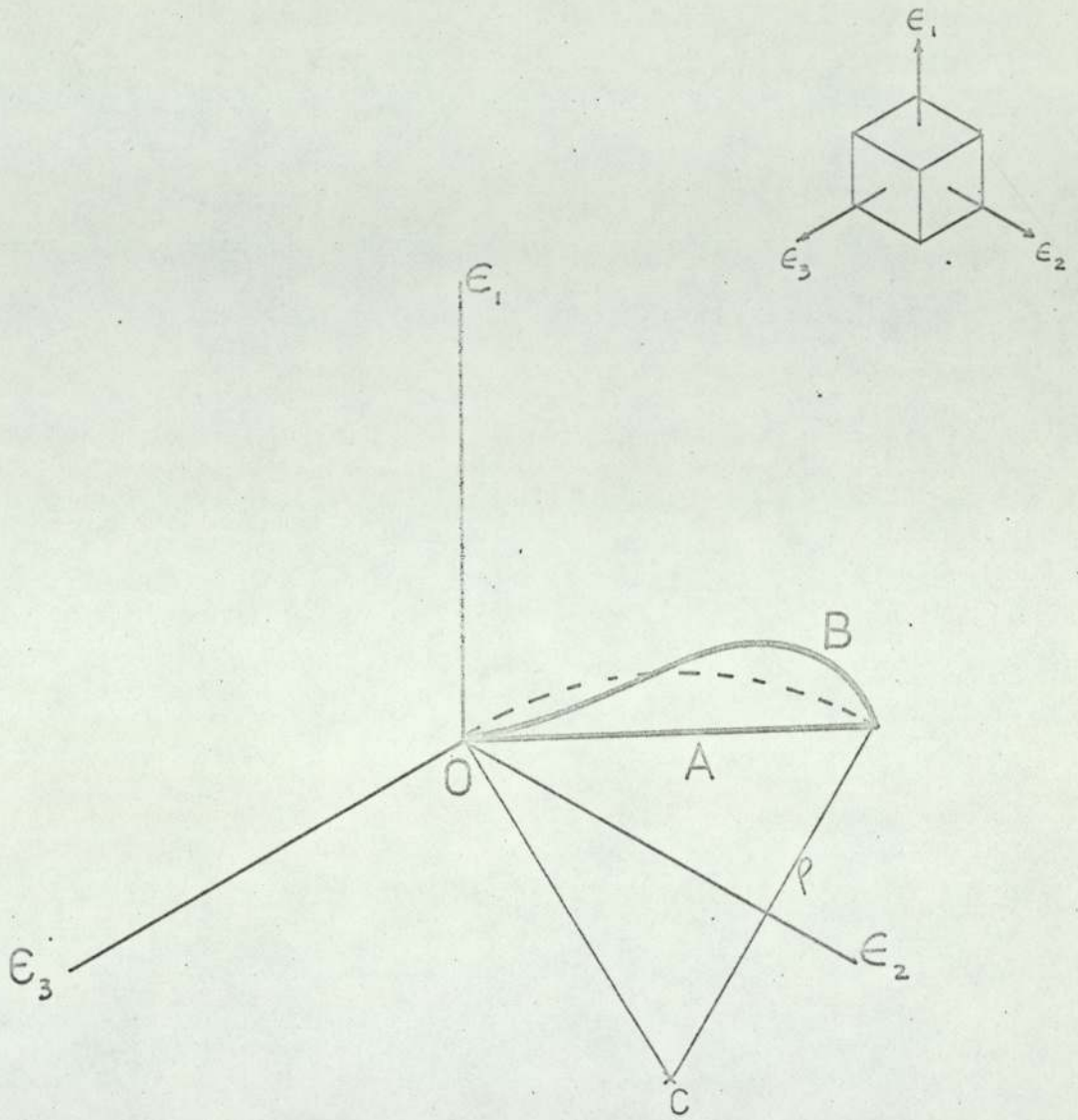


FIG. 9.30

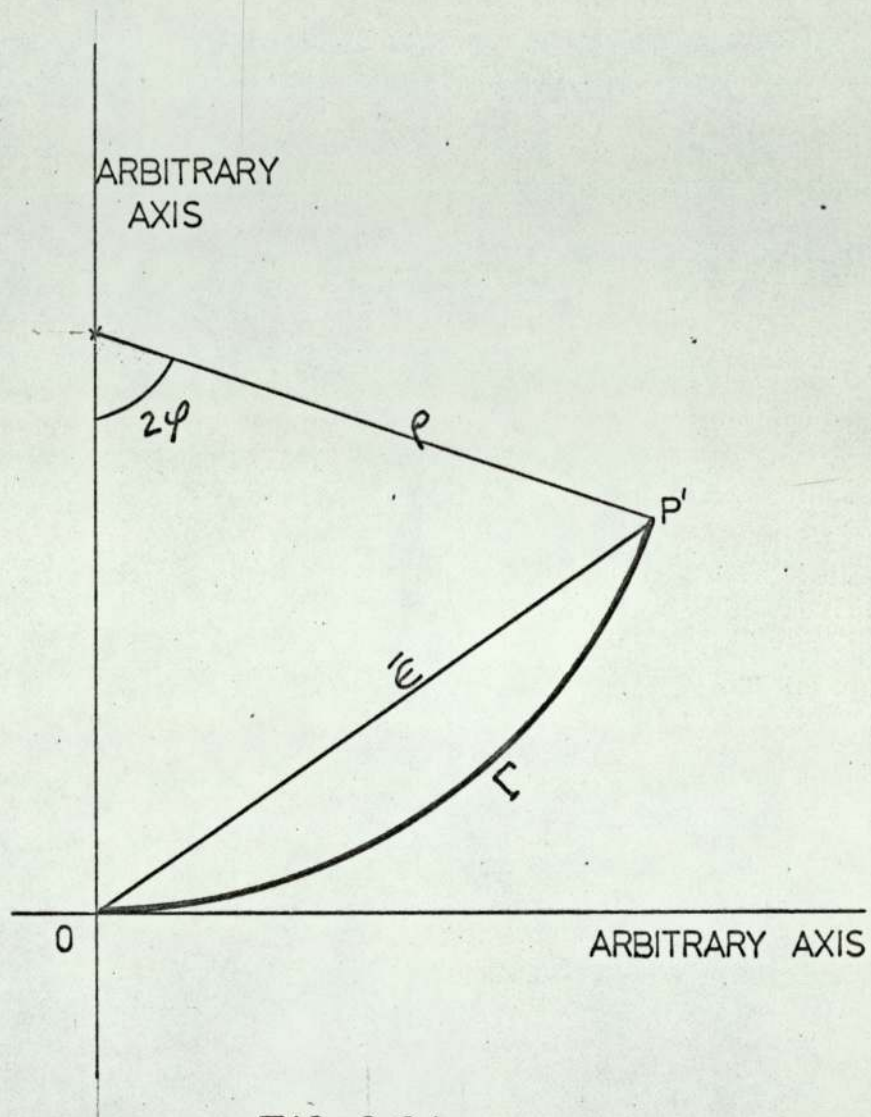


FIG. 9.31a

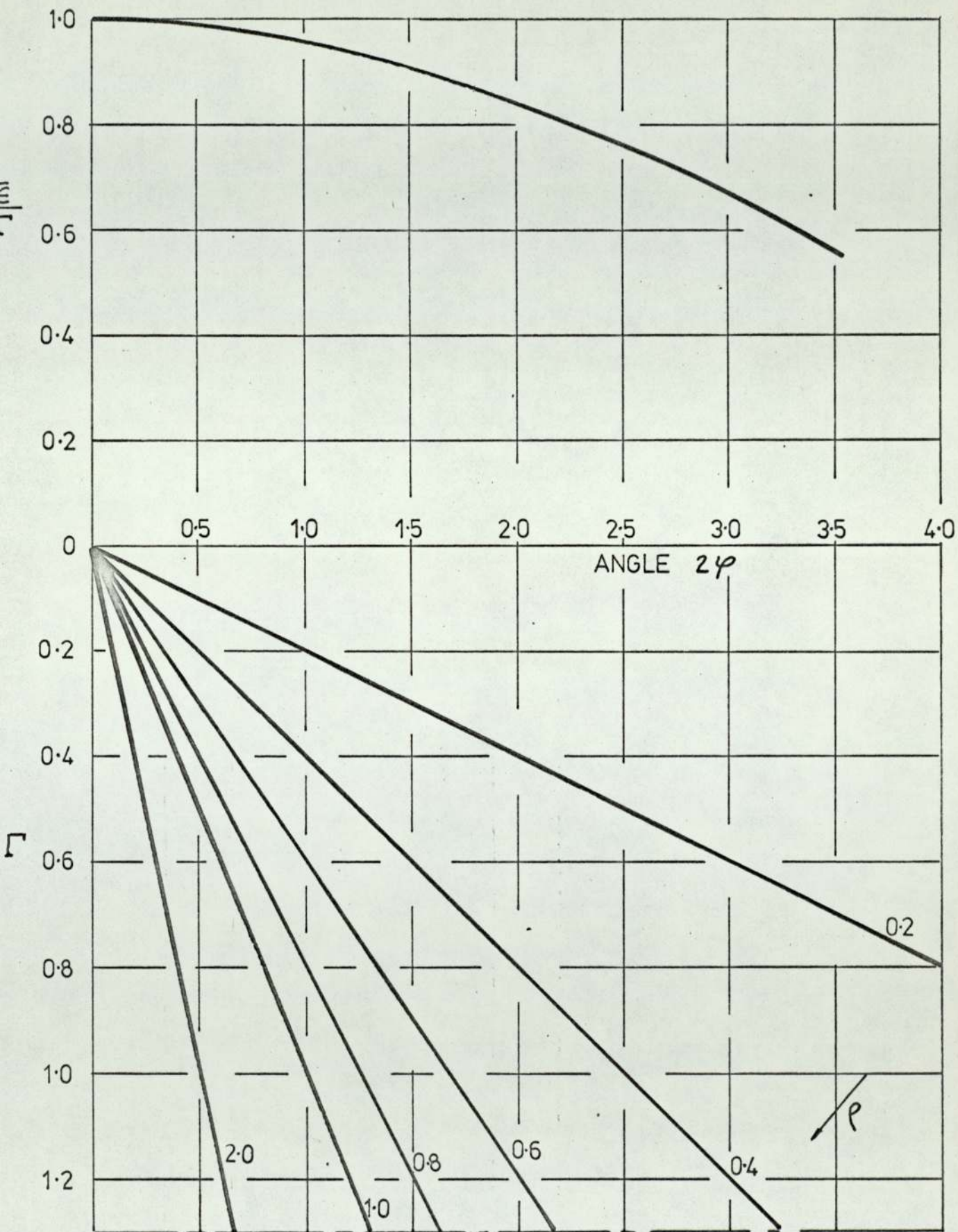


FIG. 9.31b

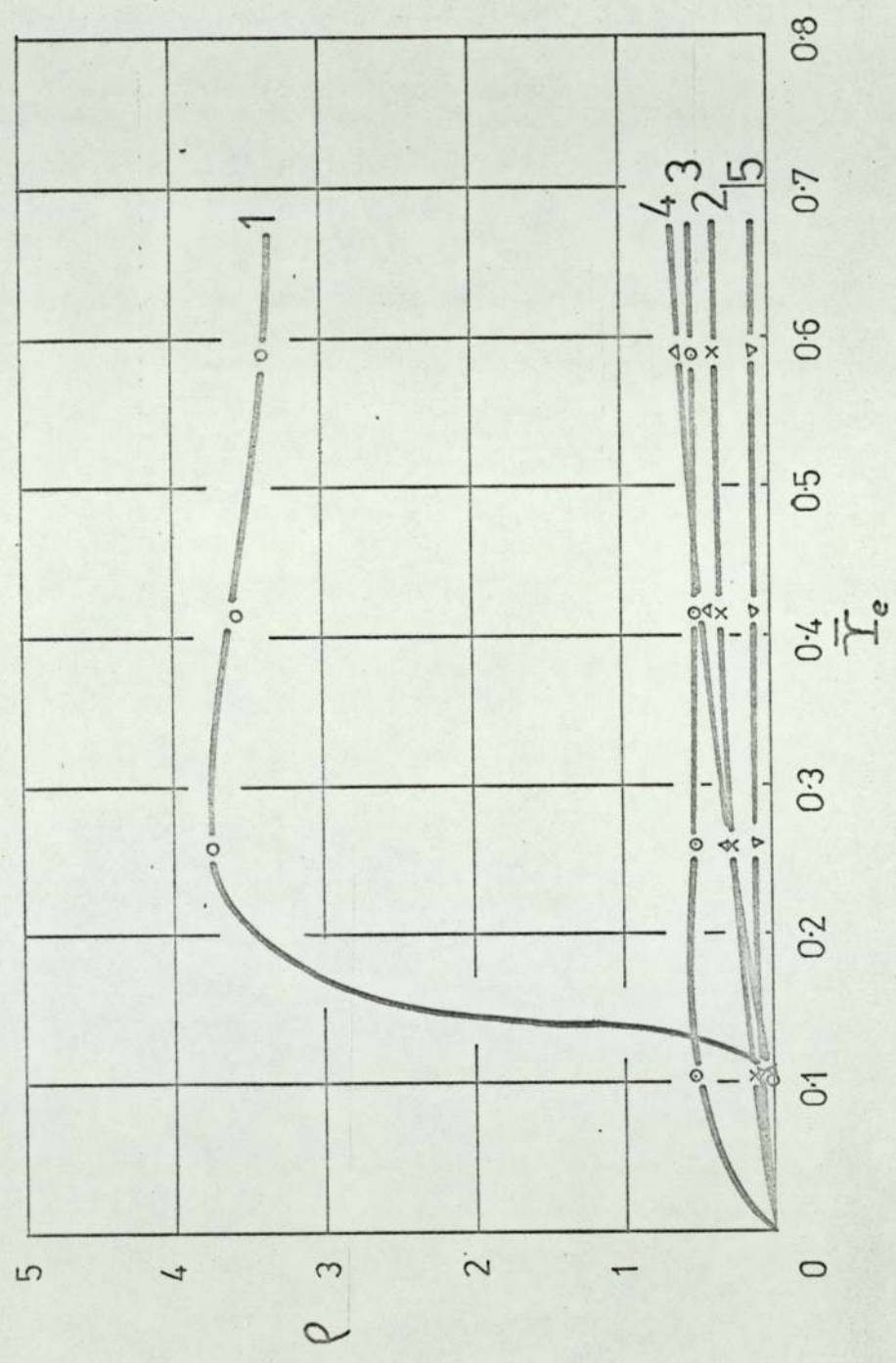
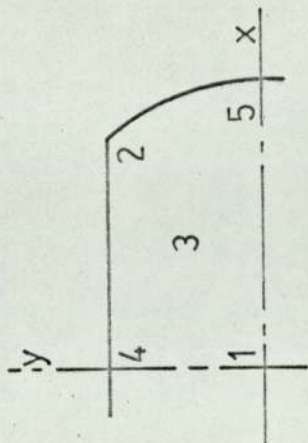


FIG. 9.32

LUBRICATED SPECIMEN

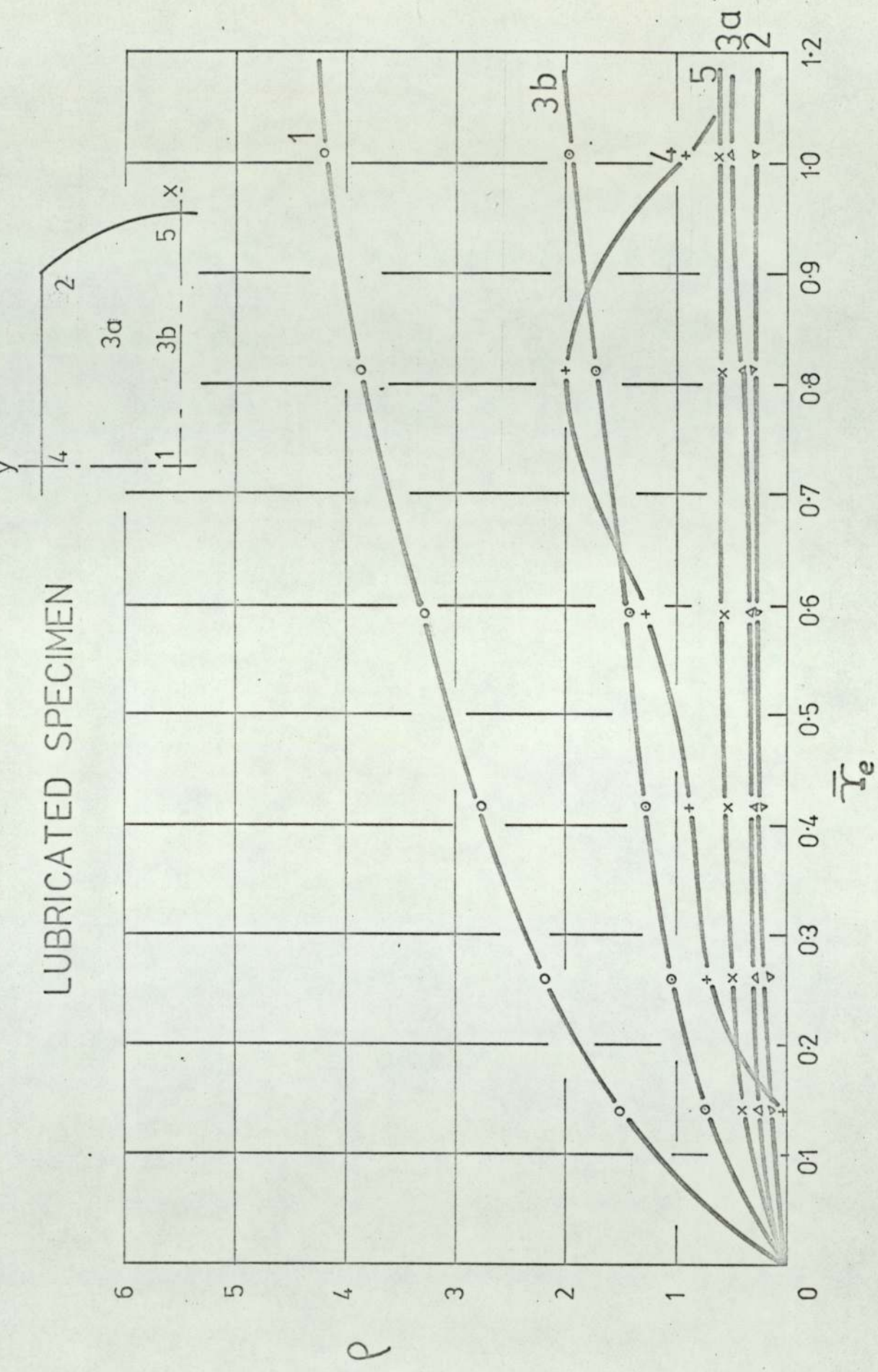


FIG. 9.33

UNLUBRICATED SPECIMEN

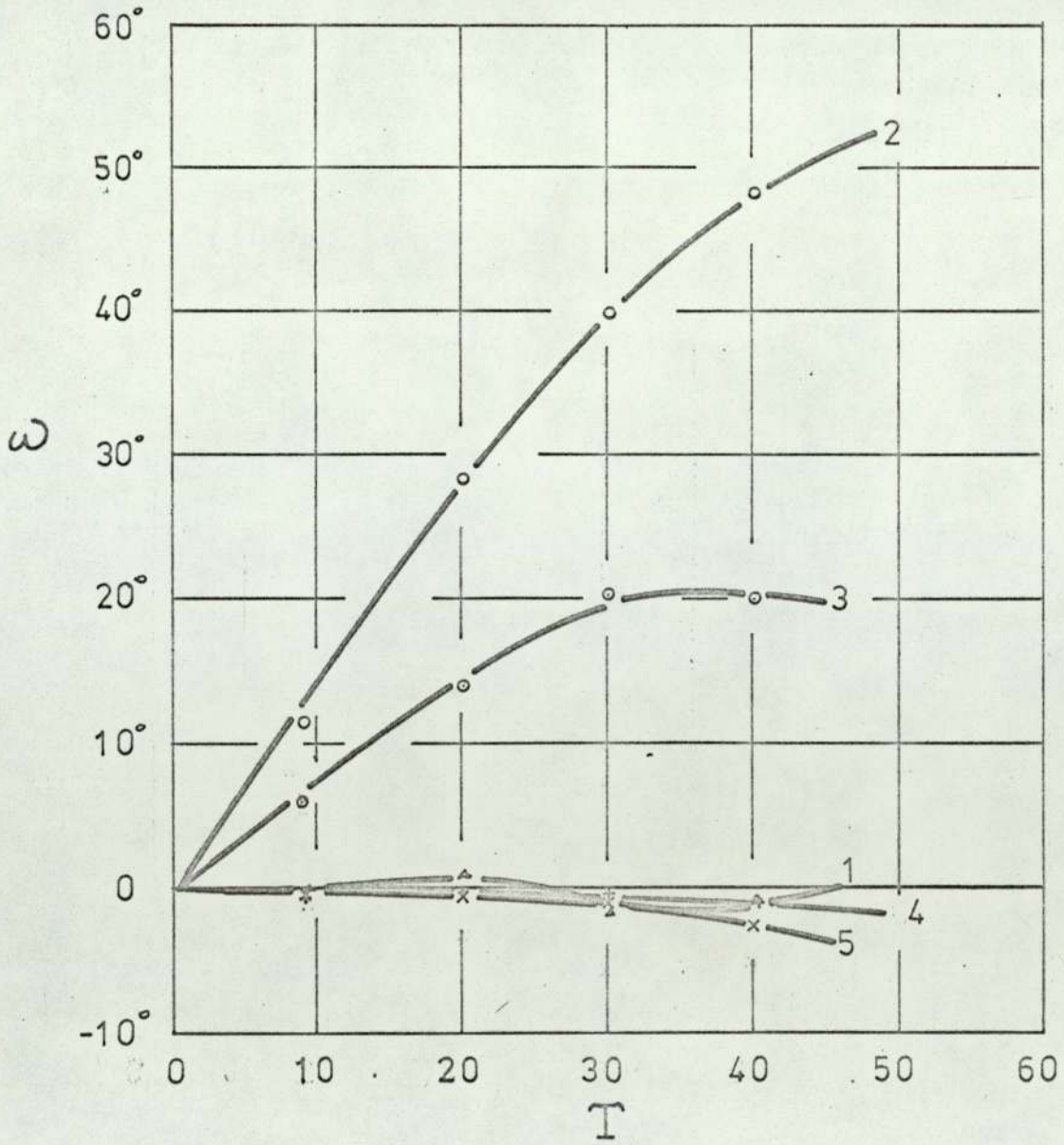
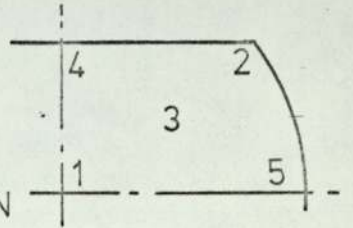
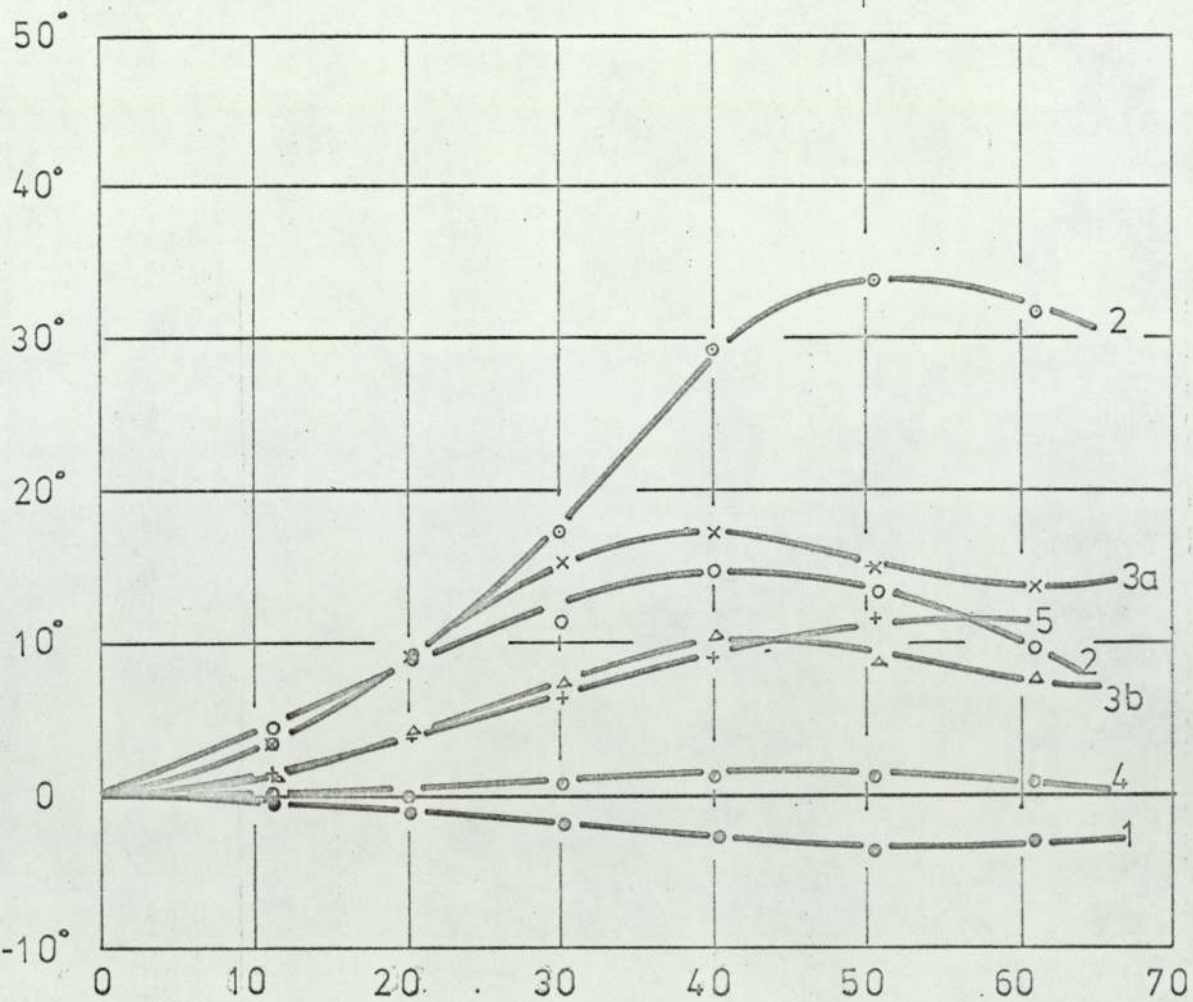
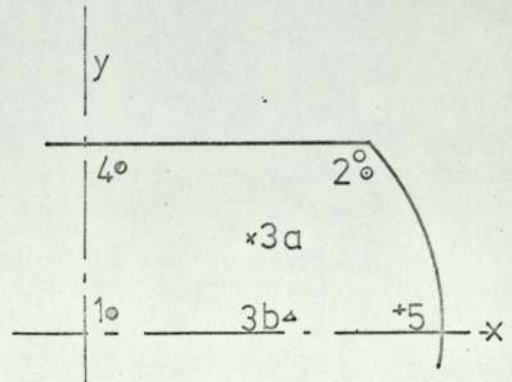


FIG. 9.34

LUBRICATED SPECIMEN



% of REDUCTION in HEIGHT

FIG. 9.35

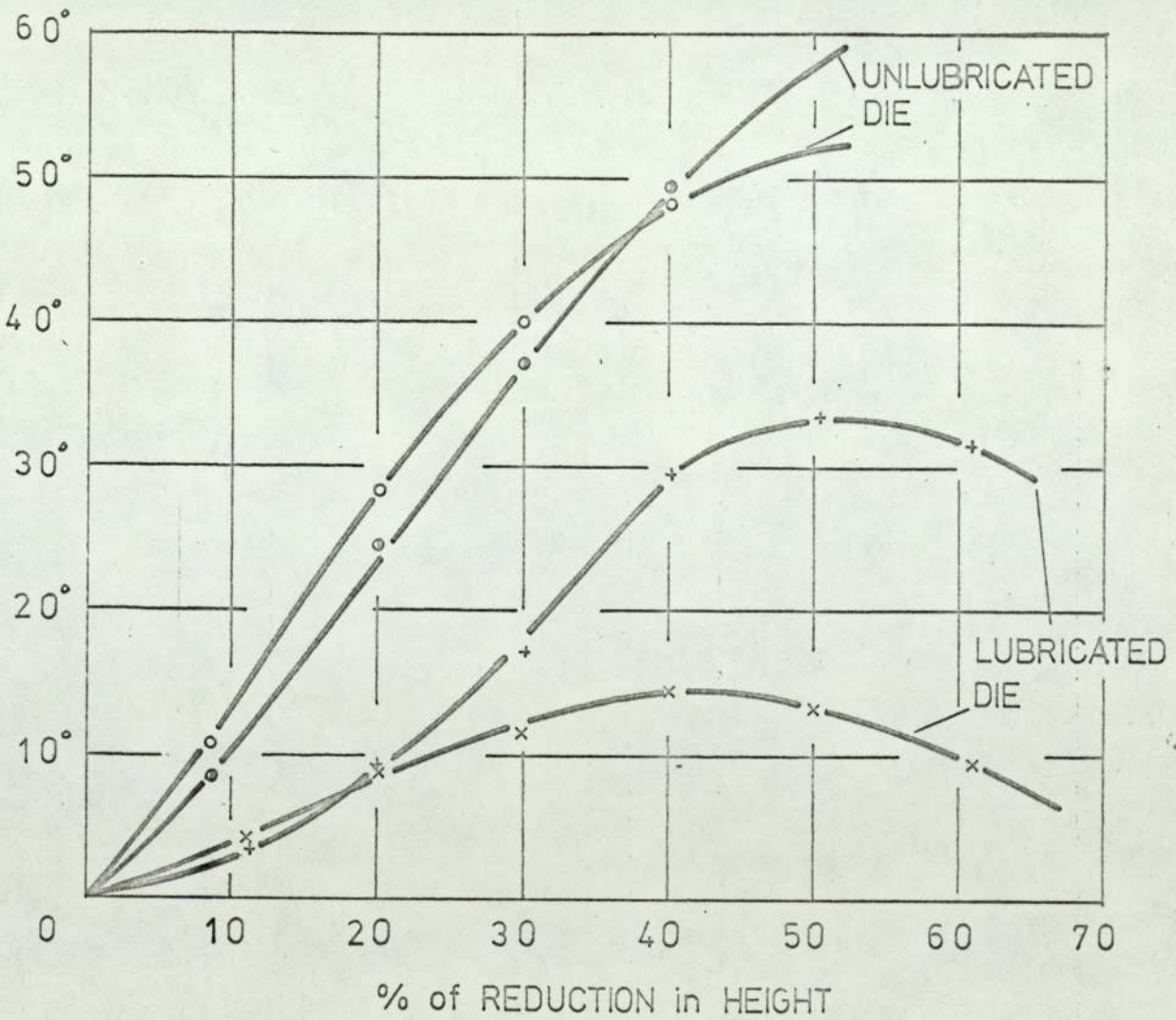
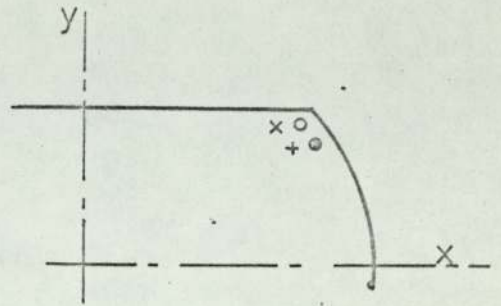


FIG. 936

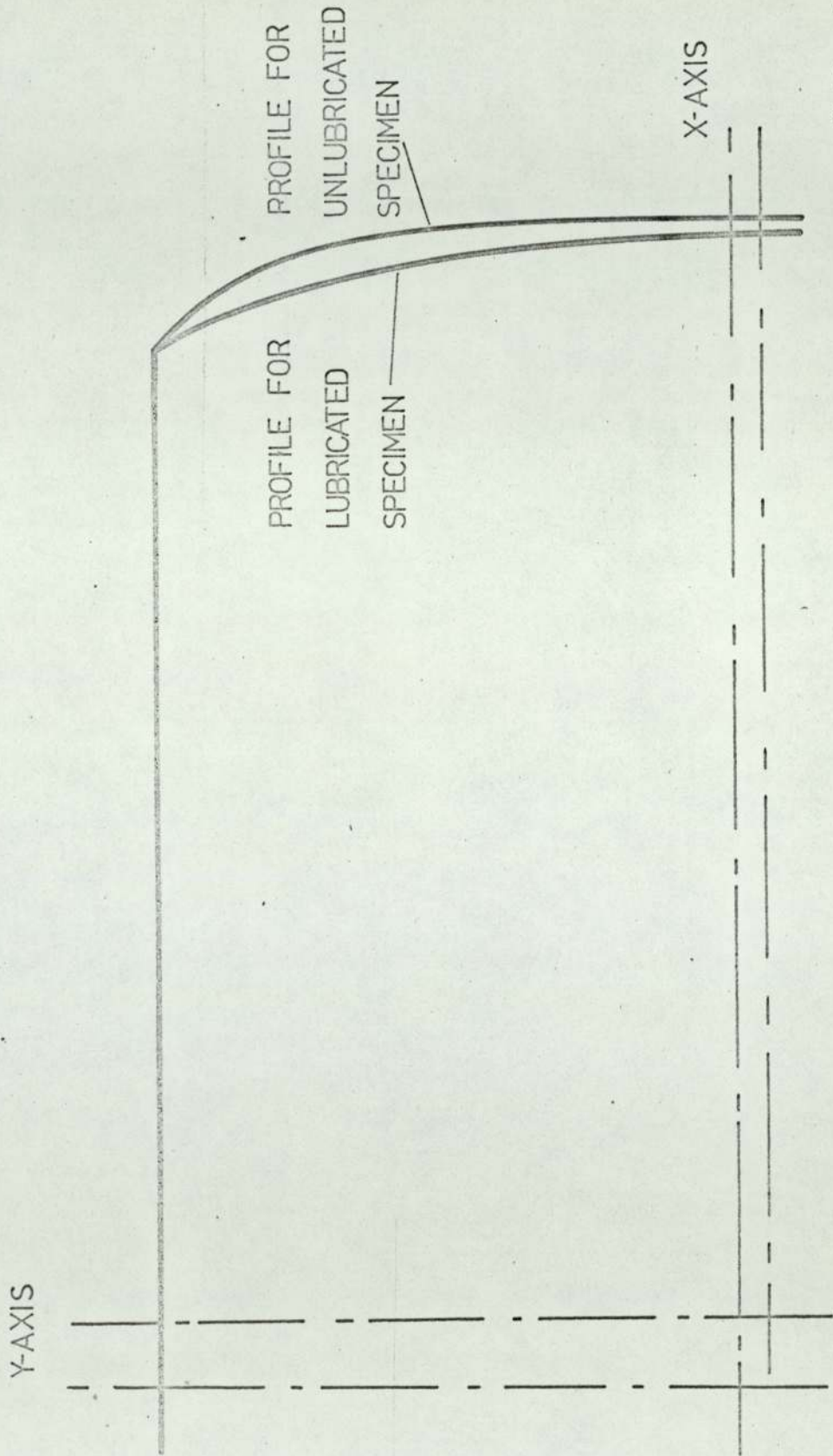
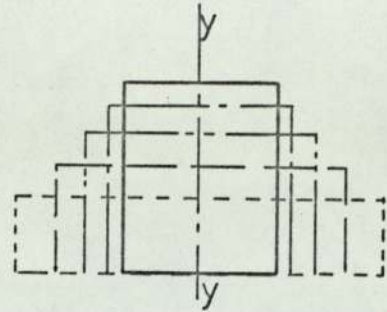


FIG. 9,37



	% of RED. in HEIGHT	MEAN STRAIN
A	8.7	0.11
B	20.2	0.26
C	30.3	0.42
D	40.3	0.60

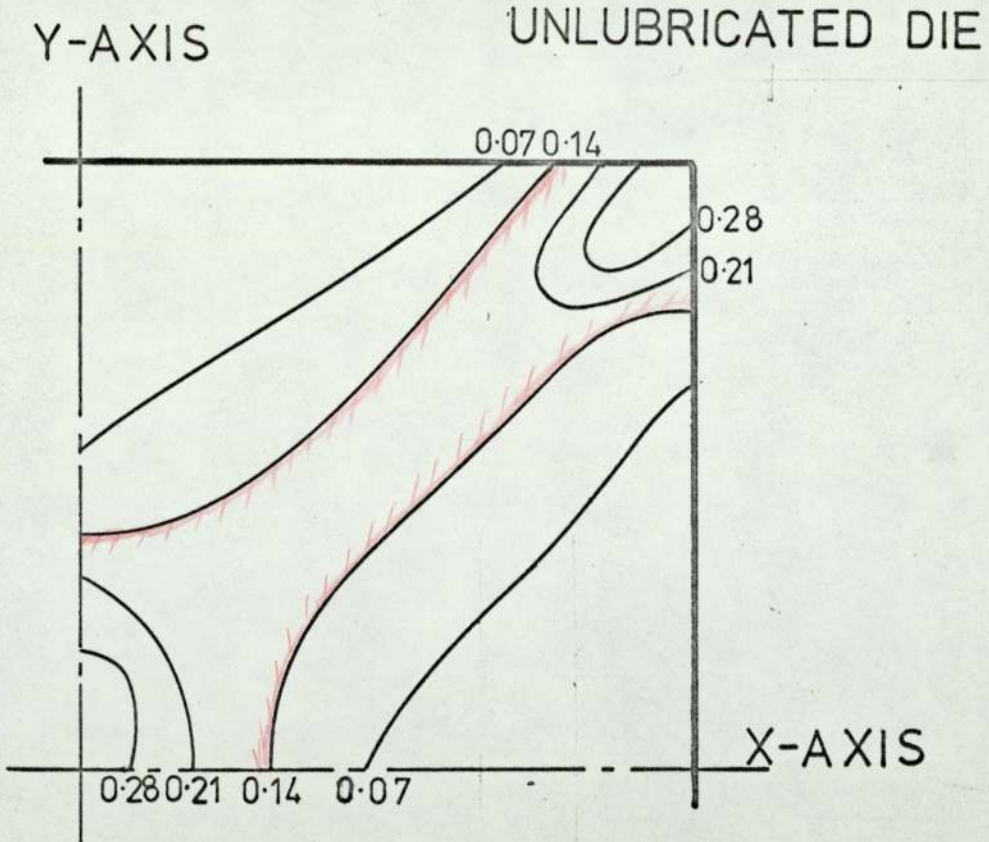
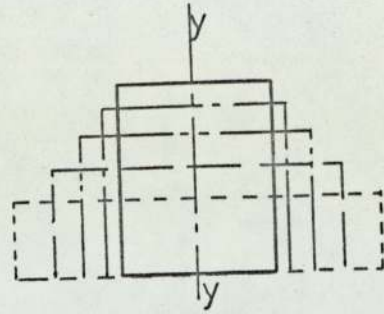
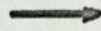


FIG. 9.38



	% of RED. in HEIGHT	MEAN STRAIN
A	8.7	0.11
B	20.2	0.26
C	30.3	0.42
D	40.3	0.60



UNLUBRICATED DIE

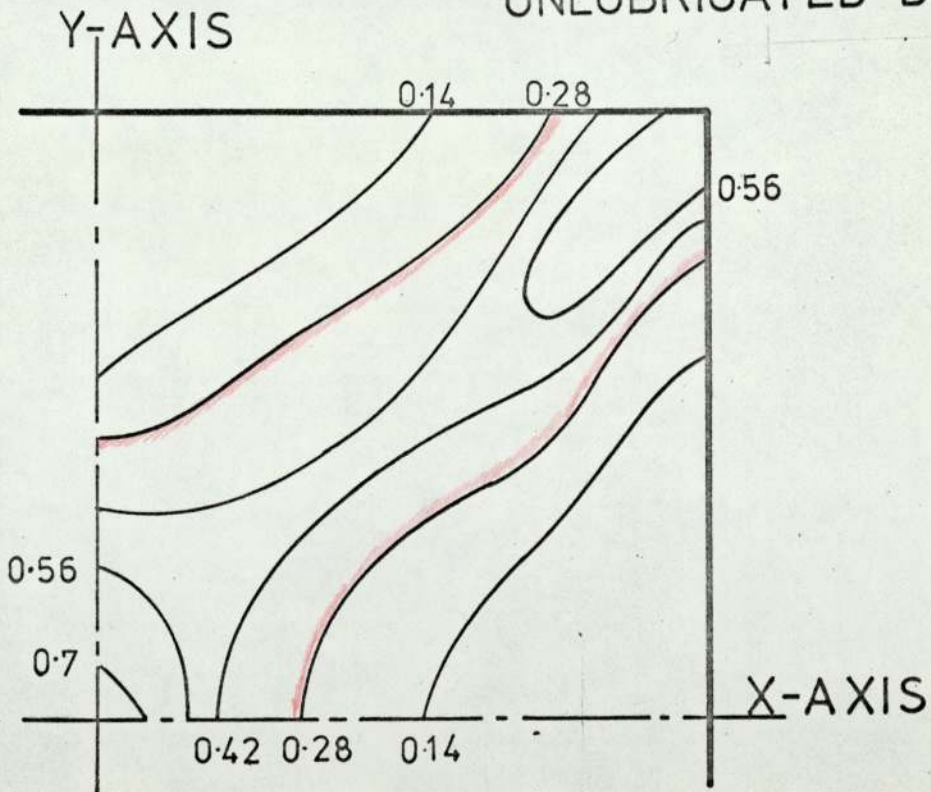
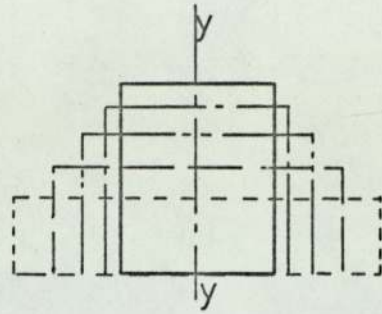


FIG. 9.39



	% of RED. in HEIGHT	MEAN STRAIN
A	8.7	0.11
B	20.2	0.26
C	30.3	0.42
D	40.3	0.60

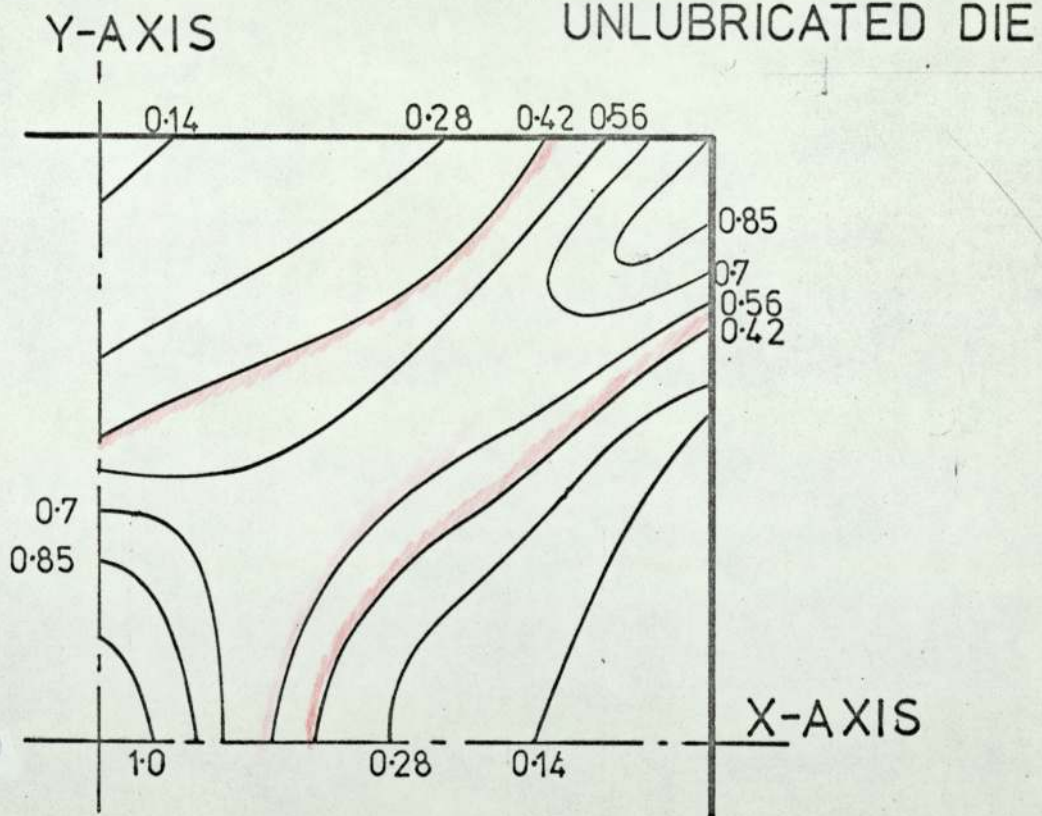
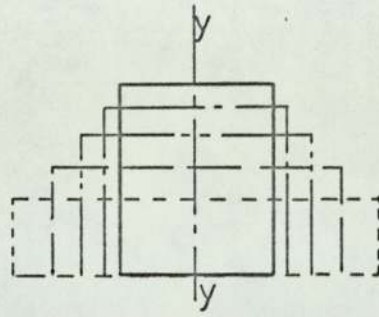


FIG. 9.40



	% of RED. in HEIGHT	MEAN STRAIN
A	8.7	0.11
B	20.2	0.26
C	30.3	0.42
D	40.3	0.60

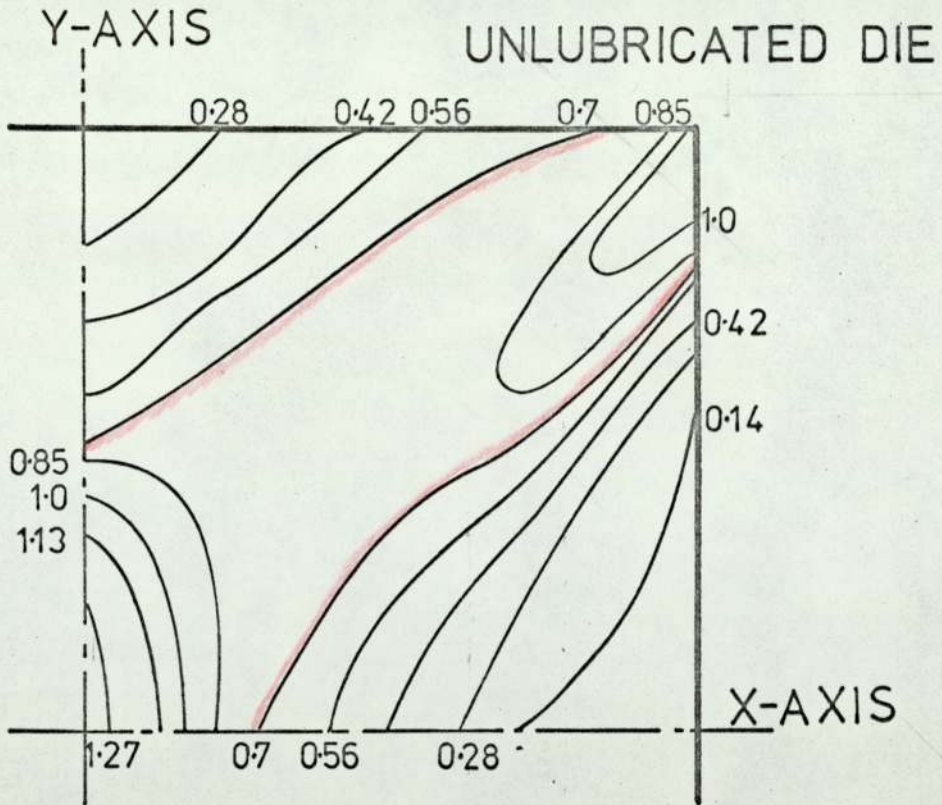
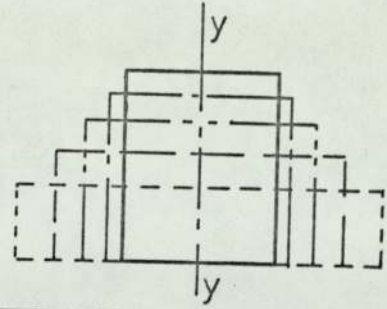


FIG. 9.41



	% of RED. in HEIGHT	MEAN STRAIN
E	11.4	0.12
F	20.1	0.25
G	30.0	0.40
H	40.0	0.58

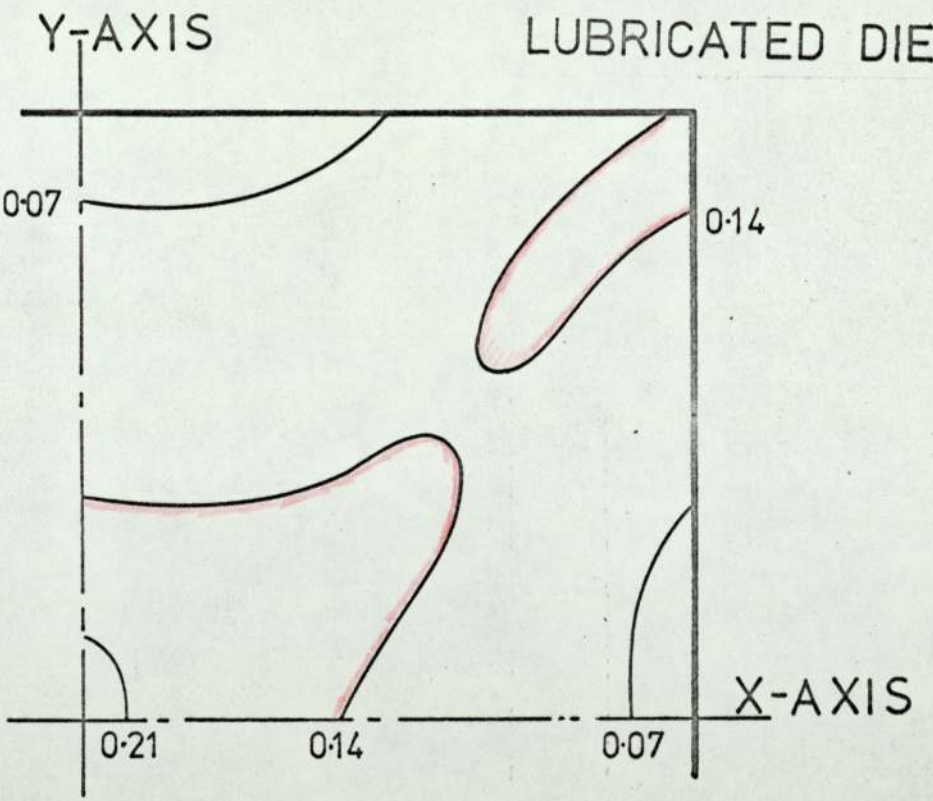
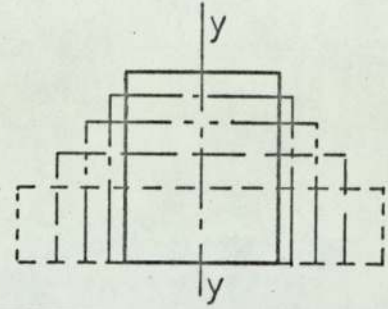


FIG. 9.42



	% of RED. in HEIGHT	MEAN STRAIN
E	11.4	0.12
F	20.1	0.25
G	30.0	0.40
H	40.0	0.58

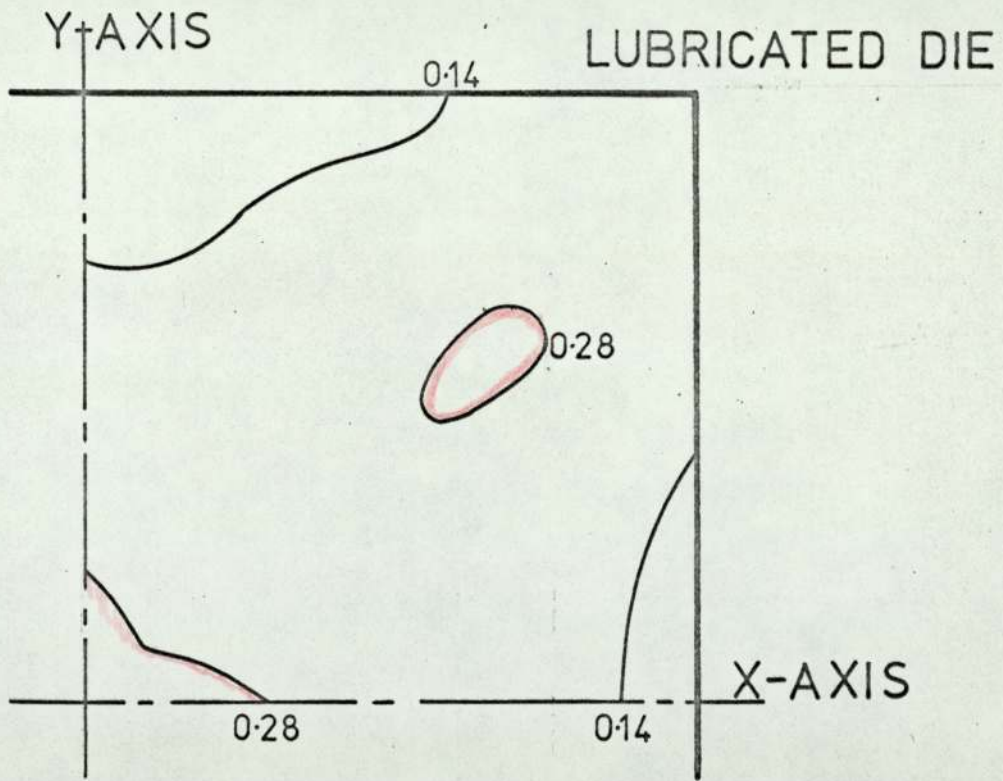
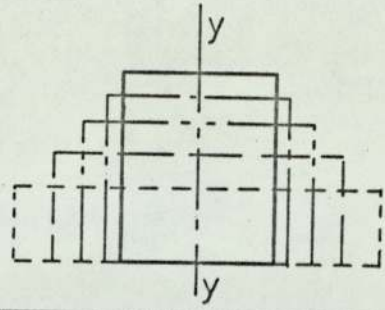


FIG. 9.43



	% of RED. in HEIGHT	MEAN STRAIN
E	11.4	0.12
F	20.1	0.25
G	30.0	0.40
H	40.0	0.58

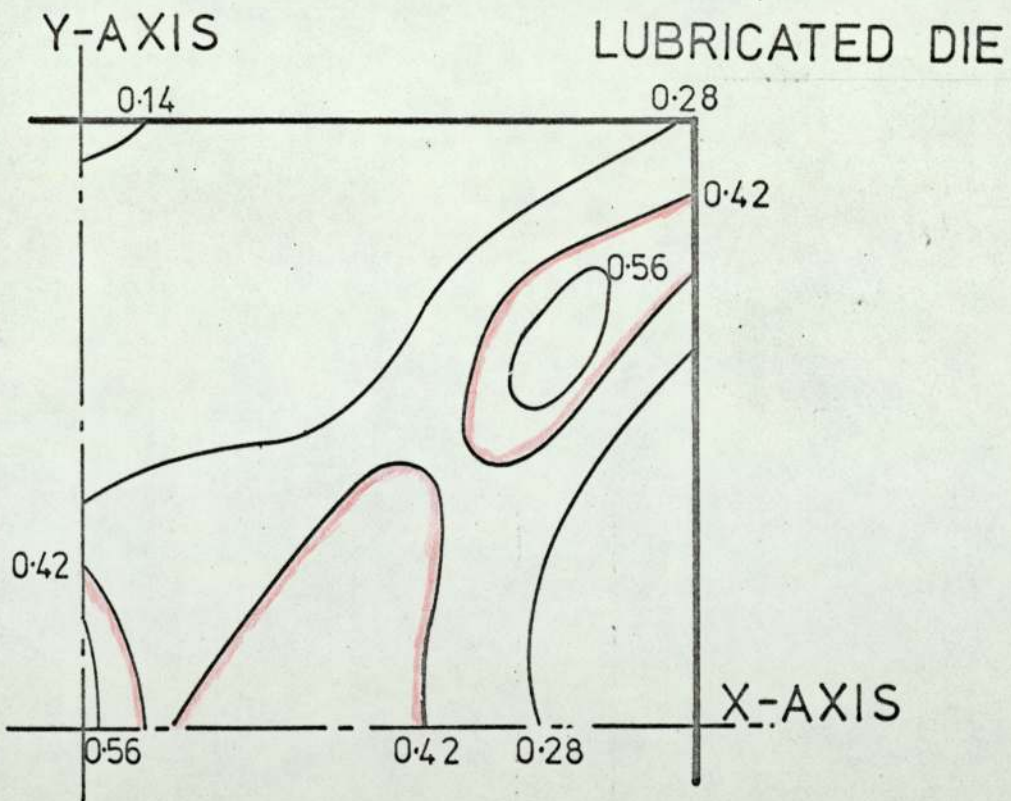
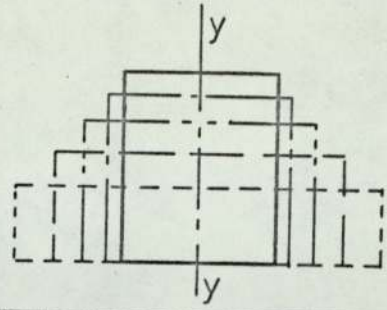


FIG. 9.44



	% of RED. in HEIGHT	MEAN STRAIN
E	11.4	0.12
F	20.1	0.25
G	30.0	0.40
H	40.0	0.58

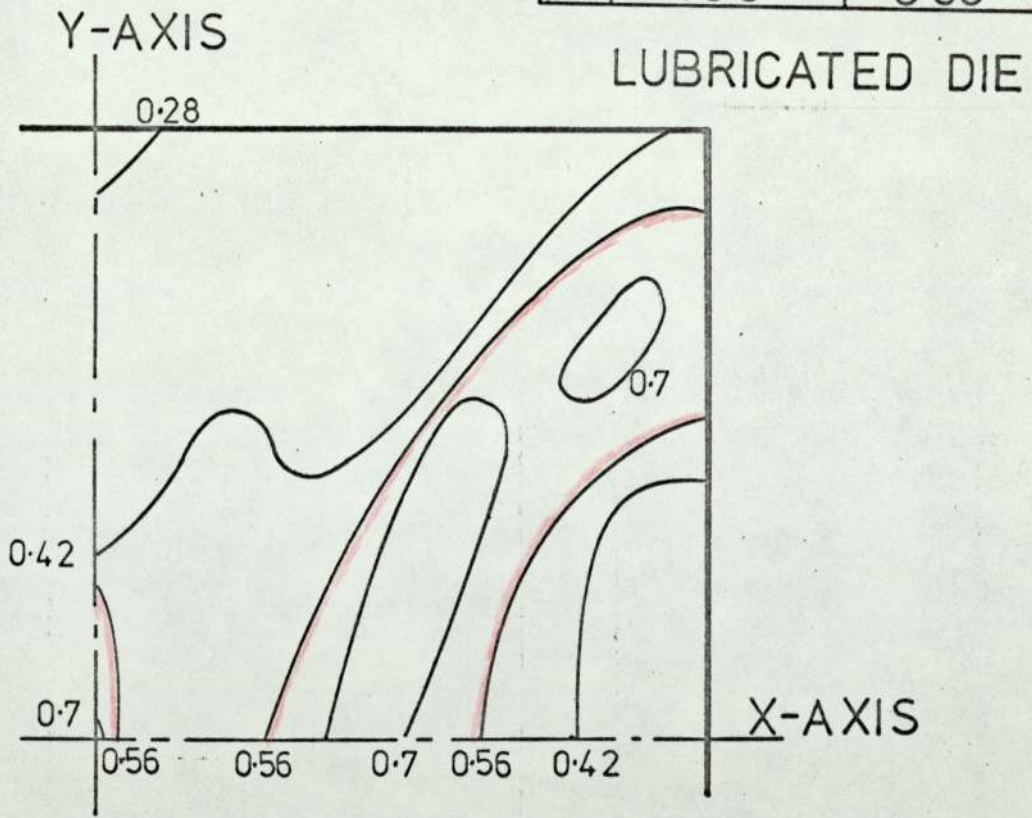
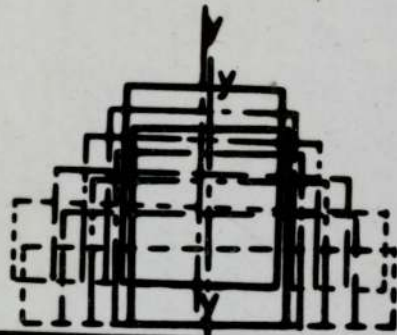


FIG. 9.45



	% of PUNCH HEIGHT	MEAN STRAIN
A	0.0	0.12
B	20.34	0.56
C	30.91	0.75
D	40.90	0.70
H	40.0	0.58

UNLUBRICATED DIE
LUBRICATED DIE

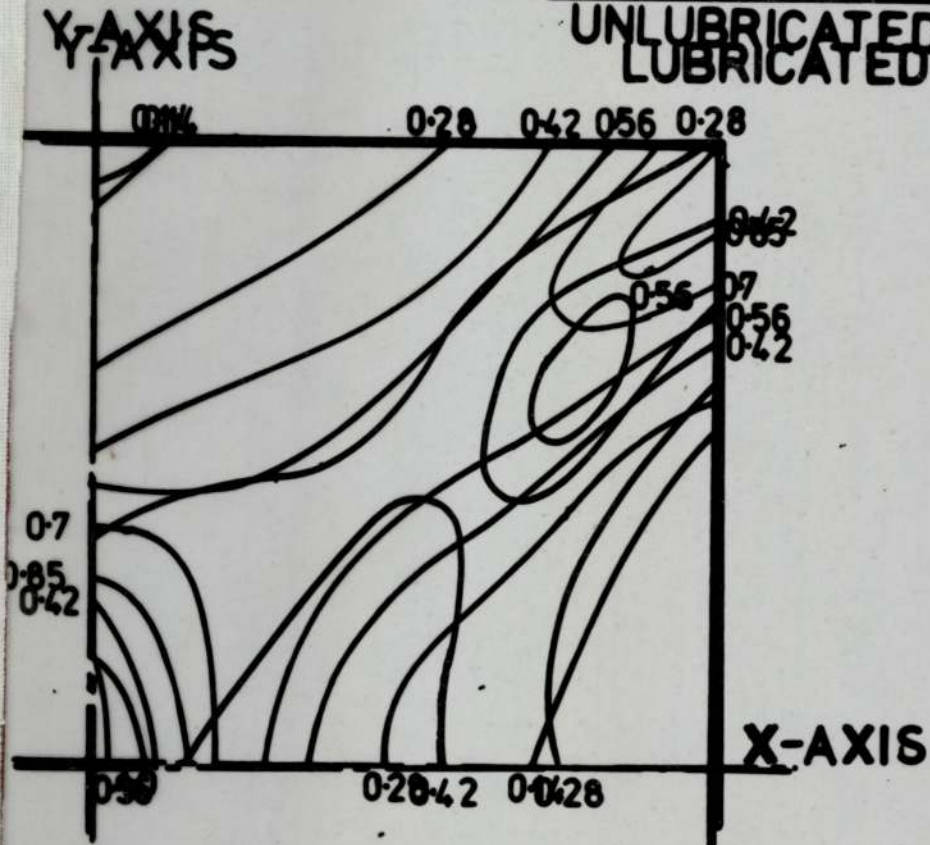


FIG. 9.46B

UNLUBRICATED
DIE

	γ % OF RED. IN HEIGHT
A	8.7
B	20.2
C	30.3
D	40.3

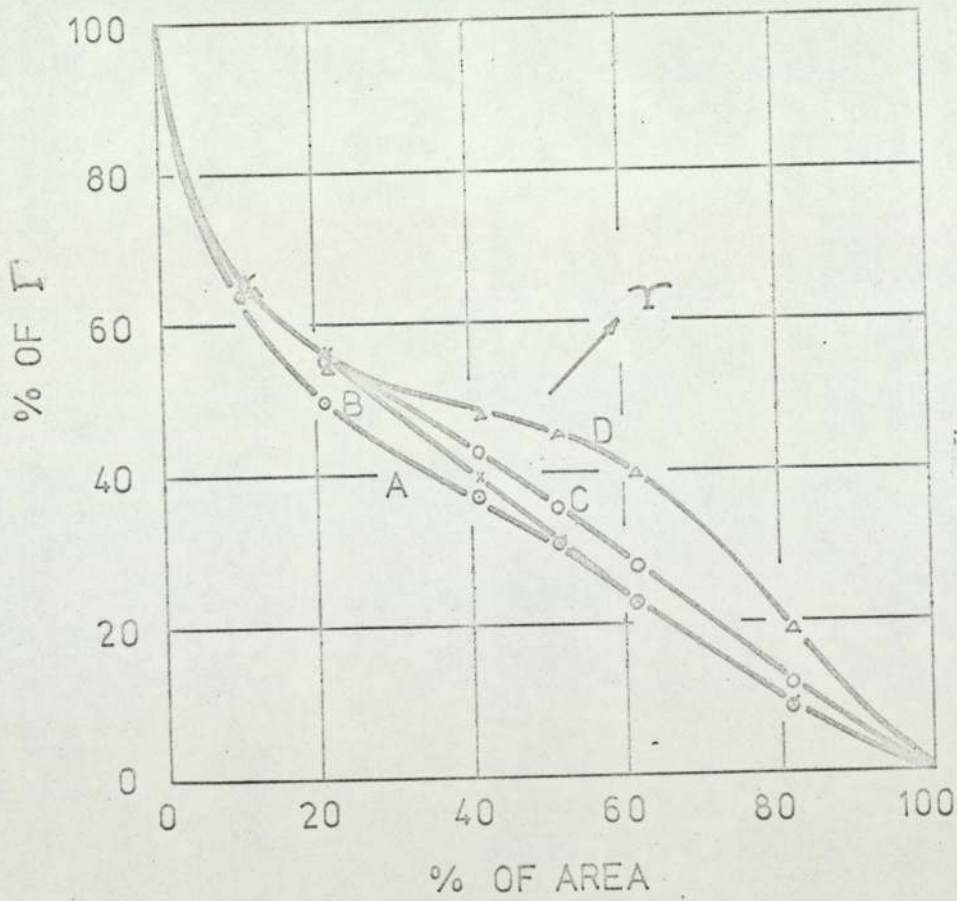
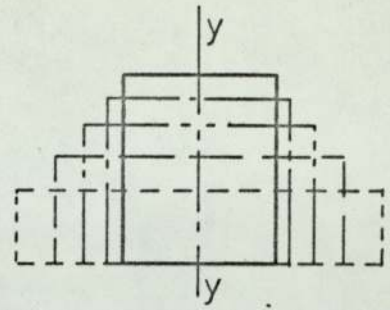


FIG. 10.1



	% of RED. in HEIGHT	MEAN STRAIN
E	11.4	0.12
F	20.1	0.25
G	30.0	0.40
H	40.0	0.58

LUBRICATED DIE

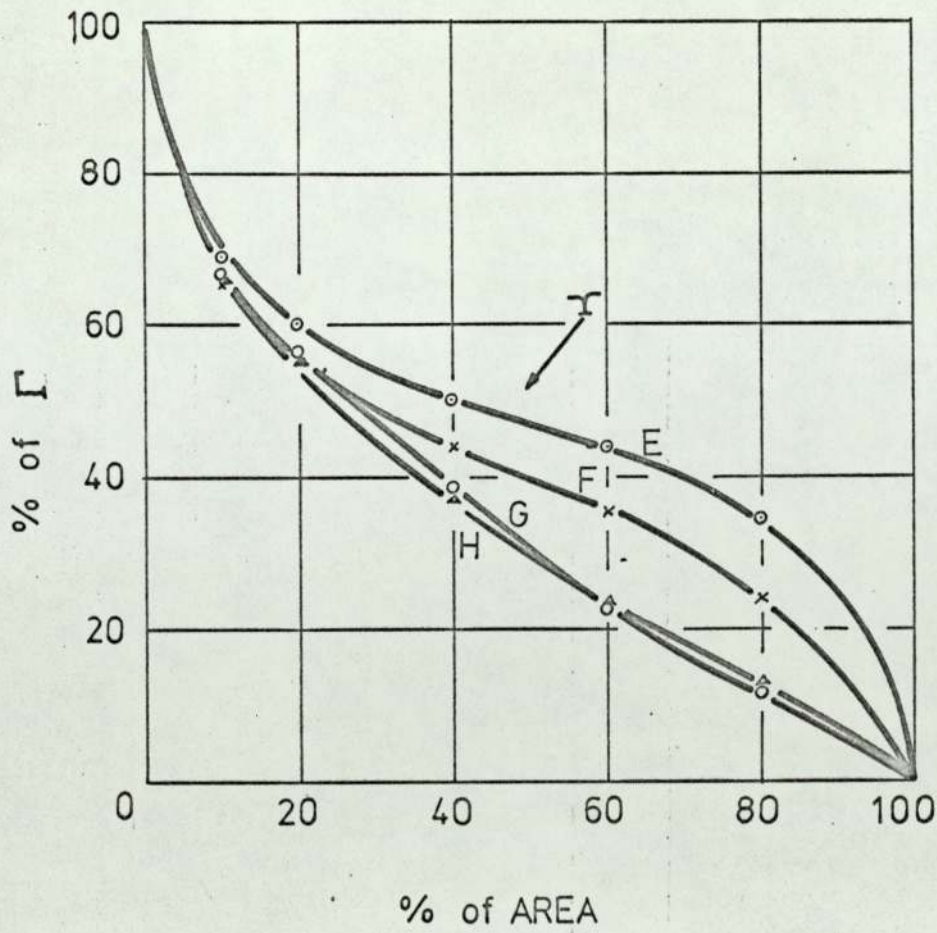


FIG. 10.2

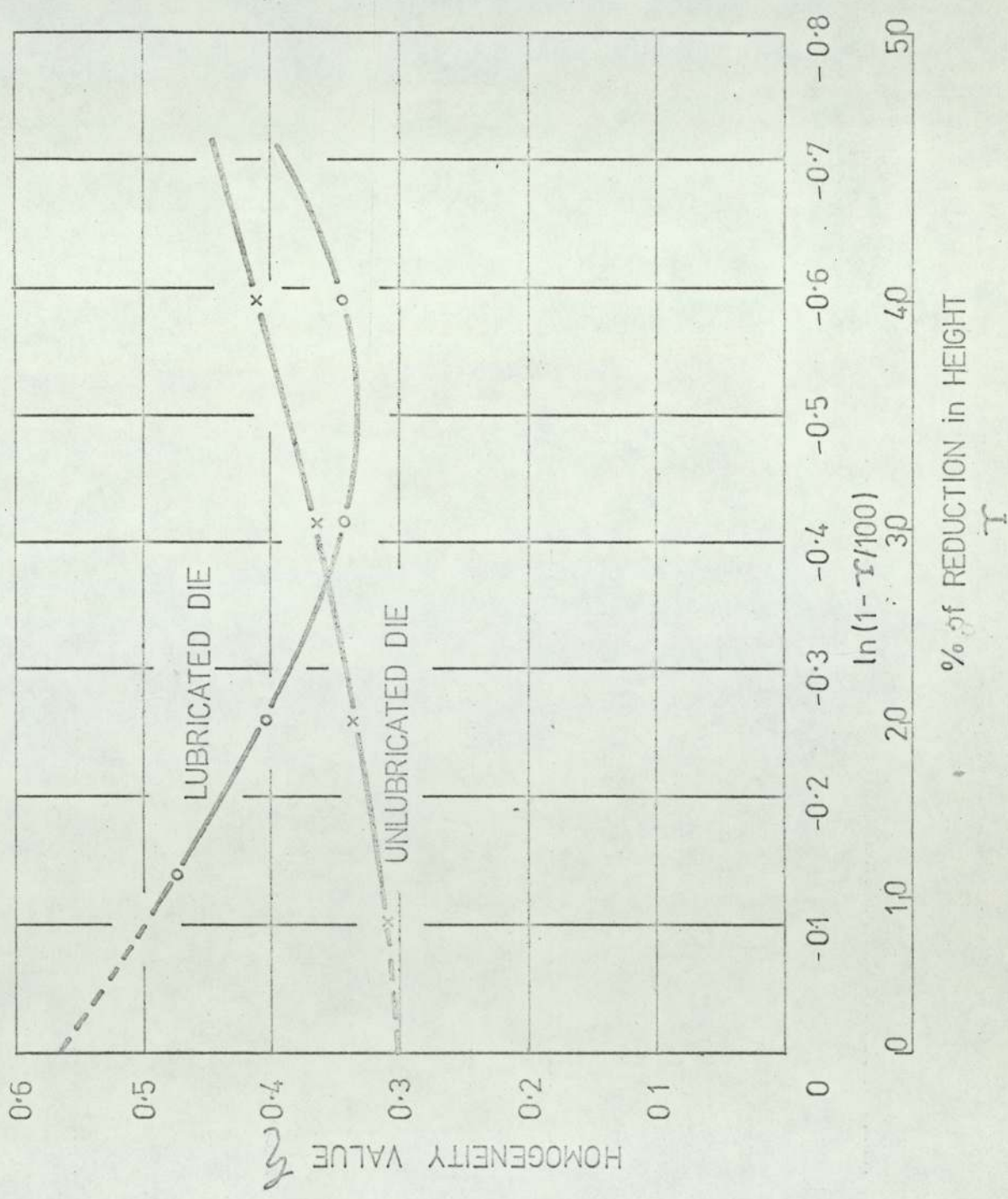
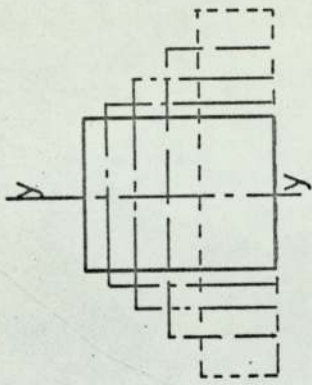


FIG.10.3



	% of RED. in HEIGHT	MEAN STRAIN
A	8.7	0.11
B	20.2	0.26
C	30.3	0.42
D	40.3	0.60

UNLUBRICATED DIE

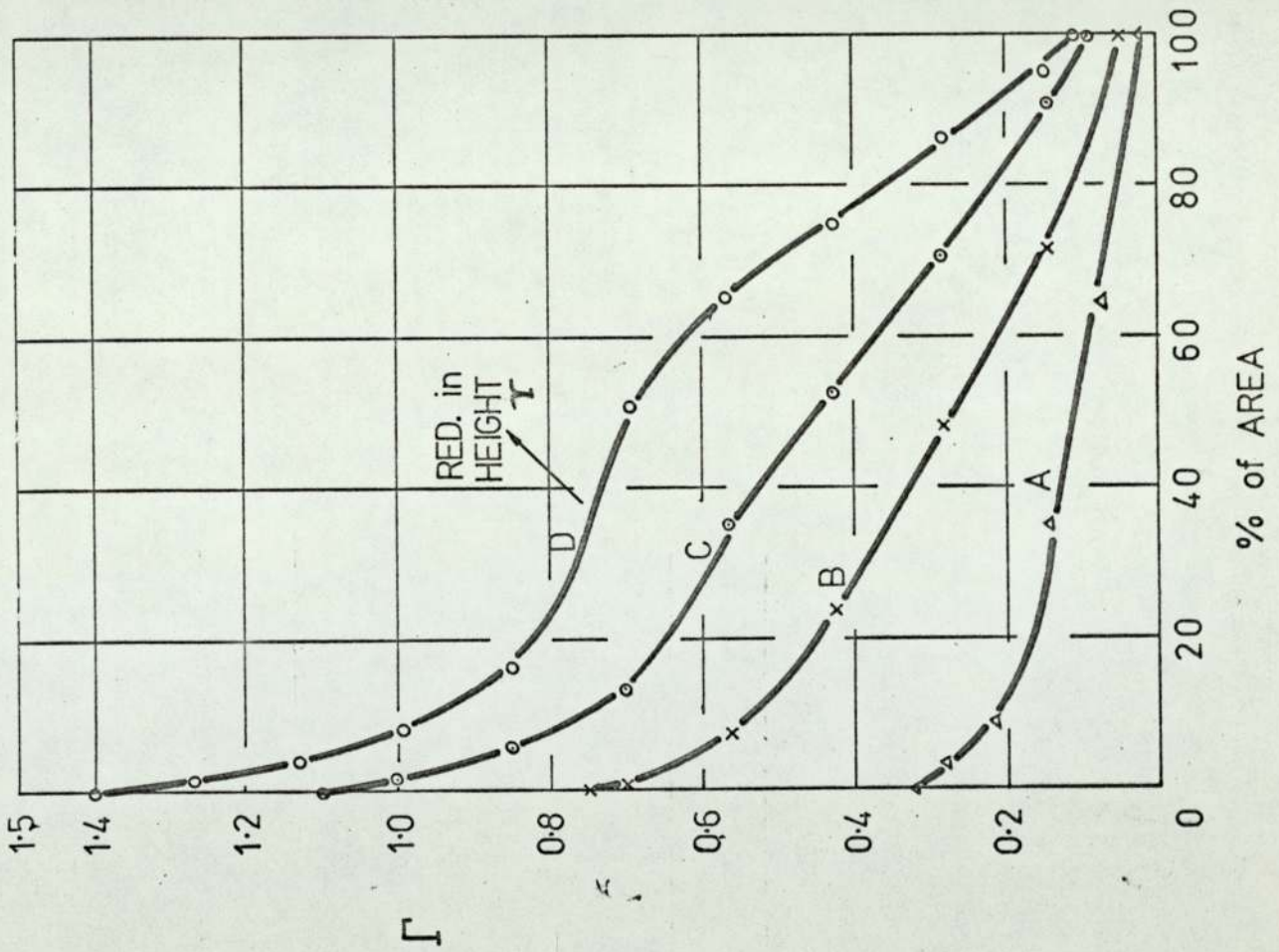
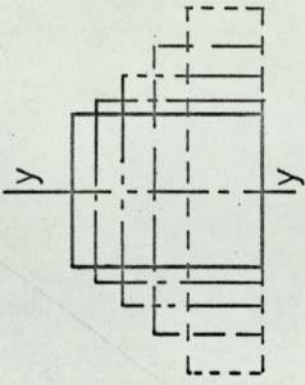


FIG.11.1



	% of RED. in HEIGHT	MEAN STRAIN
E	11.4	0.12
F	20.1	0.25
G	30.0	0.40
H	40.0	0.58

LUBRICATED DIE

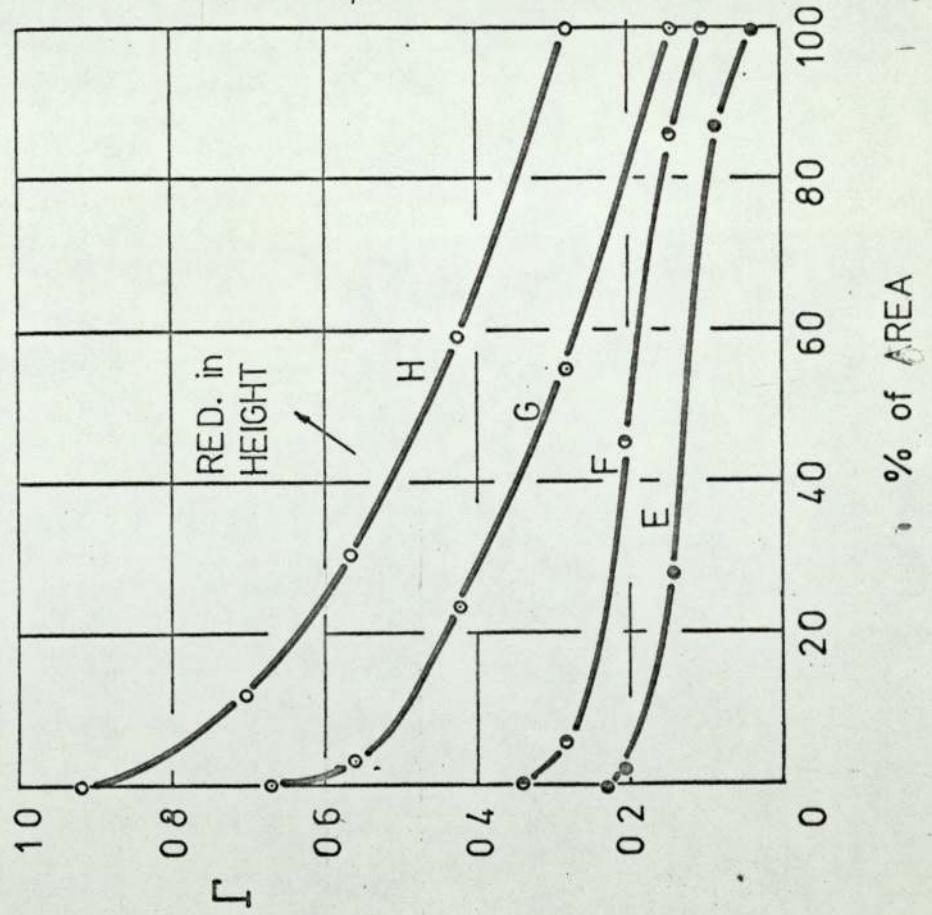


FIG. 11.2

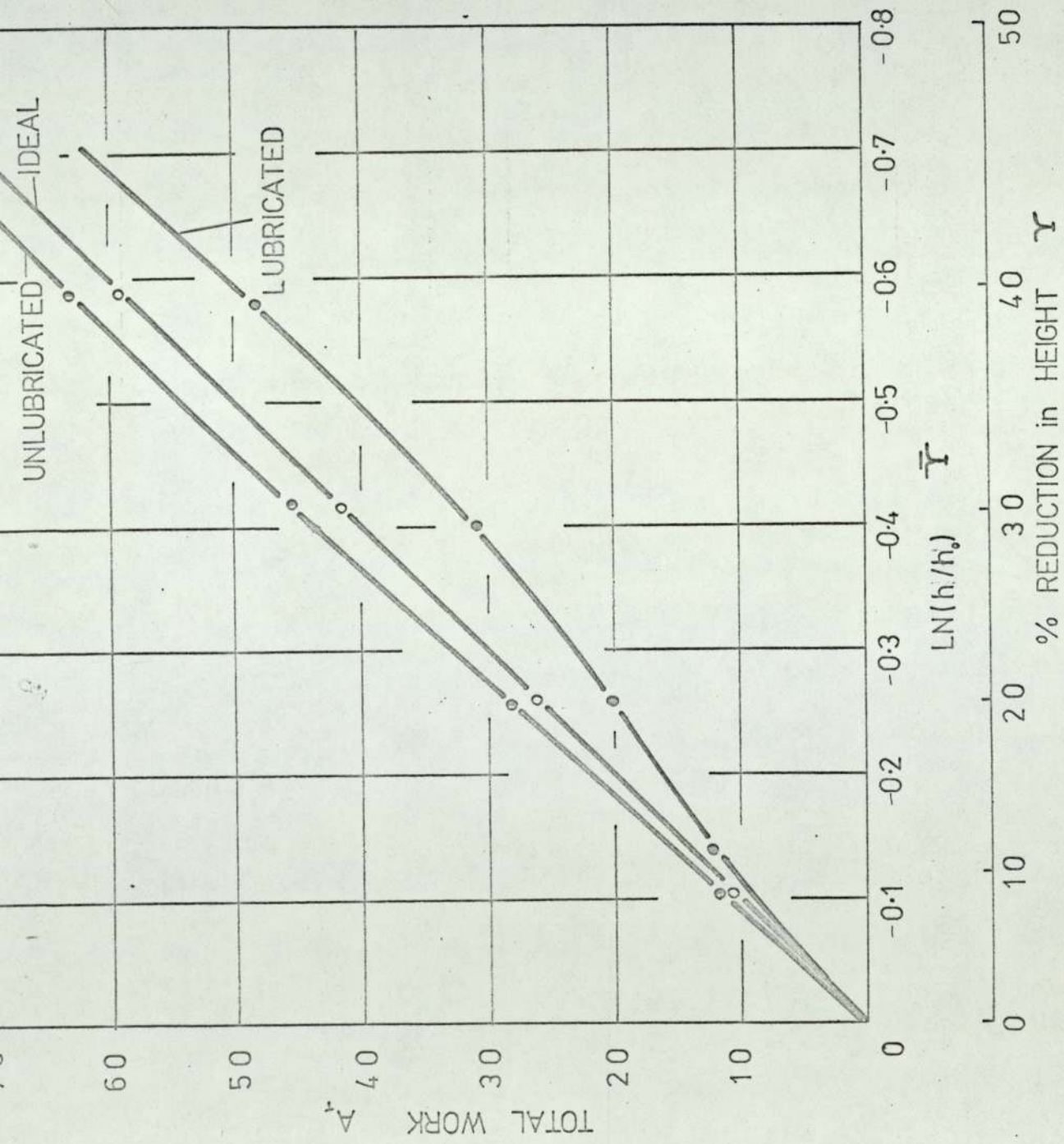


FIG. 11.3

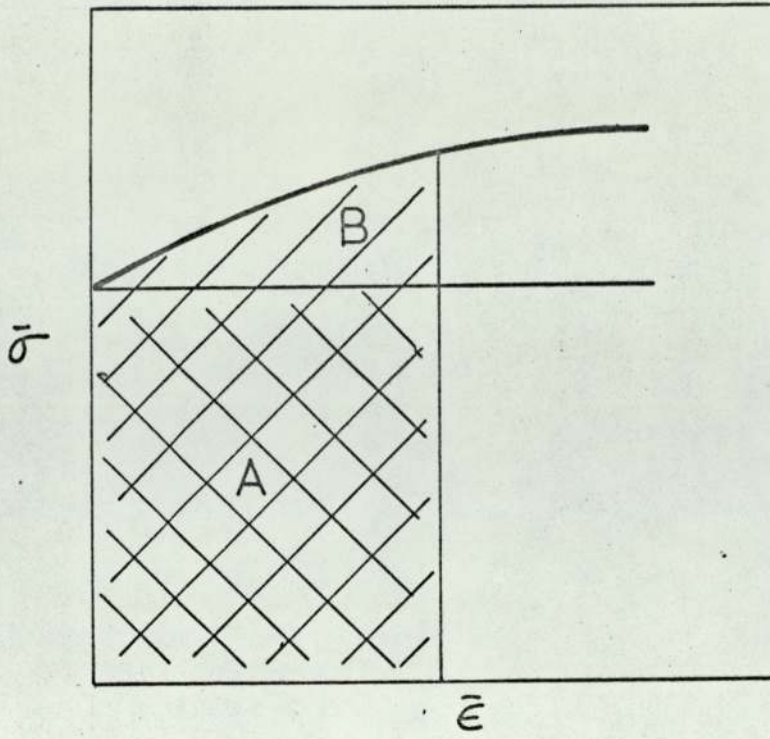


FIG. 11.4

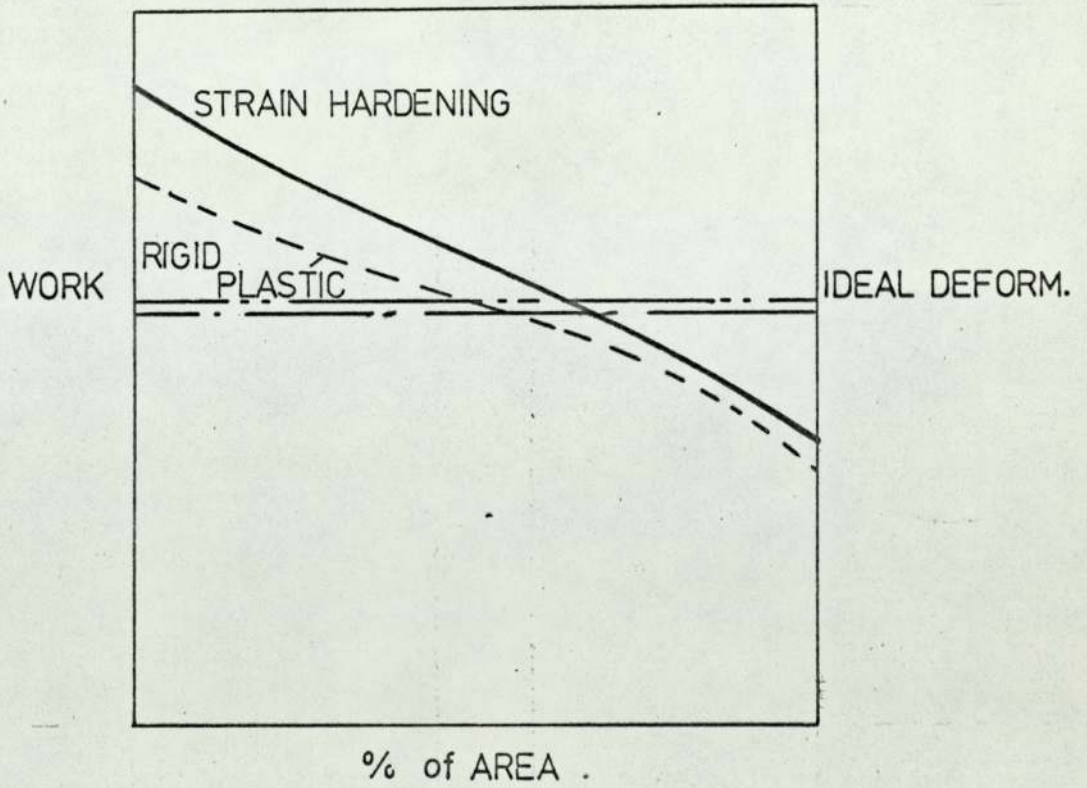


FIG. 11.5

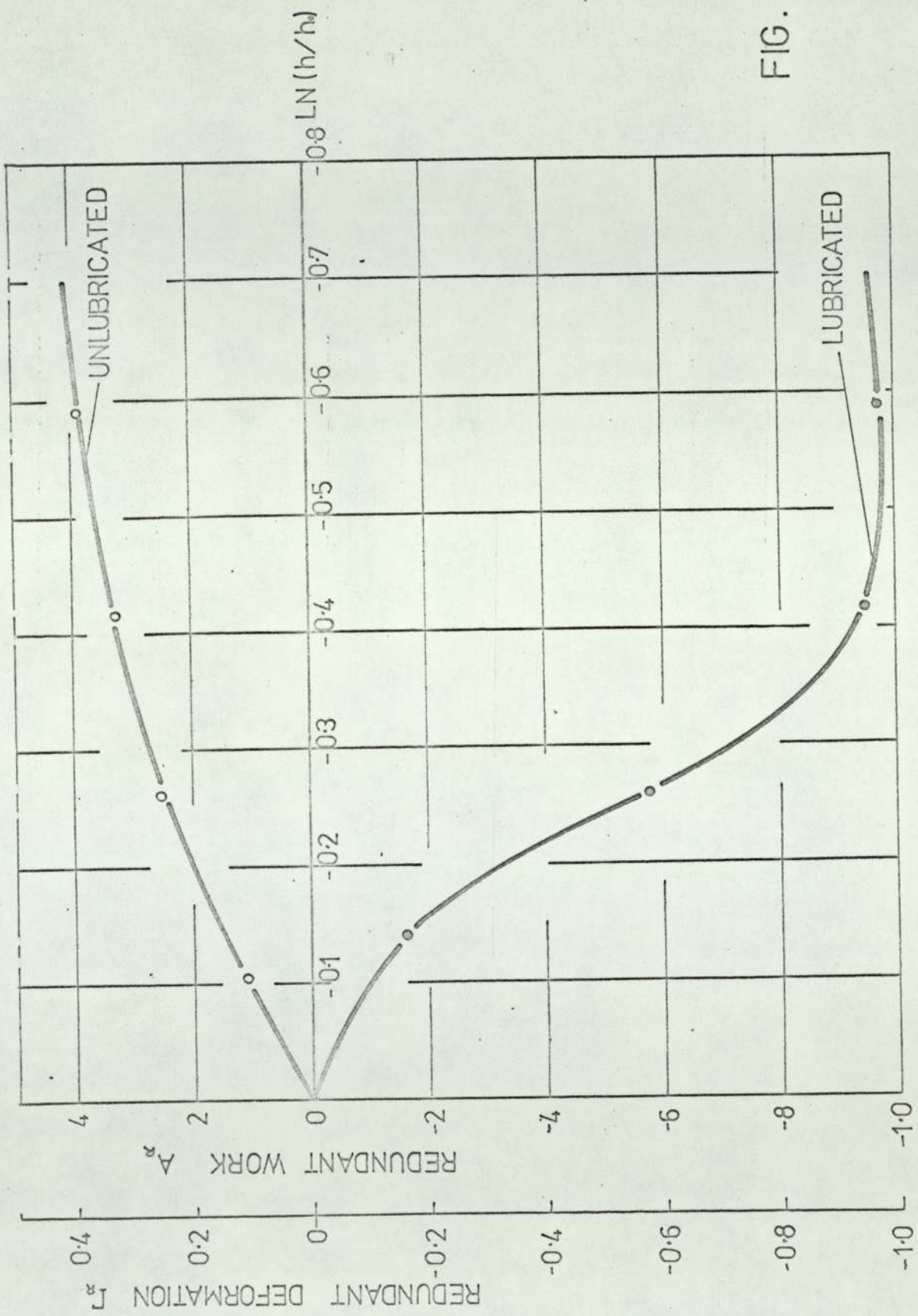


FIG. 11.6

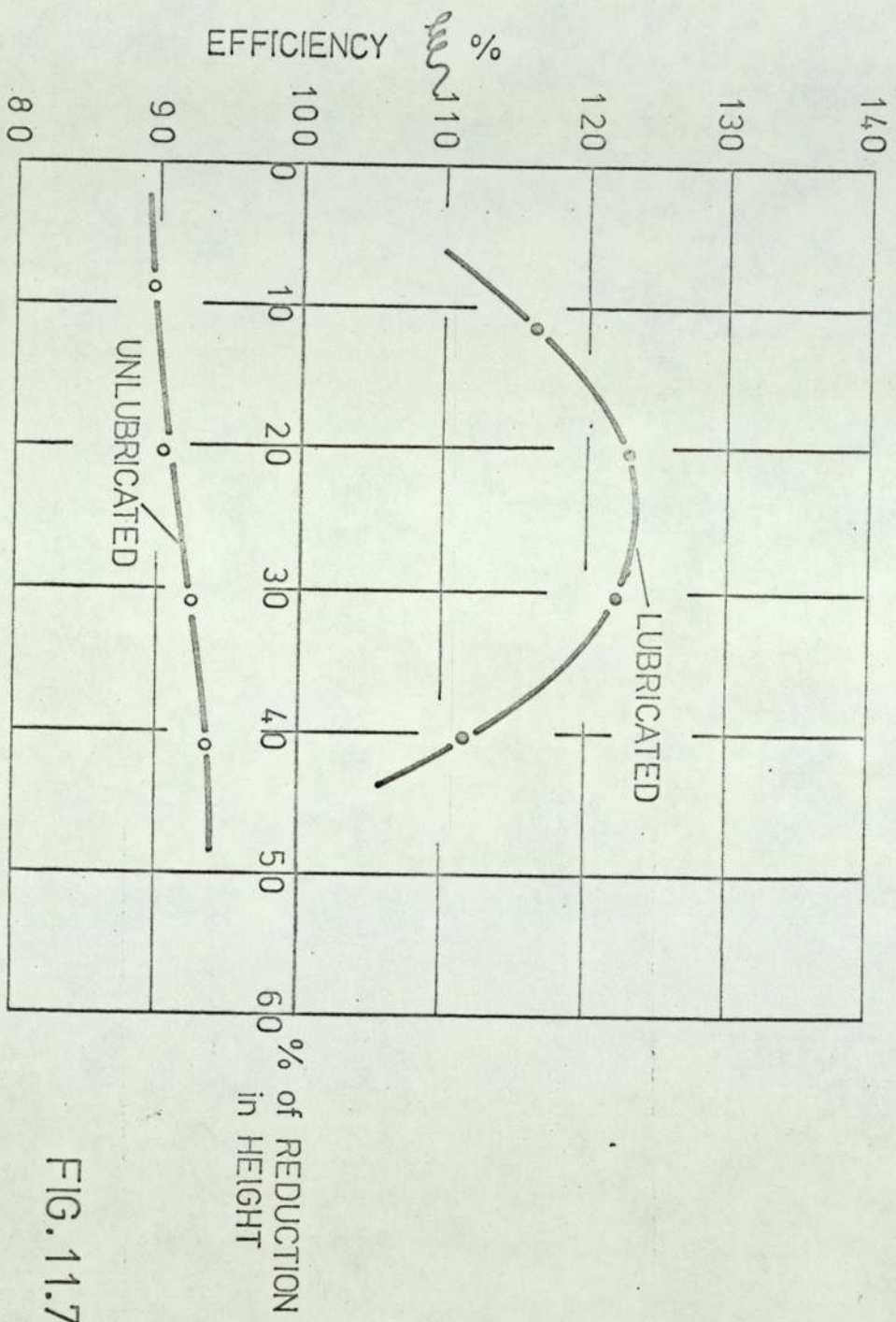


FIG. 11.7

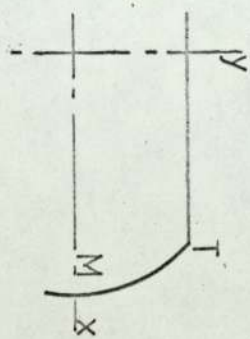
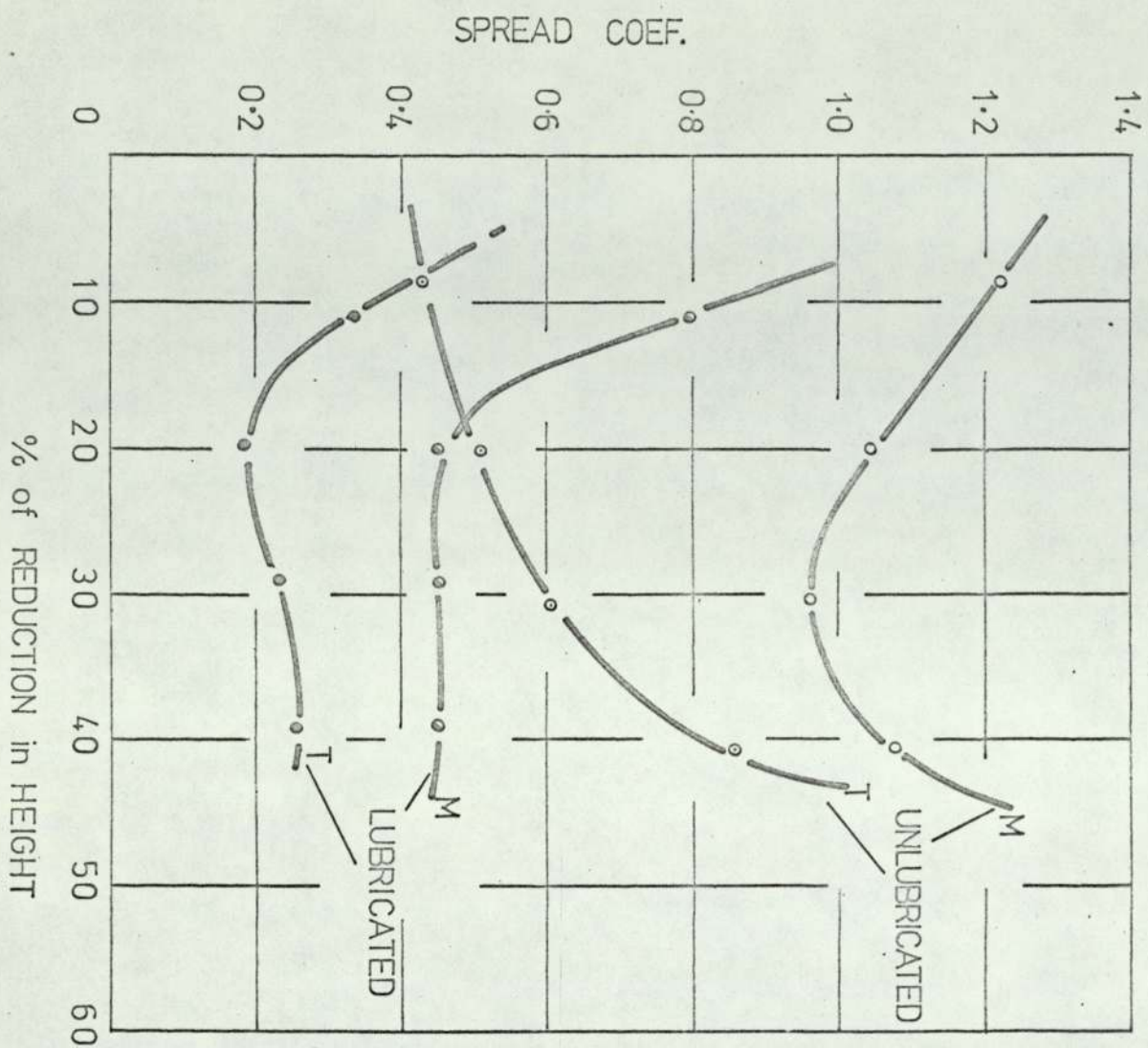


FIG. 12.1

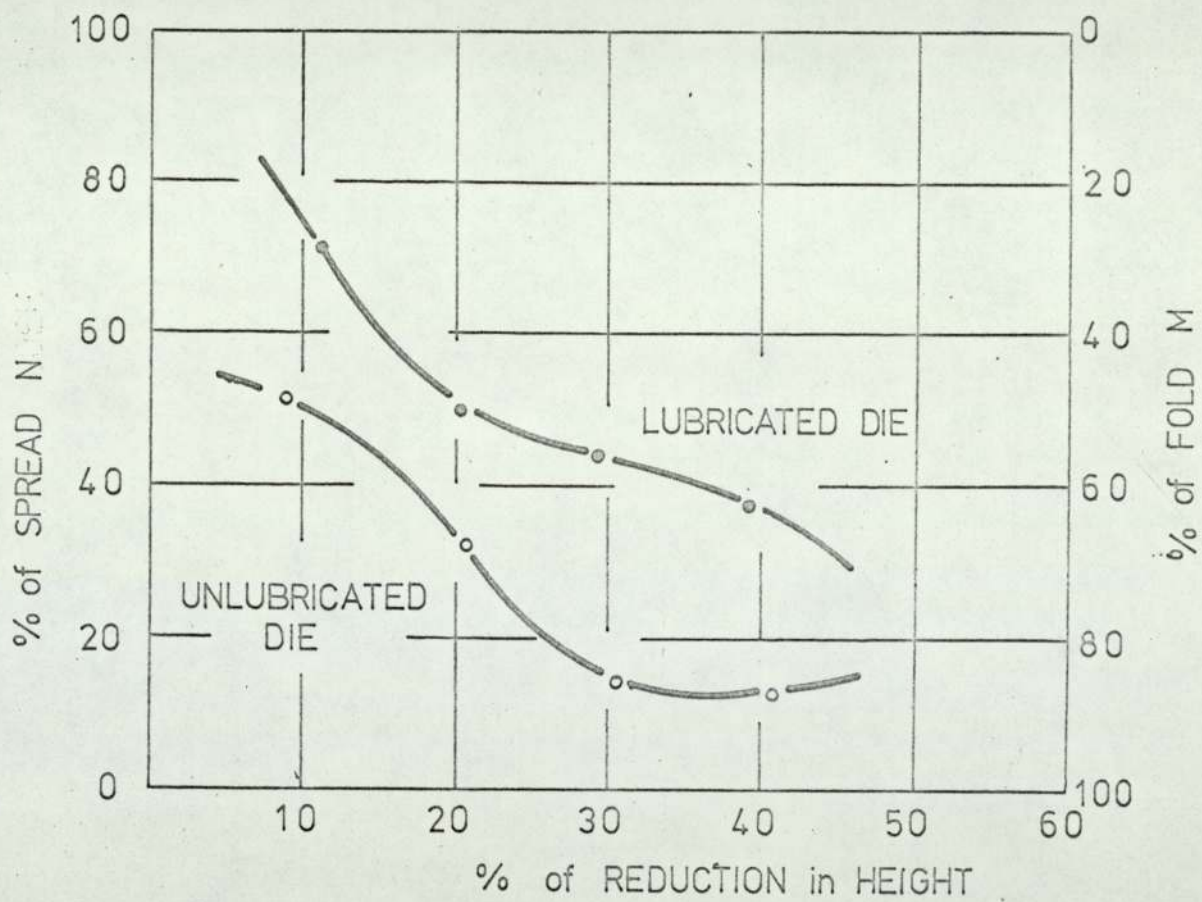


FIG.12.2

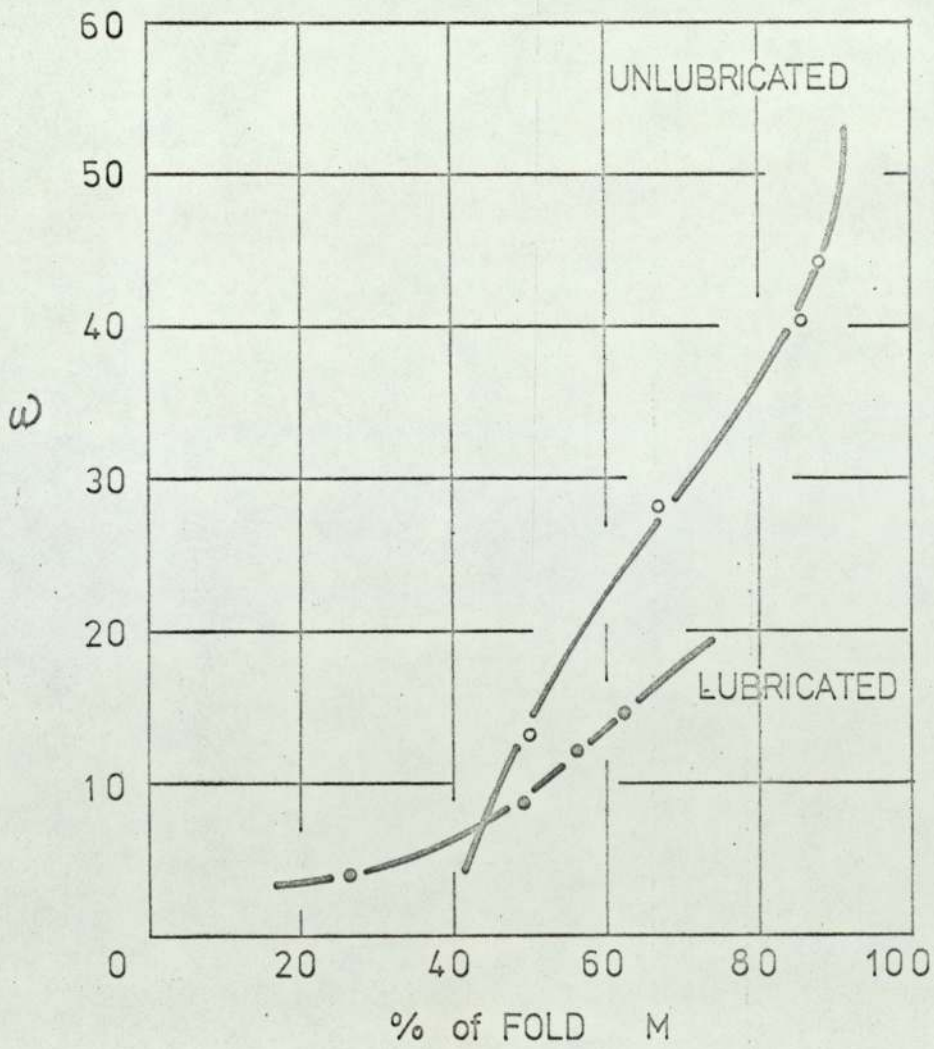
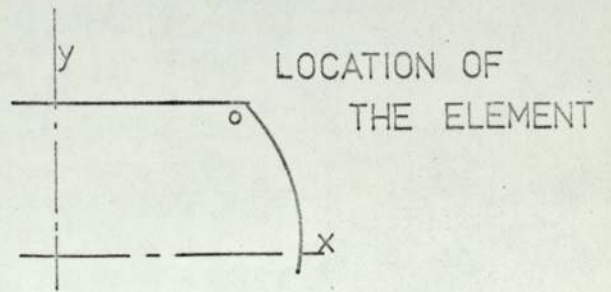


FIG.12.3

H/D
 A 1.5
 B 1.8
 C 2.0

DIE DIA. 1 INCH

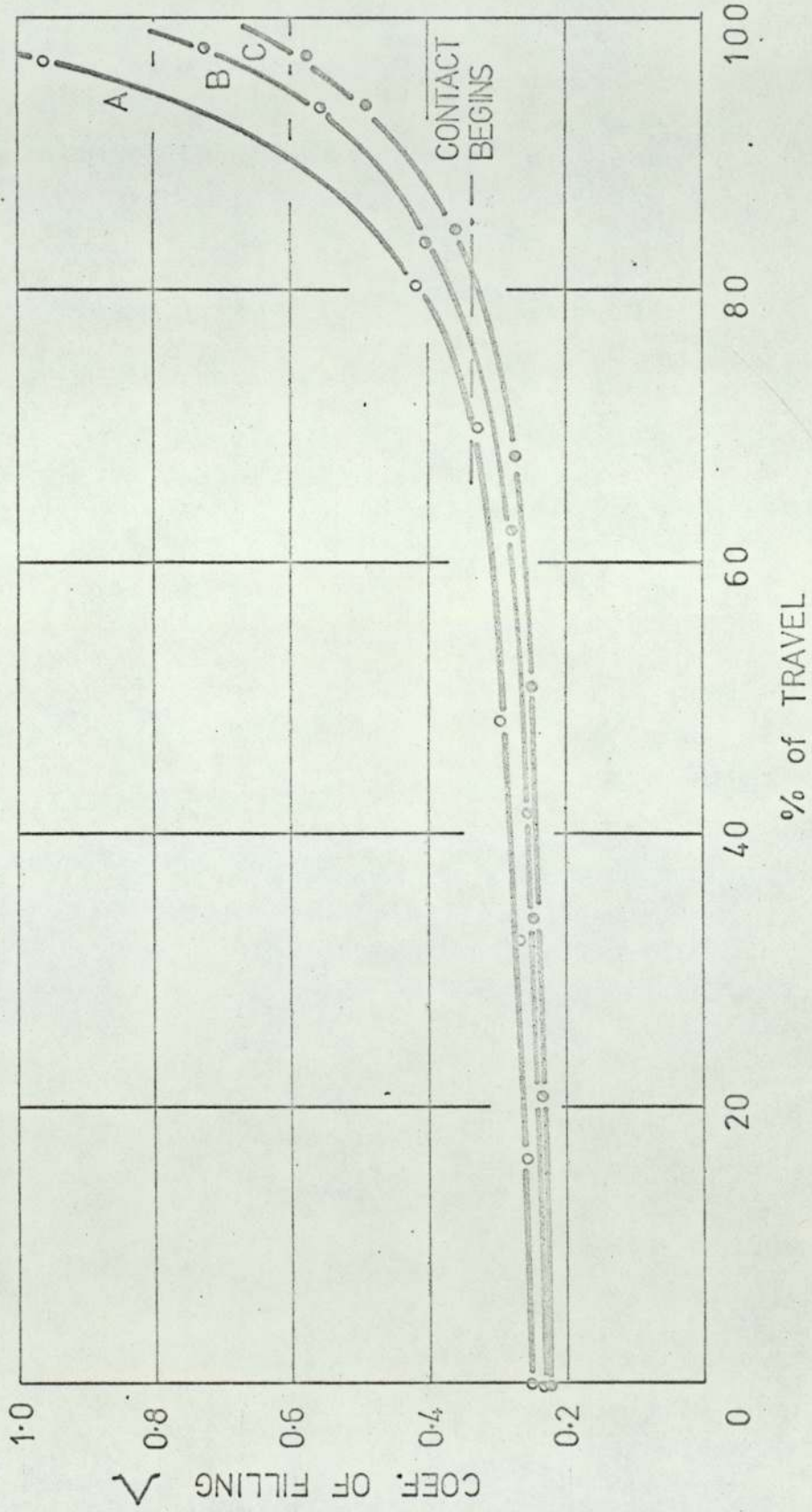


FIG. 12.4

H/D
 A 1.5
 B 1.8
 C 2.0

DIE DIA. 1 1/2 INCH

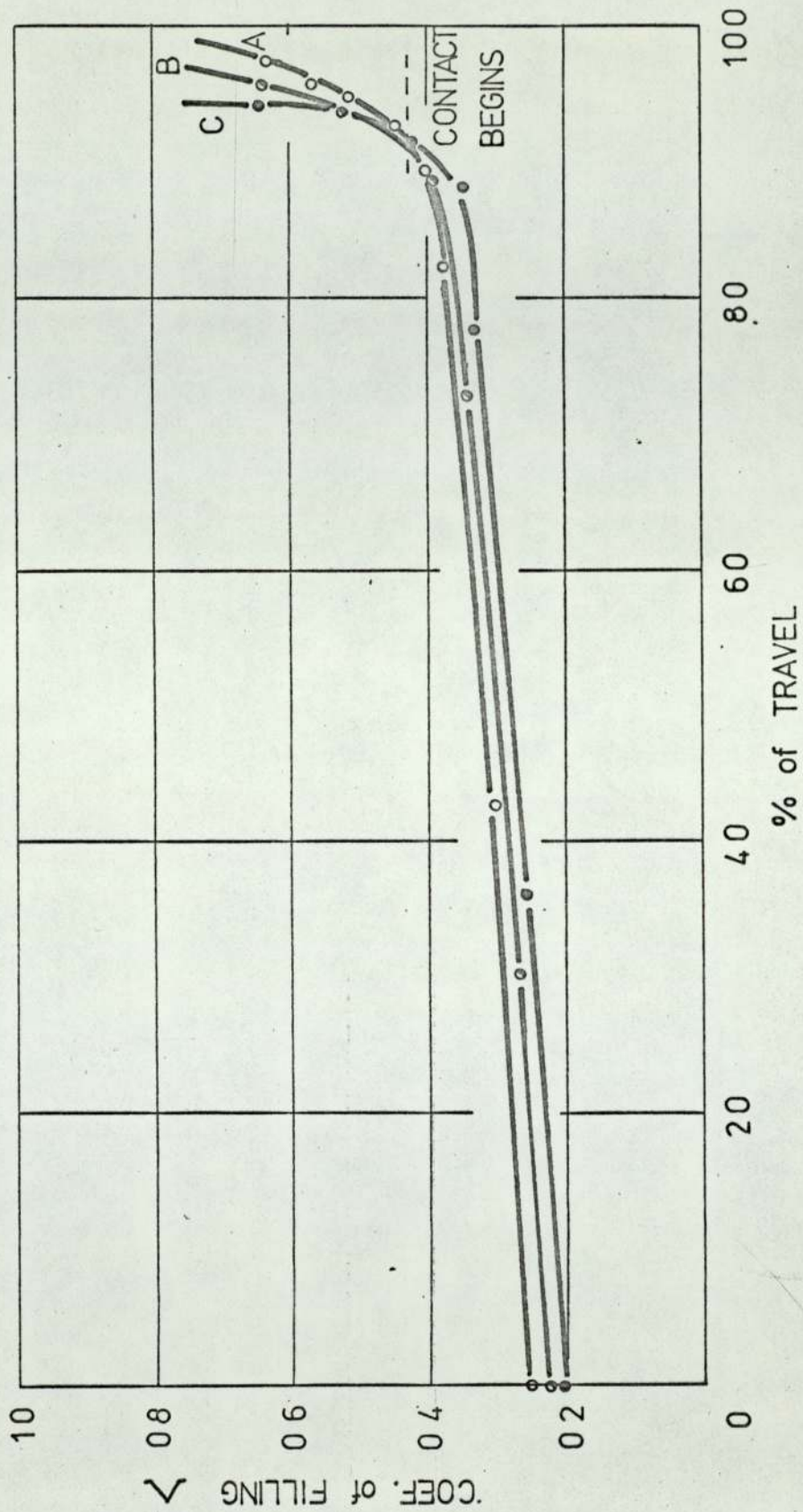


FIG. 12.5

A 1.5
B 1.8
C 2.0

DIE DIA. 1 3/4 INCH

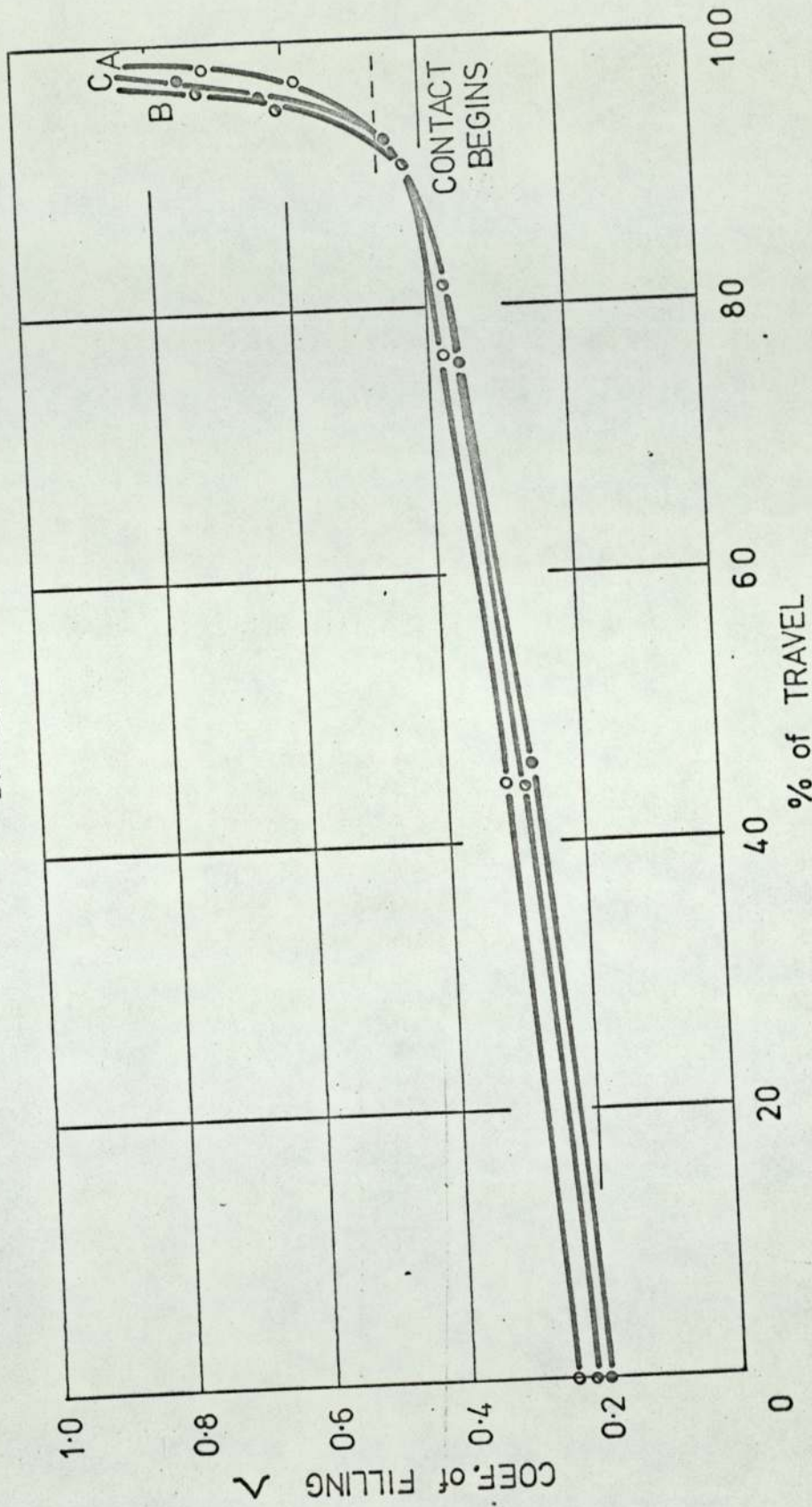


FIG. 12.6

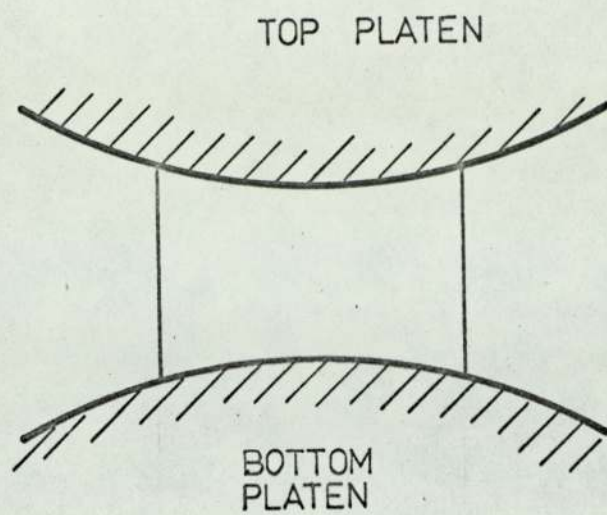


FIG. 12.7a

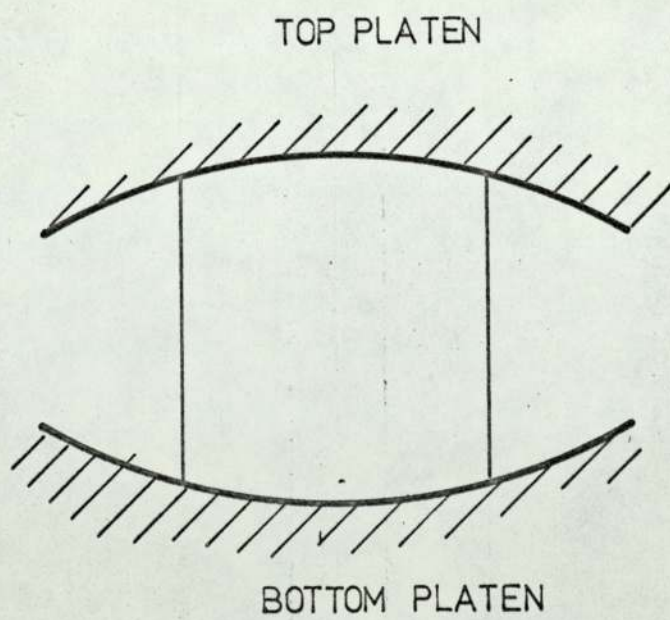


FIG. 12.7b

% of EXTRA
 VOL.
 A 10
 B 15
 C 20

DIE DIA. 1 1/2 INCH

SPECIMEN H/D 1.5

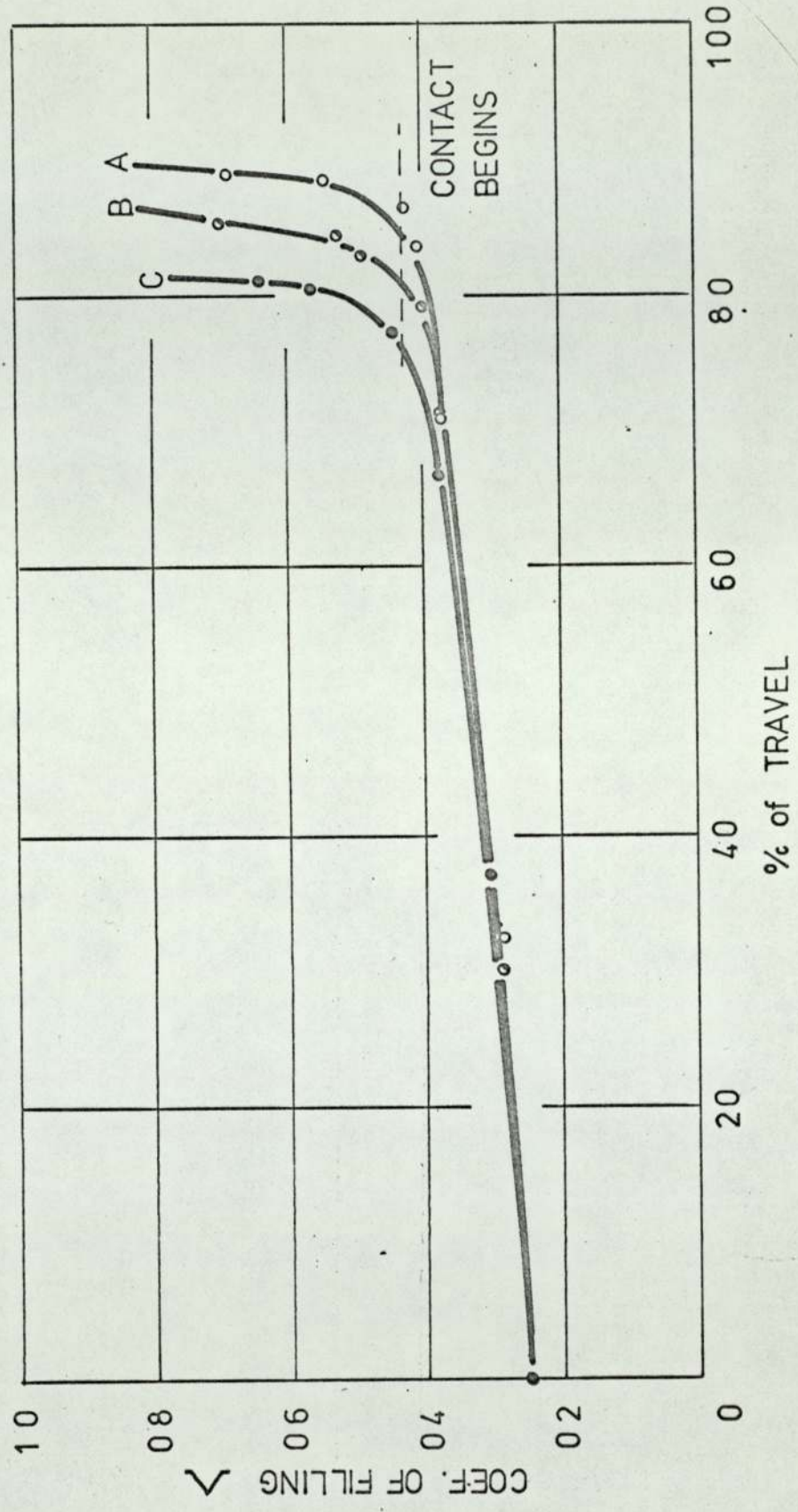


FIG. 12.8

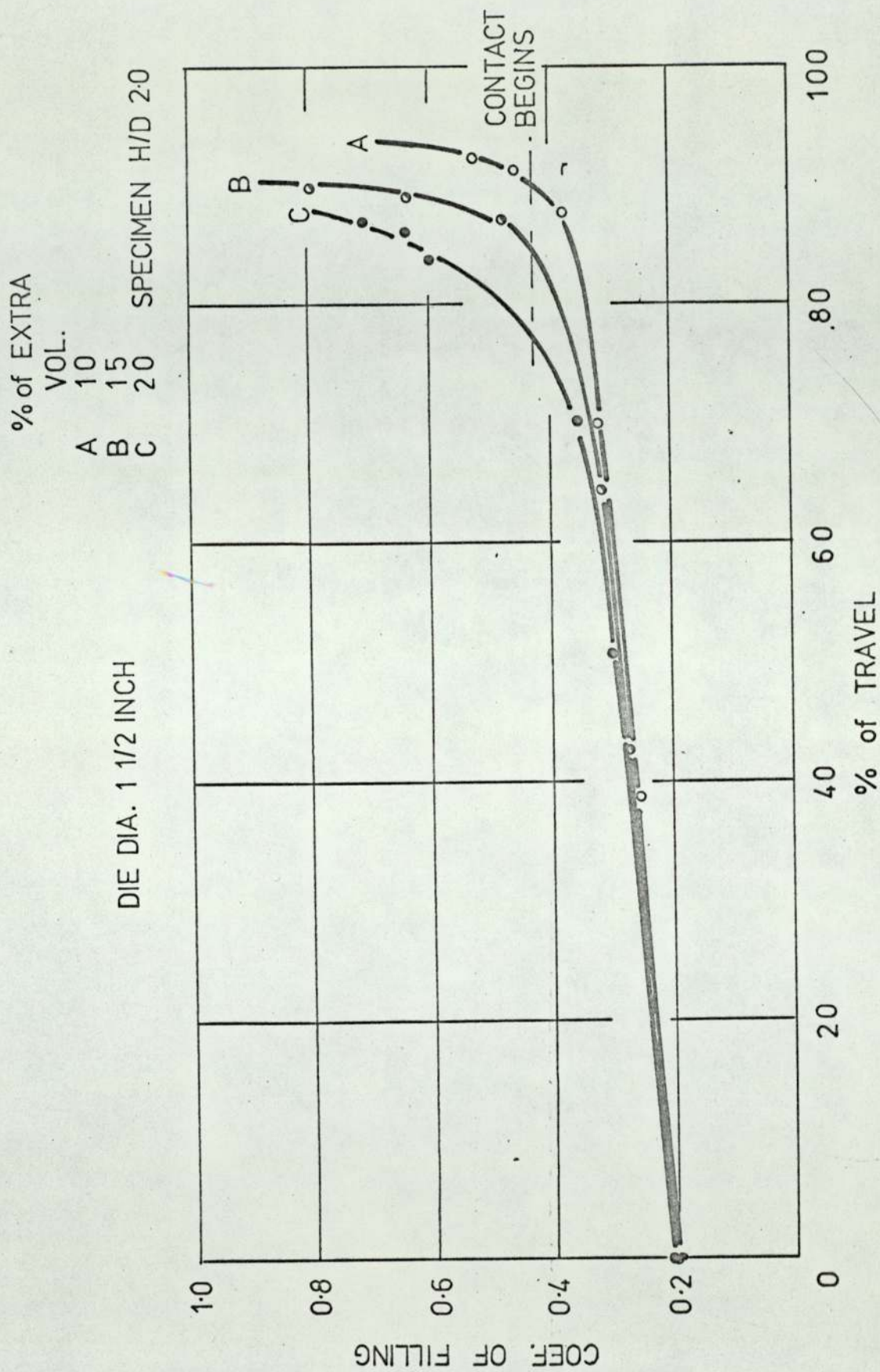


FIG. 12.9

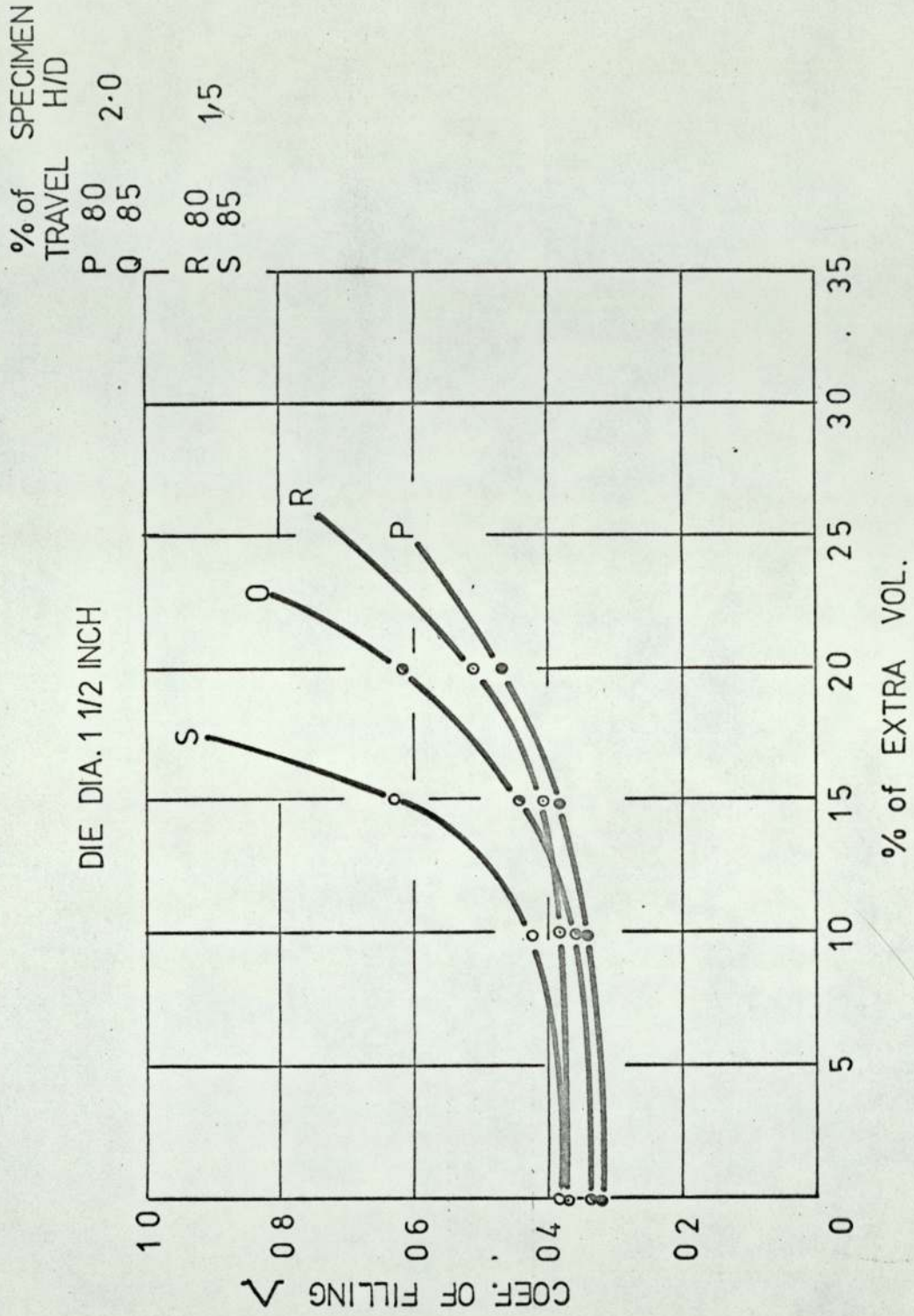


FIG.12.10

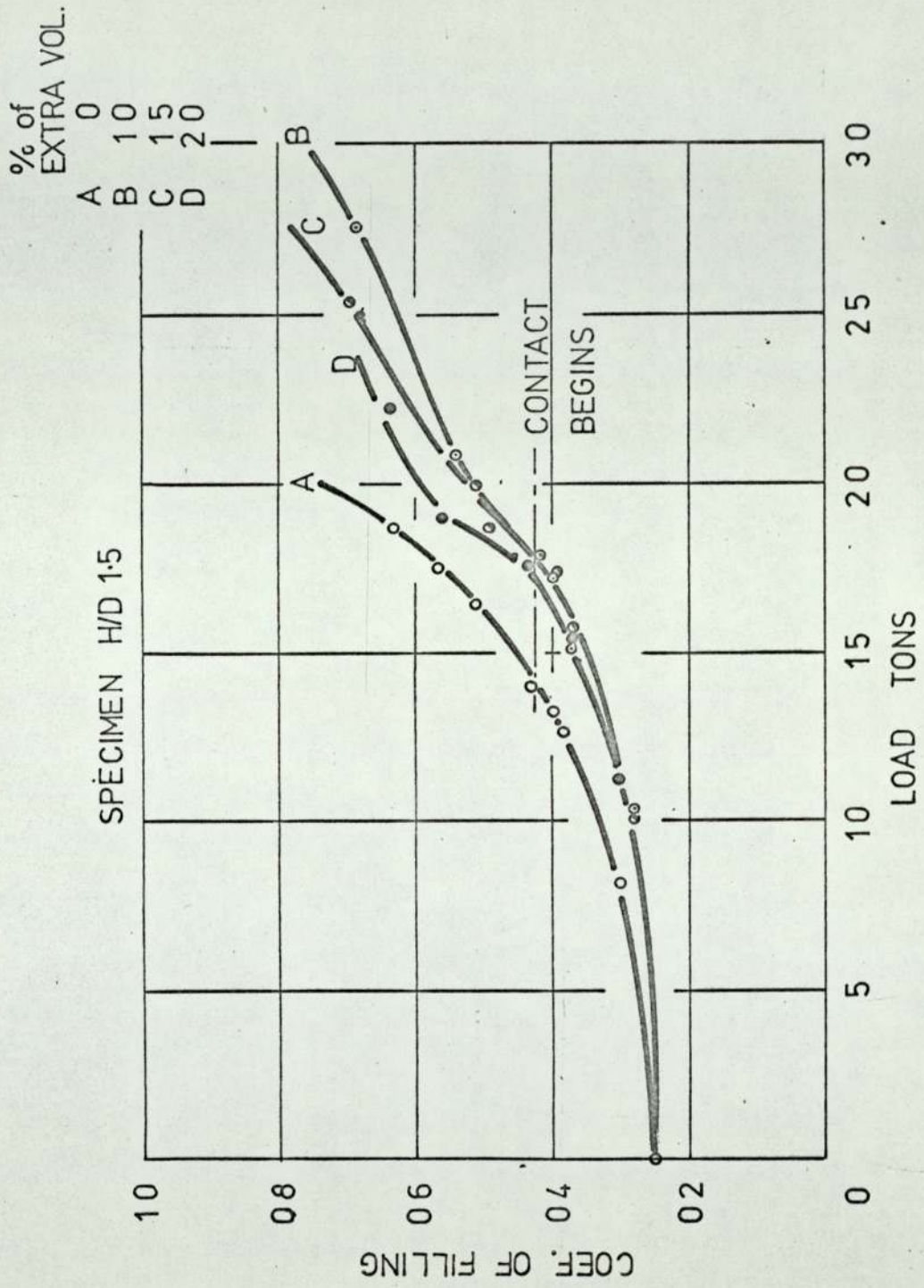


FIG.12.11

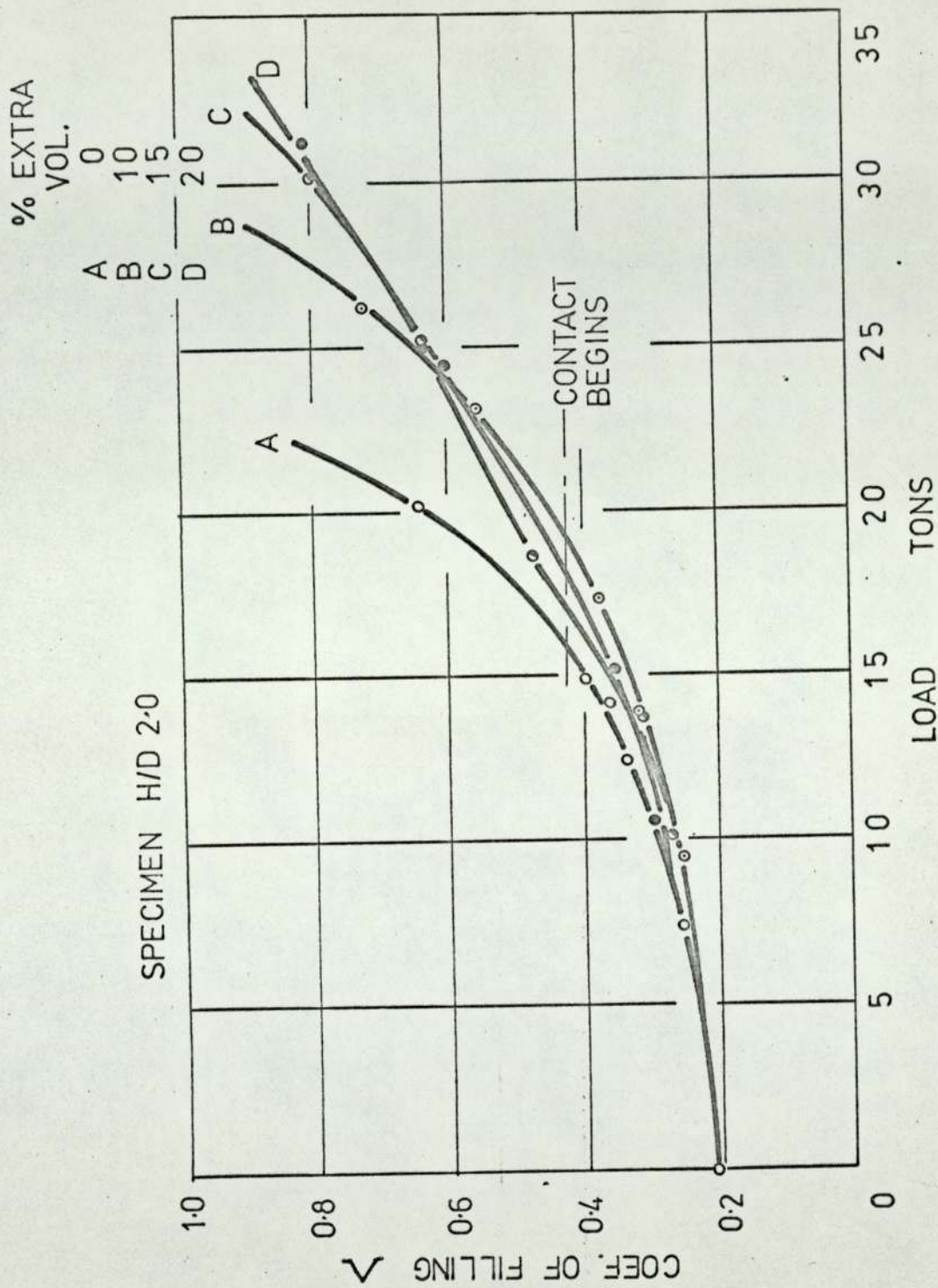


FIG. 12.12

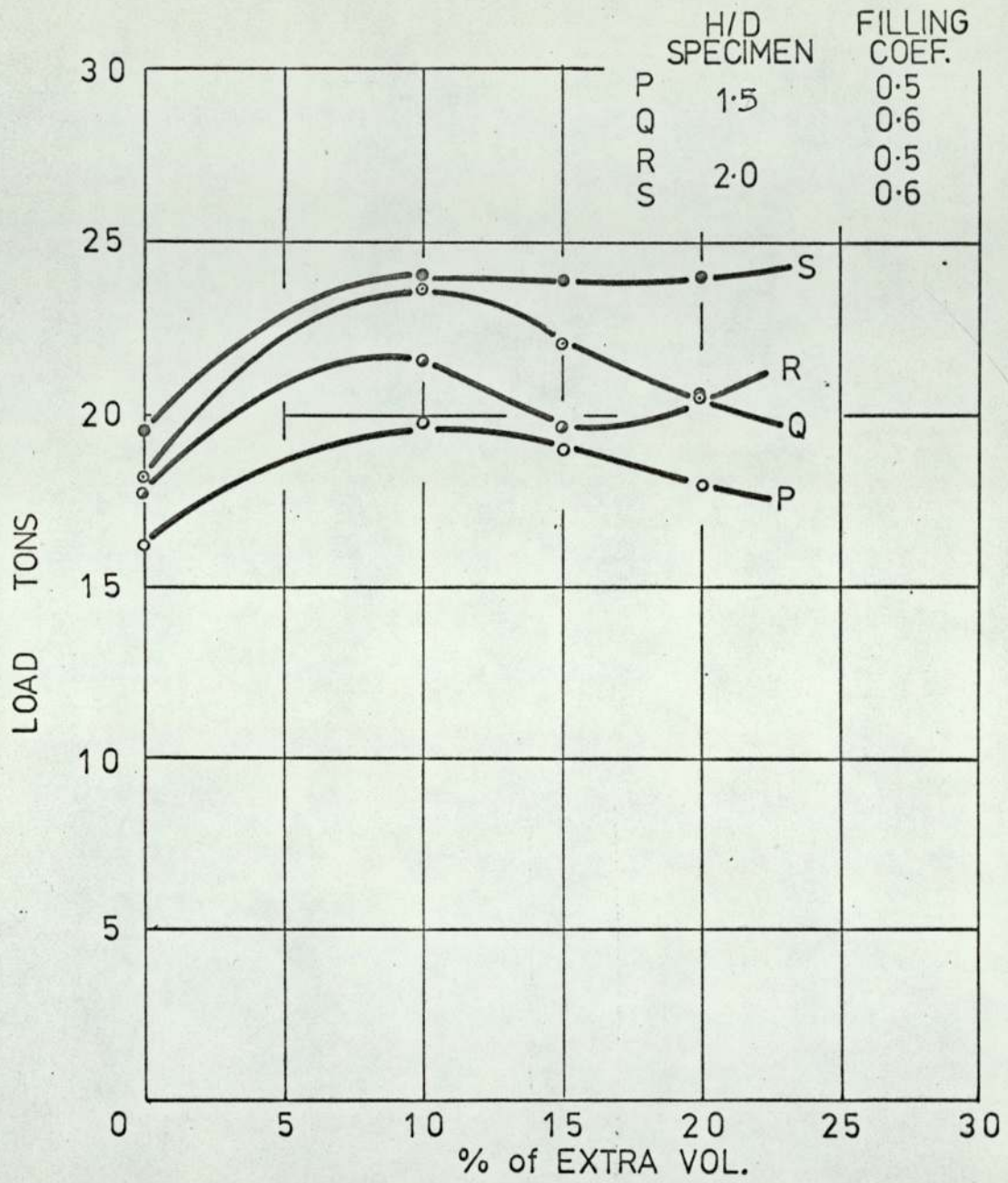


FIG. 12.13

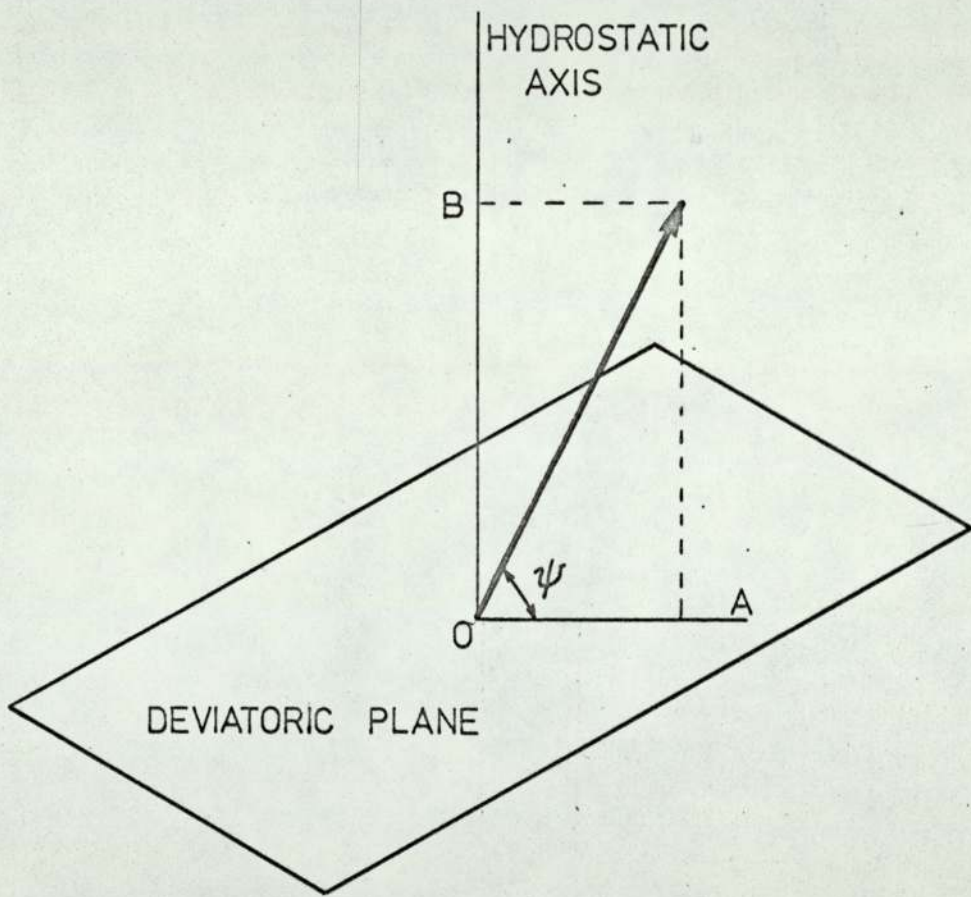


FIG. 13.1

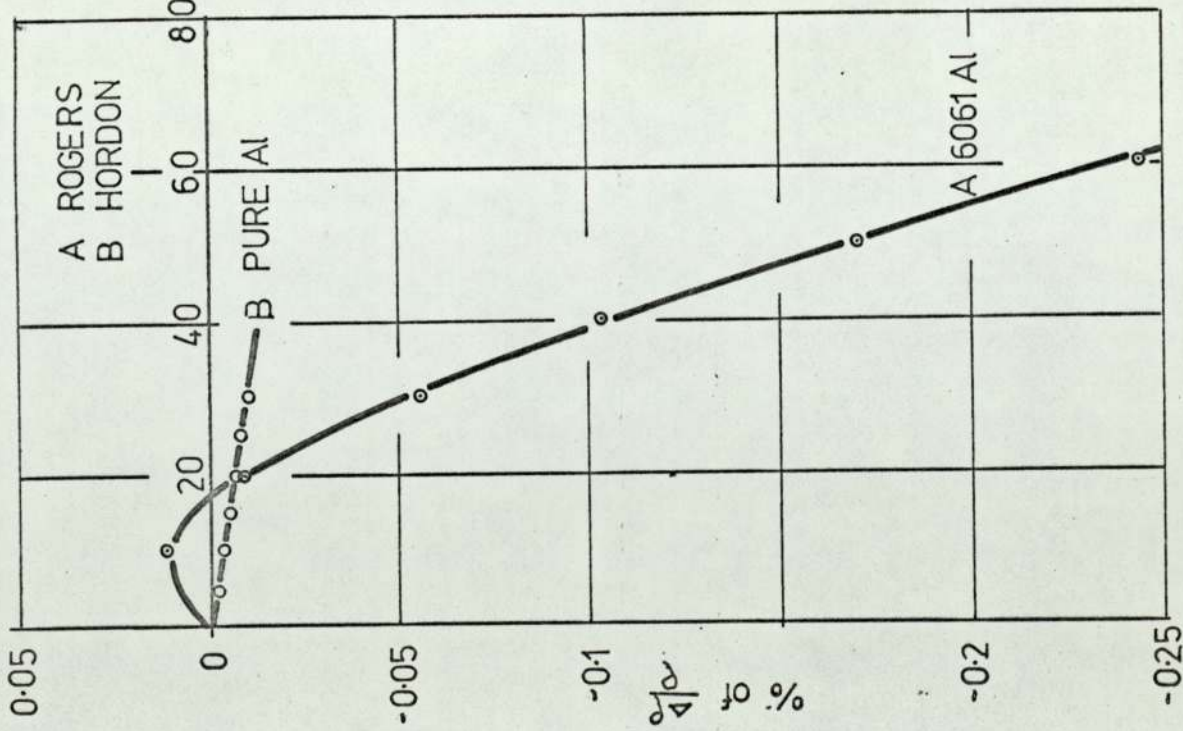
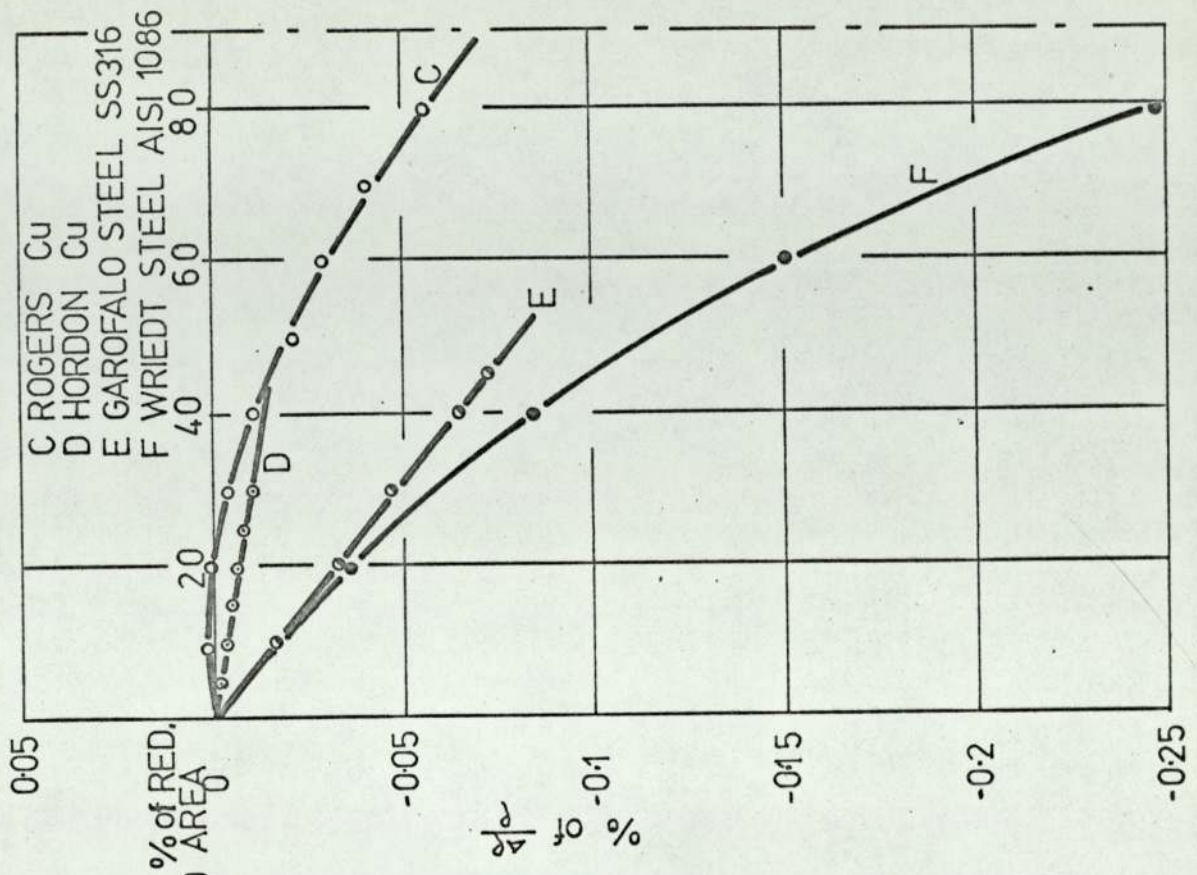


FIG.14.1

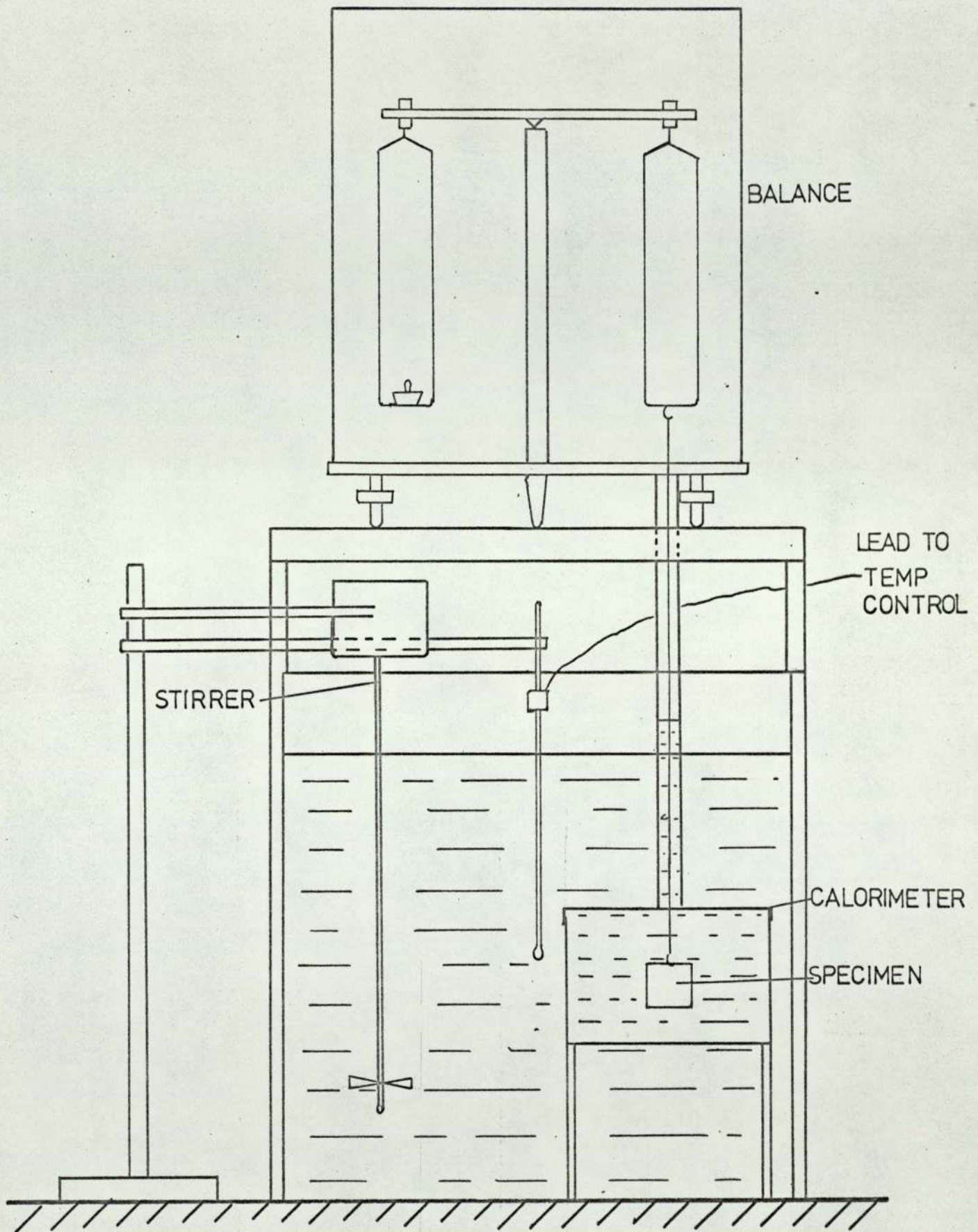


FIG. 14.2

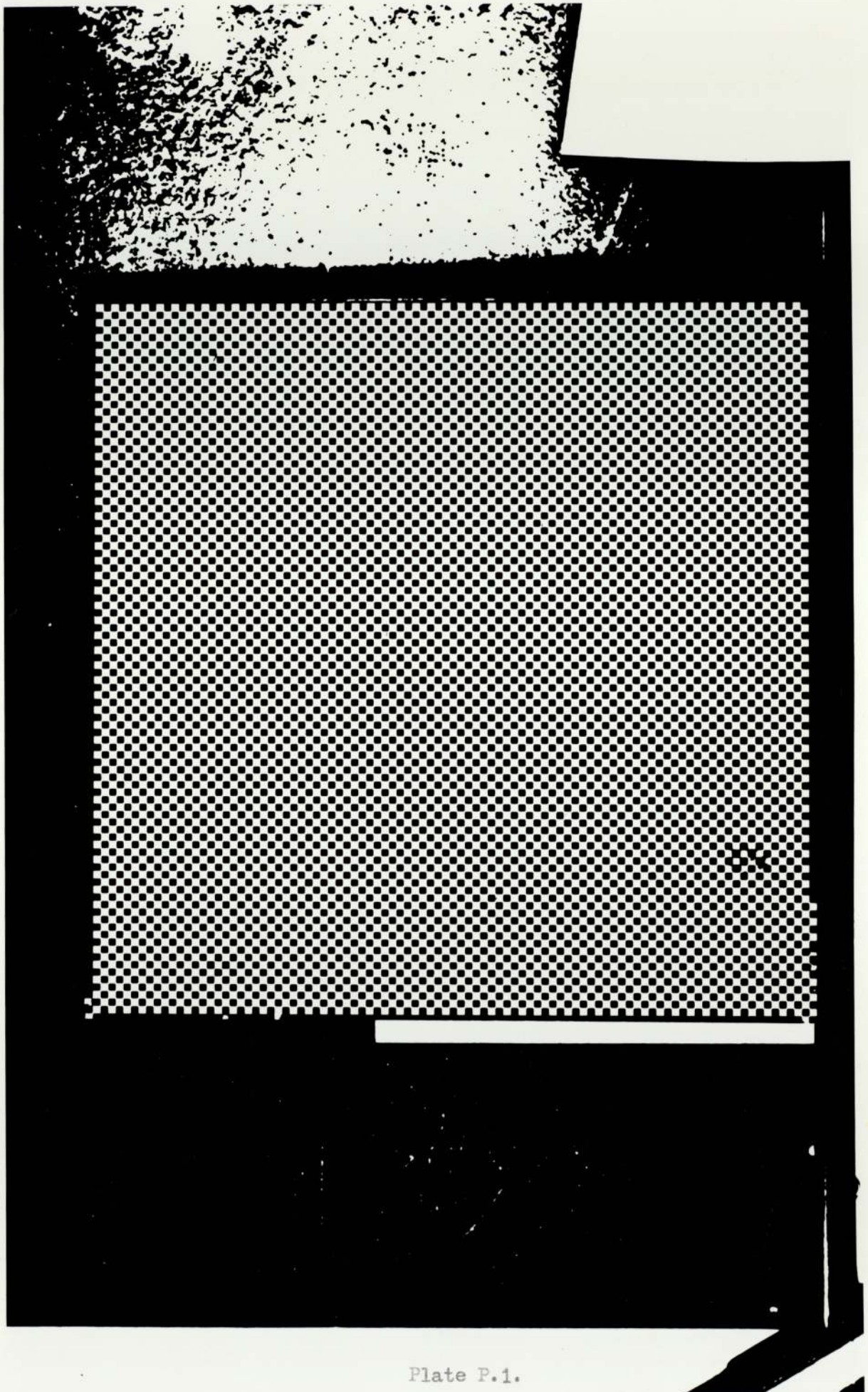


Plate P.1.

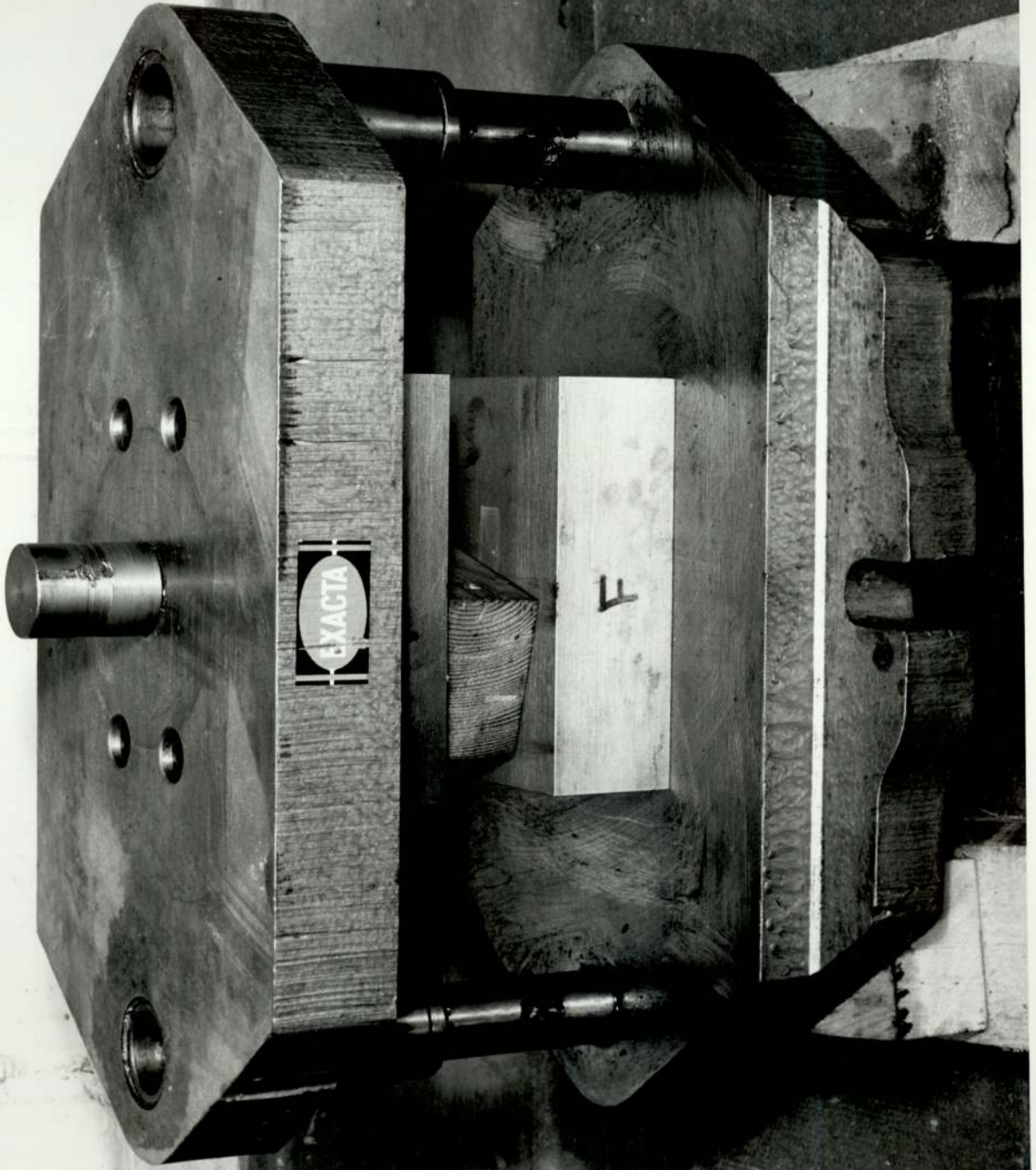


Plate P.2.

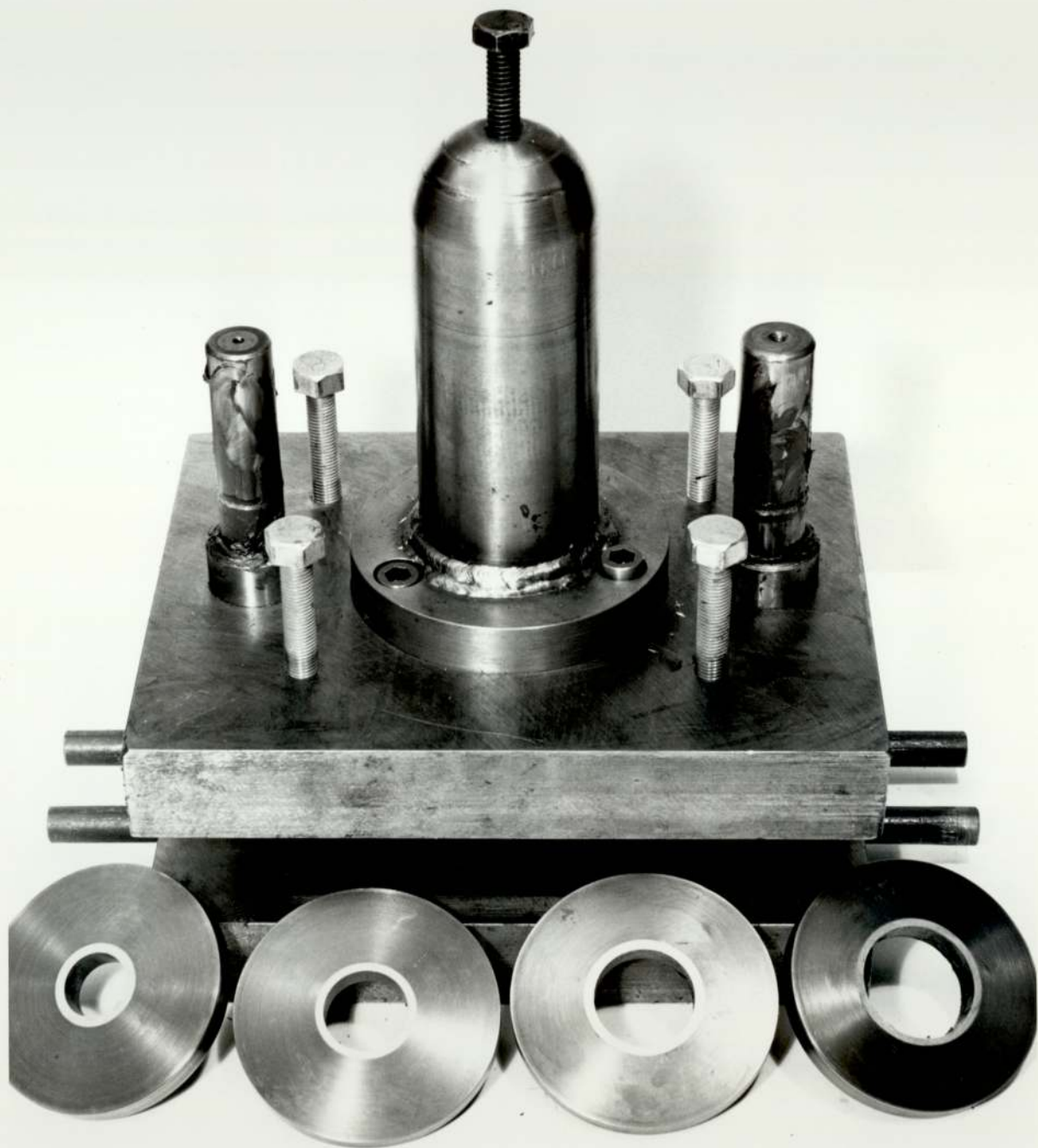


Plate P.3.

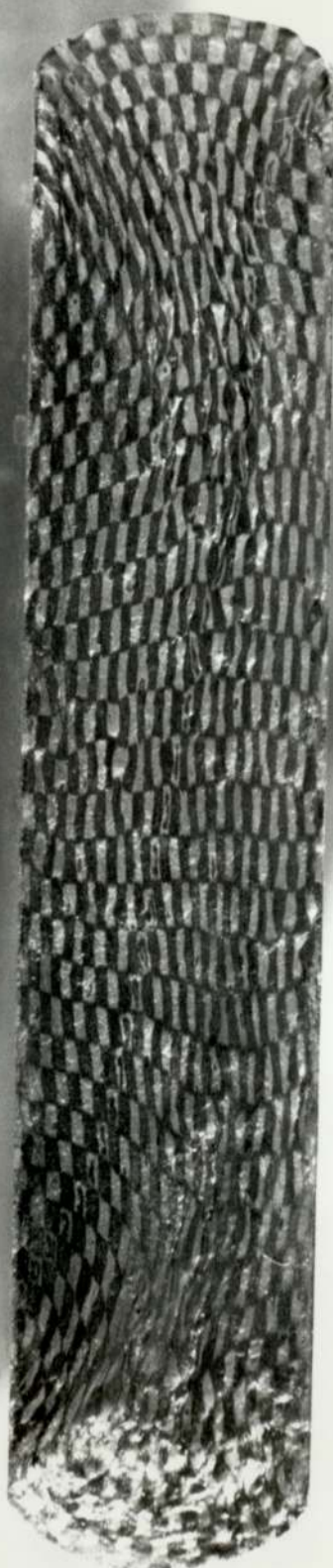


Plate P.4.